UNIVERSITY OF LIVERPOOL

Characterising the effect of S100P overexpression in cell adhesion

Thesis submitted in accordance with the requirements of the University

of Liverpool for the degree of Doctor in Philosophy by

Richard Thomas Smith

September 2015

Acknowledgements

Abstract

S100P is overexpressed in a number of different cancers and this overexpression has been shown to be associated with a significant decrease in patient survival. This decrease in survival is thought to be due to unregulated high levels of S100P within the cells of the primary tumour resulting in an increased risk of metastasis. In this thesis it is demonstrated, in an S100P-inducible cancer cell system, that overexpression of S100P decreases cell-extracellular matrix adhesion and increases cell migration and invasion. These effects caused by overexpression of S100P are shown to be dependent on the breakdown of NMIIA-containing cytoskeletal filaments and are coupled with a reduction in the abundance and alteration in the distribution of immunofluorescently-stained focal adhesions. In order to determine whether there were any alterations in the abundance of proteins within S100P-overexpressing cells, whole cell mass spectrometry was utilized which yielded several proteins although none that would directly account for the observed reduction in cell adhesion. A novel adhesome isolation technique is presented using both non-ionic detergents and hydrodynamic shearing which was used to study the effect of overexpression of S100P on the cell adhesome fraction. Western blotting of this cell fraction showed that S100P-overexpression did not cause any changes in the abundance of core focal adhesion proteins. However, mass spectrometry of the cell adhesome did identify several key proteins, the cellular level of which was significantly altered due to S100P-overexpression. In particular, the scaffold protein IQGAP1 was identified using this method, the redistribution of which can have substantial effects on cell dynamics. Finally it was determined that there was an alteration in the rate of focal adhesion maturation possibly due to a loss of NMIIA-mediated tension caused by S100P overexpression, as demonstrated by a reduction in the phosphorylation state of focal adhesion signalling proteins, linked to adhesion maturation. It is concluded that overexpression of S100P results in a breakdown of NMIIA filaments, which reduces cellular tension leading to a reduction in focal adhesion maturation which, in turn, leads to a reduction in the rate and strength of cell-extracellular matrix adhesion within this system. With a greater understanding of the way in which overexpression of S100P mechanistically affects the adhesive properties of carcinogenic cells, it may be possible to develop therapeutic drugs targeting these pathways, thus inhibiting the harmful effects of S100P overexpression in cancers.

Contents

List of Figures

List of Tables

Chapter 1

Introduction

1.1 Cancer

It is well established that the initiation of cancer can be caused by a wide range of agents including genetic disposition, lifestyle factors, radiation, exposure to carcinogenic chemicals and ageing [1]. Exposure to these results in mutations within normal healthy cells, such that they take on oncogenic properties. These mutations are commonly either in proto-oncogenes or tumour suppressor genes. In the former, such as genes like RAS, gene mutations result in increased activity of the protein, at which time they are referred to as oncogenes [2]. In many cases the increased expression of these proteins amplifies the effect they have on a cell. It is often common for such proteins to have functions that include: increasing cell proliferation, decreasing cell differentiation, decreasing cell adhesion, inhibiting apoptosis and promoting cell migration. All of these factors, when altered, can result in tumorigenesis [3]. Tumour suppressors are, in many ways the reverse, having functions that prevent or limit the aforementioned properties that would promote tumorigenesis. Mutations in tumour suppressor genes such as Retinoblastoma protein or p53 either lower or completely knock-out their activity, thus leading to an increased chance of the affected cells becoming carcinogenic [4, 5].

Despite the incidence of cancer is increasing, early detection and improved drug treatments are allowing a larger percentage of people to survive. However, once the cancer has spread, treatment options are dramatically reduced as surgery is no longer as easy on a larger number of smaller tumours. The result of this is patient mortality increases significantly in these cases [6]. The process by which cancerous cells disseminate from the

primary tumour and form secondary tumours elsewhere in the body is known as cancer metastasis.

1.2 Cancer metastasis

Metastasis is described as the spread of cancerous cells from one organ to another via either the circulatory or lymphatic system, these cells can then attach to the lining of the endothelium or other vessel walls and form secondary tumours [1]. Just as normal healthy cells require specific mutations in order to become tumorigenic, cancer cells from the primary tumour also require additional mutations, which cause specific cellular alterations in order to become metastatic. These cellular alterations produce an increase in cell migration, increased cell invasion, promotion of angiogenesis, increased epithelial to mesenchymal transitions and a decrease in cell adhesion [7, 8]. These factors for cancer progression are likely caused by a number of proteins in overlapping pathways forming a complex cascade which self propagates and causes cells to become more and more metastatic over time. This study is primarily focused on alterations which lead to cancer cells becoming more metastatic, as such each of these factors will be considered individually in more detail.

1.3 Changes in cellular adhesion

1.3.1 Cell-cell adhesion

For cells to become metastatic, cells need to break away from the primary tumour, and a crucial first step is breaking or inhibiting the adhesion sites which bind cells together [9]. Cell-cell intracellular adhesions are divided into three main groups: adherens junctions, tight junctions and desmosomes [10]. The first group, adherens junctions are composed of two distinct protein families; cadherins and catenins (Figure 1.1) [11]. The former are transmembrane polypeptides of about 730 residues in length, consisting of a small intracellular component, a transmembrane region and a large extracellular domain [12]. Cadherins form calcium-dependent extracellular linkages between one another, adhering adjacent cells together, with the action of this linkage being dependent on the specific cadherins [13]. The family of cadherins encompasses over 100 different proteins. Many

cadherins are given single letter designations depending on their tissue specificity, e.g. P-cadherin (placental), H-cadherin (heart) [14].The two most common cadherins are E-cadherin and N-cadherin. E-cadherin (epithelial) is located in all epithelial tissues, whereas N-cadherin (neural), which was originally discovered in neurons, is present in other cell types, crucially including mesenchymal cells [15-17]. Catenin proteins are structural cytoplasmic proteins and occur as two major types: α-catenin and β-catenin [18, 19]. The former α-catenin type forms a linkage between β-catenin and the actin cytoskeleton, while β-catenin also binds to the cytoplasmic tail domain of cadherins. In this manner a chain is formed between two cells, where their cadherins bind extracellularly and then catenins bind this linkage intracellularly to the actin cytoskeleton [11]. In many ways this form of cell-cell binding is analogous to the way in which integrins activate during cell-extracellular adhesion by binding of talin. Similar to that system, the structural adhesion proteins alpha-actinin and vinculin are recruited to strengthen and organise the intracellular actin linkages formed by the adherens junction [20, 21].

Tight junctions act in a very different manner, whereby the junction firmly holds the cell membrane of two cells together, so they are in contact, acting as a physical barrier [22]. This physical barrier prevents the passage of extracellular ligands, other diffusible molecules and controls ion passage between bound cells [23]. This function allows for tight regulation of the molecules which pass through a particular tissue and into other cellular compartments. These junctions are primarily formed from three transmembrane proteins: occuldin, tricellulin and junction adhesion molecule proteins (JAM) (Figure 1.1) [24]. These proteins complex at the cell membrane, with their extracellular domains binding to their complementary protein on adjacent cells. The intracellular domains of each bind to zonula occludens (ZO) proteins which, in turn, bind to the actin cytoskeleton [25].

Lastly desmosomes form cell-cell junctions with the aim of reducing mechanical and shearing stresses on the cells [26]. They contain desmocollins (1-3) and desmogleins (1-4), which are members of the cadherin protein family (Figure 1.1). These proteins form heterodimeric transmembrane linkages, where their extracellular domains bind to complementary homotypic partners from adjacent cells [27]. On the intracellular side, desmocollin and desmoglein bind to plakoglobin-containing and plakophilin-containing dense plaques [28, 29]. These plaques consist of two parts, outer and inner, where the outer part binds to the desmocollin and desmoglein, and the inner part binds to

desmoplakin. Desmoplakin then binds to intermediate filaments within the cell cytoskeleton [26].

In the context of cancer metastasis, deregulation of the above adhesion junctions allows cells to break away from the primary tumour more easily. At the cell-cell interface alterations in the cadherin or catenin, adherens junction proteins is also indicative of an epithelial to mesenchymal transition (EMT), a key hallmark in the progression of epithelial cancers (see Section 1.5). The breakdown of adherens junctions not only has a significant structural impact, but also results in increased cytoplasmic β-catenin which, through the Wnt signalling pathway, is able to promote expression of additional EMT proteins[30]. In tight junctions a loss or reduction of occuldin or claudin results in a loss of cell polarity and an increase in cell proliferation, and their loss has been associated with cancer cell metastasis [31-33]. Mutations in the genes expressing desmosomal proteins such as desmoplakin results in a similar situation to that found in adherens junctions, where there is promotion of the Wnt signalling pathway and, therefore, increased EMT protein production [34, 35]. A reduction in the desmosomal proteins has also been associated with a decrease in cell adhesion, an increase in cell invasion and promotion of cancer metastasis [36, 37]. For these reasons it is extremely common to find that cells in secondary tumour sites have undergone substantial loss of all three of these cell-cell junctions.
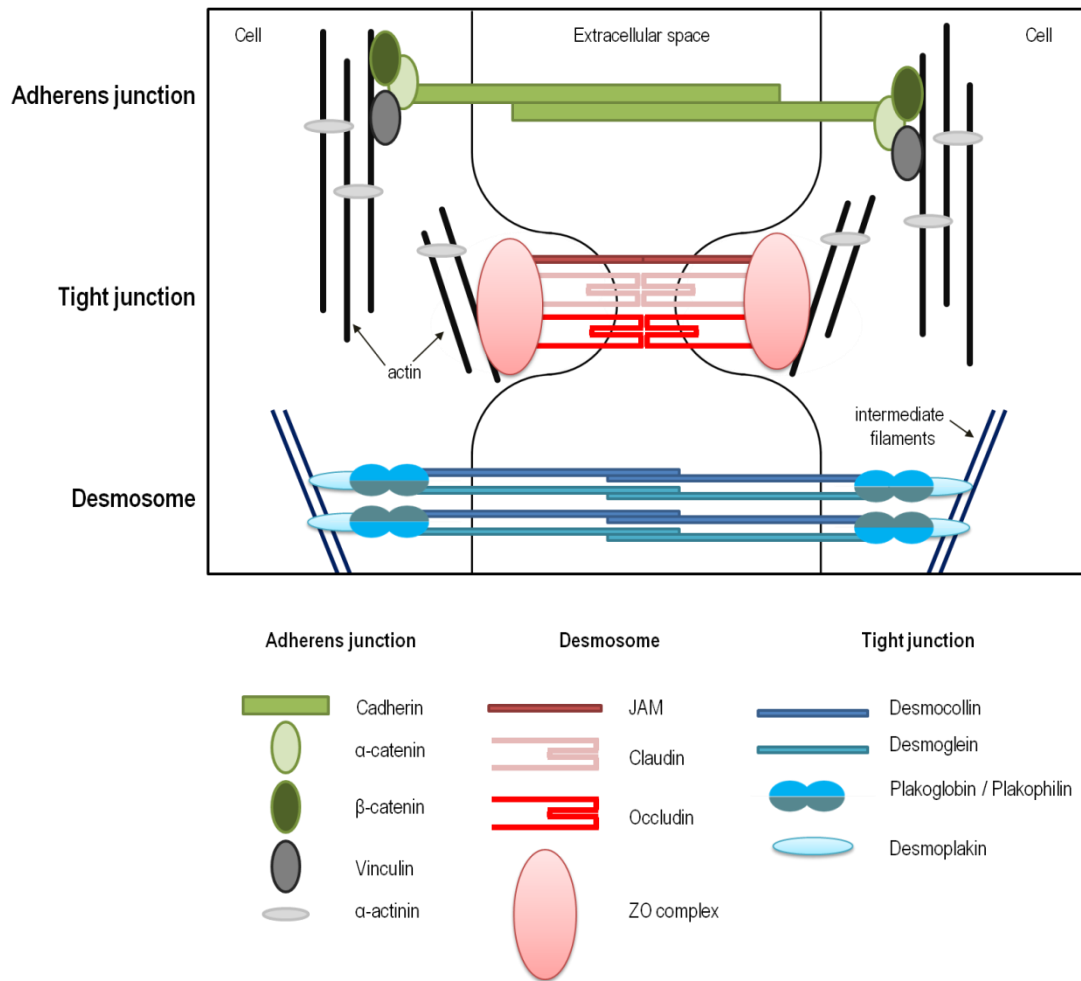
Figure 1.1. Cell-cell adhesion junctions in epithelial cells. Schematic representation of the way in which adherens junctions, tight junctions and desmosomes form cell-cell adhesions in epithelial cells. Abbreviations used are: junctional adhesion molecule (Jam), zonulae occludentes complex (ZO complex). Figure adapted from Neunlist, M. *et al.,* 2012 [10]

1.3.2 Cell-extracellular matrix adhesion

The mechanism by which cells adhere to the extracellular matrix is complex and has been an area of intense research over the last 10 years. There are over 200 molecules that make up cell-extracellular matrix adhesion sites and up to as many as 800 proteins and roughly 500 phosphoproteins, depending on how the adhesive cell fraction analysis was carried out [38-40]. These proteins have all been identified to have a role in cell to extracellular matrix adhesion and many of them form structural and signalling-based complexes at the cell membrane [41]. In its most simplistic form, cell-extracellular matrix adhesion takes place via integrin binding to the extracellular matrix which, via focal adhesion proteins, forms a

linkage to the cell cytoskeleton. This integrin and focal adhesion-based form of adhesion takes place in three phases: adhesion initiation, maturation and degradation [21, 42, 43].

1.3.2.1 Adhesion initiation

The first stage in cellular adhesion to the extracellular matrix is initial binding. This binding is initiated when protrusions from the cell's lamellipodium extend outwards from the cell during cell migration forming filopodia [43, 44]. Initial cell binding is undertaken by binding of the integrin receptor to the extracellular matrix along the periphery of a filopodia which protrudes from the cell at the leading edge [45].

Integrins are a family of transmembrane heterodimeric receptor proteins which bind the cell to the extracellular matrix via their extracellular domains [21]. The structure of each integrin consists of 3 main parts, the first is a large globular extracellular domain, which binds to the extracellular matrix or to extracellular ligands. The second is a transmembrane region and the third is a short intracellular domain, which binds to the actin cytoskeleton through focal adhesion proteins. The heterodimeric structure of integrins consists of one α and one β subunit. There are a total of 18 α subunits and 8 β subunits with 24 known αβ integrin pairings (Figure 1.2). The various combinations determine tissue specificity, cellular distribution and to which component of the extracellular matrix the pair will bind (Table 1.1) [46, 47]. In many cases, the binding of integrins to the extracellular matrix is via the RDG motif recognition sites; these sites allow binding to fibronectin, vitronectin and fibrinogen [48].

Integrin activation, which is required for extracellular binding, involves a conformational change in the α and β subunits [40]. When inactive, the extracellular region of the integrin is bent and has a low affinity for extracellular ligands. When active, the extracellular regions straighten up and are considered to be in a high affinity state. Integrin inactivity is maintained by the α and β subunits associating with one another, forming a salt bridge between the two [21]. Activation takes place in two ways, either through initial binding to extracellular ligands, which is known as "outside-in" integrin signalling, or through the binding of intracellular adhesion proteins to the integrin's intracellular regions, which is known as "inside-out" integrin signalling [49-51]. Furthermore single molecule microscopy of integrins has shown that Integrins undergo fast free-diffusion while inactive and not bound into focal adhesions. It was also shown that integrin activation correlated

with integrin immobilization to the focal adhesion site, and that this process of diffusion and immobilization occurs in a cycle matching both the activation state of the integrin and formation of nascent focal adhesions.
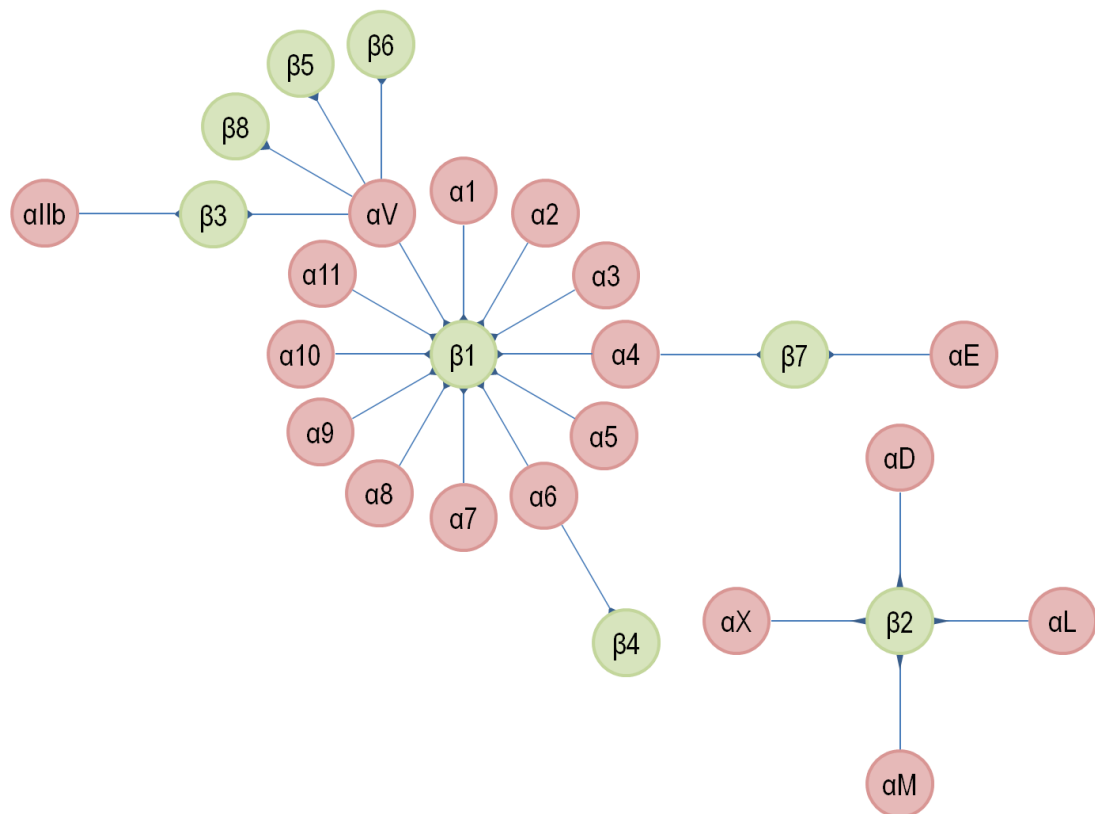
Figure 1.2. Integrin α and β subunit binding partners. Integrin alpha (α) subunits are indicated in red and beta (β) in green, with the blue lines indicating possible heterodimeric partners. Figure adapted from Bouvard *et al.,* 2001 [52]

Integrin	Extracellular binding ligands
Integrin α1β1	Laminin, Collagen
Integrin α2β1	Laminin, Thrombospondin, Collagen
Integrin α3β1	Laminin, Thrombospondin
Integrin α4β1	Thrombospondin, Fibronectin, Osteopontin
Integrin α4β7	Fibronectin, Osteopontin
Integrin α5β1	Fibronectin, Osteopontin
Integrin α6β1	Laminin
Integrin α6β4	Laminin
Integrin α7β1	Laminin
Integrin α8β1	Fibronectin, Osteopontin, Vitronectin, Tenascin
Integrin α9β1	Osteopontin, Tenascin
Integrin α10β1	Laminin, Collagen
Integrin α11β1	Collagen
Integrin αIIbβ3	Thrombospondin, Fibronectin, Vitronectin, Fibrinogen
Integrin αDβ2	ICAM
Integrin αEβ7	E-cadherin
Integrin αLβ2	ICAM
Integrin αMβ2	Fibrinogen, ICAM
Integrin αVβ1	Fibronectin, Osteopontin, LAP-TGF-β
Integrin αVβ3	Thrombospondin, Fibronectin, Osteopontin, Bone sialoprotein, MFG-E8, Vitronectin,

	Tenascin, Fibrillin, Fibrinogen, LAP-TGF-β
Integrin αVβ5	Osteopontin, Bone sialoprotein, MFG-E8, Vitronectin
Integrin αVβ6	Fibronectin, Osteopontin, LAP-TGF-β
Integrin αVβ8	LAP-TGF-β
Integrin αXβ2	Fibrinogen, ICAM

Table 1.1 List of integrins with their known extracellular binding ligands. List taken from Humphries, J.D. *et al.,* 2006 [53]

1.3.2.1.1 Inside-out integrin activation

Inside-out integrin activation is more common in situations where cells are in close proximity to the integrin extracellular ligands, but activation is only required in response to specific external stimuli [51]. An example of this would be in the circulatory system where cells in the blood need only bind to the vascular walls as a wound response or due to inflammation [54]. Indeed this has been shown in platelets containg the inactive platelet integrin αIIbβ3 which is activated by this mechanism [55].

In the "Inside-out" integrin mechanism, talin, an actin binding and structural adhesion protein binds to the NPxY motif on the intracellular region of the β integrin subunit [56]. Talin is found in two forms distinct isoforms, talin-1 and talin-2, both of which are large proteins at ~270 kDa [57]. The N-terminal head domain of talin is ~47 kDa and contains a FERM ((F) 4.1 protein, (E) ezrin, (R) radixin, (M) moesin) domain which binds to the NPxY motif of the β integrin [58, 59]. Talin also has a long (~220 kDa) C-terminal rod region, which contains multiple binding sites for other structural and signalling-based adhesion proteins. Included amongst these binding sites is one for vinculin, which is only activated when the talin tail is exposed to tensile force and an actin binding site [60-62]. Upon binding of talin to the β integrin tail, there is destabilisation of the salt bridge between the two integrin subunits and this destabilisation results in an extracellular conformational change which promotes binding to the extracellular matrix [63, 64]. Other

proteins are also able to bind in a similar manner to talin, such as Dok1 and tensin; however, binding of these proteins does not result in the conformational activation of the integrin. This difference is because the integrin-binding FERM domain on talin contains four subdomains F0, F1, F2 and F3. The last of these domains, F3, is unique to talin and assists in additional binding to a proximal site on the β integrin tail [58, 65]. This binding is achieved by the F2 and F3 subdomains acting in tandem to form the bond with integrin-binding site 1 (IBS1). The correct positioning of F3 during IBS1 binding is required in order to facilitate correct binding of the F2 subdomain [66].

The activation of integrins via the "Inside-out" pathway is tightly regulated. Talin, when not bound to integrins, is located in the cytoplasm in an inactive, auto-inhibitory form, which cannot bind to the β integrin tail [66, 67]. This auto-inhibition is caused by the N-terminal F3 subdomain of talin being bound to a region of its C-terminal rod. Homodimerization of talin takes place when in this inactive form and this self association masks the remaining integrin binding sites [68]. The way in which talin becomes activated is still not fully understood. The best current hypothesis is that phosphatidylinositol 4,5-bisphosphate (PIP2) interrupts talin auto-inhibition and sequesters it to the membrane, where it binds to the β integrins [69]. PIP2 regulation is mediated by PIP-kinase type 1γ which, when bound to talin, results in increased expression of PIP2. Talin activation and recruitment to the plasma membrane can also be mediated by Rap1-GTP-interacting adaptor molecule (RIAM) which contains an N-terminal domain which binds to and activates talin [70, 71]. These two pathways interact, in that RIAM is sequestered to the plasma membrane by Rap1A which is recruited by increased PIP2.

Besides talin, integrins can also become activated by kindlins. Like talin, kindlins have a FERM domain which contains the all important F3 subdomain; this F3 subdomain allows binding to β1, β2 and β3 integrin tails [72]. However, unlike talin, kindlins alone are not sufficient to form focal adhesions, since they are unable to bind to the actin cytoskeleton. *In vitro* experiments have demonstrated that a complex is formed between the NxxY motif on the β integrin and the FERM domains of both kindlin and talin [73, 74]. Knock-down experiments have shown that kindlin alone is not sufficient to activate fully the integrins. Moreover, in the absence of kindlin, the ability of talin to activate integrins was also diminished, with the overall binding affinity of the extracellular integrin being reduced [75, 76]. The net result is that for full activation of integrins from a low affinity to a

high affinity state in the "Inside-out" signalling model, both talin and kindlins are required [57].

1.3.2.1.2 Outside-in integrin activation

When ligands of the extracellular matrix bind to the extracellular domains of the integrin proteins, a signal is transmitted altering the intracellular domains and affecting the adhesion signalling cascade [21]. Similar to the "Inside-out" pathway, talin is recruited first and this molecule completes a structural chain from the extracellular matrix to the actin cytoskeleton. Once this chain is formed, a nascent adhesion is said to have formed, after which a large number of proteins bind and interact with the early adhesion, as will be discussed later in adhesion maturation. This manner of integrin activation and adhesion initiation is more common in cells which are present in an ECM rich environment [77, 78]. In these situations the reduced affinity of the inactive integrins is lessened by the abundance of the ECM proteins.

1.3.2.1.3 Syndecans in cell adhesion

Syndecans are transmembrane proteoglycans, which act as co-receptors with transmembrane proteins such as integrins and growth factor receptors. There are four members of the syndecan family with syndecans 1-3 having tissue-specific expression and syndecan 4 being expressed ubiquitously across all tissues [79]. Structurally syndecans consist of a small cytoplasmic domain, which contains two conserved regions, present in all syndecan isoforms, and a variable region, which is distinctive for each isoform. Each syndecan has a single transmembrane domain leading to an extracellular protein core bound to three to five glycosaminoglycan chains (heparan sulfate or chondroitin sulfate), depending on the isoform. These long, flexible extracellular glycosaminoglycans allow for interactions with ligands that are slightly more distant from the membrane or are very dilute, as well as with key extracellular matrix proteins [80]. Functionally syndecans can perform several roles, the first of which is in growth factor receptor activation via binding of the extracellular glycosaminoglycans to ligands such as FGFs, VEGF, TGF-β and EGFs. The second main function is in promoting cell to extracellular matrix adhesion via binding to

structural extracellular matrix proteins, such as collagens I, III and V, fibronectin, thrombospondin, and tenascin.

In regards to focal adhesion initiation, it has been previously shown that cells grown on fibronectin are dependent on both integrin activation ($\alpha5\beta1$) and syndecan 4 for formation of a nascent adhesion [81]. The manner in which this takes place is due to syndecan 4 activating PKCα and localising it to a newly-forming adhesion site, where it stimulates the Rac-Rho pathway. This happens by syndecan 4 binding fibronectin via its extracellular glycosaminoglycan chains; this allows the cytoplasmic variable region of syndecan 4 to bind to the kinase domain of PKCα, in conjunction with the inositol lipid PIP2. This activated tertiary complex, in conjunction with activated integrins, is then able to activate Rac1 which, in turn, promotes focal adhesion formation, although the exact manner in which the syndecan PKCα complex promotes this activation is still unclear [82, 83]. Furthermore, it has been shown that once activated by extracellular matrix binding, syndecan 3 can activate FAK and SRCn, and it has been proposed that syndecan 4 is likely to possess the same ability. Again the exact manner in which this takes place is not known, although there is also evidence of syndecan 4 contributing to FAK regulation. FAK is activated by autophosphorylation at Y397, and in syndecan 4 knockout experiments it has been shown to be significantly inhibited, resulting in reduced cellular adhesion[82].

1.3.2.1.4 Adhesion initiation and cancer metastasis

Within a tumour, a reduction in cell adhesion is often associated with local invasion, since cells can break away more easily from the surrounding cells of the tumour and from the extracellular matrix to which they are anchored [1]. With regards to adhesion initiation, changes in the integrins present within the cell can drastically change the adhesive phenotype. In metastatic cells, there is a reduction in the level of expression of integrins which bind cells to the basement membrane, such as $\alpha6\beta4$ and $\alpha6\beta1$. In place of these integrins, there is an increase in the abundance of $\beta1$-containing integrins that bind RGD, the overabundance of which is associated with a disruption of cell-cell E-cadherin adhesion junctions [84-86]. The fibronectin-binding integrin, $\alpha5\beta1$ is also often overexpressed in these cells to promote further cell migration [87]. Metastatic cancer cells are frequently observed to produce additional fibronectin, which allows for increased cell migration by binding these specific integrins. Other integrins can become overexpressed, such as $\alpha V\beta6$

and αVβ8, both of which have been observed in colon, lung and liver cancers [88]. In the αVβ6 and αVβ8 cases, a greater abundance of these integrins results in increased secretion of TGFβ, an important protein, which can promote EMT and angiogenesis (Section 3.4) [89]. Lastly α6β4 is overexpressed in a number of cancers, and its overabundance is associated with increased cell proliferation, migration and invasion [90-92]. All of these alterations in integrin abundance highlight how important tight regulation of adhesion initiation is within the cell.

1.3.2.2 Adhesion maturation

Following integrin activation, the binding of talin and the formation of nascent adhesions linking the extracellular matrix to the actin cytoskeleton (Figure 1.3), several other structural and signalling-based adhesion proteins bind or interact with the newly formed adhesion sites. These nascent adhesion sites have a very rapid turnover, being created and broken down in ~60 seconds in migrating cells. Nascent adhesions consist of talin, vinculin, α-actinin, paxillin [93] and FAK [94], along with other signalling-based proteins such as SRC.

1.3.2.2.1 Nascent adhesions

The first amongst the proteins to bind after integrin activation and talin binding is vinculin, a 117kDa cytoskeletal scaffold protein involved in focal adhesion maturation, as well as in stability of cell-cell adherens junctions. Structurally vinculin consists of: a globular C-terminal head domain which is able to bind to talin and α-actinin; a mid proline-rich neck region that binds VASP, vinexins and ponsin; and an N-terminal tail domain which, in turn, binds F-actin, PIP2 and paxillin [95]. The primary role of vinculin within the focal adhesion is to strengthen the integrin-talin-actin junction by forming a strong linkage between talin and the actin cytoskeleton. Inactive talin, not bound to integrins has its vinculin binding domain masked; however, due to a small amount of cellular tension exerted on talin by the integrin-actin junction, the binding site for vinculin is exposed allowing binding [61, 96].

α-actinin, a member of the spectrin superfamily, is an actin-binding protein which forms crosslinks between F-actin filaments . The N-terminal tail actin-binding domain (ABD) of α-actinin binds to a F-actin filament in an antiparallel homodimeric complex with

another α-actinin protein which binds to a second F-actin filament. This complex can then bind directly to talin-bound vinculin via the C-terminal domains which further strengthens the bond between the growing adhesion site and the actin cytoskeleton [97].

Paxillin, a signal transduction adaptor and scaffold protein, is the first major adhesion scaffold and signalling protein that binds to the growing nascent adhesion, alongside FAK. The C-termini of paxillin contains four LIM (Lin11, Isl1, Mec3) domains which target paxillin to focal adhesion sites. The N-terminal domain contains five leucine aspartic acid repeat (LD) motifs, these act as protein binding/interacting domains, with specific LD motifs. These LD motifs are responsible for binding FAK, Src and vinculin, as well as other proteins that interact later in adhesion maturation, such as the IPP (ILK-PINCH-parvin) complex. Paxillin can also become phosphorylated at several tyrosine sites by FAK and these phosphorylations have implications in mediating later stages of adhesion maturation [98, 99].

FAK is a tyrosine kinase, and the main signalling protein which results in the adhesion-mediated signalling cascades due to formation of focal adhesions. FAK activity is crucial during development of organisms and affects a large number of cellular processes, including cell-extracellular matrix adhesion, cell migration, control over cell polarity, cell proliferation and apoptotic pathways [94]. Structurally, FAK consists of a focal adhesion targeting domain (FAT) at the C-terminus, a central catalytic kinase domain and an N-terminus containing a FERM domain (consisting of F1, F2 and F3 sub-domains). FAK can bind to the main nascent adhesion complex via the C-terminal FAT domain binding to the LD2 and LD4 sub-domains on paxillin's N-termini or to the F3 sub-domain on the C-terminal FERM domain of talin. There is also some evidence to suggest that FAK can bind to β-integrins through the FERM domain, although the exact way in which this takes place is still not fully understood. FAK kinase activity is auto inhibited by binding of its FERM domain to a FERM binding site in the kinase domain. Full activation of FAK is achieved via phosphorylation of tyrosine 397 (Y397) near the N-terminus between the FERM domain and the kinase domain. Initial FAK activation is caused by autophosphorylation at Y397 is mediated by FAK binding to the proteins in the nascent adhesion, as described above. Upon phosphorylation, Y397 and an adjacent proline motif act as a recruitment and binding site for SRC. This binding of SRC to FAK is via its SRC homology 2 (SH2) and SRC homology 3 domains (SH3) present on the C-terminal of SRC. Furthermore, SRC binding at this site enables src to phosphorylate FAK at Y925 which, in turn, increases FAK activity [100-102].

SRC is a tyrosine kinase and acts as a proto-oncogene meaning that its overexpression, or activity has been linked with tumorigenesis. SRC activity influences a wide range of cellular functions, including promoting cell survival, cytoskeletal integrations, angiogenesis, cell proliferation and cellular invasion [103]. This is achieved by interacting with a number of different signalling proteins and pathways including RAC/RHO signalling, RAS, MAPK, P13K, CAS and paxillin [104, 105]. A structural organisation of nascent adhesions is shown diagrammatically in Figure 1.3.
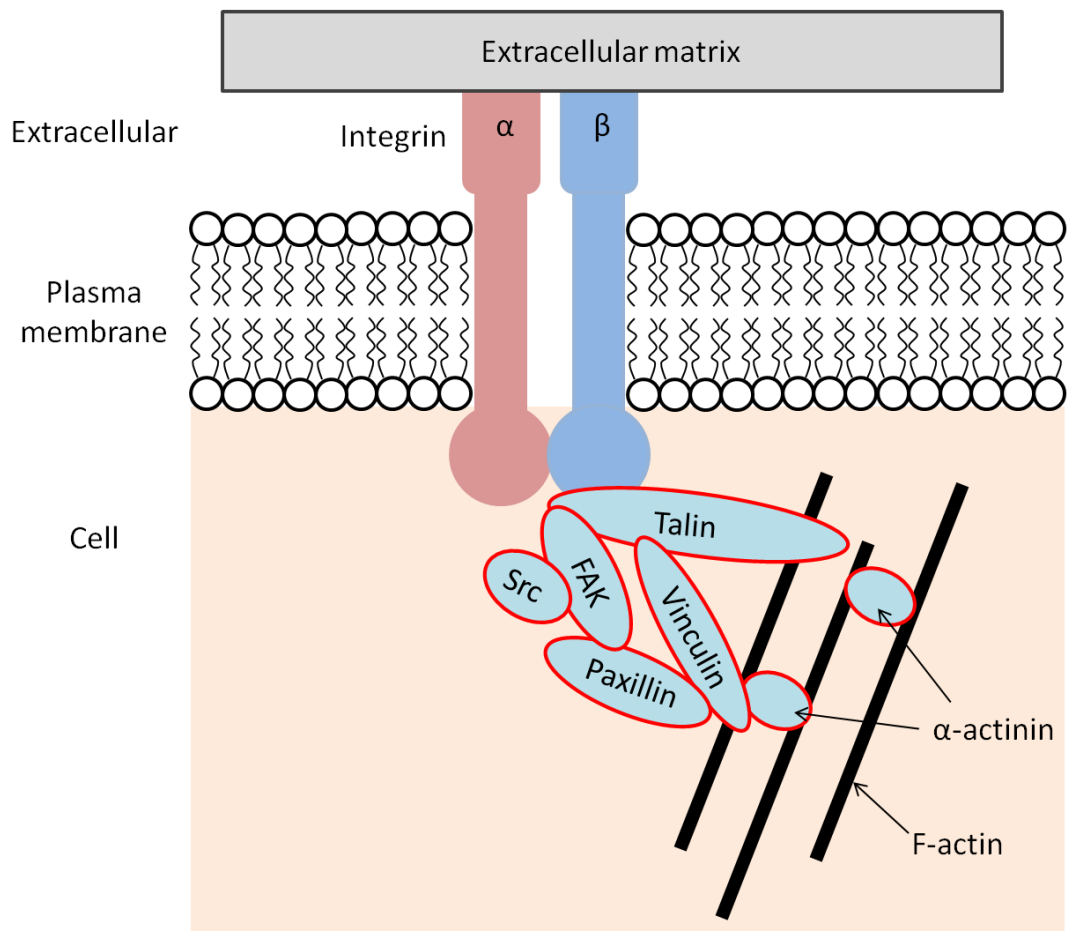
Figure 1.3. Nascent cell-extracellular matrix adhesion.

1.3.2.2.2 Adhesion complexes

As cells continue to migrate forward forming new nascent adhesions at sites of filopodia, the majority of those adhesion sites are degraded; however, some begin to mature moving back to the lamellipodium–lamellum interface. These maturing adhesion foci are referred

to as focal complexes and are larger in size than nascent adhesions at roughly 1 μm. Focal complexes are also considerably more stable, being able to exist for several minutes after which they will either be broken down or continue to mature [42]. The control of nascent adhesion to focal complex maturation is still not fully understood, although it is known that binding to myosin stress fibres is required for focal complex maturation. RhoA signalling (Section 1.3.2.2.4) has also been implicated in the maturation of nascent adhesions, as it directly controls myosin contractions, actin polymerization, as well as other aspects of adhesion initiation and maturation [106-108]. Structurally, focal complexes are similar to nascent adhesions in that they contain a common set of proteins, with additional proteins such as the structural scaffold proteins, tensin and zyxin, which accumulate at these adhesion sites [109, 110]. These focal complexes contain a greater abundance of all the previously mentioned proteins due to integrin clustering and an expansion of the size, of the intracellular adhesion site along with cross linking of intracellular focal adhesion proteins. The first notable protein addition is a much greater abundance in α-actinin, since this protein is required to bind the focal complex tightly to the actomyosin stress fibres.

Tensins give increased structural strength to the growing adhesion site by binding β-integrins together, as well as binding them to F-actin filaments. The exact manner in which tensins are regulated and interact with adhesion sites is currently not fully understood, although it is observed in higher abundance in more mature adhesions [111]. Zyxin acts in a somewhat similar manner, since it is able to bind to F-actin and to α-actinin; however, it also has an important role in regulating actin dynamics. This regulation is achieved by active bound zyxin recruiting and directly binding to vasodilator-stimulated phosphoprotein (VASP). This binding is achieved either through proline rich FPPPPP motifs near the N-termini of zyxin, or via the C-terminal LIM domains [112]. VASP is able to bind several crucial signalling proteins, the most important of which is profilin, which is subsequently able to promote formation of ATP-actin monomers and add them to the free barbed ends of F-actin filaments [113, 114]. This results in increased actin polymerisation which strengthens the adhesion site, as well as being important in cellular migration. Crucially profilin activity is also mediated by RhoA signalling (Section 1.3.2.2.4), although the manner in which zyxin and VASP are regulated is less well understood [115].

The signalling cascade continues to grow as adhesion complexes mature further, with other signalling complexes such as the ILK/PINCH/parvin complex (IPP) which binds to paxillin, being added to the adhesion site. These additional proteins mediate a wide range

of cellular processes and, as such, disruptions in adhesion maturation at this stage can cause alterations in many pathways [116].

1.3.2.2.3 Focal adhesions and fibrillar adhesions

If the focal complexes are not degraded, they continue to mature and move further back into the cell lamellum via mediated myosin tension. At this stage, they are referred to as mature focal adhesions and are typically elongated in the direction of cell migration, being roughly 2μm wide and 3-10 μm long. Focal adhesions are attached to myosin-containing ventral stress fibres and act as the strongest anchoring points for the cell [117, 118]. They are also the points where the highest contractile forces from the myosin fibres are exerted. Structurally, focal adhesions are very similar to adhesion complexes, but contain a larger abundance of all the core structural proteins and have increased integrin clustering. As the cell moves forward, over the focal adhesion sites, the focal adhesions slowly move backwards towards the trailing edge of the cell, where they are then disassembled.

In environments which are rich in fibronectin, cells are also able to form highly elongated fibrillar adhesions which are a specialised form of focal adhesion dependent on the presence of fibronectin. These are the strongest of all focal adhesion, containing a large abundance of tensins and are not present in highly migratory cells. They also have a secondary function, whereby they are involved in fibronectin matrix assembly and reorganization of the extracellular matrix [119].

1.3.2.3 Myosin structure and function

Myosins encompass a large family of ATP-dependent motor proteins and are best known for their role in actin contractibility, both in muscle fibres, as well as within many migratory cell types. In total there are 18 distinct forms of myosin, many of which are not involved in actin contractions, but instead walk along actin cables transporting large intercellular components like vesicles or organelles[118]. Myosin II is the main myosin involved in actin contractibility and is found in two sub-types, muscle myosin and non-muscle myosin. Structurally myosin II is a homodimer and consists of 3 distinct pairs of polypeptides. The first of these are two large (230 kDa) myosin heavy chains, each of which have a long C-

terminal tail that is helically coiled to the adjacent heavy chain. These heavy chains also contain an N-terminal globular head domain, which contains the binding site for both ATP and actin. Bound to the head domain of the heavy chain are 2 essential light chains, one on each chain which stabilises the heavy chains. Lastly there are 2 regulatory light chains which bind to the neck region of the heavy chain, between the globular head and coiled alpha helix. While these regulatory chains are unphosphorylated, myosin II folds in on itself in a compact, inactive form. In this form the globular head domains are still able to bind actin, however, myosin polymerization is not possible, as the alpha helix tails are folded. Upon phosphorylation of these chains at Ser19, the full myosin structure unfolds, allowing polymerisation in a bipolar manner via interactions between the helical tail domains on adjacent myosin molecules (Figure 1.4). While in this phosphorylated, polymerized state, actin which is bound to the heavy chain head domain, is moved in an anti-parallel way due to the ATPase activity of the myosin head domain initiating a conformation change.
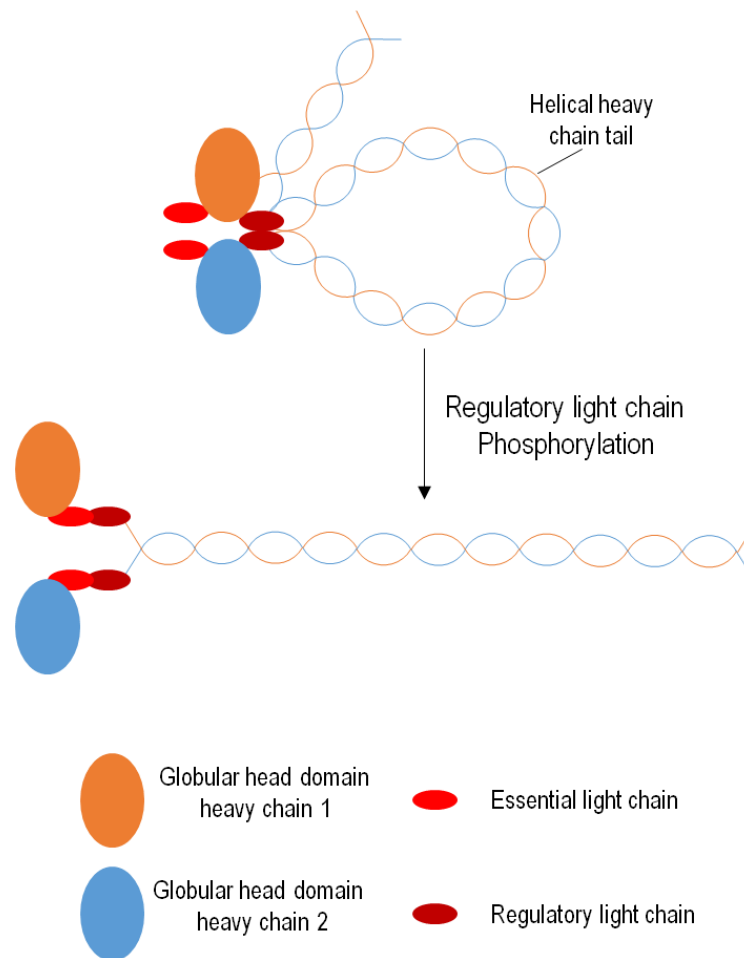
Figure 1.4. Structure of Myosin II. Schematic representation of myosin II structure showing a dimerised inactive and active form. Figure adapted from Vicente-Manzanares, M. *et.al* 2009 [118].

1.3.2.3.1 NMII isoforms

Normal mammalian cells are able to express three forms of non-muscle myosin, although the abundance of each is dependent on the cell type. Three different genes code for these non-muscle myosins; myosin heavy chain 9, 10 and 11, which lead to the production of non-muscle myosin heavy chain IIA, IIB and IIC [118]. The whole myosin molecule with associated light chains is then referred to by its respective heavy chain isoform. In regards to function, there are two main properties that define NMII activity and distinguish the three isoforms. The first is actin activated ATPase activity, which is measured by the increase in ATPase activity of NMII when bound to actin. For this, NMIIA has the highest activity and as such is able to pull on actin cables more quickly than the other isoforms. The

second property is duty ratio, which is the amount of time that NMII can remain bound to actin in a force creating form. NMIIB has the highest duty ratio of the isoforms making it specialised in exerting tension for longer periods of time than NMIIA.

1.3.2.4 Regulation of maturation of cell-extracellular matrix adhesion

The regulatory mechanisms by which cell-extracellular matrix adhesion foci mature is not fully understood, although it is known that maturation from a nascent adhesion to a focal adhesion is not unidirectional, but dynamic. In this manner, adhesion sites grow and disperse depending on both the signals involved as well as the tension that is being exerted upon them. In most cases, once adhesion foci begin to disassemble they are fully disassembled, although it has been shown that this is not always the case and that they can re-assemble depending on fluctuations in the abundance of zyxin and tensins [120]. It is also worth noting that not all cell types exhibit all forms of adhesion foci, with highly motile cells such as neutrophils and macrophages exhibiting only nascent and adhesion complexes [42].

It is clear that in order for focal adhesions to become fully mature, tensile force must be exerted upon the adhesion site via myosin contractions. The main regulator involved in this process is the RhoA signalling pathway, through which the contractile forces of NMIIA and NMIIB-containing actomyosin fibres is controlled [108, 121]. The effect of these myosin contractions has also been linked to increased adhesion maturation via phosphorylation of adhesion proteins. Increased tension on integrins due to myosin contractions has been shown to increase phosphorylation of FAK at Y397, which, while bound with SRC, subsequently promotes phosphorylation of paxillin at Y118 and Y31. The result of these phosphorylations is an increase in the rate of recruitment of focal adhesion proteins to the adhesion sites [99]. Specifically, this has been shown to be the case with vinculin recruitment, as well as with focal adhesion intermediates such as p130CAS-CRK and G protein-coupled receptor kinase interacting ArfGAP (GIT)–β-Pix; this in turn increases the rate of adhesion maturation and promotes integrin clustering and more structurally stable adhesion sites [122].

1.3.2.4.1 RhoA signalling

RAS homologue gene family member A (RhoA) is a GTPase protein, known to control the actin cytoskeleton and affect cellular tension via interactions related to stress fibres, as well as it having effects on cell proliferation [123]. RhoA influences these factors via interactions with 3 crucial proteins: ROCK1, Rac1 and DIAPH (Figure 1.5). In the case of the first protein, RhoA activates ROCK1, which in turn promotes phosphorylation of myosin light chain (MLC) by inhibiting directly myosin light chain phosphatase (MLCP). When MLC is phosphorylated, it binds to myosin filaments allowing phosphorylation of the myosin filament at S19 and T18, which results in the formation of crossbridges between myosin and actin. This binding results in contraction of the actin cytoskeleton, which increases cellular tension. This increased tension, in turn, promotes maturation of focal adhesions. Activated ROCK also phosphorylates PIP5K and this phosphorylation results in increased PIP2. The increased PIP2 leads to increased activation of talin and, therefore, increased initiation of focal adhesions, and binding of vinculin, which promotes adhesion maturation [107, 124].

RhoA further enhances this pathway by inhibiting Rac1, which results in decreased PAK2 activity. PAK2 is able to phosphorylate myosin light chain kinase (MLCK) which, in turn, inhibits MLCK's action as a kinase for MLC (Figure 1.2). The end result of the inhibition of Rac1 is, therefore, an increase in the abundance of phosphorylated, active MLC which is able to bind myosin filaments. Inhibition of Rac1 by RhoA results in a reduction in focal adhesion initiation and maturation in an inverse manner to ROCK signalling. Thus, inhibition of Rac1, inhibits activation of PIP5K, and therefore reduces PIP2 which results in less talin being activated and less binding of vinculin to mature focal complexes [125].

Finally, RhoA activates Protein diaphanous homolog 1 (DIAPH1) through preventing its auto inhibition and localising it to the adhesion sites. Active DIAPH1, via its FH1 domain then binds profilin which, in turn, binds to monomeric actin and promotes actin polymerization. The increased actin polymerization produces a larger amount of filamentous actin (F-actin) within the cell, and this increase in F-actin enhances cell migration by promoting more F-actin at the lamellipodia. A diagrammatic summary of the full pathway is shown in Figure 1.4 [107].
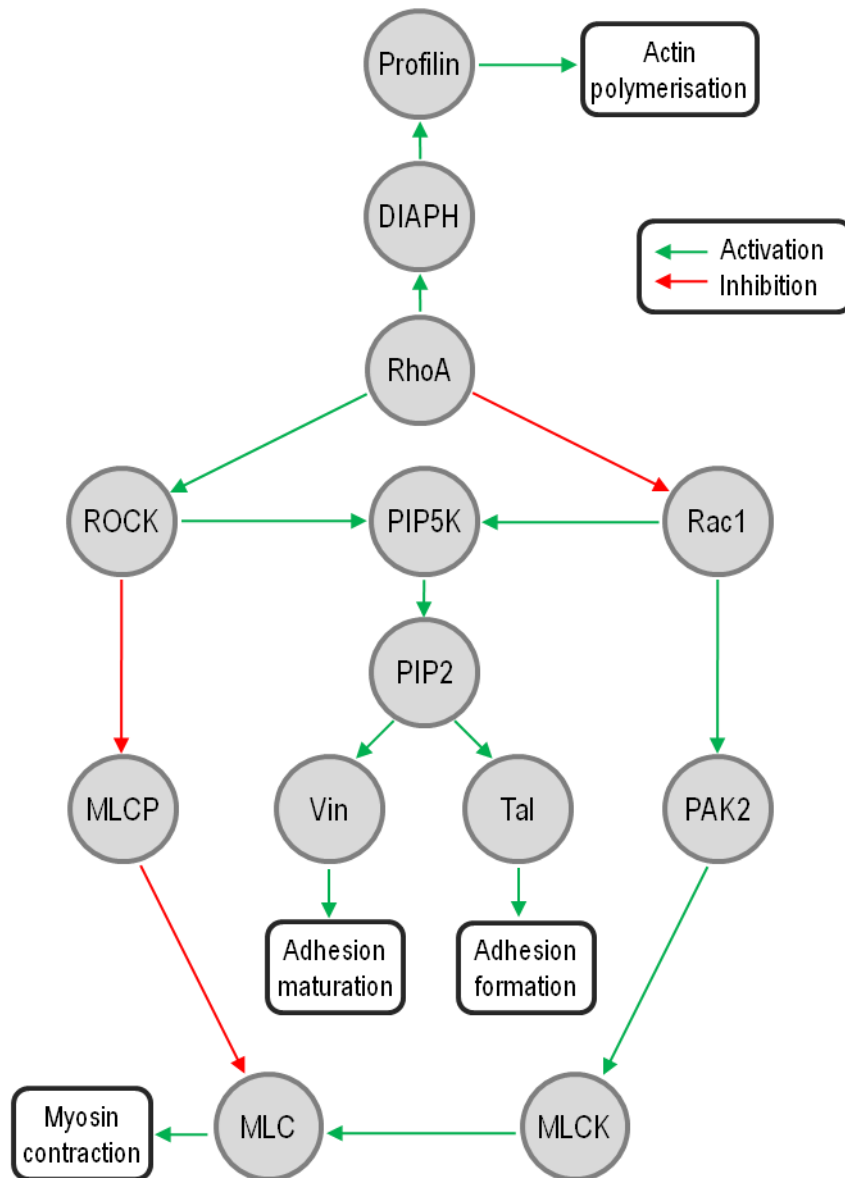
Figure 1.5. RhoA signalling pathway showing the cascade effects that lead to cellular alterations. Abbreviations used are: Protein diaphanous homolog (DIAPH), vinculin (vin), talin (tal), myosin light chain (MLC), myosin light chain kinase (MLCK) and myosin light chain phosphatase (MLCP).

1.4 Changes in cell migration

Cells migrate by the extension of filopodia from the leading edge of the cell membrane followed by attachment of the protruding filopodia to the basal substrate via either inside-out or outside-in activation of integrins. The integrins then bind to the substratum and form focal adhesions [126-128]. An intracellular adhesion protein, talin, is recruited to form these nascent adhesions, creating a bridge between the extracellular matrix and the actin cytoskeleton [55, 57, 126]. Once this attachment is formed, and the focal adhesions begin to mature, tensile forces created by the actomyosin cytoskeleton pull the cell in the direction of the leading filopodia, while at the same time, adhesion complexes at the trailing edge of the cell are disassembled. The rate at which this process takes place is dependent on a number of factors, primary amongst these is the polymerisation of actin in the lammellipodia, as this is required for adhesion maturation [129-131]. As discussed previously, it is the depolymerisation of actin at the trailing end of the cell, which, combined with integrin clustering, exerts force on the talin-actin junction, promoting recruitment of vinculin to talin and thus initiating early focal adhesion maturation [132]. Adhesion maturation is important, since this provides a much stronger anchoring point for the cell, so that it can exert a greater pulling force and drive the cell forwards.

Mature focal adhesions are strongly bound to the actin cytoskeleton and myosin contractions pull tightly on the actin structures, promoting the formation of stress fibres. This process is also mediated by changes in RhoA, ROCK and Rac1, all of which can affect adhesion maturation and actin polymerization, as well as controlling the strength and frequency of myosin contractions via myosin light chain (MLC) [108, 133]. Stress fibres consist of 10 - 30 short actin filaments bundled together through cross-linking with α-actinin, which are then bound to myosin II [134]. There are three main types of stress fibres that are formed due to cellular tension; transverse fibres, dorsal fibres and ventral fibres [135]. The first of these fibres form just behind the lamellipodium at the leading edge of the cell and are not bound to any focal adhesion [133, 136]. These transverse stress fibres contain a repeating α-actinin-myosin pattern, where both myosin IIA and IIB are present, and convey contractile forces to the cell through their interaction with dorsal stress fibres. Crucially, since transverse fibres are not bound to adhesion sites, they are able to move from the leading edge to the centre of the cell during migration in a process known as retrograde flow. This process acts in a wave-like motion as the cell migrates forward. Dorsal stress fibres form at the leading edge of the cell and bind to newly formed focal adhesion

sites. Unlike transverse and ventral fibres, dorsal fibres very rarely contain myosin II and, as a result, they are unable to contract. Although the dorsal fibres lack this contracting ability, their role is crucial in binding to the focal adhesions and force is still exerted on them by contractions of transverse stress fibres. Lastly, ventral stress fibres contain both actin and large amounts of myosin IIB. They are attached to focal adhesion sites at both ends of the stress fibre and are generally located near the trailing edge of the cell. These strong stress fibres exert the major contractile forces which drives cells forward during migration. It is known that all of the above forms of stress fibres can interact and bind to one another, although the mechanism by which this takes place is still largely unknown [137-139]. A diagrammatical representation of these stress fibres in the context of a migrating cell can be seen in Figure 1.6.

In the context of metastasis, several alterations can take place that promote increased cellular migration [140]. One pathway that is frequently altered involves RhoA, which through ROCK, Rac1 and DIAPH has effects on initiation of focal adhesion, focal adhesion maturation, actin polymerization and myosin contraction (Section 3.3.2.2.2) [141]. Overexpression of RhoA is, therefore, common in many metastatic cancers and a reduction in RhoA has been shown to inhibit metastasis in lung cancer cell lines [142]. Mutations or cellular events such as epithelial to mesenchymal transitions (EMT) that cause alterations in cell-cell junctions are also common in metastatic cancers and can cause an increase in cell migration due to a reduction in cell-cell adhesion and disorganisation of the actin cytoskeleton [143].
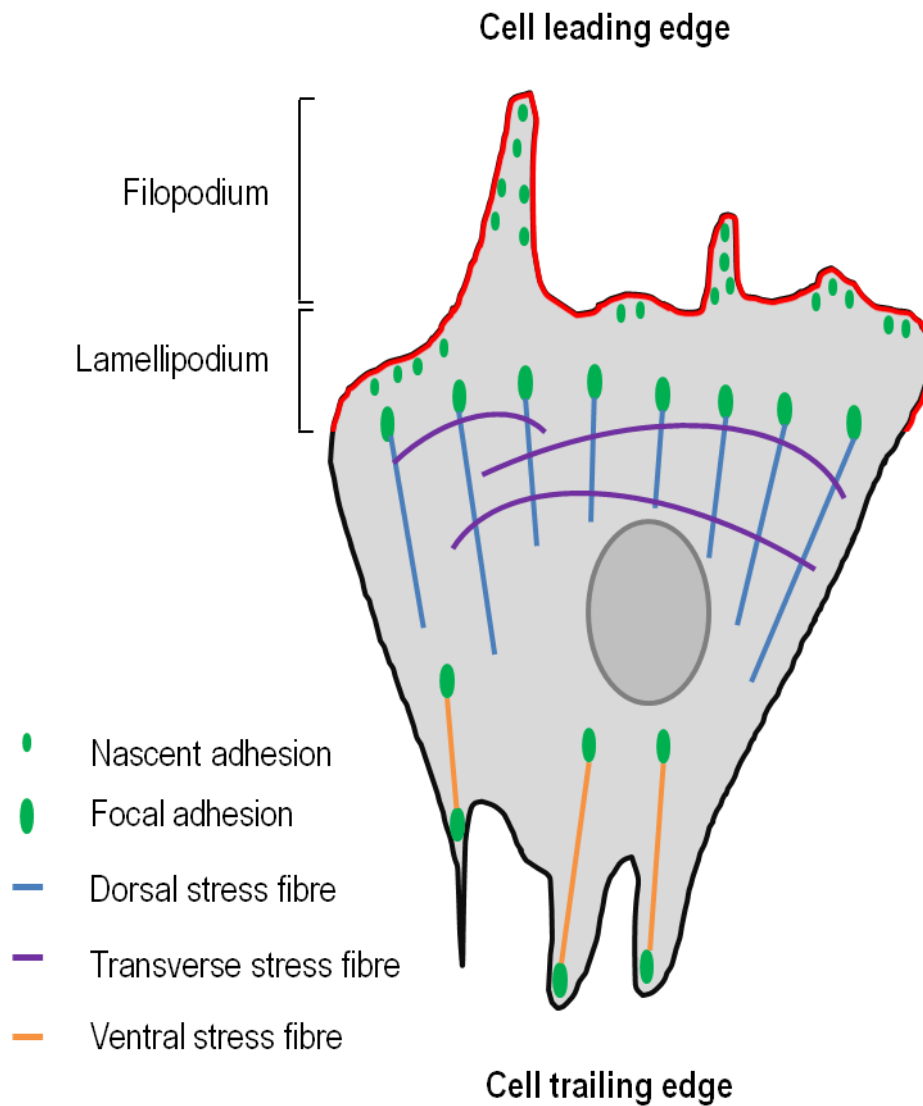
Figure 1.6. Stress fibre and adhesion foci localisation in a migrating epithelial cell. Figure adapted from Vallenius, T. *et.al* 2013 [136].

1.4.1 Microtubules in cell migration

The dynamic nature of microtubules is required for the migration of most mammalian cells[144]. During cell migration microtubules are oriented towards the leading edge of the cell. Dynamic microtubules regulate the levels of key proteins involved in adhesion and migration such as RhoA and Rac1. However, the exact manner in which cross-linking proteins coordinate the functions of the actin and microtubule cytoskeleton during migration is poorly understood [145]. Specifically, it is not known how exactly the mechanical properties of the F-actin filamental structure changes the outcome of actin to

microtubule interactions. These interactions do occur, however, such as F-actin coordination of microtubule growth. This microtubule growth is targeted towards focal adhesions present at the ends of stress fibres to regulate their turnover and promote migration. The main family of proteins known to be involved in the process of actin to microtubule crosslinking are spectraplakins, a family that contains proteins like microtubule-actin crosslinking factor (MACF), which is capable of physically cross-linking F-actin and microtubules [146].

1.5 Epithelial to mesenchymal transition

An epithelial to mesenchymal transition (EMT) is a process whereby cells from an epithelial tissue begin to lose their epithelial characteristics and take on more mesenchymal-like properties in exchange [147, 148]. This process is not linked solely to cancer progression, since it also occurs naturally during embryonic development and would healing [143, 149, 150]. In either natural cases or as a result of mutation, EMT usually results in a decrease in cellular adhesion and an increase in cellular migration. In cancers, an increase in invasive properties is also commonly observed, this increase can sometimes be due to EMT. Recently, it has become apparent that EMT is not a linear pathway and cells can partially undergo an EMT or indeed the process can be reversed [148].

1.5.1 Characteristics changes in an EMT

One of the core alterations that is observed in EMT is the reduction of E-cadherin in cell-cell adherens junctions [148, 151]. This loss has the immediate effect of reducing the strength of cell-cell junctions, making it easier for cells to break away from neighbouring cells. Disruptions in these junctions also leads to a loss of cell polarity which, in turn, directly affects the dynamics of cytoskeletal actin within the cell, leading to increased cell migration due to an increase in the number of filopodia [140, 151]. This alteration in the actin cytoskelton and increase in filopodia at the leading edge of the lamellipodia causes elongation and flattening of the cells, making them both visually distinct, and more able to traverse the narrow gaps between cells and stromal tissues. A secondary effect caused by the loss of E-cadherin is a release of bound β-catenin into the cytoplasm, where it causes a signalling cascade which results in increased transcription of additional EMT proteins, such

as the mesenchymal intermediate filamental protein vimentin [117, 152]. This overexpression of vimentin reduces the abundance of epithelial cytokeratins which, is associated with a reduction in E-cadherin transport to the cell membrane. In this way, as is common with many of these changes, the result is a positive feedback loop, which drives the cell's transformation forward. Vimentin filaments also interact with the proteins involved in cell migration such as the actin bundling protein fimbrin to promote further cell migration [153]. Lastly, with respect to E-cadherin, is what is commonly referred to as the "cadherin switch", whereby the reduction in E-cadherin is counteracted by the increased expression of N-cadherin [148, 154]. N-cadherin is found usually in neuronal cells, as well as in mesenchymal cells and its presence in adherens junctions forms much weaker interactions with neighbouring cells [155]. Crucially, the expression of N-cadherin due to EMT results in the expression of neural cell adhesion molecule (NCAM) which, in turn, causes an increase in assembly of focal adhesions, thus promoting migration [151, 156, 157]. As well as the observed alterations in cell-cell junction proteins due to EMT, cell-substrate proteins are also altered. Similar to the "cadherin switch", there is an "integrin switch" in which basement membrane binding integrins like α6β4 are down-regulated in favour of fibronectin-binding integrins like α6β1 or αVβ1 [84, 86].

1.5.2 Causes of EMT

1.5.2.1 Transforming growth factor beta

The transforming growth factor-β (TGFβ) superfamily encompasses a large range of proteins consisting of TGFβs, activins, NODAL, bone morphogenetic proteins (BMPs), growth and differentiation factors (GDFs) and anti-Müllerian hormone (AMH). Within these groups there are more than 30 TGFβ superfamily ligands, which are then divided into many more subfamilies based on their sequence similarity and biological function. Of particular interest in regards to EMT is the TGFβ subfamily [158]. TGFβs are secreted protein ligands that bind to the transmembrane TGF receptor TGFRII and have a role in cell proliferation, migration and differentiation [159-161]. Upon TGF binding, TGFRII associates with TGFRI resulting in receptor activity and intracellular signalling. The primary intracellular pathway activated by this process is SMAD signalling, which can be either activated or inhibited by the TGF signal [162-164]. Once TGFβ is bound to its receptor, SMAD2 or SMAD3 is recruited to the active TGF receptor by SARA to which it is bound, until SMAD2 or SMAD3 is

phosphorylated by the activated TGF receptor, thereby allowing SARA to dissociate. At this stage phosphorylated SMAD2/3 binds to SMAD4 in a heterodimeric complex and translocates to the nucleus, where it acts as a transcriptional activator inducing expression of EMT genes. These upregulated EMT genes include: Snail, Slug, ZEB1 and Twist, all of which contribute to promoting a more mesenchymal phenotype [148, 161, 165, 166].

As well as its effect on SMAD signalling, TGFβ also affects various other pathways that lead to an increase in EMT. During the formative stages of EMT, TGFβ causes degradation of RhoA, and then in the later stages, switches to promote increased RhoA expression and activation [167, 168]. As detailed in Section 3.3.2.2.2, RhoA signalling has effects on cellular migration, adhesion initiation, adhesion maturation and cytoskeletal remodelling. In the early stages of EMT, when RhoA is being degraded, this leads to increased Rac1 and a reduction in actin polymerization due to signalling through DIAPH [169, 170]. The exact manner and timing in which TGFβ performs this function is not fully understood; however, the initial degradation of RhoA is known to be via TGFβ, promoting upregulation of SMURF1 which then applies ubiquitin to RhoA [171].

TGFβ also has an effect on the AKT and MAPK pathways, where increased TGFβR activation promotes EMT through up-regulation of Snail and MMPs, although the exact manner in which these changes take place is still not clear [172-174].

1.5.2.3 Key transcriptional regulating proteins

As stated above, several transcriptional activators are up-regulated due to the initial EMT signalling. There are three major families of transcription factors that have their expression altered, The most significant of these are the Snail proteins (Snail1, Slug, Smuc) [175, 176], the ZEB proteins (ZEB1, ZEB2) [177] and the bHLH proteins (Twist1, Twist2) [178]. In many cases, these proteins act to inhibit the expression of E-cadherin, and, therefore, drive the EMT cascade forwards.

The Snail family of proteins have also been implicated in a range of developmental pathways, including cell survival and cell left-right identity and their overexpression has been strongly linked with cancer progression in several cancers [179, 180]. All Snail proteins contain four to six zinc finger domains at the C-terminus end, which bind to E-box motifs (5'CANNTG) on target genes. Curiously, elevated Snail expression has been associated with

suppressed tumour development during the early stages, but then switches to promote tumour progression via EMT when cells become resistant to TGF-β signals. It is during the later stages of EMT that TGF-β highly up-regulates Snail, via SMAD signalling. It has also been demonstrated that GSK-3β is the primary kinase for Snail, which causes its degradation. GSK-3β activity is inhibited by TGF-β signalling through AKT and integrin-linked kinase (ILK), further promoting increased levels of Snail in the cell [176, 181].

1.5.3 Mesenchymal to epithelial transition

As discussed, EMT within a primary tumour results in a reduction in cell-cell and cell-extracellular matrix adhesion, as well as an increase in cell migration and invasion. All of these changes are necessary to facilitate the breaking away of carcinogenic cells and their invasion into either the circulatory or lymphatic system, where they can then be transported to secondary sites. However, at this stage there is increasing evidence that these carcinogenic cells can begin to undergo a mesenchymal to epithelial transition (MET), whereby the changes wrought by EMT begin to be reversed, resulting in a return of some epithelial-like characteristics [182]. In theory this process makes sense, since cells transported by the blood or lymph system need to bind to other cells at a secondary sites and then grow into a secondary tumour. This process of cell growth and binding would be greatly hindered by the significant reduction in cell adhesion that cells which have undergone EMT exhibit. Evidence for this has been reported, in that secondary sites of metastasis seem to contain cells with a more epithelial-like phenotype, compared to those of the parental primary tumour [183, 184]. However, since single cells have not yet been followed from the primary tumour to secondary sites, it may be possible that more successful metastasising cells are simply less mesenchymal. Furthermore, the exact mechanism by which MET takes place and is regulated is still poorly understood, although these MET cells seem to exhibit almost the exact reverse of EMT in regards to their expression of EMT related proteins. Thus, MET of cells is currently characterised by the re-acquisition and expression of E-cadherin and its localisation at adherens junctions [185]. Transcriptional regulators of EMT such as Snail, ZEB and Twist also show reduced expression, presumably driving the cells back towards a more epithelial phenotype. The final result is a heterogeneous tumour consisting of cells at different stages on the EMT-MET continuum [182].

1.6 Metastasis-inducing proteins

Over the last 50 years, several different proteins have been identified which lack either oncogenic or tumour suppressor activity, but can promote the progression of cancer. All of these proteins, when expressed within normal cells, cause no adverse effects. However, when overexpressed within benign tumours they dramatically increase the chance of cancer metastasis. Due to this unique property these proteins have been termed metastasis-inducing proteins (MIPs). The three major proteins or protein groups described currently are the S100 proteins, AGR2 and osteopontin [186-188].

1.6.1 S100 proteins

The S100 proteins encompass 25 distinct members, which have a range of cellular functions including regulation of cell growth, differentiation and cell survival [189-191]. It has been previously shown that several of these proteins have an acute effect on cellular migration, and their overexpression in cancer cell models can result in dissemination and formation of secondary tumours when implanted into rat model systems [192, 193]. The S100 proteins are of low molecular weight (10 – 25 kDa) and all retain the ability to bind calcium. Of the 25 known members designated as S100 proteins, 16 are S100A proteins (S100A1 – S100A16) and there are 9 other proteins including S100B, S100G, S100P and S100Z, all of which share between 16-98% sequence homology [188, 194, 195]. The ability of S100 proteins to bind calcium is via a pair of highly conserved, calcium-binding regions; the first a C-terminal EF-hand motif containing 12 amino acids, and the second a 14 amino acid N-terminal loop [196, 197]. S100 proteins are expressed naturally in a range of different tissues and cell types, as well as being overexpressed in several different cancers [198, 199]. Over the past decade two S100 proteins, S100A4 and S100P have been shown to have the greatest clinical, metastasis-associated effects in patients, and in this study the latter, S100P, will be examined in detail [200, 201].

1.6.2 S100P

S100P is not limited to a role in disease-based systems and is found in abundance in developing placental and oesophagal tissues [199, 202]. The role of S100P within these cell types is poorly understood, as is the method by which its expression is regulated. However, recent evidence has suggested that its role in the placenta may be in mediating endometrial implantation via alterations in cell migration and invasion, and its expression seems to coincide with the ovarian cycle [202]. Evidence from disease systems support this idea, since in many cancers and in endometriosis, S100P has been observed to increase cell migration and invasion [203-205]. The link between the research in healthy tissues and diseased tissues is tenuous, since the majority of published information on S100P has all been conducted in either cancers or in endometriosis.

1.6.2.1 Cellular effect of S100P

The effect of S100P on cells is still not fully understood within either normal or disease cell systems, although it has been shown to interact directly with and affect various proteins, which are involved in cytoskeletal remodelling [206, 207]. S100P has been shown to interact directly with ezrin, a member of the Ezrin, Radixin, Moesin (ERM) protein family, which acts as cross-linking proteins between the plasma membrane and the cytoskeleton [203, 208]. This cross-linking is caused by ezrin activation via S100P, where the C-terminal ERM domain of ezrin binds to F-actin, and the N-terminal ((F) 4.1 protein, (E) ezrin, (R) radixin, (M) moesin) FERM domain binds to membrane proteins such as CD44 and ICAM-2 [209, 210]. Ezrin can also be activated by other routes, such as through RhoA signalling, but regardless of its source of activation, binding results in alterations in migration due to F-actin relocalisation [211, 212].

S100P has also been shown to interact with IQGAP1 a multi-domain 190 kDa protein involved in actin regulation and adhesion through interactions with Cdc42 and the Rac1 pathway [213-216]. IQGAP1 has also been shown to crosslink actin filaments and may be important in tumorigenesis, as knock-out studies have shown tumour formation is significantly inhibited due to a loss of IQGAP1. IQGAP1 also binds to b-RAF, MEK1, MEK2, ERK1 and ERK2 and, as such, is important in the MAPK pathway which leads to cell proliferation, differentiation, and apoptosis [217]. Due to IQGAP1 affecting so many crucial

pathways, it has been linked to a number of cancers, including colorectal, squamous cell, breast, liver, gastric and lung, where an increase in IQGAP1 is associated with a poor patient prognosis [218, 219]. The manner in which S100P affects IQGAP1 via its binding is still not fully understood.

Previous work by Du *et.al.* 2012 showed that using an IAsys two-channel resonant mirror biosensor, S100P binds directly to NMIIA *in vitro*. The exact binding site for S100P was determined by creating NMIIA mutants. Through these it was shown that, like S100A4, S100P binds to amino acids 1909-1937 on NMIIA. This region lies directly adjacent to a domain that regulates NMIIA filament polymerisation and due to a small overlap in sequence is thought to be the reason why S100P binding results in a decrease in NMIIA filament polymerisation. Extracellular S100P has also been suggested to be a factor in affecting the migratory properties of cells by interacting with RAGE receptors, although this interaction is poorly understood, as is the mechanism by which S100P could become released from a cell [220-222].

1.6.2.2 S100P in cancer

A number of studies have been carried out linking the overexpression of S100P to the clinical outcome for patients in a range of cancers by using immunohistochemistry to stain for S100P in patient biopsies. In all cancers tested, including breast, colon, lung, prostate, gastric and cholangiocarcinoma, an increase in S100P within a tumour correlated with a very poor patient prognosis [193, 223-227].

Furthermore, recent *in-vitro* research has shown that overexpression of S100P in both HeLa and benign Rama 37 mammary cell lines results in a more metastatic phenotype via increased cellular migration [206]. Knock-downs have also been carried out on S100P highly-expressing colon and pancreatic cancer cell lines. In both cases knock-downs of S100P resulted in a reduction in cell migration, as well as in cellular invasion [228, 229].

1.7 Project aims

As S100P has been shown to have a role in cancer progression, the main aim of this study is to investigate the mechanism by which S100P causes these phenotypic alterations leading to the promotion of metastatic characteristics. This goal will be broken down into two major parts, the first aim will be to determine and characterise the effect S100P has on cellular migration, adhesion and invasion and to try and ascertain possible causes for any observed alterations. The second major aim is to establish the levels of those proteins which are altered as a consequence of S100P overexpression. These aims will be achieved using the HeLa A3 cells as a model system. The overall aim, therefore, is to build up a better understanding of what the function of S100P is, as well as its effect in a cancer-based system. Utilizing this knowledge, longer term goals would therefore be to identify drugs which specifically target S100P in cancers.

Chapter 2

Materials and Methods

2.1 Chemicals and equipment

All chemicals and equipment utilized during this study were used from communal stocks and obtained from Sigma (Sigma-Aldrich Co., St. Louis, MO, USA), Cell Signaling (Cell Signaling Technology, Inc., Danvers, MA, USA) or Fisher Scientific (Fisher Scientific UK Ltd., Loughborough, UK), unless otherwise stated. All equipment utilized for eukaryotic tissue culture was obtained from Corning (Corning Inc., Corning, NY, USA), unless otherwise stated. All solutions were made up to their required volume using deionised water, unless otherwise stated.

2.2 Tissue culture

All standard cell culture was carried out using Dulbecco's Modified Eagle's Medium (DMEM), which in all cases contained 4500mg/ml glucose, non-essential amino acids, 3.7g/l sodium bicarbonate and phenol red. All DMEM solutions had the following chemicals added to aid in cell growth: 100µg/µl penicillin, 100µg/µl streptomycin (added as a mixture), 4mM L-glutamine and 10% (v/v) foetal bovine serum (FBS); this solution will hereafter be referred to as Standard Culture Medium (SCM). All chemicals used were obtained from Gibco (Thermo Fisher Scientific, Waltham, MA, USA).

Routine cell culture was undertaken using 10cm diameter tissue culture-treated Petri dishes containing 10ml of SCM. All cell culture was carried out under sterile conditions in a

negative air pressure Laminar Flow Hood. Cells were maintained in a 37°C humidified incubator set with an atmospheric carbon dioxide (CO_2) concentration of 10% (v/v).

2.2.1 Cell lines

2.2.1.1 Parental cell lines

The following parental cell lines were used during this study:

HeLa cells - epithelial, human cancer cells originally derived from a human cervical cancer from Helen Lane; these cuboidal-like cells culture easily and have a clear and well defined cytoskeleton (including NMIIA) and adhesive structures [230, 231]. It has been shown in previous studies that HeLa cells are no longer true epithelial cells, as they have undergone an epithelial to mesenchymal transition to some extent, meaning that any alterations observed in adhesive or migratory properties due to S100P are unlikely to be due solely to this transformation. All of these properties are useful for studying the effect of S100P on the cytoskeleton and adhesive structures and, as such, HeLa cells were chosen as the primary model system for this thesis. Moreover an S100P-inducible HeLa cell system was available, which had previously been used for similar work.

Cos7 cells - originally derived from the immortalization of CV-1 monkey kidney cells [232]. These are spindly epithelial cells and were utilized because they do not contain any NMIIA filaments. NMIIA is a known target of S100P and, as such, Cos7 cells were used to study the effects of S100P when this interaction is impossible.

2.2.1.2 Transfected cell lines

Prior to this study, HeLa and Cos7 cells had been transfected to create S100P inducible cell lines by Drs Min Du and Guogong Wang in our laboratory, as described in [206]. The inducible systems, stimulated by doxycyclin are achieved by the integration of two plasmids. The first, pBTE is integrated in order to express the regulatory element rtTA2(S)-M2 which is responsible for acting as a doxycyclin switch. The second plasmid, pTRE-ins is

then integrated in order to express the S100P protein. The result of these transfections yielded the cell lines shown in Table 2.1.

Parental cell name	Transfected cell name	Transfected cell characteristics
HeLa	HeLa A3	Epithelial cancer cell, overexpresses S100P upon induction with doxycyclin
Cos7	Cos7-S10	Elongated epithelial-derived cell, no cytoskeletal NMIIA, overexpresses S100P upon induction with doxycyclin

Table 2.1. Overview of S100P-inducible cell lines. Both transfected cell lines used during this study are inducible for S100P by doxycyclin.

2.2.2 Cell passage

Unless otherwise stated, cells were passaged once their confluence reached 70-80%, usually over the course of 2-3 days. All solutions used during a cell passage were pre-warmed to 37°C to prevent thermal shock to the cells. SCM was removed from the Petri dishes using an aspirator and the cells were gently washed twice with phosphate-buffered saline (PBS). One ml of 0.05% (v/v) trypsin in versene was then added for 3 minutes for HeLa A3 cells or 2 minutes for Cos7-S10 cells, during which time the Petri dishes were returned to the 37°C incubator. Trypsin activity was then halted by the addition of SCM. The volume of SCM added was dependent on the ratio at which the cells were split, with HeLa A3 cells routinely split at a ratio of 1:6 and Cos7-S10 cells at 1:8. The ratios of these splits were altered in order to obtain a greater or lower cell confluency as required.

2.2.3 Freezing cells

Cells were detached using the methods described in Section 2.2.2. The cell medium suspension was transferred to a 50ml Falcon tube and centrifuged at 1000 x *g* for 5 minutes. The SCM was then removed by aspiration ensuring not to disturb the cell pellet. Two ml of Freezing Medium was then added for every 10cm diameter dish which was used during the initial collection. Freezing Medium is SCM as described in Section 2.2 with the addition of 7.5% (v/v) dimethyl sulfoxide (DMSO) to inhibit ice crystal formation during freezing. One ml of freezing medium / cell suspension was added per cryovial (STARLAB UK, Ltd., Milton Keynes, UK). Vials were then placed into a freezing container (Nalgene, Nalge Nunc International., Rochester, NY, USA) and were stored in a -80°C freezer overnight to ensure a rate of temperature decrease of roughly -1°C per minute. Cell vials were then transferred to a -135°C freezer for long term storage.

2.2.4 Thawing cells

Cryovials of cells were rapidly thawed in a 37°C water bath before the resultant solution was poured into a 10cm diameter tissue culture Petri dish containing 9ml of pre-warmed SCM. The dishes were then incubated for 24 hours, after which the SCM was replaced to remove any remaining DMSO. This was due to the fact that DMSO is toxic to cells at either high concentrations or over a prolonged period of time.

2.2.5 Doxycyclin induction of S100P

Doxycyclin powder (Clontech Laboratories Inc., Mountain View, CA, USA) was dissolved in reverse osmosis water to make a 5mg/ml stock solution. HeLa A3 or Cos7-S10 cells (as the experiment requires) were split as detailed in Section 2.2.2. Dishes marked as induced were inoculated with 10μl of stock doxycyclin solution giving a final concentration of 5μg/ml. Unless otherwise stated, cells were then left for 48 hour for S100P protein expression to reach acceptably detectable levels. In cases where long term induction was required, doxycyclin-containing SCM was replaced every 48 hour, either as part of a cell passage or by aspirating and reapplying this fresh medium to the cells.

2.2.6 Whole cell lysis

Unless otherwise stated, cells were lysed once their confluence had reached 70-80%. Cell culture dishes were placed on ice and washed three times with ice-cold PBS. They were then tilted to 45° and left for 1 minute to allow residual PBS to pool. The residual PBS was then aspirated and replaced by 100μl of standard SDS Lysis Buffer per 10cm dish (Table 2.2). The dishes were then thoroughly scraped using a cell scraper and the resultant lysis solutions pooled and collected in an Eppendorf. Samples were then sonicated on ice using a MSE Soniprep 150 plus (MSE UK, London, UK) with the 3mm exponential microprobe attachment at an amplitude of 12 microns for 15 seconds. Samples were then heated at 95°C for 5 minutes, cooled on ice and stored at -80°C until needed.

Standard SDS Lysis Buffer
0.5% (w/v) SDS
50mM Tris-HCL pH 6.8
1mM EDTANa$_2$
150mM NaCl
10% (w/v) Protease inhibitor cocktail*

Table 2.2. Standard SDS-containing lysis buffer used for routine whole cell lysis. *Protease inhibitor cocktail complete EDTA-free tablets purchased from Roche (Roche Holding AG. Basel, Switzerland) were prepared in distilled water at 1 tablet per ml. The solution was then aliquotted and frozen at -20°C. Protease inhibitor cocktail solution was added to the Lysis Buffer just before use.

2.3 Cellular dynamics assays

2.3.1 Migration assay

This assay was carried out using Corning®, 6.5mm diameter, 24 well Transwells with 8μm diameter pore polycarbonate membrane inserts. FBS-free SCM was added (200μl) to the interior and exterior of the Transwells for 1 hour while the Transwell dish was placed in the incubator. This medium was aspirated just before the cells were added to the wells. Either HeLa A3 or Cos7-S10 cells (as required) were induced with doxycyclin 48 hours before this experiment was conducted, as described in Section 2.2.6. Control and induced cells were initially collected via the methods described in Section 2.2.3 and counted using a Z1 Coulter® particle counter (Beckman Coulter., Brea, CA, USA). The cells were collected by centrifugation at 1000 x g and resuspended at 15000 cells/mL in 1% (v/v) FBS containing DMEM culture medium. SCM was added (200μl) to the exterior of the Transwell chambers followed by 100μl of the cell suspension containing 15000 cells into the Transwell chamber interior. These solutions were prepared to create a 1% to 10% (v/v) FBS difference between the inside and outside of the Transwell chamber in order for the cells to migrate via serum chemotaxis. Cells were incubated for 24 hours, after which time all medium was removed by aspiration and the interior of the membrane wiped clean using cotton buds purchased from Tesco (Tesco PLC., Cheshunt, UK). The Transwell membranes were then stained using a REAstain Quick Diff kit (Reagena., Siilinjärvi, Finland). The total number of cells that had migrated across the membrane were then counted per membrane using a light microscope with a 10x objective lense. All cell treatments were prepared in triplicate with the mean number of cells migrated +/- SD being used as the final value.

2.3.2 Invasion assay

This assay was carried out using Corning® BioCoat Matrigel 6.5mm diameter, 24 well Invasion Chambers with 8μm diameter pore polycarbonate membrane inserts. The method used in this assay was the same as that described in Section 2.3.1 with the following alteration. FBS-free culture medium was added (200μl) to the interior and exterior of the Matrigel-coated chambers for 2 hour prior to the addition of cells. This medium was then removed by aspiration before 20000 cells were seeded in the invasion chambers. All cell

treatments were prepared in triplicate with the mean number of cells migrated +/- SD being used as the final value.

2.3.3 Time course adhesion assay

Either HeLa A3 or Cos7-S10 cells (as required) were induced by addition of doxycyclin 48 hours prior to this experiment being conducted, as described in Section 2.2.6. Uninduced control and induced cells were initially collected using the methods described in Section 2.2.3 and counted using a Z1 Coulter® particle counter. The cells were collected by centrifugation at 1000 x g and resuspended at 200000 cells/mL in SCM. One ml per well of cell suspension was added into a 24 well tissue culture dish and cells were allowed to adhere at 37°C. At the appropriate time (30 min to 2 hours) the wells were carefully washed two times with PBS to remove unbound cells and 0.05% (v/v) trypsin in versene solution was added for 5 minutes. SCM was then added and the number of cells counted. The percentage of the original 200000 cells that had seeded compared to the number remaining was then calculated to give an adhesion efficiency. All cell treatments were prepared in triplicate.

2.3.4 Strength of adhesion assay

Either HeLa A3 or Cos7-S10 cells (as required) were induced with doxycyclin 48 hours prior to the experiment being conducted, as described in Section 2.2.6. Control and induced cells were initially collected using the methods described in Section 2.2.3. Cells were seeded in a 24 well tissue culture dishes so as to yield an 80% confluent culture in 24 hours. Two identical dishes were set up in all experiments, with one acting as a test plate and the other a control plate, to aid in cell normalisation. After 24 hours, the wells on the dish were washed two times with PBS, and 250µl of 0.0125% (v/v) trypsin in versene solution was added for 5 minutes at 37°C. Wells were then carefully washed two times with PBS to remove weakly bound cells. Trypsin in versene solution was then added (250µl of 0.05% (v/v)) to both the test dish and the control dish for five minutes to remove all cells from the wells. SCM was added and the cells in all wells were then counted. The cell counts from the test dish were then compared to the cell counts from the control dish to calculate the proportion of cells which remained attached after the weak trypsin digestion step. All cell

treatments were prepared in triplicate with the mean number of cells migrated +/- SD being used as the final value.

2.4 SDS-PAGE

2.4.1 BCA assay

The total protein concentration of cell lysates was determined using a bicinchoninic acid assay (BCA assay) using a BCA protein assay kit (Pierce Biotechnology, Waltham, MA, USA). A standard curve was constructed from the known concentrations of bovine serum albumin (BSA) using a 2mg/ml BSA standard (part of BCA kit). Protein range for the standard curve was 0-2000µg/ml. Unless otherwise stated, cell lysate samples were diluted five times in order to bring them within the range of the calibration curve. Ten µl of lysate sample or BSA standard were pipetted into a 96 well plate in triplicate. BCA reagent (mix of reagent A and B) was then pippeted into each well (200µl) and the dish briefly shaken before it was incubated at 37°C for 30 minutes. The absorbance of the samples was then read at 562nm using a Spectramax plu384 (Molecular Devices, Sunnyvale, CA, USA). The absorbance was plotted alongside the concentration of the known BSA standards to construct a linear calibration curve from which the unknown protein concentrations of the lysate samples could be determined.
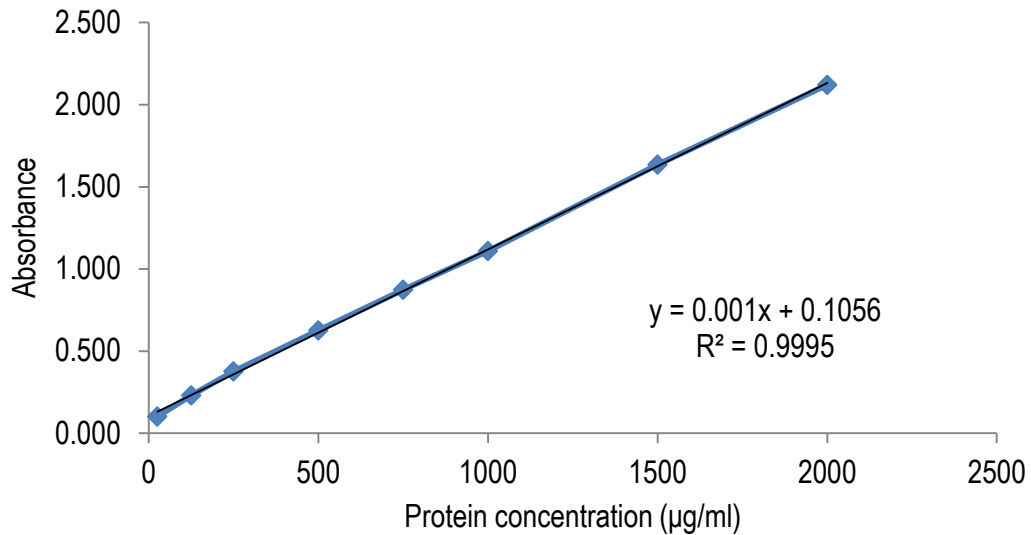
Figure 2.1. Example of a BCA standard curve. Black line shows the linear fit determined by least square regression, with the adjacent equation used in determining the protein concentration of the samples.

2.4.2 Assembly of polyacrylamide gels

Polyacrylamide gels were erected using 1mm thick, mini-gel glass plates held together using a Biorad gel assembly kit (Bio-Rad Laboratories Inc., Hercules, CA, USA). Resolving Gel (Table 2.3) was poured and layered with 100μl of butanol to ensure an even surface during setting. The resolving gel was allowed to set for a minimum of 1 hour (this time was increased if required), after which all butanol was carefully removed using filter paper. Stacking Gel (Table 2.3) was poured into the remaining space above the resolving gel and a 1mm comb (10 well or 15 well as required) was inserted. The resolving gel was allowed to set for a further 1 hour, after which the comb was carefully removed and the wells washed with distilled water. Gels were then either used immediately, or stored overnight for use the next day. Gels were stored by wrapping them in distilled water-soaked blue paper roll and then wrapping in polythene at 4°C.

Stacking Gel	Resolving Gel
250mM Tris-HCl pH 6.8	750mM Tris-HCl pH 8.9
0.1% (w/v) SDS	0.1% (w/v) SDS
4% (v/v) acrylamide:bis-acrylamide	15%, 10%, 8% (v/v) acrylamide:bis-acrylamide
0.06% (w/v) ammonium persulfate (APS)	0.06% (w/v) ammonium persulfate (APS)
0.015% (v/v) tetramethylethylenediamine (TEMED)	0.015% (v/v) tetramethylethylenediamine (TEMED)

Table 2.3. Composition of Stacking and Resolving Gel.

2.4.3 Running polyacrylamide gels

Prior to loading, cell lysate samples were defrosted and 3x SDS containing loading buffer was added in a 1:3 ratio. Samples were then heated at 95°C for 5 minutes.

3x SDS containing Loading Buffer
188mM Tris-HCl pH 6.8
6% (w/v) SDS
30% (v/v) glycerol
300mM DTT
0.625% (v/v) bromophenol blue

Table 2.4. Composition of 3x SDS-containing Loading Buffer.

Previously cast polyacrylamide gels (Section 2.2.4) were inserted into a Biorad gel electrophoresis tank and the tank filled with SDS running buffer. Precision Plus Protein™ Dual Color Standards protein ladder (purchased from Biorad) was loaded onto the gel followed by the samples using gel loading tips. Gels were run at 200V for 1-2 hours depending on the acrylamide concentration used for the gel. Gels were then removed and the stacking gel removed, leaving the resolving gel for further analysis.

SDS-containing Running Buffer (pH 8.3)
50mM Tris
192mM Glycine
0.1% (w/v) SDS

Table 2.5. Composition of SDS-containing running buffer.

2.4.4 Coomassie Blue staining

Once gels had been run and removed (Section 2.4.3), they were washed in distilled water before being immersed in coomassie blue stain. Gels were left to stain at room temperature for a minimum of 1 hour. After staining, gels were removed and washed with distilled water to remove any unbound stain. They were then immersed in coomassie destain three times for 15 minutes each time, in a container placed on a rocking apparatus to cause constant mixing of the solution. The gels were then left overnight in coomassie destain to remove as much unbound coomassie blue stain as possible, so that clearly stained protein bands were easily visible. Images were then recorded by scanning the gel inside a polythene pouch using an ImageScanner III gel scanner from GE Life Sciences (GE Healthcare., Little Chalfont, UK).

Coomassie Blue stain	Coomassie Destain
0.1% (w/v) Coomassie Brilliant Blue 50% (v/v) methanol 7% (v/v) glacial acetic acid	20% (v/v) methanol 10% (v/v) glacial acetic acid

Table 2.6. Composition of Coomassie Blue stain and Destain solutions.

2.4.5 Western blotting

2.4.5.1 Main Western blot protocol

Protein Transfer buffer	TBS-Tween
120mM Tris 192mM Glycine 20% (v/v) Methanol	20mM Tris-HCl pH 7.5 150mM NaCl 0.1% (v/v) Tween20

Table 2.7. Composition of Western blot transfer and TBS-Tween buffers.

Once gels had been run (Section 2.4.3), the proteins within the gel were transferred onto Immobilon-P PVDF membrane (EMD Millipore, Billerica, MA, USA). Gels were washed in distilled water before being immersed in transfer buffer for 15 minutes at room temperature to equilibrate to the new buffer. During this time the PVDF membrane was cut to size and activated by immersing it in methanol for 20 seconds. Following this, the membrane was placed into the protein transfer buffer (Table 2.7). The gels, membrane, filter paper and sponges were assembled in a transfer cassette, with care taken to avoid any air bubbles in the apparatus. The cassette was then placed into a protein gel tank

within a tray filled with ice and water to ensure the temperature during transfer was kept as low as possible. Protein transfer was completed at 100V for 2 hour.

After transfer, the membranes were removed and the efficiency of the transfer assessed using ATX Ponceau S stain (Fluka - part of the Sigma-Aldrich group) to visualise any protein bands. Excess stain was removed, first with distilled water and then with a short incubation in Tris-buffered saline-Tween20 (TBST) (Table 2.7). Membranes were then blocked for one hour at room temperature in a protein-blocking solution consisting of either 5% (w/v) BSA in TBST or 5% (w/v) Marvel skimmed-milk powder in TBST, depending on the primary antibody. During this time, primary antibody (Table 2.8) was made up to the correct concentration in blocking solution in a total volume of 5ml in a 50ml Falcon tube. After blocking, membranes were inserted into the Falcon tubes, which were then incubated on a roller mixer overnight at 4°C.

Following primary incubation, the membranes were removed and washed for 10 min, three times in TBST to remove any unbound primary antibody. Secondary antibody against the species of origin of the primary (Table 2.9) was made up to the correct concentration in blocking solution, in a total volume of 5ml in a 50ml Falcon tube. Membranes were again inserted into the new Falcon tubes and incubated on a roller mixer for 2 hours at room temperature. After the incubation with secondary antibody, the membranes were removed and washed for 5 minutes, three times in TBST, to remove any unbound secondary antibody. Excess TBST was then drained off the membrane, after which the membranes were incubated with 1ml of Amersham™ ECL™ substrate (GE Life Sciences) per membrane for 5 minutes. Membranes were then placed inside a developing cassette and taken to a dark room for film-based development. Super RX X-ray film (Kodak, Rochester, NY, USA) was exposed to the membranes for 10 seconds to 60 minutes, as required for adequate exposure, followed by development and fixation. In cases where long exposures with standard ECL proved insufficient to give clear bands, membranes were removed and washed for 5 min in TBST. Membranes were then incubated with 1ml of Amersham™ ECL Select™ substrate (purchased from GE Life Sciences) for 1 minute, after which exposure to X-ray film was repeated.

Primary antibodies						
Antibody	**Company**	**Product code**	**Host species**	**Monoclonal or polyclonal**	**Concentration used**	**Block in**
S100P	R&D Systems	AF2957	Goat	Polyclonal	1:1000	BSA
Vinculin	Abcam[1]	ab18058	Mouse	Monoclonal	1:1000	Milk
Paxillin	Abcam[1]	ab32084	Rabbit	Monoclonal	1:2000	Milk
Non-Muscle Myosin IIA	Thermo Scientific	PA1-24943	Rabbit	Polyclonal	1:1000	Milk
Integrin αV	Cell Signaling	4711S	Rabbit	Polyclonal	1:1000	Milk
Integrin α5	Cell Signaling	4705S	Rabbit	Polyclonal	1:500	Milk
Integrin β1	Cell Signaling	9699S	Rabbit	Monoclonal	1:1000	Milk
Integrin β3	Cell Signaling	13166S	Rabbit	Monoclonal	1:1000	Milk
Vimentin	Cell Signaling	5741S	Rabbit	Monoclonal	1:2000	Milk
N-cadherin	Cell Signaling	13116S	Rabbit	Monoclonal	1:1000	Milk
E-cadherin	Cell Signaling	3195S	Rabbit	Monoclonal	1:1000	Milk
Snail	Cell Signaling	3879S	Rabbit	Monoclonal	1:500	Milk

Slug	Cell Signaling	9585S	Rabbit	Monoclonal	1:500	Milk
Talin	Abcam[1]	ab11188	Mouse	Monoclonal	1:1000	Milk
FAK	Abcam[1]	ab40794	Rabbit	Monoclonal	1:500	Milk
Lamin β1	Abcam[1]	ab16048	Rabbit	Polyclonal	1:1000	Milk
VDAC	Abcam[1]	ab14734	Mouse	Monoclonal	1:1000	Milk
GAP-DH	Abcam[1]	ab8245	Mouse	Monoclonal	1:10000	Milk
Endoglin	Abcam[1]	ab169545	Rabbit	Monoclonal	1:1000	Milk
Paxillin Y118	Abcam[1]	ab4833	Rabbit	Polyclonal	1:500	BSA
Paxillin Y31	Abcam[1]	ab32115	Rabbit	Monoclonal	1:500	BSA
FAK Y397	Abcam[1]	ab81298	Rabbit	Monoclonal	1:500	BSA

Table 2.8. Primary antibodies used during Western blotting. [1]Abcam plc, Cambridge, UK.

Secondary antibodies					
Antibody	**Company**	**Product code**	**Host species**	**Monoclonal or polyclonal**	**Concentration used**
HRP conjugated Rabbit Anti – Mouse IgG	DAKO[1]	P0260	Rabbit	Polyclonal	1:5000
HRP conjugated Swine Anti – Rabbit IgG	DAKO[1]	P0217	Swine	Polyclonal	1:5000
HRP conjugated Rabbit Anti - Goat IgG	DAKO[1]	P0160	Rabbit	Polyclonal	1:5000

Table 2.9. Secondary antibodies used during Western blotting. [1]DAKO, Copenhagen, Denmark.

2.4.5.2 Probing with multiple antibodies

In many cases membranes were cut so that several antibodies for proteins with substantially different molecular weights could be probed using the same membrane. This was primarily carried out when looking at focal adhesion and integrin proteins, since their high molecular weight made it appropriate to cut the membrane so that GAP-DH, a control for equal loading of total protein in the sample, could also be probed on the same membrane. It was decided that this multiple probing technique was a more accurate method than stripping the membrane, since the latter can result in proteins being lost. Stripping was, however, used in scenarios where cutting the membrane was not possible due to the proteins having a similar molecular weight, such as studies on phosphorylation.

In cases where stripping was required, membranes were washed for 5 minutes in TBST followed by immersion in Mild Stripping Buffer (Table 2.10) for 10 minutes at room temperature. The buffer was then removed and replaced with fresh buffer and the membranes incubated for a further 10 minutes. Membranes were washed two times in PBS for 10 minutes then two times in TBST for 5 minutes. After this step the membranes were ready to be blocked again (protocol provided by Abcam).

Mild Stripping Buffer pH 2.2[1]
20mM Glycine
0.1% (w/v) SDS
1% (v/v) Tween20

Table 2.10. Composition of Mild Stripping Buffer. [1]The pH of the buffer was corrected using HCL and NaOH.

2.4.5.3 Densitometic analysis

Once X-ray films were developed, fixed and dried, they were scanned using a flatbed scanner (Ricoh, Tokyo, Japan). Analysis of the pixel density of protein bands was undertaken using Image J (http://imagej.nih.gov/ij/) to acquire the raw data and further analysed using Microsoft Excel (Microsoft Corporation, Redmond, WA, USA).

2.5 Immunofluorescent staining

2.5.1 Preparation of paraformaldehyde

Paraformaldehyde (PFA) was made up at 4% (w/v) in PBS and then heated to 70°C in a water bath. Once heated, 10M NaOH was added, drop-wise, until all the PFA had dissolved. The solution was then cooled and filtered under sterile tissue culture conditions using a 0.22μm filter. PFA was then stored in aliquots at -20°C until needed. Frozen PFA was stored for a maximum of 2 weeks, after which a new fresh stock was made.

2.5.2 Cell fixation, staining and imaging

Multi-well culture slides (Beckman Coulter) were coated with 250μl of 15μg/ml bovine fibronectin in PBS. PBS was evaporated at room temperature for 4 hour in a Laminar Flow Hood, after which any residual PBS was aspirated and the slides allowed to dry completely.

Either HeLa A3 or Cos7-S10 cells (as required) were induced by addition of doxycyclin 48 hours prior to this experiment, as described in Section 2.2.6. Control and induced cells were initially collected using the methods described in Section 2.2.3. The cells were then counted and 5000 cells were seeded in the fibronectin-coated wells and left to grow overnight.

The next day all culture medium was removed by aspiration, and the cells were washed two times with warmed PBS. PFA at 4% (w/v) was added (200μl) for 10 min at room temperature to fix the cells, after which the cells were washed two times in PBS. Ammonium chloride (NH_4Cl) was added (200μl) to the cells for 20 min in order to remove any remaining unreacted aldehyde groups. The cells were then washed a further two times with PBS prior to permeabilization.

Permeabilization was undertaken by adding 250μl of 0.5% (v/v) Triton X-100 in PBS for 10 minutes at room temperature. The cells were then blocked in immunofluorescent blocking solution (Table 2.11) for 1 hour at room temperature, after which all blocking solution was aspirated. Primary antibody (Table 2.11) was made up to the correct concentration in Immunofluorescent Blocking Solution and 100μl was added to the wells.

The cells were then incubated overnight at 4°C. In cases where co-localisation staining was being undertaken, both primary antibodies were added to the cells at the same time.

The next day the solution within the wells was aspirated and the cells washed for 10 min, four times with 0.1% (v/v) Triton X-100 in PBS. Secondary antibody (Table 2.12) was made up to the correct concentration in immunofluorescent blocking solution and 100μl added to the wells for 30 min at room temperature, taking care to avoid any excessive exposure to light. The cells were again washed for 10 min, four times with 0.1% (v/v) Triton X-100 in PBS. In cases where nuclear staining with DAPI was carried out, 0.1μg/ml DAPI was added for 10 min at room temperature before its removal by aspiration. The culture slide was then placed in a shallow container of methanol for 10 minutes. This was undertaken so that the methanol only reached just over the glass slide, so as to loosen the glass slide from the plastic wells. The plastic wells were then removed and a glass cover slip mounted on the glass slide using Hydromount mounting medium (National Diagnostics, Atlanta, GA, USA). The slides were allowed to dry for at least 30 minutes at room temperature to ensure the mounting medium was sufficiently set before imaging.

Cells were imaged using an EVOS® FL microscope imaging system (Life Technologies, Carlsbad, CA, USA).

Immunofluorescent Blocking solution[1]
2% (w/v) BSA
3% (w/v) Marvel skimmed milk powder
0.5% (v/v) Triton X-100

Table 2.11. Composition of Immunofluorescent Blocking solution. [1]This solution was made up in PBS.

Primary antibodies					
Antibody	Company	Product code	Host species	Monoclonal or polyclonal	Concentration used
S100P	BD Biosciences[1]	610307	Mouse	Monoclonal	1:500
NMIIA	Abcam	ab18058	Mouse	Monoclonal	1:300
Paxillin	Abcam	ab32084	Rabbit	Monoclonal	1:1000
Vinculin	Sigma	V9131	Mouse	Monoclonal	1:500
Talin	Sigma	T3287	Mouse	Monoclonal	1:500
IQGAP1	Abcam	ab86064	Rabbit	Polyclonal	1:100

Table 2.12. Primary antibodies used for immunofluorescent staining. [1]BD Biosciences, Franklin Lakes, NJ, USA.

Secondary antibodies					
Antibody	Company	Product code	Host species	Monoclonal or polyclonal	Concentration used
Alexa Fluor 488 Goat Anti – mouse IgG	Life Technologies	A-11029	Rabbit	Polyclonal	1:500
Alexa Fluor 488 Goat Anti – rabbit IgG	Life Technologies	A-11034	Swine	Polyclonal	1:500
Alexa Fluor 568 Goat Anti – rabbit IgG	Life Technologies	A-11036	Rabbit	Polyclonal	1:500

Table 2.13. Secondary antibodies used for immunofluorescent staining.

2.6 Cell fraction isolation

2.6.1 Triton insoluble protein isolation

This method was undertaken to removed all cytoplasmic proteins and leave only the Triton X-100 insoluble cytoskeletal proteins and structural adhesion proteins. Triton X-100 is a non-ionic detergent that causes a breakdown in the phospholipid membrane of the cell by solubilising the lipid fraction. At very low concentrations Triton X-100 can, therefore, be used to permeabilise the cell membrane or at higher concentrations can be used to fully lyse the cell. This solubilisation, and therefore lysing, is not ubiquitous, however, as eukaryotic cell membranes often contain detergent-insoluble sphingolipids and cholesterol rafts. As these lipid rafts may not be solubilised by the addition of Triton X-100, any

proteins associated with these membrane structures may be retained and so not be found present in the lysed cell sample.

Cells were grown to 80% confluency before being washed three times in warm PBS. Cells were treated with 1ml of 0.5% (v/v) Triton X-100 in PBS containing protease-inhibitor cocktail for 2 minutes. During this time the cell culture dishes were gently rocked, side to side, to provide a slight shearing force to aid in initial lysis. All residual solution was removed by aspiration and the cell residue was washed three times in PBS. Following this, the cell residue was removed as described in Section 2.2.6 for cell lysis, with the following modification. The volume of Lysis Buffer used was reduced to 50µl to ensure a more concentrated sample. The sample was diluted two times during BCA analysis (Section 2.4.1), rather than five times, due to the samples having a low protein concentration. When the SDS-PAGE gel was loaded (Section 2.4.3) only 4µg of protein per lane was available due to concentration limitations.

2.6.2 Hydrodynamic shearing isolation

2.6.2.1 Sample collection

This method was undertaken due to limitations found in other methods for isolation of focal adhesions and was based on a method kindly provided by Professor Martin Humphries' group at The University of Manchester (The University of Manchester, Michael Smith Building, Manchester, UK). Cells were seeded in a 10cm diameter tissue culture dish (1.5×10^6) and grown to 80% confluency overnight, before they were washed in warmed PBS. Each dish of cells was exposed to pressurised reverse osmosis water from a Mira 4 Spray Mode White Shower Head (B&Q, Liverpool, UK). The shower head was connected to an RO water tap using a Cooke & Lewis White PVC Shower Hose (B&Q) (Figure 2.2). The shower head was set so that the water jet was as tight as possible and the RO water tap opened to maximum. The amount of time the cells were exposed to the water flow was dependent on the cell type used. The time was varied to find the point where all cells are removed, while minimising subsequent additional damage. For HeLa A3 and Cos7-S10 cells, 5 seconds of exposure per dish were found to be sufficient. This exposure was carefully timed, while ensuring the distance travelled by the water jet from shower head to the dish was maintained at 6 inches. The angle at which the plates were showered was 90° with a

set pattern being traced with the water jet each time to ensure consistency between dishes (Figure 2.3).

Once the cells had been sheared off the dish, the dish was immediately inspected under a light microscope to ensure all cells had been removed. The dishes were then placed on ice and washed five times with 10ml of ice-cold PBS. Plates were then tilted to 45° for 1 minute to allow residual PBS to pool. This PBS was then removed by aspiration and 30µl per dish of modified SDS Lysis Buffer (as shown in Table 2.2 plus 300µM DTT) was added. The addition of DTT to the Standard Lysis Buffer was to prevent any aggregation of the large adhesion, cytoskeletal or extracellular proteins through their cysteine residues. The dishes were then thoroughly scraped using a cell scraper and the lysis solution pooled and collected in a 1.5ml Eppendorf tube. Another 30µl of modified SDS Lysis Buffer was then added and the scraping and collecting repeated. This procedure was undertaken to ensure the maximum amount of protein was removed from the dish using the minimum volume of modified SDS Lysis Buffer. Samples were then heated at 95°C for 5 minutes, after which samples were cooled and were either stored at -80°C or immediately processed for protein precipitation.

Figure 2.2. Set up of the hydrodynamic shearing apparatus.
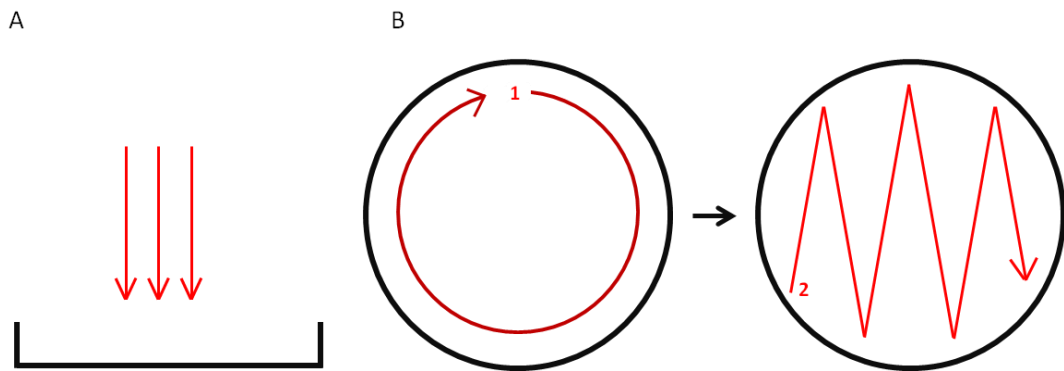
Figure 2.3. Hydrodynamic shearing. A) Red arrows indicated the angle at which the water jet was aligned to the tissue culture dish. B) Red arrows indicated the direction of the water jet pattern traced over 5 seconds to cover the maximum surface area in the minimum amount of time. The circular pattern was traced first followed by the zigzag pattern.

2.6.2.2 Acetone precipitation

A volume of cold (-20°C) acetone was added to the isolated samples, equal to 4 times the volume of sample in the Eppendorf. In cases where this volume was too large, the sample was first transferred to a larger receptacle before adding the acetone. Samples were then mixed and stored overnight at -80°C to allow the proteins to precipitate. The following day the Eppendorfs were centrifuged at 16.1 x g for 15 minutes at 4°C. The acetone supernatant was then carefully removed, and the pellet washed two times with the same volume of cold (-20°C) acetone. Care was taken at this step to ensure minimum agitation to the protein pellet. As much acetone was removed as possible without disturbing the protein pellet, and all remaining acetone allowed to evaporate at room temperature over 10-20 min, depending on atmospheric conditions. The samples were then resuspended in SDS-containing loading buffer (Table 2.4). The volume used was 30µl per 2 dishes that were lysed. The pellet was solubilised by sonication three times in a water bath for 5 minutes followed by heating at 95°C for 5 minutes. Samples were then either immediately loaded onto SDS-PAGE gels or stored at -80°C until needed. For each whole-cell mass spectrometry analysis the above procedure was completed 4 times for control samples and 4 times for induced cell samples to give a total of 8 samples for every run.

2.6.2.3 Hydrodynamically-sheared sample analysis

In order to determine the content of the isolated samples, Western blots were performed to ensure proteins not found in the cell-extracellular matrix adhesion fraction of the cell were absent from the sample. Western blots were also carried out looking for the presence of known cell-extracellular matrix adhesion proteins as a positive control for the isolated fraction. Blots for three negative control proteins were carried out; the first, GAP-DH was used to determine if any cytosolic proteins remained in the sample. The concentration of this antibody was increased from 1:10000 to 1:5000 to increase the detection sensitivity. Blots for Lamin-β1 were undertaken to ensure the cell nuclei had been completely removed. Lastly blots for voltage-dependent anion channel (VDAC), a mitochondrial membrane protein were used to ensure there were no remaining mitochondrial proteins present in the sample. Positive controls for talin, vinculin and paxillin were also run each time to ensure the expected proteins were present.

2.6.2.4 Immunofluorescent staining of hydrodynamically-sheared cultures

In order to ensure the adhesion foci remained intact after hydrodynamic shearing, immunofluorescent staining for vinculin was performed. The methodology used for this was the same as stated in Section 2.5.2 with the following alterations. Unlike with whole cells fixation with PFA no fixation or permeabilisation step was performed, since preliminary experiments determined that the addition of PFA prevented any signal being seen during imaging. Since no cell boundaries were visible when imaging, it was not possible to determine which vinculin-stained focal adhesions were derived from which cells during counting. To resolve this, the number of focal adhesions was counted per field of view in control, uninduced cells and in cells induced with doxycyclin, and the values compared.

2.7 Mass spectrometry

2.7.1 Whole cell analysis

2.7.1.1 Cell preparation

HeLa A3 cells were thawed as stated in Section 2.2.4. After the first passage, cells were grown in phenol red-free DMEM supplemented, as stated in Section 2.2 with 4% (v/v) non-essential amino acids. Cells were allowed to equilibrate in the new culture medium for two passages prior to S100P induction with doxycyclin. Four dishes of either control, uninduced HeLa A3 cells or doxycyclin-induced HeLa A3 cells were grown to 80% confluency. Cells from these 4 dishes were washed three times in warm PBS and incubated with enzyme-free Dissociation Buffer (Millipore) for 30 min at 37°C. This buffer was used instead of trypsin as it provides a far more gentle method of detachment. Following incubation, cells were collected in warmed PBS and centrifuged at 1250 x g for 10 minutes. The PBS was aspirated to remove all remaining enzyme-free Dissociation Buffer from the sample. Cells were washed in 20ml of warmed PBS, centrifuged again and resuspended in 10ml of PBS. The cell suspension (100µl) was counted using a Z1 Coulter® particle counter (Beckman Coulter) and 1×10^7 cells were transferred into a 15ml Falcon tube. This tube was then centrifuged and the supernatant aspirated. The pelleted cells were then snap frozen in liquid nitrogen and stored at -80°C.

All further steps were conducted by the Protein Function Group in the Institute of Integrative Biology at the University of Liverpool.

2.7.1.2 Cell lysis and peptide formation

Cell pellets were thawed from the -80°C freezer and resuspended in 25mM ammonium bicarbonate (NH_4HCO_3). Cells were then lysed by sonication and the DNA removed from the sample via digestion with 25 units of Benzonase nuclease (Novagen, Darmstadt, Germany). The protein concentration of the samples was then determined using the Brandford assay and the samples normalised accordingly.

A volume of protein was then taken (100µl) from each sample and incubated with 0.05% (v/v) of RapiGest SF™ (Waters, Milford, MA, USA) in 25mM NH_4HCO_3 for 10 minutes at

80°C. DTT at 60mM was then added and the samples heated at 60°C for a further 10 min. Following this, 178mM iodoacetamide was added and the samples incubated in the dark at room temperature. To cleave the proteins and form peptide fragments, Gold mass spectrometry grade trypsin (Promega, Madison, WI, USA) was added and the samples incubated for 45 minutes at 37°C. Samples were then centrifuged at 17,000 x g for 30 min at room temperature to pellet any cell debris or insoluble proteins. To the supernatant 0.1% (w/v) trifluoroacetic acid (TFA) was added to remove the RapiGest SF™ and trypsin, as well as acting as an ion-pairing agent for the liquid chromatography (LC).

2.7.1.3 Liquid chromatograpic separation

Peptide separation was carried out using an Ultimate 3000 nano High Pressure Liquid Chromatography (HPLC) system (Thermo Fisher Scientific). Sample was loaded (5µl/min) onto a trap column (Acclaim PepMap 100, 2cm x 75µm inner diameter, C18, 3µm, 100Å) with an aqueous solution containing 0.1% (v/v) trifluoroacetic acid (TFA) and 2% (v/v) acetonitrile and allowed to run for 3 min. Following this, the trap column was connected to an analytical column (Easy-Spray PepMap® RSLC 50cm x 75µm inner diameter, C18, 2µm, 100Å) (Dionex, Sunnyvale, CA, USA) and peptide elution was performed by applying a mixture of 0.1% (v/v) formic acid in HPLC grade water (Solution A) and 80% (v/v) HPLC grade acetonitrile in 0.1% (v/v) formic acid (Solution B) to the column. The separation of peptides was carried out by applying a linear gradient of Solution B ranging from 3.8% (v/v) up to 50% (v/v) over 95 minutes at a flow rate of 300 µl/min. The column was then washed with 99% Solution B for 5 minutes. Finally the column was equilibrated with 3.8% (v/v) Solution B for 15 minutes before the next sample was loaded. MS/MS analysis was then performed on the eluted peptides.

2.7.1.4 MS/MS mass spectrometry

Mass spectrometric analysis was carried out using a Q Exactive™ Hybrid Quadrupole-Orbitrap mass spectrometer (Thermo Scientific) operating in data-dependent positive mode, so as to switch automatically between full scan MS and MS/MS data acquisition.

2.7.1.5 Protein identification, quantification and analysis

The raw MS data files were uploaded to proteome discoverer 1.3 and searched against the human Uniprot database using the Mascot search engine (version 2.4.1). This gave a list of possible proteins for each sample based on the peptides analysed. In order to quantify changes in protein abundance between different samples, Progenesis LC-MS label-free quantification software (Nonlinear Dynamics, Newcastle upon Tyne, UK) was used. For protein pathway analysis to determine the cellular localisation of each protein, QIAGEN'S Ingenuity Pathway Analysis was used (Qiagen, Limburg, Netherlands).

2.7.2 Analysis of hydrodynamically-sheared fraction

Two different purification methods were employed after initial hydrodynamic shearing (Section 2.6.2.1) in order to obtain the mass spectrometric data on this cell fraction. SDS is incompatible with mass spectrometry, and as such, any protocol needed to ensure that all SDS from the Lysis Buffer was removed. The first purification method followed that described in Section 2.6.2.2 with some alterations (noted below) using acetone precipitation to remove the SDS. This method was found to lead to removal, but still resulted in a low level of SDS contamination which caused peak drift of the peptide ions during LC-MS. As a result, a second method was used, Filter Aided Sample Preparation (FASP). This method involved a SDS to urea exchange step using spin filters to ensure all the SDS was removed.

2.7.2.1 SDS removal

Methods for hydrodynamic shearing and preparation of samples to be analysed by LC-MS were identical to that stated in Section 2.6.2.2 with the following alterations. The acetone precipitation of proteins in the samples was altered, since the proteins were not going to be resuspended in buffer following removal of SDS. Additional washing steps were also added to ensure maximum removal of SDS. The speed of centrifugation was reduced to prevent the pellet from becoming overly compacted, as this would cause problems during sample preparation for LC.

When the samples had been precipitated in acetone overnight, they were centrifuged at 7.5 x *g* for 10 min at 4°C. The supernatant was carefully removed and the same volume of cold (-20°C) acetone was added and the sample centrifuged at 7.5 x *g* for 3 minutes at 4°C. After this first wash, the supernatant was removed and fresh acetone was added. The protein pellet was then agitated with a pipette tip to release any SDS in the pellet. The sample was then centrifuged at 7.5 x *g* for 10 min at 4°C. Fresh acetone was added and the sample centrifuged at 7.5 x *g* for 3 min at 4°C twice more, discarding all supernatant in between washes. As much acetone was then removed as possible without disturbing the protein pellet, and all remaining acetone allowed to evaporate at room temperature over 10-20 min, depending on atmospheric conditions. The protein pellets were then frozen and stored at -80°C until needed.

LC-MC preparation was performed as reported in Section 2.6.2.2, but only from the RapiGest SF™ step onwards. Due to the low protein concentration of the samples, all the protein was treated as if the normalisation had been carried out beforehand, based on cell number, as was the case. This was to avoid wasting any sample in a Bradford assay.

2.7.2.2 Filter aided sample preparation (FASP) digestion

FASP filter units were prepared prior to receiving the samples. Formic acid was added (300µl of 1% (v/v)) to a VivaCon 500 10kDa MWCO HydroSart Filter unit (Millipore) and centrifuged at 14691 x *g* at 20°C for 15 min. Because FASP caused exchange of SDS in the Lysis Buffer for urea, no precipitation step was necessary after lysis, and the complete sample was sent for digestion.

The sample was gradually added to the filter unit and, with each arbitrary volume added, was centrifuged for 15 min at 14691 x *g* at 20°C. Once all the protein had been captured on the filter, 300µl of urea buffer (100mM Tris-HCl pH 8.5 and 8M urea) was added and the filter centrifuged for 15 min at 14691 x *g* at 20°C. This step was then repeated, followed by an additional, short 5 min centrifugation to ensure all urea buffer was removed. DTT Buffer (10mM DTT in urea buffer) was added (150µl) and the filter was briefly agitated by vortexing, before it was incubated at 56°C for 20 min. The filter was then centrifuged for 10 min at 14691 x *g* at 20°C. Then 150µl of urea buffer was added successively twice, and the filter was centrifuged for 10 min after each addition. Iodoacetamide buffer (50mM iodoacetamide in urea buffer) was added (150µl) and the

filter was briefly agitated by vortexing and then it was incubated at room temperature for 20 minutes in the dark. The filter was then centrifuged for 10 min at 14691 x g at 20°C. Urea Buffer was added (150µl) successively twice, and the filter was centrifuged for 15 min after each addition. NH_4HCO_3 was added (150µl of 25mM) successively twice, and the filter was centrifuged again for 15 min after each addition. The filter unit was then transferred into a fresh collection tube which had been prewashed with 500µl of 1% (v/v) formic acid. Gold mass spectrometry grade trypsin was added (40µl) and the samples were left to incubate overnight at 37°C. The following day, the filter unit was centrifuged for 15 min before adding 30µl of NH_4HCO_3 successively twice, and the filter was centrifuged for 15 min after each addition. This procedure resulted in an approximate sample recovery volume of 120µl. The flowthrough from the filter was then transferred to a new Eppendorf. TFA was added to a final concentration of 0.2% (v/v) to remove the trypsin, as well as acting as an ion-pairing agent for LC. The samples were then stored on ice and were analysed on the same day, as described in Section 2.7.1.3.

2.8 Cell morphological analysis

2.8.1 Time course of S100P induction

HeLa A3 cells were thawed and passaged twice prior to beginning the time course. S100P was induced in the cells using doxycyclin, as described in Section 2.2.5. Cells were split into three 10cm diameter tissue culture dishes every two days, so as to yield a 60% confluent culture 48 hours after passage. Cultures at 60% confluence were selected, since trial runs showed these to be optimal for image analysis. Upon every passage, the doxycyclin was re-applied to the cells at a concentration of 5µg/µl. At every time point (including before induction) images of the cells were recorded using a DC5000 CMEX microscope camera (Euromex, Edegem, Belgium) connected to a light microscope. Eight images were taken per dish in a regular arrangement. Two dishes each passage were lysed (Section 2.2.6), and the third was split to continue the culture. A control for this experiment was also carried out, where untransfected HeLa cells were incubated with 5µg/µl of doxycyclin over a two week time course, as described above. Images were taken of these cells to determine if the doxycyclin was having any effect on cell morphology independent of S100P induction.

2.8.2 Image analysis

All cell morphology analyses were carried out using Fiji: ImageJ 2.0.0.rc24/1.49m_v64 (http://fiji.sc/Fiji). To ensure the correct data was collected, the settings shown in Figure 2.4 (A) were selected by running the [Analyze -> Set Measurements] command. Cell images were imported into the programme and the freehand selection tool was selected. The boundaries of each cell were traced and the information about the shape drawn stored by running the [Edit -> Selection -> Add to Manager] command after each cell (Figure 2.4). Once all the cells were selected for the current image, the shape properties were saved using ROI manager. Values for key morphological characteristics were determined for each of the cells by selecting "measure" in the ROI manager. This data was then copied into an Excel document. Multiple images were analysed for each time point, until 270 cells had been analysed for that time point.
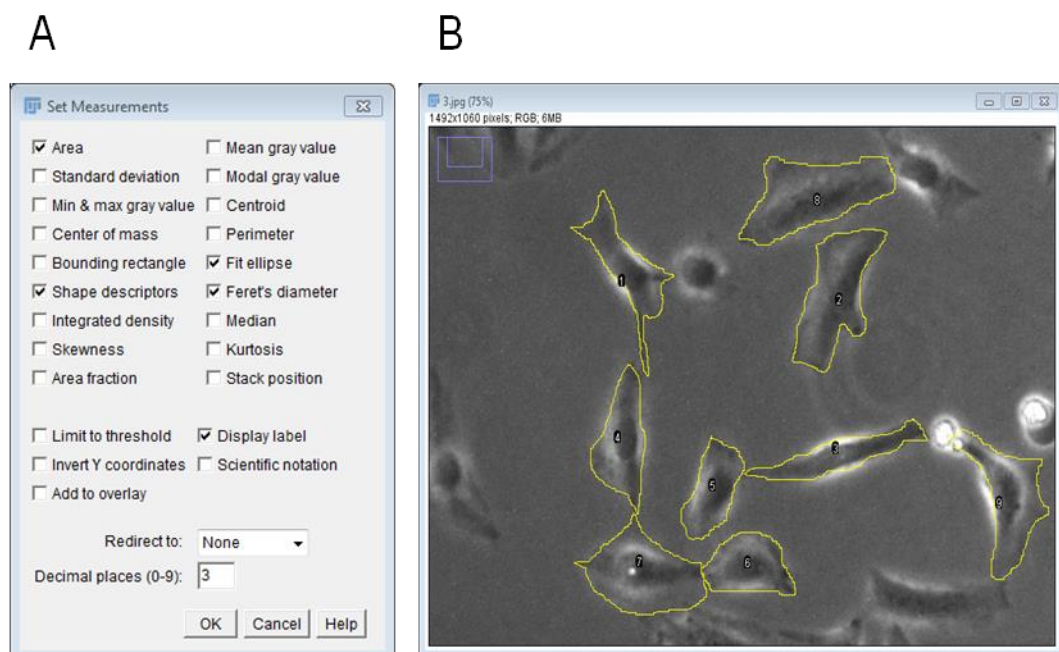
Figure 2.4. Analysis of cell morphology using Fiji: ImageJ programme. A) Set measurements menu showing parameters that were selected for image analysis. B) Traced cells using freehand selection tool. Numbers indicate the shape designations in the ROI manager.

2.8.3 Characterisation of cell morphology values

The method by which Fiji: ImageJ program analyses the selected shapes inputted into the ROI manager is by using ellipse fitting macros. The dimensions of the selected shape are used in conjunction with the fitted ellipse to give shape parameters which relate directly to cell morphology (Figure 2.5). The key shape parameters that have been used in this study are characterised as follows:

<u>Area</u> – The number of pixels present in the selected area of the shapes.
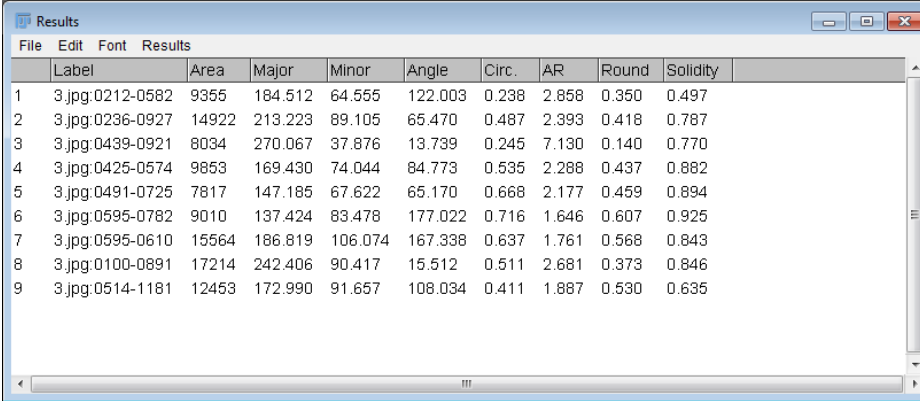
<u>Major axis</u> – The longest possible diameter using the fitted ellipse that runs directly through the central foci of the ellipse.

<u>Minor axis</u> – The longest possible diameter using the fitted ellipse that runs through the central foci of the ellipse and also runs perpendicularly to the major axis.

<u>Aspect ratio</u> – The ratio of the major axis to the minor axis as obtained from the ellipse model.

<u>Roundness</u> – A measure of how round the shape is based upon the fitted ellipse. This is calculated using $4([Area]/\pi[Major\ axis]^2)$, where a value of 1 would be a perfect circle.

<u>Solidity</u> – A measure of how much unfilled space is present between the selected shape and the fitted ellipse. This is calculated using (Area/Convex area) and is an expression of how convex the shape is, where a value of 1 would be a shape with no convex surfaces. Solidity can be used as an indication of exaggerated filopodia formation, as this results in increased convex surfaces and therefore lower solidity.

	Label	Area	Major	Minor	Angle	Circ.	AR	Round	Solidity
1	3.jpg:0212-0582	9355	184.512	64.555	122.003	0.238	2.858	0.350	0.497
2	3.jpg:0236-0927	14922	213.223	89.105	65.470	0.487	2.393	0.418	0.787
3	3.jpg:0439-0921	8034	270.067	37.876	13.739	0.245	7.130	0.140	0.770
4	3.jpg:0425-0574	9853	169.430	74.044	84.773	0.535	2.288	0.437	0.882
5	3.jpg:0491-0725	7817	147.185	67.622	65.170	0.668	2.177	0.459	0.894
6	3.jpg:0595-0782	9010	137.424	83.478	177.022	0.716	1.646	0.607	0.925
7	3.jpg:0595-0610	15564	186.819	106.074	167.338	0.637	1.761	0.568	0.843
8	3.jpg:0100-0891	17214	242.406	90.417	15.512	0.511	2.681	0.373	0.846
9	3.jpg:0514-1181	12453	172.990	91.657	108.034	0.411	1.887	0.530	0.635

Figure 2.5. Measured parameters of selected cells. Parameters used are defined in Section 2.8.3 above.

2.9 Endoglin siRNA

siRNA endoglin knock-downs were carried out on uninduced HeLa A3 cells. Cells (100000) in 2ml of SCM were seeded into the wells of a six-well tissue culture dish. Cells were then incubated under normal growth conditions for two hours. siRNA (150ng) (Table 2.13) was added to 400μl of serum-free culture medium followed by 12μl of HiPerFect Transfection Reagent (Qiagen, Limburg, Netherlands). This mixture was then incubated at room temperature for 10 min, to allow formation of the transfection complexes. The mixture was then added, drop-wise, onto the cells in one well of the six-well dish and the dish gently swirled to allow even distribution of the transfection complexes. This process was repeated for the scramble control siRNA, four separate endoglin siRNAs and a mixture of Hs_ENG_2 siRNA and Hs_ENG_4 siRNA (50% of each present in the 150ng added). The cells were then allowed to grow under normal conditions and were lysed at 24 and 48 hours to determine the knock-down efficiency using Western blotting for their target, endoglin.

Following this control experiment, migration assays (Section 2.3.1) and adhesion rate assays (Section 2.3.3) were carried out on cells where endoglin had been knocked-down by the most efficient siRNA. Due to the increased number of cells needed for these bio-assays, 10cm diameter tissue culture dishes were employed. This increased demand for cells required all values indicated above to be scaled up by a factor of five.

siRNA Name	Product code	Target sequence
Negative control siRNA	1022076	5'- AATTCTCCGAACGTGTCACGT
Hs_ENG_2 siRNA	SI00002317	5'- AAGGGAGAACTTGAAACAGAT
Hs_ENG_4 siRNA	SI00002331	5'- ACCAATAAATCAGACCATGAA
Hs_ENG_5 siRNA	SI02663024	5'- CGCCATGACCCTGGTACTAAA
Hs_ENG_6 siRNA	SI02663031	5'- CAGCAATGAGGCGGTGGTCAA

Table 2.14. siRNA used during endoglin knock-down experiments. All siRNAs were purchased as a kit from Qiagen.

2.10 Statistical analysis

All statistical analysis was performed using either the SPSS software package, version 20

(IBM) or StatsDirect statistical software, version 2.7.9.

Chapter 3

Characterisation of the effect of S100P on inducible cell lines

3.1 Introduction

As previously discussed, overexpression of S100P in primary tumours results in an increased chance of metastasis in number of different cancers. The steps by which benign cells transform into metastatic cells is a multifaceted process involving changes in cellular morphology and dynamics, both properties that S100P is suspected to affect. It has been shown that S100P binds directly to NMIIA, a crucial cytoskeletal protein involved in maintaining cell morphology and inhibiting cellular migration via stress fibre tension. The binding of S100P to NMIIA has been demonstrated to cause a breakdown in the NMIIA filamental structure and, as such, it was proposed that this promotes an increase in cell migration [206]. These experiments have been undertaken using HeLa A3 cells, a S100P transfected HeLa cell line, with expression of S100P placed under the control of a doxycyclin-inducible promoter. Thus, when doxycyclin is added to the medium, the cells overexpress S100P. Immunofluorescence staining for vinculin in these S100P overexpressing cells has also been carried out, which showed a reduction in the number of stained focal adhesions. This result may suggest that, indeed, cell-extracellular matrix adhesion, at least to the plastic surface of the Petri dish, is altered in some way by S100P overexpression. Similar observations have also been made looking at changes in cell morphology and cytoskeletal organisation in S100P overexpressing pancreatic (Panc-1) [233] and colon (LS174T) [234] cell lines. In all of these cases, significant alterations were observed whereby S100P-overexpressing cells appeared more elongated and had a less organised actin cytoskeleton. All cell lines were also observed to be

significantly more motile compared to control cells. Small hairpin RNA (shRNA) knockdowns of S100P have also been carried out using LS174T cells which resulted in reduced cellular motility, as well as a decrease in the rate of filopodia formation and retraction [235].

All of these studies suggest that S100P is having an important role in cytoskeletal organisation and cell migration, and this mechanism may involve NMIIA; however, this process is still not fully understood.

3.1.1 Chapter objectives

Utilising S100P-overexpressing, inducible cell lines, the aim of this chapter is to explore the effect of S100P induction on the adhesive, migratory and invasive properties of the cells using cell-based bioassays, as well as to observe any morphological alterations that take place upon induction. Furthermore, if any alterations are observed in these properties, they will be investigated further to determine if there are any alterations in the abundance or distribution of key focal adhesion or integrin proteins. This investigation will be conducted using the S100P-inducible HeLa A3 cells and the S100P-inducible Cos7-S10 cells (Section 2.2.1), the latter contain no NMIIA, so the effect of S100P can be studied in the absence of its binding to NMIIA.

Furthermore, determining if S100P causes an epithelial to mesenchymal transition (EMT) in HeLa A3 cells is an important factor to ascertain, since if this were the case, it would likely cause alterations in cell migration and adhesion. HeLa A3 cells are known to have previously undergone an EMT to some extent, but it is important to identify if this process is further progressed via overexpression of S100P. Described in detail in the Introduction, Section 1.5, EMT is the process by which epithelial cells lose epithelial cell characteristics in place of a more mesenchymal-like phenotype [151]. EMT is also common in many metastatic cancers, and has been shown to occur in cells overexpressing S100A4, another member of the S100 protein family closely related to S100P [236, 237]. EMT is characterised by several genotypic alterations in protein expression which are: a reduction in E-cadherin, replaced by an increase in N-cadherin, overexpression of the mesenchymal intermediate filament, vimentin and upregulation of several transcription factors including Snail and Slug [148]. The levels of these proteins in S100P overexpressing cells will therefore be determined.

Finally it is important to consider the signalling mechanisms behind any observed changes in focal adhesion distribution. These signalling mechanism can be investigated by looking at the phosphorylation state of focal adhesion proteins involved in vinculin recruitment and promotion of adhesion maturation. Expanding on themes in Section 1.3.2.3, NMIIA-mediated tension results in FAK phosphorylation at Y397, which subsequently phosphorylates paxillin at Y118 and Y31, leading to an increased rate of recruitment of adhesion proteins to the adhesion sites [99]. Therefore, if the S100P-dependent breakdown of NMIIA is causing a loss in cell tension resulting in reduced mature focal adhesions, it would be expected that there would be a reduction in the levels of phosphorylated Y397 FAK and Y118 / Y31 paxillin.

3.2 Results

3.2.1 S100P overexpression in relation to cell morphology

In order to determine the effect of S100P on cells in general, it was necessary to study its overexpression *in vitro*. A cell line was selected that could be induced with 5µg/ml of doxycyclin to overexpress S100P after a set time. HeLa A3 cells were used, as they provided an epithelial cancer cell line that could be easily cultured. The transfection of this cell line has also been achieved in-house and as such the cells were readily available.

In order to gain an insight into what was happening to the cells morphologically as a result of S100P overexpression, HeLa A3 cells were induced with doxycyclin (Section 2.2.5) and imaged using a light microscope 48 hours after induction. Whole cell lysates were taken from the cultured dishes after imaging and Western blots were also carried out to determine the level of S100P expression compared to uninduced, control HeLa A3 cells.

When S100P was induced, the cells appeared more elongated with more clearly defined protrusions and an overall flatter appearance. The morphology of the control, uninduced cells was typical for subconfluent cultures in that they appeared somewhat irregular for these epithelial cells. At higher confluence, however, control uninduced HeLa A3 cells took on a more classical cuboidal appearance. Subconfluent cultures were henceforth selected, as at a higher confluence the differences between the uninduced and induced cells was less clear.

When observed under a light microscope (Figure 3.1), a clear and substantial morphological alteration occurred between the control, uninduced cells (Figure 3.1A) and the S100P-induced cells (Figure 3.1B). There was a significant 2.8-fold increase in the percentage of elongated cells present in the S100P-overexpressing HeLa A3 cell population (percentage of elongated cells in: control, uninduced cells 16.7%, S100P-induced cells 48.1%, Student's t = 8.04, P = 0.0013). This does emphasize one issue with the inducible HeLa A3 cell system, however, in that there is heterogeneity within the cell population since not all cells responded in the same manner to doxycyclin treatment at the same time period.

The Western blot (Figure 3.1C) from whole-cell lysates of control, uninduced HeLa A3 cells and lysates from cells growing in the presence of 5µg/ml doxycyclin for 48 hours resulted in a band at the correct apparent molecular weight of 9kDa corresponding to

S100P. The intensity of this band was very high, however, due to a lack of detectable S100P in the uninduced, control cells, thus densitometry-based comparative analysis would be rather meaningless.
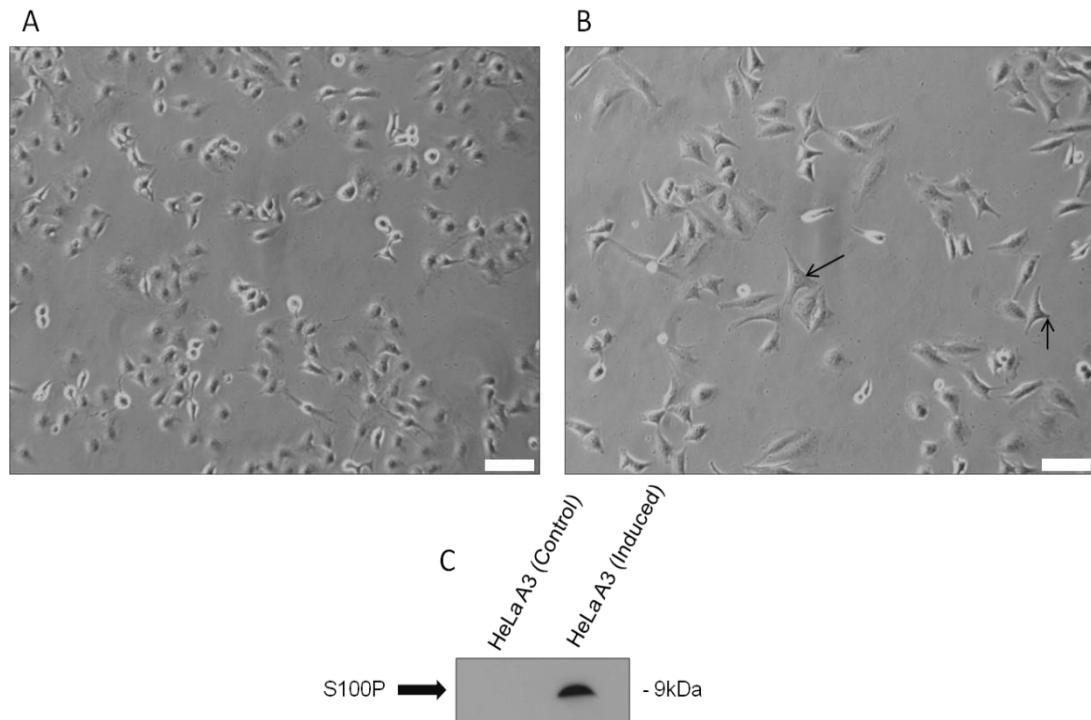
Figure 3.1. HeLa A3 cell morphology in relation to S100P overexpression. A) Control, untreated more-cuboidal HeLa A3 cells show irregular morphology, but no clearly defined protrusions. B) HeLa A3 cells 48 hour after addition of doxycyclin show a more elongated shape and an increase in filopodia. Arrows point to good examples of the more elongated cells. White bars = 100μm. A significant difference is seen in the percentage of elongated cells in the S100P-induced cells compared to the control, uninduced cells. Percentage of elongated cells in: control-uninduced cells 16.7%, SD = 6.4% and S100P-induced cells 48.1%, SD = 2.2% (Student's t = 8.04, P < 0.05), 400 cells were used for measurements across n = 3 experiments. C) Western blot of S100P expression in HeLa A3 cells, 48 hour after addition of 5μg/ml doxycyclin (for full gel see Appendix 1). Twenty μg of protein was loaded per well on a 15% (w/v) polyacrylamide gel. Arrow points to position of S100P at an apparent molecular weight of 9kDa.

3.2.2 NMIIA null cells and S100P

Since the main interaction of S100P reported previously was its binding to NMIIA, a S100P-inducible cell line was used that contained no NMIIA. To study the effect of S100P overexpression in a system with no NMIIA, Cos7-S10 cells were utilized. These cells were inducible for S100P with 5µg/ml of doxycyclin, via the same transfection system used in the HeLa A3 cells. These cells are a more elongated cell line and were created in-house by Dr Min Du.

The same experiment was conducted as for the HeLa A3 cells, whereby Cos-S10 cells were induced for 48 hour, imaged and then lysed to determine the levels of S100P using Western blotting (Figure 3.2). In contrast to the HeLa A3 cells, there was no observable difference between the cell morphology of uninduced, control and the S100P-induced Cos7-S10 cells. The Western blot (Figure 3.2C) from whole-cell lysates of control, uninduced Cos7-S10 cells and lysates from cells growing in the presence of 5µg/ml doxycyclin for 48 hours resulted in a band at the correct apparent molecular weight of 9kDa corresponding to S100P. The intensity of this band, similar to that shown in the S100P-overexpressing HeLa A3 cells, was very high, however, due to a lack of detectable S100P in the control, uninduced cells densitometry-based comparative analysis was of no value.

The lack of a clear morphological change in the Cos7-S10 cells may indicate that it is the interaction between S100P and NMIIA that is required for changes in cell shape.
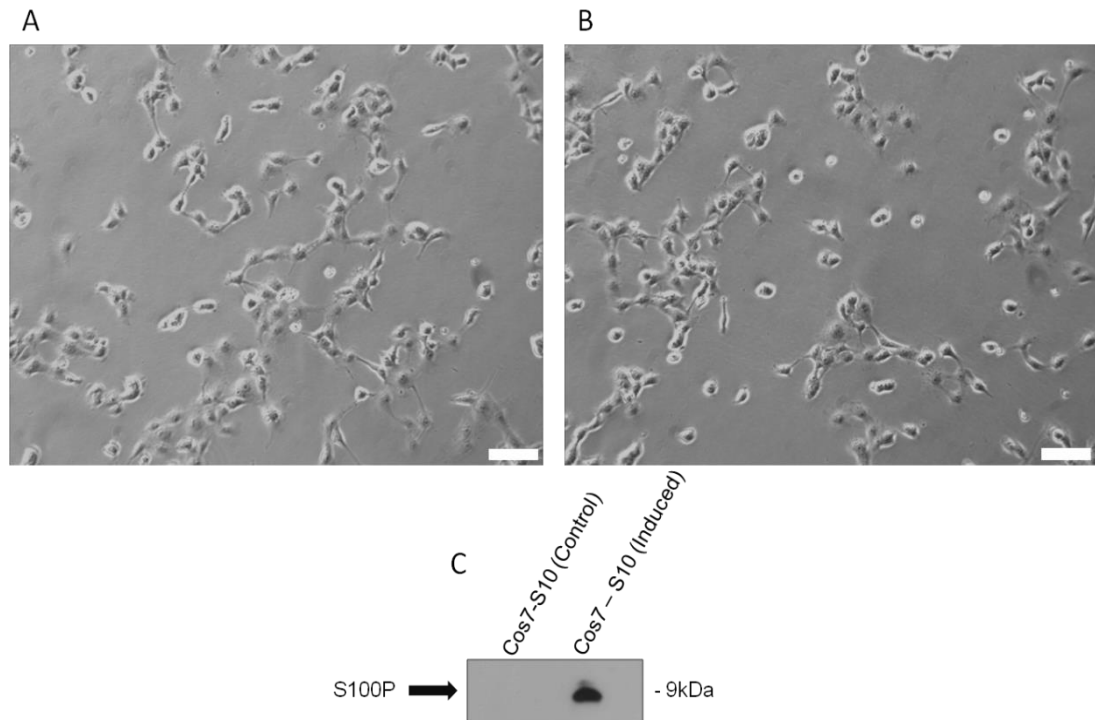
Figure 3.2. Cos7-S10 cell morphology in relation to S100P overexpression. A) Control, untreated Cos7-S10 cells showing a more cuboidal to spherical appearance except while dividing. B) Cos7-S10 cells 48 hour after addition of doxycyclin show no observable difference in cell morphology compared to control, uninduced cells which were not doxycyclin treated. 100% of the Cos7-S10 cells showed standard morphology with or without induction of S100P. White bars = 100µm. C) Western blot of S100P expression in Cos7-S10 cells 48 hour after addition of doxycyclin. Twenty µg of protein was loaded per well on a 15% (w/v) polyacrylamide gel. Arrow points to position of S100P at an apparent molecular weight of 9kDa.

3.2.3 Changes in NMIIA in whole-cell lysates

Since the alterations in cell morphology appeared dependent on the presence of NMIIA, it was important to determine the expression of NMIIA in the HeLa A3 and Cos7-S10 cell lines. As anticipated there was no visible NMIIA protein band for the Cos-S10 cells in either the uninduced, control or S100P-induced samples. In contrast, there was an observable band for NMIIA at the correct molecular weight of 230kDa in both HeLa A3 samples, but there was no significant difference between the levels of NMIIA in uninduced, control HeLa A3 samples compared to the S100P-induced cell samples. This may, therefore, suggest that

S100P in the HeLa A3 cells is not causing the NMIIA to be degraded, rather just depolymerising or preventing the formation of the NMIIA filamental structures.
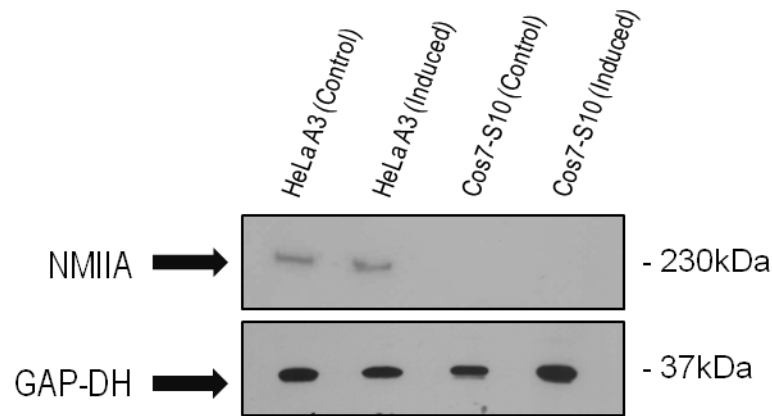
Figure 3.3. Identification of non-muscle myosin IIA (NMIIA) protein in HeLa A3 and Cos7-S10 cells. Western blot of NMIIA protein using HeLa A3 and Cos7-S10 whole-cell lysates 48 hours after induction with doxycyclin showing NMIIA at 230kDa present in the HeLa A3 cells, but no observable band in Cos7-S10 cells. No significant difference is seen in the mean levels of NMIIA bands in HeLa A3 cells (0.99-fold change, Student's $t = 0.054$, $p = 0.96$, $n = 3$). GAP-DH bands at 37kDa are shown as a loading control. Ten µg of protein was loaded per well on an 8% (w/v) polyacrylamide gel.

3.2.4 Phenotypic changes in cell dynamics

3.2.4.1 S100P and cellular adhesion

As mentioned in 3.1, there are many cellular properties that could be altered by a change in the cell's cytoskeleton. Chief amongst these were potential changes in the cell's adhesive properties, which are reliant both on cellular tension and the actin-myosin cytoskeleton for adhesion initiation and maturation. As previously described, some studies found links between S100P and alterations in cellular adhesion and, as such, this aspect needed to be explored in more detail.

3.2.4.1.1 Rate of adhesion

The rate at which cells can adhere to a surface is crucially important in the context of cancer. Once cells invade through into the circulatory system and break off to be carried by the blood/lymph flow, they need to be carried sufficiently far away and not adhere immediately to the adjacent vessel walls. HeLa A3 and Cos7-S10 cells were assayed to determine whether S100P had an effect on the rate of adhesion (Figure 3.4). The HeLa A3 cells (Figure 3.4A) showed a significant decrease in the number of cells adhering at each time point in the doxycyclin-induced cells compared to the uninduced control cells (30 min Student's $t = 3.6$, $P = 0.022$; 1 hour $t = 4.3$, $P = 0.013$; 2 hour $t = 9.3$, $P = 0.0007$, $n = 3$). The Cos7-S10 cells (Figure 3.4B) showed no significant difference in the number of cells adhering at each time point (30 min $t = 0.4$, $P = 0.69$; 1 hour $t = 1.6$, $P= 0.19$; 2 hour $t = 1.6$, $P = 0.18$, $n = 3$). These results may suggest that it is the depolymerisation of the filaments of NMIIA by S100P that causes the decrease in cell adhesion seen here.
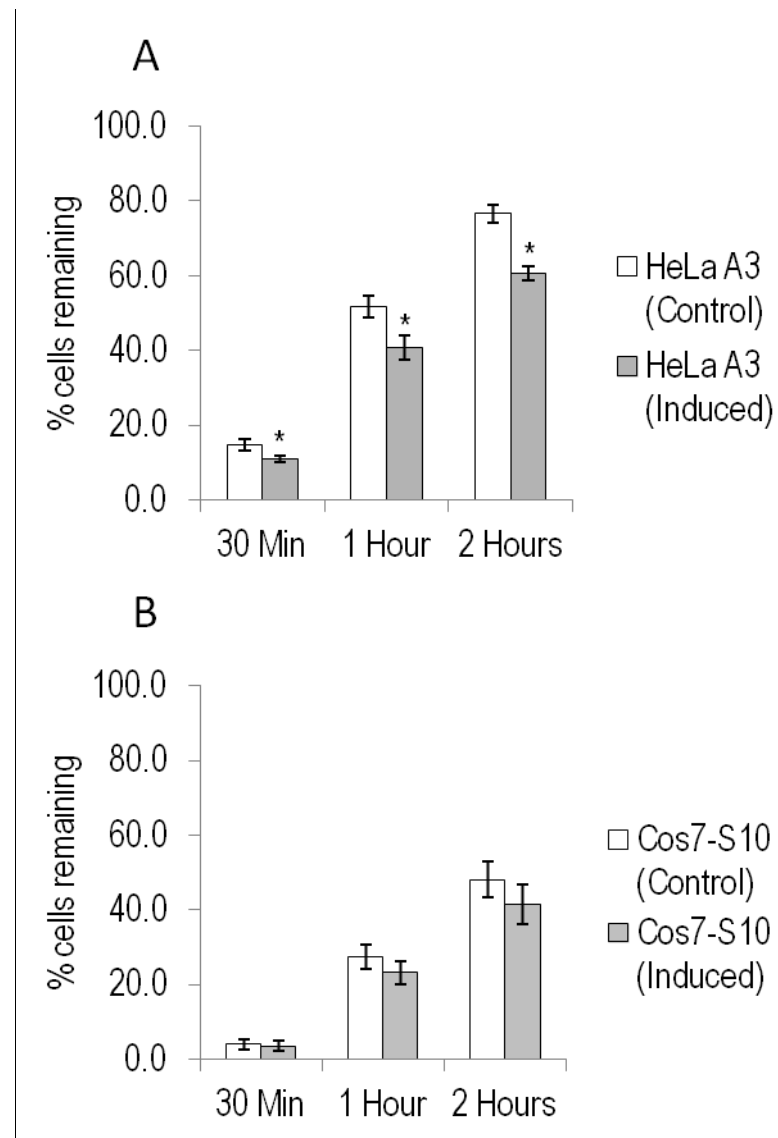
Figure 3.4. Rate of adhesion assay time course. The percentage of cells remaining which have adhered to tissue culture dishes at different times after initial seeding are shown. Originally 200000 cells were seeded in each well using a 24 well plate. A) Control uninduced HeLa A3 cells and doxycyclin-induced HeLa A3 cells. Differences at 30 min Student's t = 3.6, P < 0.05; 1 hour t = 4.3, P < 0.05; 2 hour t = 9.3, P < 0.05, n = 3. B) Control uninduced Cos7-S10 cells and doxycyclin-induced Cos7-S10 cells. Differences at 30 min t = 0.4, P = 0.69; 1 hour t = 1.6, P= 0.19; 2 hour t = 1.6, P = 0.18, n = 3. The induced cells were exposed to doxycyclin for 48 hour prior to the experiment and means +/- SD of each experiment are shown. Asterisk (*) indicates time points that are significantly different between uninduced, control and S100P-induced cells (Student's t-test, P < 0.05).

3.2.4.1.2 Strength of adhesion

As well as assessing the rate of cell adhesion, it was also necessary to determine how strongly the cells were bound to the culture dishes. Ultimately, if cells were bound less strongly to the surrounding matrix, then it would be easier for them to break free from a tumour. HeLa A3 and Cos7-S10 cells were, therefore, assayed to determine whether S100P had an effect on the strength of cell adhesion. The HeLa A3 cells (Figure 3.5A) showed a significant decrease in the number of cells that remained adhered to the tissue culture dish in the doxycyclin-induced cells compared to the uninduced control cells after weak trypsination (Student's $t = 6.7$, $P = 0.022$, $n = 3$). The Cos7-S10 cells (Figure 3.5B) showed no significant difference in the number of cells that remained adhered to the tissue culture dish after weak trypsination ($t = 0.6$, $P = 0.95$, $n = 3$). These results, as with the rate of adhesion assay, suggest that it is the breakdown of filamental NMIIA by S100P that causes the decrease in strength of adhesion seen here.
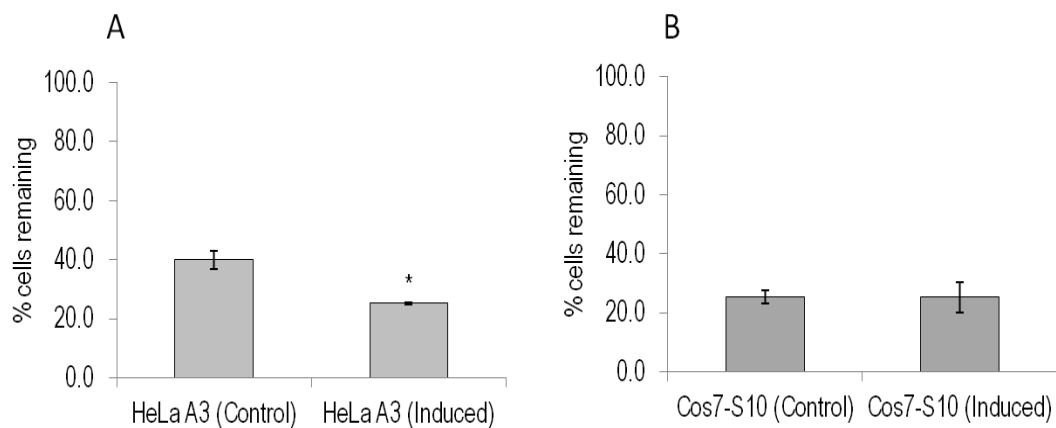
Figure 3.5. Strength of adhesion assay. Cells were seeded in a 24 well plate to form an 80% confluent monolayer 16 hours later. Cells were then digested with dilute 0.0125% (w/v) trypsin/versene for 5 min to remove weakly bound cells. The remaining bound cells were removed and counted using standard procedures (Materials and Methods). The values are expressed as a percentage of the original number of cells seeded. A) Control, uninduced HeLa A3 cells and doxycyclin-induced HeLa A3 cells. There was a significant 1.6-fold decrease in the strength of adhesion upon induction of S100P (Student's $t = 6.7$, $P < 0.05$, $n = 3$). B) Control uninduced Cos7-S10 cells and doxycyclin-induced Cos7-S10 cells. There was no significant change in the strength of adhesion upon induction of S100P ($t = 0.6$, $P = 0.95$, $n = 3$). The induced cells were exposed to doxycyclin for 48 hour prior to the experiment.

Asterisk (*) indicates time points that are significantly different between uninduced, control and S100P-induced cells (Student's t-test P < 0.05).

3.2.4.2 Cell migration assays

In order to substantiate previous studies, cell migration was measured in order to ensure S100P overexpression was causing the reported increase in cell motility. Cos7-S10 cells were also used in this assay to determine if any changes in migration were independent of the S100P-NMIIA interaction.

HeLa A3 cells showed a significant 4.7-fold increase in cell migration in doxyclin-induced cells compared to uninduced, control cells (Student's t = 20.8, P < 0.0001, n = 3) (Figure 3.6A). The Cos7-S10 cells were very variable when performing migration assays, with the values substantially deviating around the means. The results in Figure 3.6B shows that there was a near 1.4-fold increase in cell migration between the uninduced and induced Cos7-S10 cells. However, due to the variability of the results, this increase due to S100P-overexpression was not significant (1.4 fold increase t = 1.68, P = 0.144, n = 4).

The HeLa A3 results are consistent with those in the literature and, as with the adhesion assays, the Cos7-S10 results may imply that NMIIA is required, in part, for S100P to have a full effect on increasing cell migration.
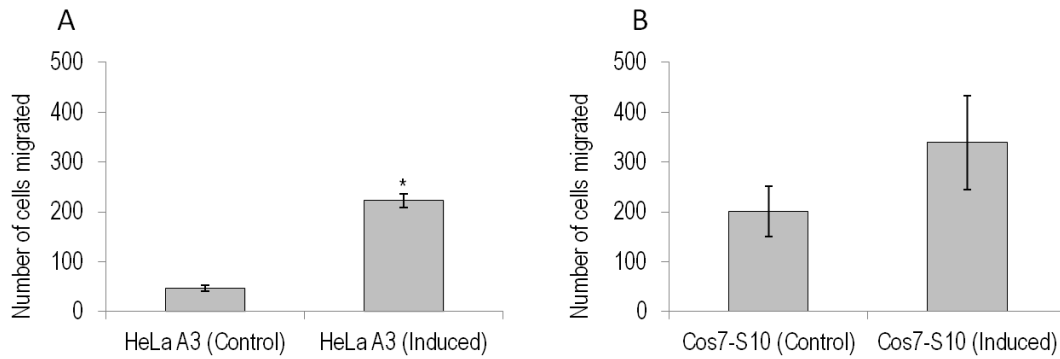
Figure 3.6. Effect of S100P on cell migration. Cells were seeded in Boyden chambers and allowed to migrate across a permeable membrane via chemotaxis induced by a 1% to 10% (v/v) serum difference. The number of cells migrated 16 hour after seeding was scored. A) Control uninduced HeLa A3 cells and doxycyclin-induced HeLa A3 cells. There was a significant 4.8 fold increase in migration upon induction of S100P (Student's t = 20.8, P < 0.05, n = 3). B) Control, uninduced Cos7-S10 cells and doxycyclin-induced Cos7-S10 cells. There was a 1.4 fold increase in migration upon induction of S100P, which proved not to be significant (t = 1.68, P = 0.144, n = 4). The induced cells were exposed to doxycyclin for 48 hour prior to the experiment and means +/- SD of each experiment are shown. Asterisk (*) indicates samples that are significantly increased (Student's t-test, P < 0.05)**.**

3.2.4.3 Cell invasion assays

As well as cell migration, an indication of a cell's invasive properties was sought to determine if S100P was causing alterations in the cell's ability to break down and traverse the extracellular matrix. Figure 3.7A shows that doxycyclin-induced HeLa A3 were more invasive than the control, uninduced HeLa A3 cells, showing a significant 3.2-fold increase in the number of invading cells compared to the control, uninduced HeLa A3 cells (Student's t = 7.01, P = 0.0022, n = 3). Surprisingly, however, the opposite was observed for Cos7-S10 cells (Figure 3.7B) with a significant 2.5-fold decrease in cell invasion upon induction of S100P with doxycyclin compared to the control, uninduced cells (t = 3.81, P = 0.0189, n = 3). This reduction rather than increase for Cos7-S10 cells may suggest that, unlike the HeLa A3 cells, S100P is having an inhibitory effect on the cell's ability to invade via serum chemotaxis, when no NMIIA is present.
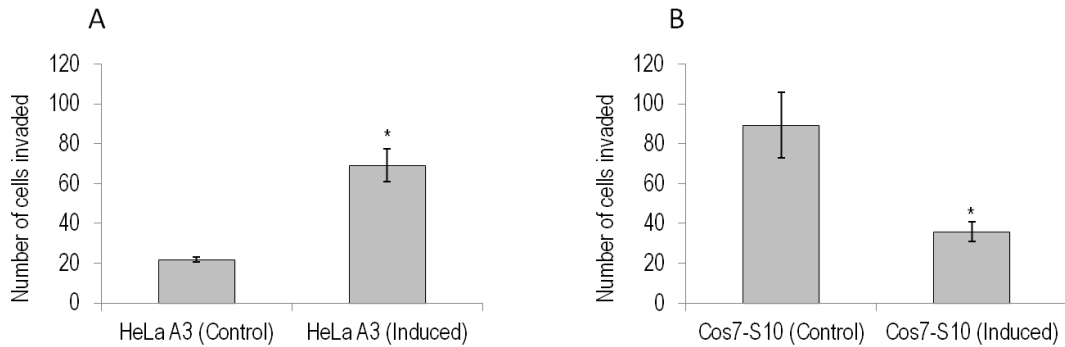
Figure 3.7. Effect of S100P on cell invasion. Cells were seeded in Boyden chambers and allowed to invade across a Matrigel-coated permeable membrane via a 1% to 10% (w/v) serum gradient. The number of cells migrated 16 hour after seeding was scored. A) Control, uninduced HeLa A3 cells and doxycyclin-induced HeLa A3 cells. There was a significant 3.2 fold increase on induction of S100P (Student's t = 7.01, P < 0.05, n = 3) B) Control, uninduced Cos7-S10 cells and doxycyclin-induced Cos7-S10 cells. There was a significant 2.5 fold decrease on induction of S100P (t = 3.81, P < 0.05, n = 3). The induced cells were exposed to doxycyclin for 48 hours prior to the experiment and means +/- SD of each experiment are shown. Asterisk (*) indicates samples that are significantly different (Student's t-test, P < 0.05)**.**

3.2.5 Epithelial to mesenchymal cell transition in HeLa A3 cells

As a significant difference was observed in the percentage of elongated cells in the S100P-induced cells compared to the control, uninduced cells, combined with an increase in migration and a decrease in cell adhesion, it was crucial to determine if these alterations were taking place due to an epithelial to mesenchymal transition (EMT) alongside the depolymerisation of NMIIA. HeLa cells have been previously shown to have undergone EMT, at least partially, but due to the observed changes, it was important to assess the extent of this EMT. EMTs are mediated by a range of both signalling and structural proteins. The abundance of these EMT-related proteins was assessed using Western blotting in control, uninduced and S100P-overexpressing HeLa A3 cells (Figure 3.8). These results show that the abundance of immunoreactive N-cadherin (140 kDa band), a crucial cell-cell adhesion protein, is significantly increased by 1.5 fold (Student's t = 10.64, P = 0.0035, n=3). This increase is consistent with an EMT; however, in most cell systems this increase in N-cadherin is paralleled by a decrease in E-cadherin. However, no detectable E-cadherin band

was visible in either the control or S100P-induced HeLa A3 samples. This lack of E-cadherin may suggest that HeLa A3 cells have already undergone a partial EMT which is supported by previous evidence on this cell line. Vimentin expression is characteristically increased in cells undergoing an EMT; however, S100P-overexpressing HeLa A3 cells showed no significant increase in the ratio of immunoreactive vimentin (57 kDa band) (fold increase = 1.11, t = 0.28, P = 0.81, n = 3). Increased expression of the transcription factors Snail and Slug are also considered major factors in EMT progression. However, no significant increase was observed in the levels of immunoreactive Slug (30 kDa band) in S100P-overexpressing cells (fold increase = 1.27, t = 2.23, P = 0.16, n = 3) compared to the control, uninduced samples. Immunoreactive Snail (30 kDa band) showed a small, but significant reduction in protein abundance in the S100P-overexpressing HeLa A3 cells (fold decrease = 1.5, t = 10.64, P = 0.0087, n = 3), the opposite of what is normally associated with EMT. From these results it is, therefore, difficult to decide whether there is an EMT taking place or not, as a result of S100P overexpression.
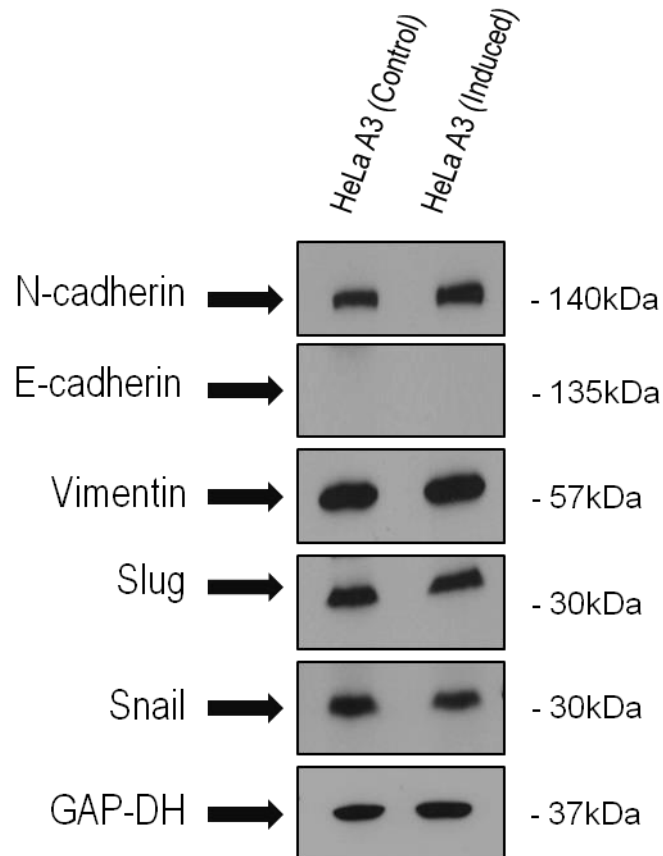
Figure 3.8. Levels of EMT proteins in S100P-induced HeLa A3 cells after 48 hours.
Examples of Western blots for EMT proteins using whole-cell extracts of control, uninduced
HeLa A3 cells and doxycyclin-induced HeLa A3 cells, with the GAP-DH bands being shown as
a loading control. A significant increase is shown in S100P-overexpressing cells for N-
cadherin (fold increase = 1.5, Student's t = 16.85, P < 0.05, n=3) and a significant decrease
for Snail (fold decrease = 1.5, t = 10.64, P < 0.05, n = 3). No significant alteration is seen in
vimentin (fold difference = 1.1, t = 0.28, P = 0.81, n = 3) or Slug (fold difference = 1.3, t =
2.23, P = 0.16, n = 3). No E-cadherin protein was detectable. The induced cells were
exposed to doxycyclin for 48 hour prior to the experiment and 10μg of protein was loaded
on a 10% (w/v) polyacrylamide gel for each well.

3.2.6 The effect of S100P over time

3.2.6.1 Analysis of cellular morphology over time

Due to the inconsistency of the expression of different EMT marker proteins reported in
Section 3.3, it was decided that the morphology of the S100P-overexpressing cells should

be studied in more detail over longer time periods. Three key parameters of cell morphology were measured over a two week time course (Figure 3.9A). The first of these parameters, Aspect Ratio, measures how elongated or spindle-like are the cells, and is derived by dividing the major axis of the cell by the minor axis. An increase in Aspect Ratio signifies an increase in cell elongation. When S100P was induced in HeLa A3 cells, there was an immediate and significant 1.3 fold increase (Student's $t = 5.47$, $P < 0.0001$, 270 cells examined) (Table 3.1) in Aspect Ratio 24 hours after induction of S100P. The Aspect Ratio of the S100P-overexpressing cells then increased steadily over the remainder of the two week period. Between the 24 hour and 334 hour time points the Aspect Ratio, and thus the cell elongation, increased significantly by another 1.3 fold ($t = 8.52$, $P < 0.0001$, 270 cells examined).

The second morphological parameter monitored is Solidity which is a measure of the cell's convex area. Morphologically, a decrease in Solidity is correlated with an increase in the number of convex surfaces present at the cellular periphery, which, in turn, implies an increase in filopodia-like protrusions. A small but significant 1.1 fold reduction in cellular solidity was observed at 24 hours (Student's $t = 9.82$, $P < 0.0001$, 270 cells examined); however, unlike Aspect Ratio, no further significant change was seen between 24 and 336 hours.

Lastly cellular Roundness was monitored, which is a measure of how spherical a cell is, with a perfect circle having a Roundness value of one. Morphologically, a decrease in Roundness indicates the cells are more elongated, although without taking into account the minor axis. Cells with a low Roundness can also be very wide in addition to being elongated. There was a significant 1.2 fold decrease (Student's $t = 7.52$, $P < 0.05$, 270 cells examined) in cellular Roundness 24 hours after induction of S100P. This decrease was followed by a significant, although smaller 1.2 fold decrease ($t = 4.72$, $P < 0.0001$, 270 cells examined) between 24 and 334 hours.

In order to validate these results and ensure that any changes observed are due to S100P overexpression, this experiment was repeated by adding doxycyclin to untransfected HeLa cells. This experiment was carried out to remove the possibility that doxycyclin, itself was causing the morphological changes observed in the induced HeLa A3 cells. Figure 5.2B shows that there was no significant change in Aspect ratio (fold change = 1.005, $t = 0.12$, $P = 0.91$, 270 cells analysed), Solidity (fold change = 1.003, $t = 0.21$, $P = 0.83$, 270 cells

analysed) or Roundness (fold change = 1.014, t = 0.44, P = 0.66, 270 cells analysed) in the control, untransfected HeLa cells up to 336 hours after addition of doxycyclin.

These morphology results may suggest that S100P has an immediate effect on the cells which takes place at about 24 hours and causes an increase in cell elongation (increase in Aspect Ratio, decrease in Roundness), and an increase in filopodia (decrease in Solidity). A second effect then occurs between 24 and 334 hours, where elongation of cells continues to increase (1.25 fold increase in Aspect Ratio and 1.21 fold decrease in Roundness).
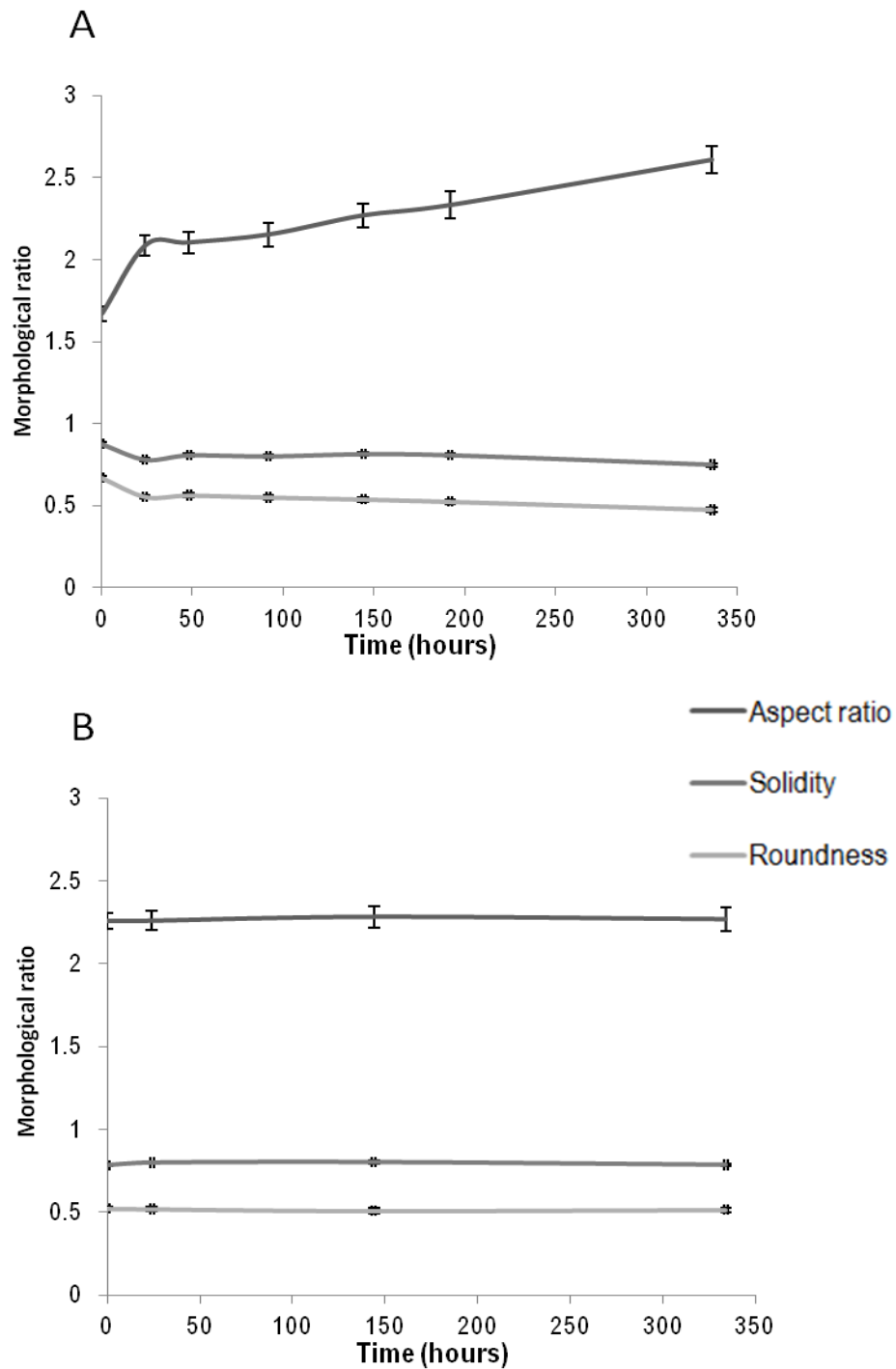
3.9. Time course of changes in HeLa A3 cell morphology upon induction of S100P. A) Morphological changes in Aspect Ratio (major axis/minor axis), Solidity (area/convex area) and Roundness ($4[area]/\pi[major\ axis]^2$) in S100P-induced HeLa A3 cells over two weeks of S100P induction with 270 cells being analysed per time point. Significant fold changes are noted in Table 5.1. B) Morphological changes in Aspect ratio, Solidity and Roundness in untransfected HeLa cells. Doxycyclin was added to the medium of both cell lines every 48 hours for two weeks. No significant change in Aspect ratio (fold change = 1.005, Student's t

= 0.12, P = 0.91), Solidity (fold change = 1.003, t = 0.21, P = 0.83) or Roundness (fold change = 1.014, t = 0.44, P = 0.66) was observed 336 hours after addition of doxycyclin. Analysis was carried out using Image J-Fiji (Material and Methods, Section 2.8.2) and 270 cells were analysed per time point.

Morphological parameter	Change (0-24h)	Change (24-336h)
Aspect Ratio	1.25 fold increase, t = 5.47, P< 0.0001	1.25 fold increase, t = 8.52, P< 0.0001
Solidity	1.1 fold decrease, t= 9.82, P< 0.0001	No change
Roundness	1.21 fold decrease, t = 7.52, P< 0.0001	1.2 fold decrease, t = 4.72, P< 0.0001

Table 3.1. Fold change and statistical significance of alterations in cell morphological parameters identified from Figure 5.2A for S100P-induced HeLa A3 cells. Definitions of morphological parameters are described in Material and Methods, Section 2.8.3.

3.2.6.2 Levels of expression of S100P over time in S100P-induced HeLa A3 cells

At the same time the morphological analysis was undertaken over 336 hours (Section 3.4.1), the relative levels of S100P were also determined using Western blotting at each time point. Upon addition of doxycyclin, the relative level of S100P increased at a steady rate from 0-100 hour, after which it levelled off somewhat, but a smaller rate of increase still continued up to 334 hour. This increase in the relative levels of S100P over time may well account for the steady increase in morphological changes that occurs after 24 hours. It is, however, unlikely that this second steady change in cellular morphological parameters between 24 hour and 336 hour is due to S100P breaking down the NMIIA filaments, since it has previously be shown that this takes place at earlier times [206].
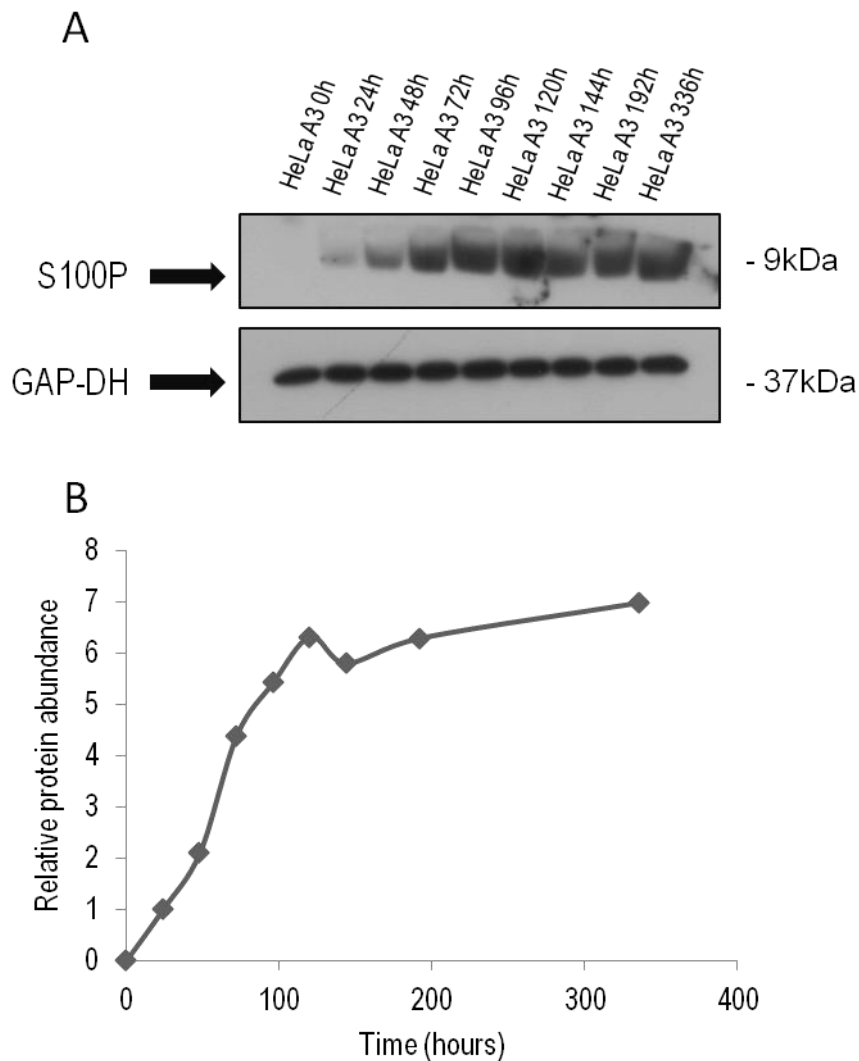
Figure 3.10. Induction of S100P in HeLa A3 cells as a function of time. A) Example of Western blot for S100P in whole-cell HeLa A3 extracts taken at different time points after addition of doxycyclin to induce S100P. GAP-DH bands are shown as a loading control. Ten μg of protein was loaded per well on 15% (w/v) polyacrylamide gels. B) Relative protein abundance of Western blots plotted against time. Protein bands for S100P were scanned and normalised against the relevant bands for GAP-DH. This ratio of pixel densities was then further normalised relative to the HeLa A3 band at t = 24 hour, since no protein band for S100P was observed at t = 0 hour.

3.2.6.3 Abundance of epithelial to mesenchymal transition (EMT)-related proteins over time

As stated in Section 3.4.2, it was unlikely that the continued morphological changes observed in S100P-overexpressing cells after 24-48 hours were caused by breakdown of NMIIA filaments, since this breakdown had already taken place. The relative levels of EMT proteins were, therefore, re-examined to see if alterations were observable after 48 hours. Figure 3.11 shows the relative levels of the main EMT proteins, Snail, vimentin and N-cadherin, over time determined by Western blots of lysates of S100P-induced HeLa A3 cells. The most striking result was a substantial drop (30-fold decrease) in the relative levels of Snail. During the initial 48 hours after doxycyclin addition, when the filaments of NMIIA depolymerize, no change in immunoreactive Snail was observed (Table 3.2). However, between 48 and 334 hours, a 30-fold decrease was observed, with the decrease occurring only after about 100 hour. This substantial decrease is the opposite of what may be expected in a cell line undergoing EMT. The relative levels of N-cadherin and vimentin were somewhat more variable (Figure 3.11B). The relative levels of N-cadherin increased (1.40 fold increase) in accordance with the early time points, as previously reported (Figure 3.8). However, N-cadherin levels did not rise substantially thereafter during the 48 to 334 hour period (1.1-fold increase). Levels of vimentin remained relatively constant with a small 1.1-fold increase between 0 to 48 hours and then another small 1.2-fold increase between 48 to 334 hours.
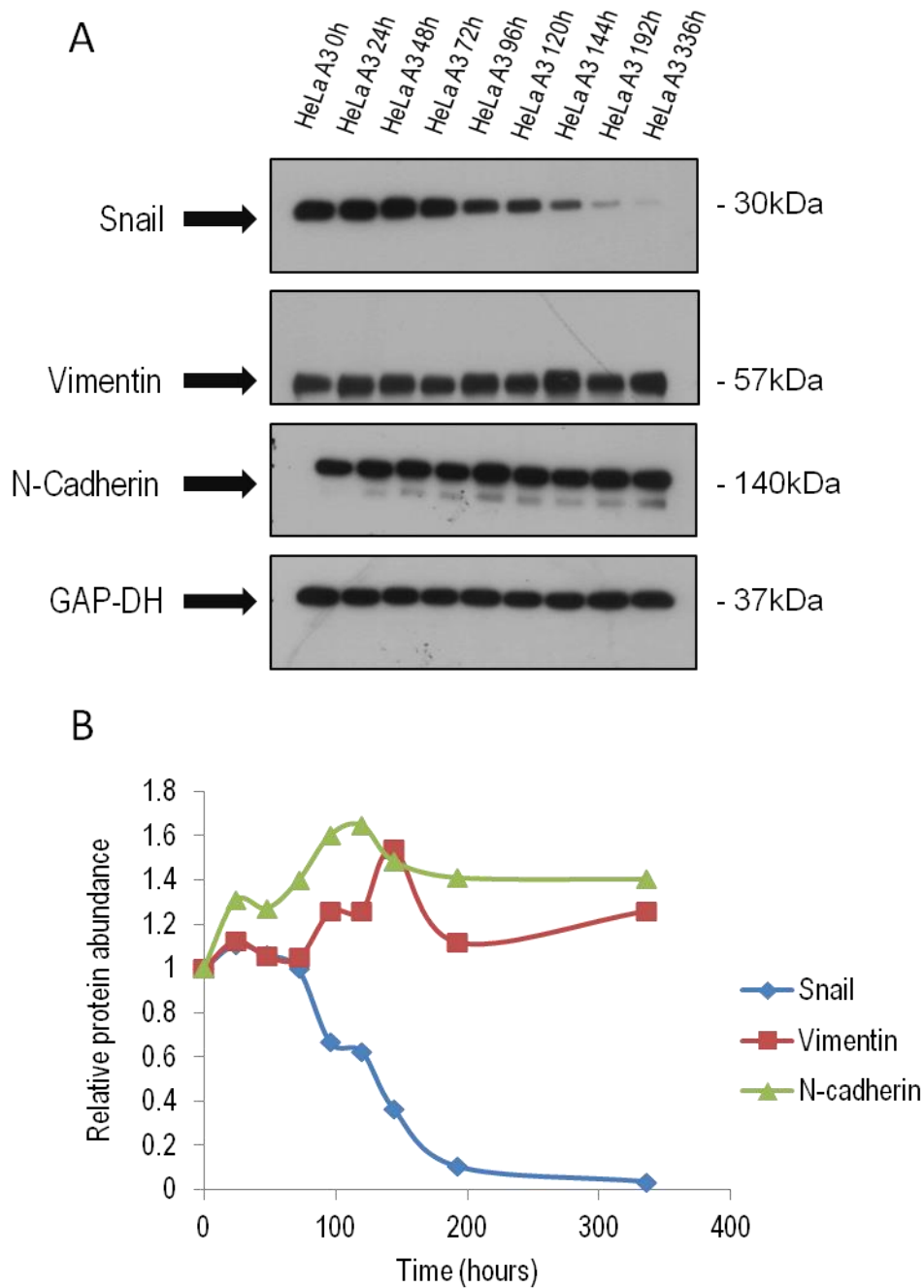
Figure 3.11. Levels of EMT proteins upon induction of S100P in HeLa A3 cells as a function of time. A) Example of Western blots for EMT proteins in whole-cell HeLa A3 extracts taken at different time points after addition of doxycyclin to induce S100P. The bands corresponding to Snail show no change up to 72 hour and then decrease dramatically from 72 to 336 hours. No substantial alterations are seen in the relative levels of vimentin. The relative levels of N-cadherin increase substantially from 0 to 24 hours and then relatively more slowly up to 120 hours. GAP-DH bands are shown as a loading control. Ten µg of protein was loaded per well on a 10% (w/v) polyacrylamide gel. B) Relative protein

abundance, determined by scanning densitometry is plotted against time for bands corresponding to Snail, vimentin and N-cadherin. Pixel densities of the scanned bands are normalised to their relevant GAP-DH bands. These relative ratios are then further normalised to their band at 0 hours.

Protein	Fold change in protein abundance after short term S100P induction (0-48h)	Fold change in protein abundance after long term S100P induction (48-336h)
Snail	1.00	30.39 fold decrease
Vimentin	1.05 fold increase	1.16 fold increase
N-cadherin	1.40 fold increase	1.09 fold increase

Table 3.2. Changes in EMT protein abundance upon long term overexpression of S100P in HeLa A3 cells. The fold increases or decreases are obtained from scans of Western blots (Figure 5.4) of the relative proteins normalised to their relevant GAP-DH bands. The change in these values is then shown as a ratio between either 0 to 48 hours or 48 to 336 hours after addition of doxycyclin and induction of S100P in whole-cell extracts of HeLa A3 cells.

3.2.7 Immunofluorescence

3.2.7.1 NMIIA cytoskeletal distribution

Following on from the cell assays, it was desirable to establish the extent to which S100P was causing changes in the cell cytoskeleton in model cell systems being used, since decreases in adhesion and increases in migration by S100P, both seemed dependent on this interaction. Thus, NMIIA was immunofluorescently stained in both HeLa A3 (Figure 3.12) and Cos7-S10 (Figure 3.13) cells. The inclusion of Cos7-S10 cells in this experiment was to determine if there was any NMIIA present in these cells that was not detectable by Western blots. Since maturation and to a lesser extent formation of focal adhesions is dependent on NMIIA filamental tension, cells were also stained for vinculin. This was

undertaken to determine the localised position of focal adhesions in relation to NMIIA in both S100P-induced and control, uninduced cells.

Control uninduced HeLa A3 cells showed clearly visible NMIIA filaments, which ran the entire length of the cell (Figure 3.8A). In contrast the S100P-induced HeLa A3 cells (Figure 3.8D) showed no distinct NMIIA filaments; these were replaced instead by a more uniform staining throughout the cell cytoplasm. This result would suggest that the protein was still present in the S100P-induced cells, but that the filaments had been depolymerized. Looking next at the focal adhesions stained for vinculin in the HeLa A3 cells, punctuate structures were clearly observed as green spots (Figure 3.12B, E). These spots are sites of vinculin bound into growing focal adhesions, strengthening the extracellular matrix interaction with actin via its binding to talin. Background cellular green staining was probably unbound, inactive cytosolic vinculin. Both the intensity of punctate staining and the number of stained foci was significantly reduced by about 2 fold in S100P-induced HeLa A3 cells (Student's t = 5.82, P = 0.002) (Figures 3.12E) compared to the uninduced control cells. In uninduced control HeLa A3 cells the merged images of staining for NMIIA and vinculin (Figure 3.8C) showed the focal adhesions were localised at the termini of the NMIIA filaments. In the S100P-induced cells, however (Figure 3.12F), it is more difficult to distinguish the distribution of focal adhesions, since the majority of the vinculin staining appears to be cytosolic.

Cos7-S10 cells did show some apparent very low level immunofluorescent staining for NMIIA (Figure 3.13A, D). This apparent weak staining was, however, thought to be non-specific, since the staining was localised in the nucleus of the cells, where no NMIIA should be present. No alteration in this very weak staining pattern was observed between the uninduced control Cos7-S10 cells and the S100P-induced cells for NMIIA. When looking at the staining for vinculin (Figure 3.13B, E), the size and clarity of the focal adhesions was substantially less pronounced than in the HeLa A3 cells. In Cos7-S10 cells there was no significant change in the number of vinculin-stained focal adhesions between uninduced control cells (panel B) and S100P-induced cells (panel E) (t = 2.55, P = 0.63) (expanded upon in Figure 3.14).
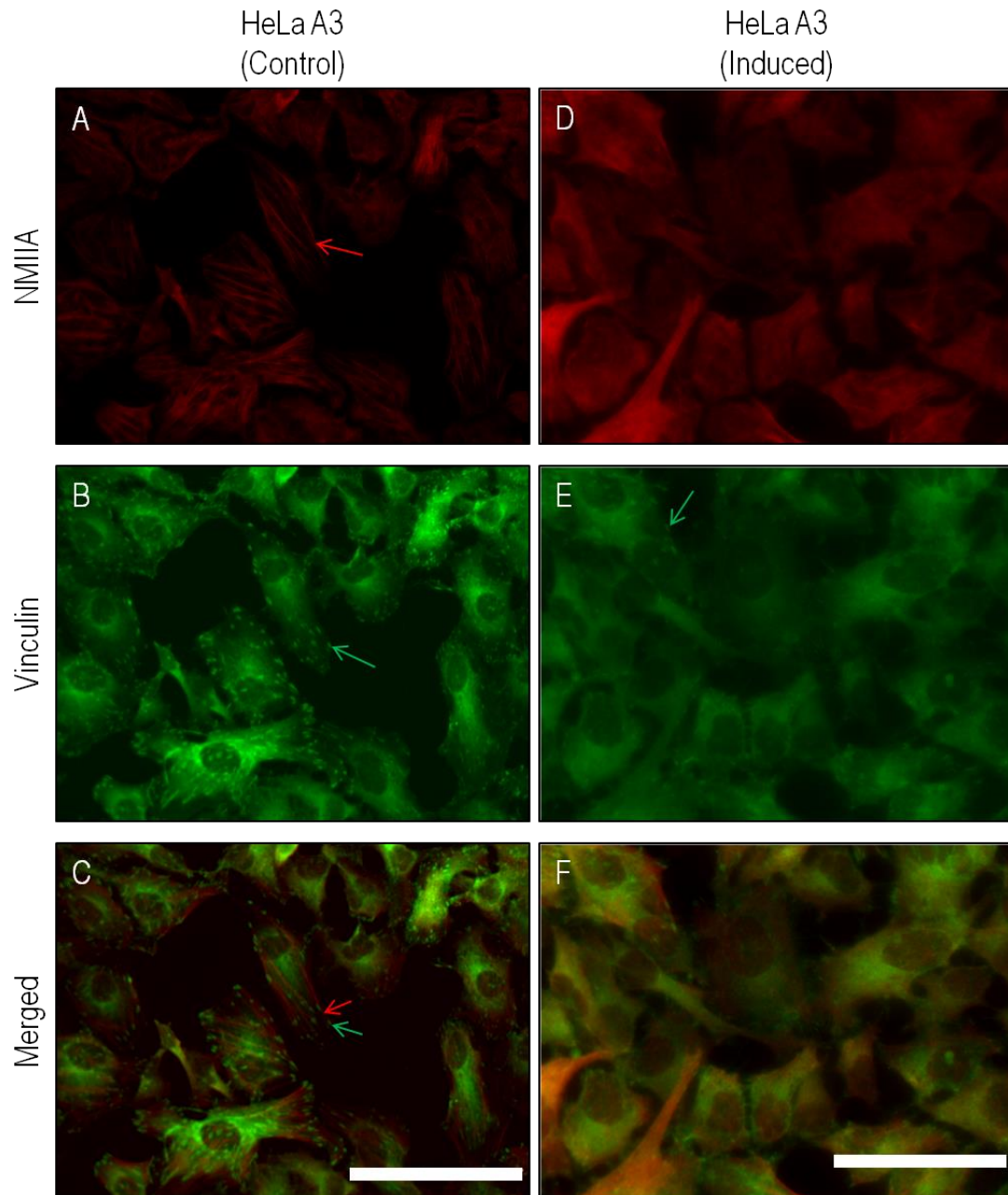
Figure 3.12. Effect of S100P expression on the NMIIA cytoskeleton of HeLa A3 cells. Cells were fixed with 4% (w/v) paraformaldehyde followed by permeabilization using 1% (w/v) Triton X-100 in PBS. Cells were immunofluorescently stained for (A,D) NMIIA (red) and (B,E) vinculin (green). Images were merged in C,F and show NMIIA filaments and vinculin co-localising at filamental termini in panel C. The NMIIA filamental structure (red arrow) in (A) control uninduced HeLa A3 cells are broken down in (D) S100P-induced HeLa A3 cells. A significant decrease was seen in the abundance of vinculin-stained focal adhesions (green arrow) in S100P-induced HeLa A3 cells (E) compared to control uninduced cells (B) (vinculin control uninduced mean = 29, SD = 3.4, induced mean = 15, SD = 2.4, 50 fields of view

measured in n = 3, Student's t = 5.82, P < 0.05). Statistical tests were carried out using Student's t test. Bars = 100μm.
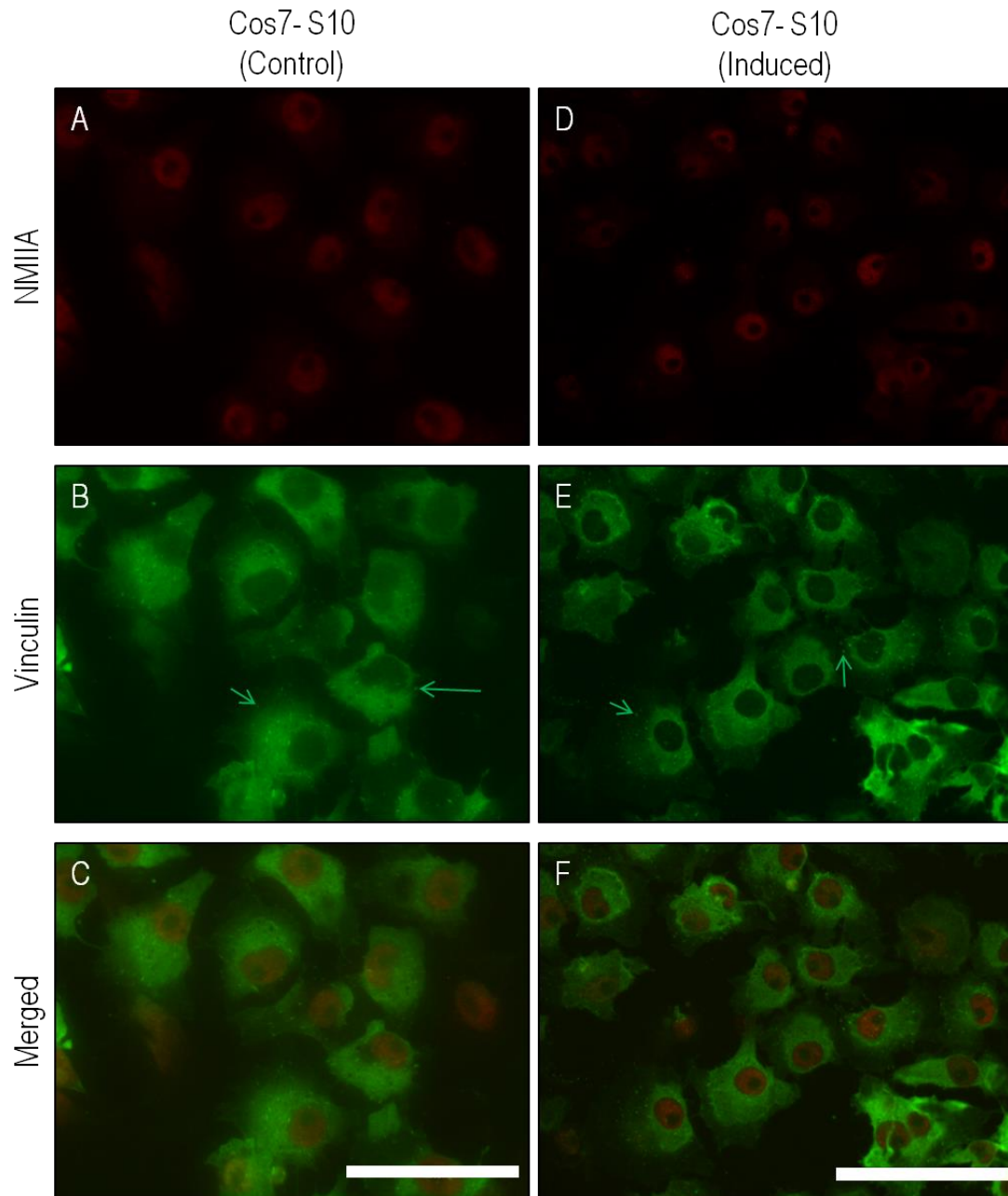
Figure 3.13. Effect of S100P expression on the NMIIA cytoskeleton of Cos7-S10 cells. Cells were fixed with 4% (w/v) paraformaldehyde followed by permeabilization using 1% (w/v) Triton X-100 in PBS. Cells were immunofluorescently stained for (A,D) NMIIA (red) and (B,E) vinculin (green). Images were merged in C,F. There was no specific staining for NMIIA in (A) Cos7-S10 uninduced control or in (D) S100P-induced Cos7-S10 cells with all staining being located in the cell nucleus. No significant change was observed in the abundance of vinculin-stained focal adhesions (green arrow) in S100P-induced Cos7-S10 cells (E) compared to control uninduced cells. (vinculin control uninduced mean = 28, SD = 2.4, induced mean = 23, SD = 2.3, 50 fields of view measured in n = 3, t = 2.55, P = 0.63)

resulting in a 1.93 fold and 1.23 fold decrease, respectively. Statistical tests were carried out using Student's t test. Bars = 100μm.

3.2.7.2 Focal adhesion fluorescence

After analysing the NMIIA data, it was clear that there was a reduction in the number of vinculin-staining focal adhesions in HeLa A3 cells when S100P was induced with doxycyclin. This result was extended to look at staining for both vinculin and paxillin, since paxillin was a crucial adhesion-signalling protein present in the adhesion complexes, in contrast to the structural role of vinculin. A significant decrease of 2.1-fold in the number of focal adhesions stained for paxillin was observed in S100P-induced HeLa A3 cells (Figure 3.10B), compared to uninduced, control HeLa cells (Figure 3.10A) (Student's t = 16.4, P < 0.0001, 50 fields of view measured in n = 3 experiments). This significant reduction was also observed in the vinculin staining focal adhesions between uninduced control cells and S100P-induced cells, accounting for a 1.9 fold reduction (Figure 3.10 C, D) (t = 5.82, P = 0.002, 50 fields of view measured in n = 3 experiments).

The Cos7-S10 cells showed a very small, but not significant 1.2-fold decrease in the number of focal adhesions upon S100P-induction. There was a 1.2-fold decrease in the number of paxillin foci in the S100P-induced Cos7-S10 cells (Figure 3.11A) compared to the uninduced control cells (Figure 3.11B) (Student's t = 1.88, P = 0.1334, 50 fields of view measured in n = 3 experiments) and a 1.2-fold decrease in vinculin between the uninduced control and the S100P-induced cells which was also not significant (Figure 3.11 C, D) (t = 2.55, P = 0.63, 50 fields of view measured in n = 3 experiments). These decreases in focal adhesion protein-stained foci are small and not significant, and are consistent with the adhesive properties of the Cos7-S10 cells not changing during adhesion-based assays upon induction of S100P.

Based on this data, it is possible to infer that the changes in adhesive characteristics exhibited by HeLa A3 cells are mainly due to a breakdown in the NMIIA cytoskeleton and/or a reduction in the number of focal adhesions active in the cell. This link between S100P expression, loss of NMIIA filaments, loss of focal adhesions and loss of adhesive properties has been established here, since none of these parameters change in S100P-induced Cos7-S10 cells that lack NMIIA. Since the aim of this study is to examine and explore possible changes in cellular adhesion based upon S100P induction, Cos7-S10 cells

will not be used further. Thus, it is clear that the S100P-NMIIA binding is necessary for most of these adhesive alterations and will now be the primary focus in this chapter.
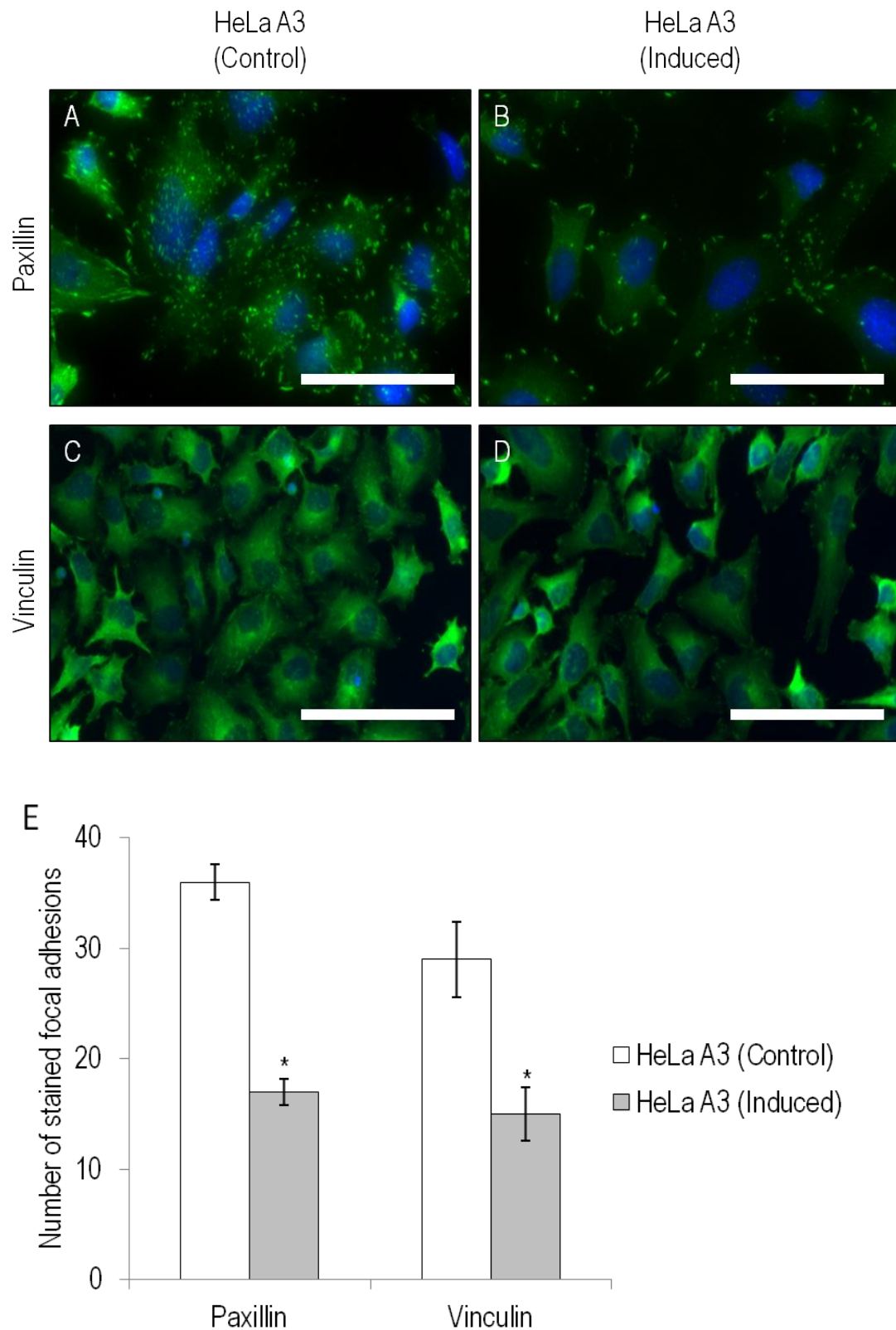
Figure 3.14. Effect of S100P overexpression on focal adhesion number and distribution in HeLa A3 cells. Cells were fixed with 4% (w/v) paraformaldehyde followed by permeabilization using 1% (v/v) Triton X-100 in PBS. HeLa A3 cells were

immunofluorescently stained for (A, B) paxillin (green) and for (C, D) vinculin (green). The numbers of punctate structures stained for paxillin or vinculin were significantly higher in the uninduced control cells compared to the S100P-induced HeLa cells (E) (paxillin control uninduced mean = 36, SD = 1.6, induced mean = 17, SD = 1.2, 50 fields of view measured in n = 3 experiments, Students' t = 16.4, P < 0.05) (vinculin control uninduced mean = 29, SD = 3.4, induced mean = 15, SD = 2.4, 50 fields of view measured in n = 3, t = 5.82, P < 0.05). This induction of S100P resulted in a 2.1 fold and 1.93 fold decrease in the number of paxillin and vinculin foci, respectively. Nuclei were stained blue using DAPI. Asterisk (*) indicates samples that are significantly different (Student's t-test, P < 0.05). Bars = 100μm.
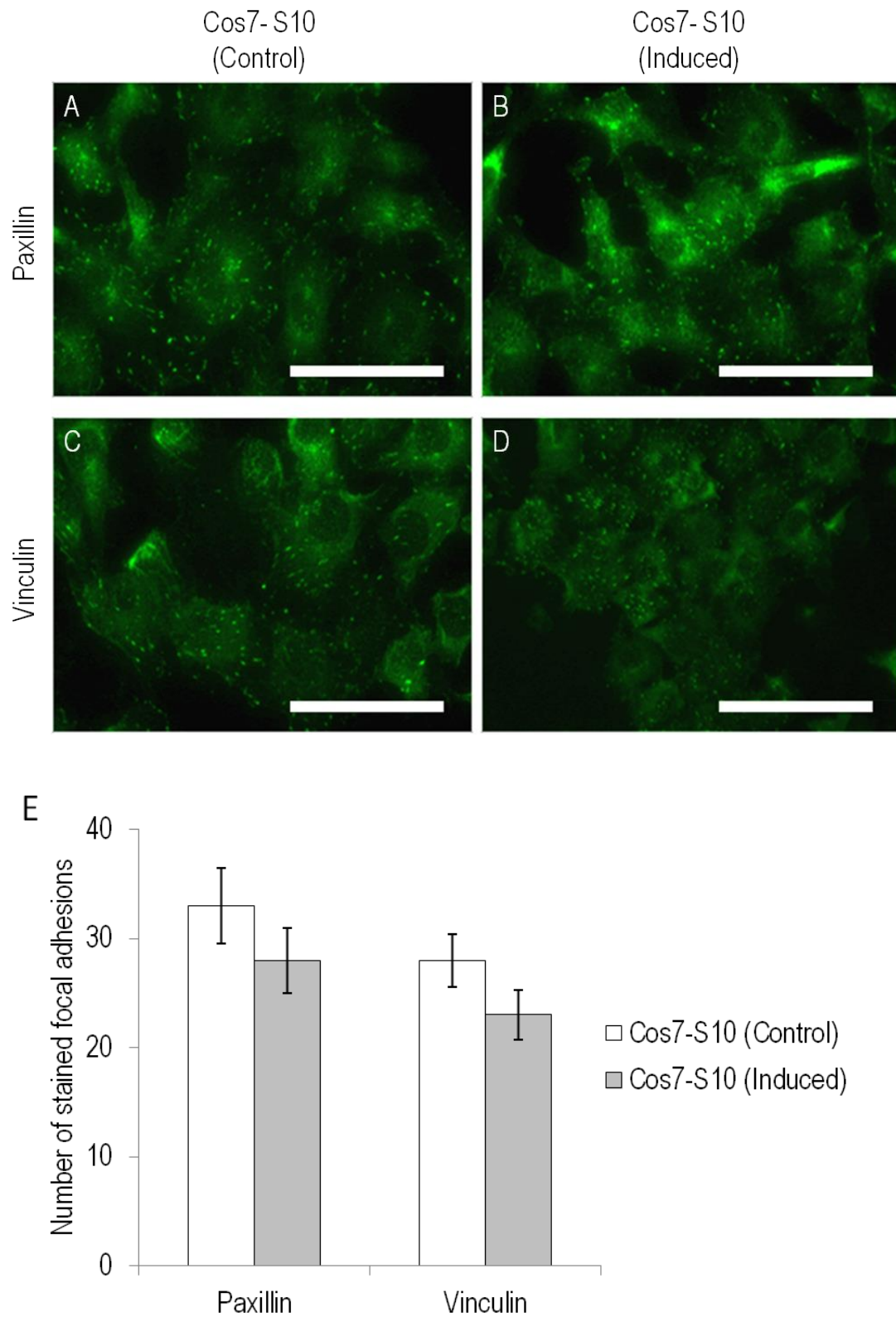
Figure 3.15. Effect of S100P overexpression on focal adhesion number and distribution in Cos7-S10 cells. Cells were fixed with 4% (w/v) paraformaldehyde followed by permeabilization using 1% (v/v) Triton X-100 in PBS. Cos7-S10 cells were immunofluorescently stained for (A, B) paxillin (green) and for (C, D) vinculin (green). The

numbers of punctate structures stained for paxillin or vinculin in Cos7-S10 cells were not significantly different in the uninduced control cells compared to the S100P-induced Cos7-S10 cells (E) (paxillin control, uninduced mean = 33, SD = 3.5, induced mean = 28, SD = 3.0, 50 fields of view measured in n = 3, t = 1.88, P = 0.13) (vinculin control uninduced mean = 28, SD = 2.4, induced mean = 23, SD = 2.3, 50 fields of view measured in n = 3, t = 2.55, P = 0.63). The fold difference was a 1.2 fold decrease in both the number of paxillin and vinculin foci. Statistical tests were carried out using Student's t test. Bars = 100µm.

3.2.7.3 S100P fluorescence

Following the reduction in the number of focal adhesions due to induction of S100P, immunofluorescence was undertaken to determine if S100P co-localised at these adhesion sites (Figure 3.12). Antibodies to paxillin were used to image the focal adhesions due to their greater clarity compared to those to vinculin. In control, uninduced HeLa A3 cells, S100P was localised in the nucleus and in the cytosol, in the latter it formed punctate, dot-like structures (Figure 3.12A). Upon overexpression of S100P, protein localisation was altered to become primarily in the nucleus, with some cytosolic staining and a loss of S100P-staining punctate structures (Figure 3.12D).

When the merged images of staining for S100P and for paxillin in the uninduced cells were examined, no co-localisation of focal adhesions and S100P foci was observed. This result may, therefore, suggest that the alterations observed in the focal adhesions are not due to any direct interaction with S100P, but due to the effect of S100P elsewhere in the cell. Since no S100P was observed in uninduced control cells using Western blotting, a no first antibody control was used to determine if the S100P-foci observed were genuine. The S100P foci were not seen when the antibody to S100P was omitted from the staining procedure and hence they are a genuine phenomenon. In the merged images for the S100P overexpressing cells (Figure 3.12D), the cells which have the highest nuclear staining for S100P appeared to have the fewest number of adhesion sites. This result may suggest that S100P is having an additional effect within the cell, possibly as a transcriptional regulator, given its prominence in the nucleus. This result also suggests that there is considerable heterogeneity within the HeLa A3 cells population, since not all cells respond in the same way to doxycyclin induction.
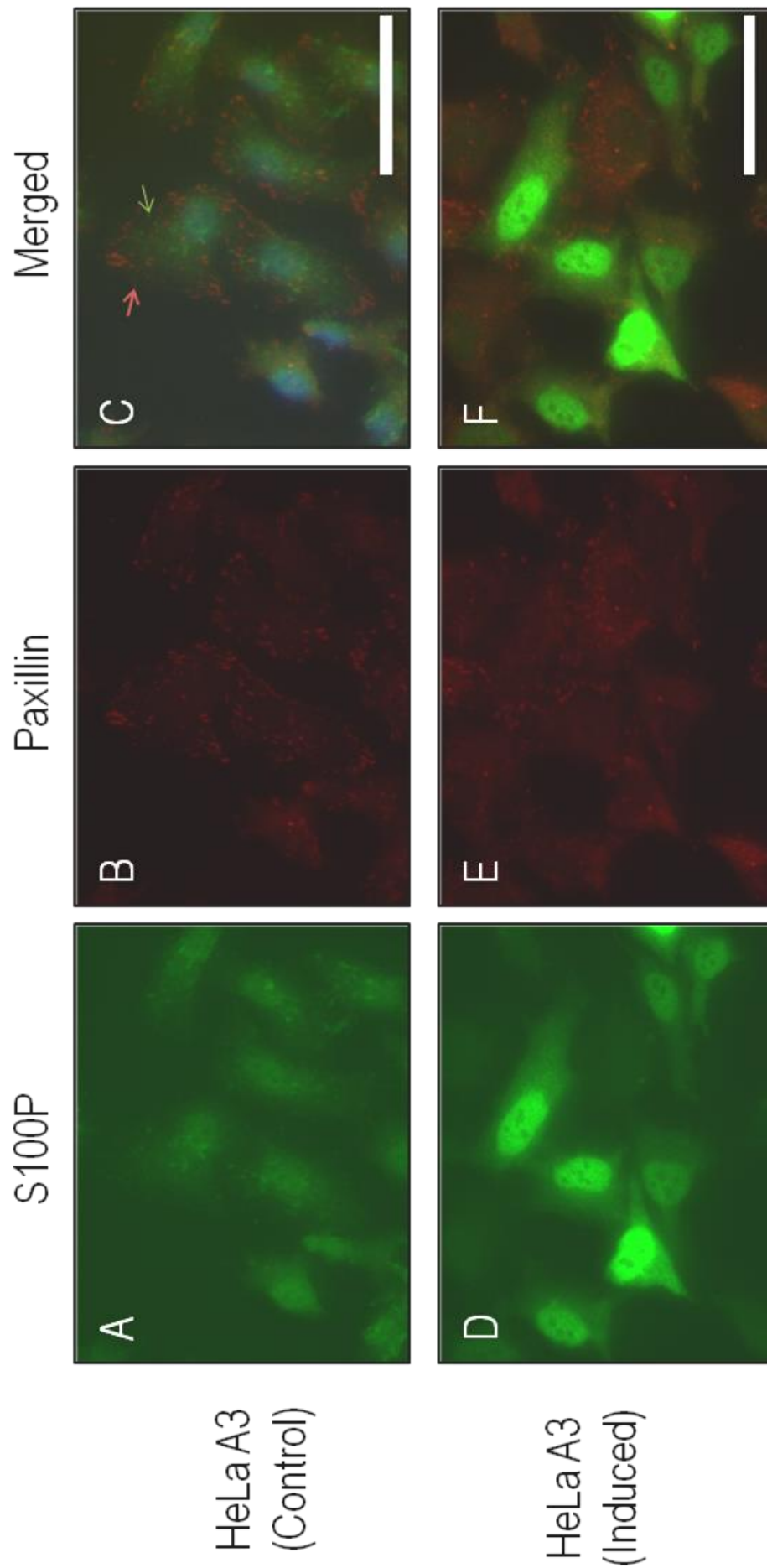
Figure 3.16. Distribution of S100P in HeLa A3 cells. Cells were fixed with 4% (w/v) paraformaldehyde followed by permeabilization using 1% (w/v) Triton X-100 in PBS. HeLa A3 cells were immunofluorescently stained for (A, D) S100P (green), and (B,E) paxillin (red). The images in C, F were merged. S100P distribution in (A) control, uninduced cells shows cytoplasmic punctate foci. This changes (D) to strong nuclear and a weaker cytoplasmic staining in S100P-induced cells with 44.4% of cells showing strong nuclear staining whereas no nuclear staining was observed in the control, uninduced HeLa A3 cells (SD = 10.7, cells from 10 fields of view used from n = 3 experiments). (B) Punctate staining for paxillin in uninduced cells was greatly reduced in (F) S100P-induced HeLa A3 cells. (C) Green arrow indicates S100P foci and Red arrow indicates paxillin foci, there is no co-localisation between the two stains. Bars = 100 μm.

3.2.8 Western blotting for adhesion proteins

3.2.8.1 Intracellular focal adhesion proteins

Following the decrease in the number of focal adhesion sites observed upon overexpression of S100P in the HeLa A3 cells, the next question was to determine if there were any alterations in the abundance of focal adhesion proteins within the cell. Western blots were carried out on whole-cell lysates using control, uninduced HeLa A3 and S100P-induced HeLa A3 cell extracts. Talin, vinculin, paxillin and focal adhesion kinase (FAK) were chosen, since they all have been reported to play a crucial role in the formation of focal adhesions. These proteins encompassed a range of functions within the adhesions; the former two are structural proteins and the latter two are signalling proteins. On Western blots they all showed bands with the correct apparent molecular weights (paxillin 60kDa, vinculin 115kDa, talin 270kDa and FAK 119kDa). The control, uninduced HeLa A3 cells showed no substantial increase or decrease in the protein levels compared to the S100P-induced HeLa A3 cells. Thus, changes in protein levels were not significant for paxillin (Student's t = 2.24, P = 0.09), vinculin (t = 2.24, P = 0.09) and talin (t = 1.21, P = 0.29), although the small 1.1-fold difference observed in FAK levels was significant (t = 4.29, P = 0.013) (Figure 3.11).
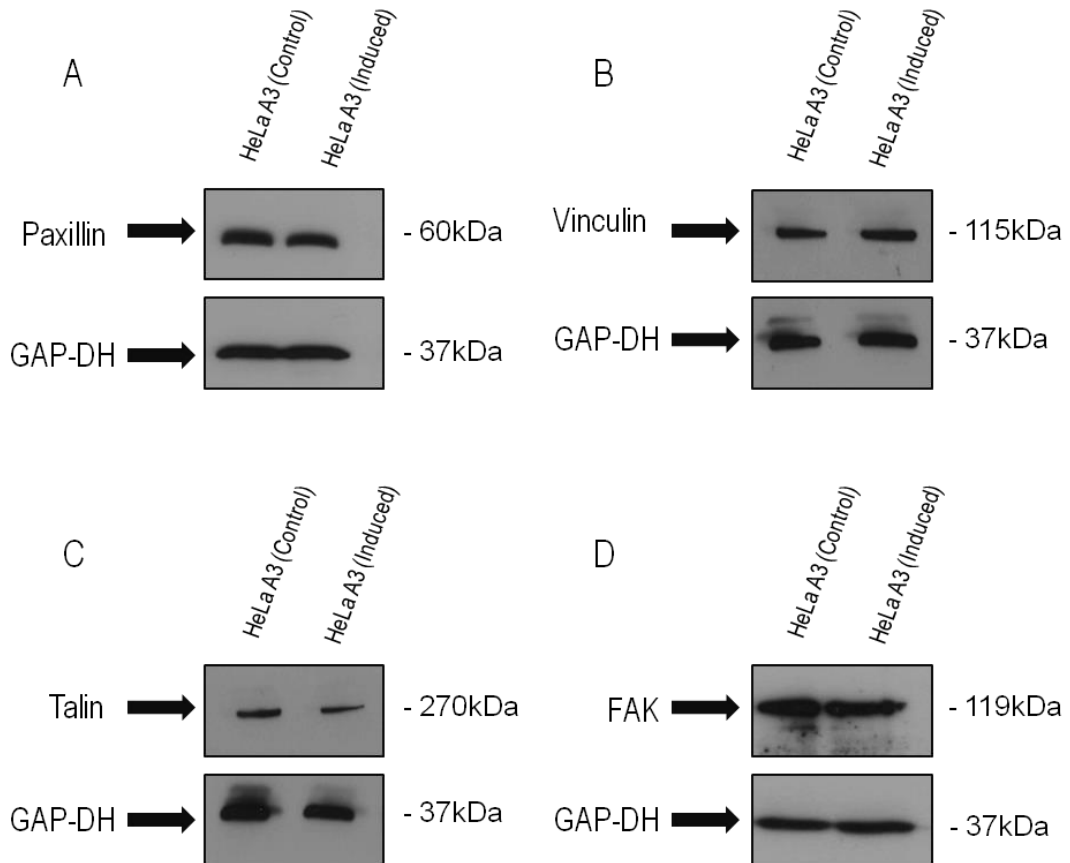
Figure 3.17. Western blotting of whole-cell lysates for key focal adhesion proteins. Western blots for (A) paxillin, (B) vinculin, (C) talin and (D) focal adhesion kinase (FAK) using whole-cell extracts of control, uninduced HeLa A3 cells and doxycyclin-induced HeLa A3 cells are shown, with GAP-DH bands being shown as a loading control. No significant alteration is seen in the mean levels of: paxillin (fold difference = 1.15, Student's t = 1.83, P = 0.14, n = 3), vinculin (fold difference = 0.90, t = 2.24, P = 0.09, n = 3), talin (fold difference = 0.95, t = 1.21, P = 0.29, n=3) and a very small, but significant difference is seen in FAK (fold difference = 1.10, t = 4.29, P < 0.05, n = 3). Fold differences are shown between bands for control, uninduced and S100P-induced cells, normalised against GAP-DH using scanning densitometry. The induced cells were exposed to doxycyclin for 48 hour prior to the experiment and 10µg protein was loaded on an 8% (w/v) polyacrylamide gel for each well.

3.2.6.1 Integrin proteins

Since there was no significant difference in the total abundance of focal adhesion proteins between the control, uninduced HeLa A3 cells and the S100P-induced cells, it was necessary to ascertain if there was a change in the total abundance of proteins at an earlier stage of cell-extracellular adhesion formation. Integrin proteins are transmembrane and, as such, are the first step in the formation of cell-substrate adhesions. The integrins that were selected for Western blotting were chosen because of their presence in epithelial cells. Western blots confirmed the presence of integrin beta-1 at 135kDa, integrin beta-3 at 100kDa, integrin alpha-V at 135kDa and integrin alpha-5 at 140kDa in whole-cell extracts of HeLa A3 cells (Figure 3.12). Once again the S100P-induced HeLa A3 extracts showed no significant increase or decrease in protein levels compared to the control, uninduced cells for integrin beta-1 (fold difference = 0.91, Student's t = 2.67, P = 0.06, n=3), integrin beta-3 (fold difference = 0.90, t = 2.58, P = 0.40, n=3), integrin alpha-V (fold difference = 1.04, t = 2.62, P = 0.11, n=3) and integrin alpha-5 (fold difference = 1.07, t = 1.18, P = 0.30, n = 3).
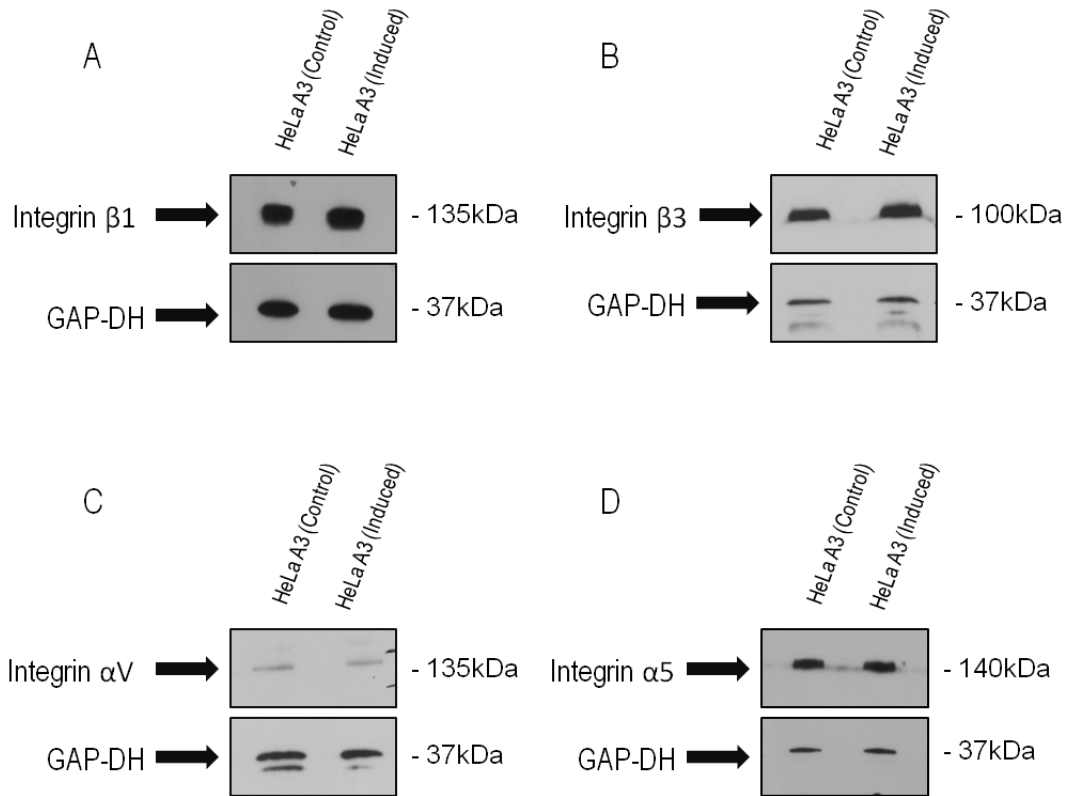
Figure 3.18. Western blotting of whole-cell lysates for integrin proteins. Western blots for (A) integrin β1, (B) integrin β3, (C) integrin αV and (D) integrin α5 using whole-cell extracts of control, uninduced HeLa A3 cells and doxycyclin-induced HeLa A3 cells are shown, with GAP-DH bands being shown as loading controls. No significant alteration is seen in the mean levels of: integrin beta-1 (fold difference = 0.91, t = 2.67, P = 0.06, n = 3), integrin beta-3 (fold difference = 0.90, t = 2.58, P = 0.40, n = 3), integrin alpha-V (fold difference = 1.04, t = 2.62, P = 0.11, n = 3) and integrin alpha-5 (fold difference = 1.07, t = 1.18, P = 0.30, n = 3). Fold differences are shown between control, uninduced and S100P-induced cell bands, normalised against GAP-DH using scanning densitometry. The S100P-induced cells were exposed to doxycyclin for 48 hour prior to the experiment and 10µg protein was loaded on an 8% (w/v) polyacrylamide gel for each well.

3.2.8.1 The effect of S100P on focal adhesion protein phosphorylation

S100P-overexpression was shown to cause a significant decrease in the adhesive strength and rate of adhesion in HeLa A3 cells (Figures 3.4 and 3.5). There was also a significant reduction in focal adhesions when visualised by immunofluorescence. However, the

abundance of key focal adhesion proteins in whole-cell lysates remained relatively unchanged between the control-uninduced and S100P-overexpressing cells (Figure 3.17). Since it is often the phosphorylation state of the focal adhesion proteins and not necessarily their levels that determines a cell's adhesive strength, phosphorylation levels of the two main focal adhesion signalling proteins, paxillin and FAK were determined in whole-cell extracts by Western blotting (Figure 3.19). In the case of paxillin, a significant 1.7-fold decrease (Student's t = 7.08, P = 0.0021, n = 3) was observed in the level of phosphorylated paxillin at tyrosine 118 (paxillin Y118), and a significant 1.6-fold decrease (t = 7.99, P = 0.0013, n = 3) in the abundance of phosphorylated paxillin at tyrosine 31 (paxillin Y31). For FAK, a significant 1.8-fold decrease (t = 9.11, P = 0.0008, n = 3) was observed in the abundance of phosphorylated FAK at tyrosine 397 (FAK Y397). Thus, although the levels of these proteins remain relatively constant, there was a significant reduction in phosphorylation of key focal adhesion signalling proteins. Phosphorylation of these focal adhesion-signalling proteins is reported to be dependent on cellular tension and extracellular signalling. Phosphorylation at these tyrosine sites on both FAK and paxillin is associated with maturation of focal adhesions, suggesting that there is a decrease in the rate at which focal adhesions mature in the S100P-induced and overexpressing HeLa A3 cells.
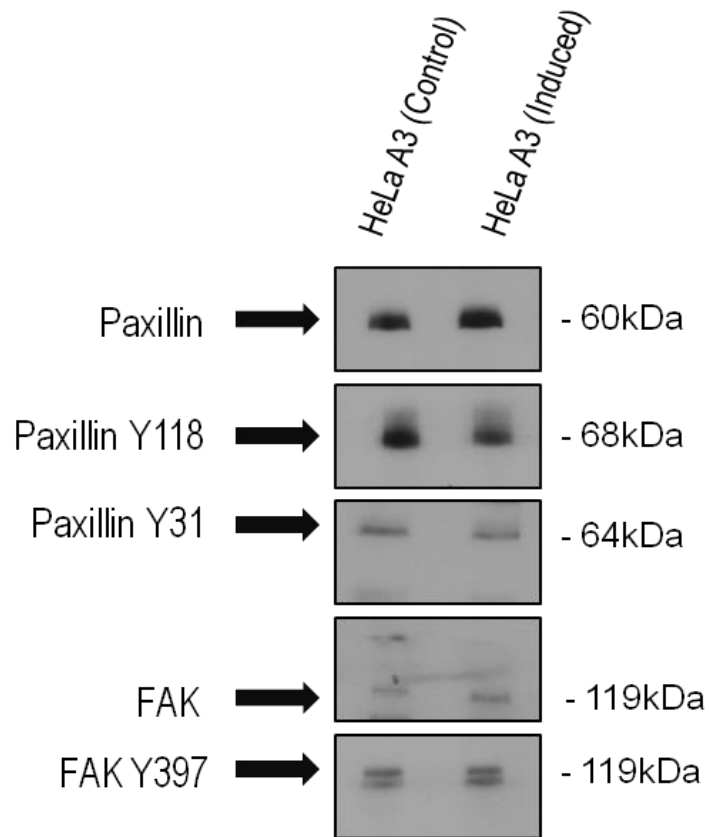
Figure 3.19. Alterations in focal adhesion protein phosphorylation upon S100P induction. Example of Western blots for paxillin and FAK phosphorylation sites in whole-cell extracts of control, uninduced and S100P-overexpressing HeLa A3 cells. A significant reduction is seen in phosphorylation of paxillin Y118 (fold decrease = 1.68, Student's t = 7.08, $P < 0.05$, n = 3), paxillin Y31 (fold decrease = 1.60, t = 7.99, $P < 0.05$, n = 3) and FAK Y397 (fold decrease = 1.83, t = 9.11, $p < 0.05$, n = 3). Unphosphorylated paxillin and FAK protein bands are shown as loading controls for normalization. The S100P-induced cells were exposed to doxycyclin for 48 hours prior to the experiment and 10 µg of protein was loaded on an 8% (w/v) polyacrylamide gel.

3.3 Discussion

3.3.1 S100P and cell morphology

3.3.1.1 S100P causes a breakdown in NMIIA altering cellular morphology

S100P has been shown to bind to NMIIA and cause the NMIIA filamental structure to be degraded in a number of studies, including one which used the same HeLa A3 cell system used in this study [206]. However, it was crucial to determine if the effect of S100P on NMIIA could be substantiated in this system (Section 3.2.5.1). NMIIA is an important element of the cytoskeleton and acts to form tension within the cell alongside its isoform NMIIB in ventral and transverse stress fibres [118]. This tensile force mediates both the rigidity of the cell, and the maturation of focal adhesion sites, as previously described (Section 1.3.2.2). In the HeLa A3 cells, when S100P is induced with doxycyclin, the NMIIA filaments are depolymerised (Figure 3.8), but the overall abundance of NMIIA within the cell remains the same (Figure 3.3). A number of previous papers have shown that loss of NMIIA in epithelial cells causes a flattening of the cell and an increase in spreading of lamellipodia. Indeed it has also been reported in the literature that the reduction in NMIIA within cells flattens and elongates the cells due to inhibition of stress fibre retraction rates [118, 141, 238]. It is therefore reasonable to assume that this breakdown in NMIIA filaments is one of the main factors in the loss of the normal HeLa cells morphology, as seen in Figure 3.1. However, in order to remove the possibility that these morphological changes are taking place due primarily to other factors, NMIIA knock-downs would need to be carried out both in the presence and absence of S100P in HeLa A3 cells.

This explanation for the change in morphology was further substantiated by the use of Cos7-S10 cells. These cells which have previously been reported not to contain any NMIIA, were a useful model to see the effect of S100P in an NMIIA-independent system. Cos7 cells are substantially different to HeLa cells in both their origin and cell type, however, the absence of NMIIA made them invaluable in determining the effect of S100P. The results presented in this chapter with the Cos7-S10 cells confirmed that there was no detectable NMIIA from Western blots of whole-cell lysates (Figure 3.3). Curiously when these cells were immunofluorescently stained for NMIIA (Figure 3.8), some nuclear staining was observed. Parallel experiments using only the secondary antibody gave no staining at all. However, it is possible that the antibody is not entirely specific for NMIIA and recognises other structures within the nucleus. To ensure that the antibody was entirely

specific, blocked controls with NMIIA protein would need to have been conducted to demonstrate that the nuclear staining was due to antibodies reacting with NMIIA. However, NMIIA is unlikely to be present in the nucleus due to its large size and, as such, the staining is assumed to be non-specific. Since there were no observable alterations in morphology of the Cos7-S10 cells 48 hours after doxycyclin induction (Figure 3.2), this suggests that indeed the morphological alterations observed in the HeLa A3 cells are primarily due to the direct effect of S100P on the breakdown of NMIIA filaments, rather than another NMIIA-independent, S100P-mediated interaction.

3.3.1.2 S100P overexpression results in a two stage effect on cell morphology

It was ascertained earlier in this Chapter (Figure 3.1) that S100P-overexpression resulted in elongation and flattening of the HeLa A3 cells. This morphological change occurred within 48 hours after induction of S100P with doxycyclin, and within this same time period the NMIIA filamental structure was also broken down. These two events were thought to be linked, since the alterations in morphology were not seen in the NMIIA-negative, Cos7-S10 cells upon induction of S100P. However, the abundance of EMT proteins did not change substantially during the first 48 hours, but then a 30-fold drop in the levels of Snail gradually occurred after this time up to 336 hours after induction of S100P. This fall in Snail may have further affected the HeLa A3 cell's morphology. Indeed a more in depth analysis of the parameters that describe cell morphology (Aspect Ratio, Solidity and Roundness) over time suggest that there may be two stages in which cellular morphology is altered in NMIIA-containing, S100P-overexpressing HeLa A3 cells. The first stage occurs in the first 24-48 hours after induction of S100P, when NMIIA filamental structures within the cell are broken down. This NMIIA breakdown stage occurs at the same time as a 1.3-fold increase in the Aspect Ratio of the cells, a 1.1-fold decrease in Solidity and a 1.2-fold decrease in cell Roundness. All of these changes are consistent with the HeLa A3 cells becoming more elongated as well as having an increased number of longer filopodia. This conclusion is also consistent with reported finding in the literature that state that a reduction in NMIIA flattens and elongates cells due to inhibition of the retraction rates in stress fibres [118, 141, 238].

The second stage of morphological change occurs slowly after the NMIIA filamental breakdown, from 48 hours up to 336 hours after induction of S100P. During this time a

further 1.3-fold increase is observed in the Aspect Ratio of the cells coupled with a further 1.2-fold decrease in cell Roundness. Both of these alterations are gradual compared to the rapid changes observed during the NMIIA filament's breakdown stage. These observations may suggest that there is an S100P-dependent alteration taking place in the cell which is further changing cellular morphology, either independent of the NMIIA filamental breakdown or more likely dependent on a subsequent event triggered by its breakdown, since no morphological changes were seen in the Cos7-S10 cells upon induction of S100P. However, in the case of the Cos7-S10 cells, their morphology was examined only at 48 hours after S100P induction. It is difficult to speculate on what may be causing this continued elongation of the S100P-overexpressing cells without further experimentation. In the future an examination of the differences in the proteome of "short term" (48 hours) S100P-overexpressing HeLa A3 cells and "long term" (336 hours) S100P-overexpressing HeLa A3 cells may give some indication as to why this change is taking place; unfortunately time did not permit these experiments to be conducted.

3.3.2 S100P overexpression causes NMIIA dependent loss in cell-extracellular matrix adhesion

Upon induction of S100P in HeLa A3 cells, a significant reduction was observed in the rate at which the induced cells adhered to a tissue culture dish compared to uninduced, control cells (Figure 3.4). This result was then shown to be dependent on the presence NMIIA, since no significant change was observed when conducting the same experiment using S100P-inducible Cos7-S10 cells (Figure 3.4). A significant reduction was also observed in the ability of monolayer-cultured S100P-induced HeLa A3 cells to resist digestion by a weak trypsin solution, compared to uninduced cells (Figure 3.5). This alteration was also dependent on NMIIA, since no change was seen in the adhesive strength of Cos7-S10 cells upon induction of S100P. However, in order to validate fully these conclusions on the effect of NMIIA on cell adhesion, NMIIA knockdowns would need to be carried out on HeLa A3 cells. These reductions in adhesive properties upon induction of S100P in HeLa A3 cells may well be due to the tension-dependent nature of focal adhesion maturation. As outlined in detail in Section 1.3.2.2, myosin tension is required for nascent adhesions and focal complexes to continue maturing into ventral stress fibre-bound focal adhesions [42, 118]. The absence of these tightly-bound, focal adhesions present in the main body and trailing edge of the cell would reduce significantly the total adhesive strength of the cells.

Regarding the decrease in the rate of cell adhesion due to overexpression of S100P in the HeLa A3 cells, as mentioned previously, loss of NMIIA has been shown to increase spreading of lamellipodia, as well as increasing significantly the number of filopodia protruding from the cell. Such changes may well imply that these cells would be faster at adhering to surfaces; however, since the cellular tension has been disrupted due to depolymerisation of filamental NMIIA, the ability of the S100P-overexpressing cells to form mature adhesions is likely to be substantially reduced. As a result, the S100P overexpressing HeLa A3 cells have a larger surface area, with reduced cellular tension and hence would be less able to form stable focal adhesions as quickly as the control, uninduced cells.

These hypotheses regarding the observed change in adhesive strength and rate of adhesion based upon NMIIA-mediated tension and adhesion maturation are confirmed by the Cos7-S10 results (Figure 3.4, 3.5), which showed that there was no change in the rate or strength of adhesion due to S100P overexpression in an NMIIA-independent system.

Regarding the viability of the two adhesion assays, the strength of adhesion assay was carried out to determine how strongly the cells adhered to the tissue culture dish. However a distinct limitation of this method is that it tests the cells' ability to resist digestion by trypsin. Although it is an appropriate method of determining how tightly bound the cells are to the dish, this method does involve an enzyme and as such other cellular alterations due to S100P may have occurred that affect the induced cells ability to resist trypsin. A more appropriate test of adhesive strength would be the application of controlled mechanical stress to the cells. However, all attempts made during this study at developing an assay, which could apply controlled mechanical stress to the cells did not produce consistently reproducible results.

3.3.3 S100P overexpression causes alterations in the migratory and invasive properties of cells.

When the migration rate of HeLa A3 cells is measured, S100P overexpression results in an increased rate of cell migration across a membrane via serum-gradient chemotaxis. This alteration, however, seems to be due, at least in part to the depolymerisation of NMIIA filaments in the S100P-overexpressing cells. There was also a considerable increase in migration in the Cos7-S10 cells of about half of that seen in the HeLa A3 cells due to S100P

overexpression. However, repeated experiments failed to show the increase was significant, largely due to the fact that the migration rates with Cos7-S10 cells were very variable. Therefore, it is not clear whether the majority or some of the increase in migration due to S100P is NMIIA dependent. The fact that at least some of the increase in cell migration is due to S100P depolymerising NMIIA filaments is supported by previous studies which suggests that removal of NMIIA, either by knock-downs or by inhibition of its activity, results in increased cell migration in this system [206, 239]. The breakdown of NMIIA filaments in these studies was shown to result in stabilization of microtubules and expansion of the tubulin structures into the lamellae. These results are, however, far from a complete story, since other studies have shown that a reduction in NMIIA in human cancer cells can result in either a reduction or increase in single cell motility, as well as, interestingly, an enhanced rate of wound closure [118, 240, 241]. Since there are so many possible pathways that can be altered during cancer metastasis that have an effect on cellular migration, it is not possible to ascertain if the increase in cell migration in S100P-overexpressing cells is due solely to the loss of NMIIA filaments.

When the ability of cells to invade across a Matrigel-coated membrane via serum gradient chemotaxis is observed, a more complex picture emerges regarding the effect of S100P (Figure 3.7). In S100P-overexpressing HeLa A3 cells a significant increase was observed in the ability of cells to traverse the Matrigel-coated membrane. This result concurs with the bulk of the literature, which demonstrates clearly that, in the majority of normal/cancer cells, induction of S100P or S100A4 causes an increase in cell invasion [233, 242]. In contrast the reverse was observed in Cos7-S10 cells, which showed a significant reduction in cell invasion due to S100P overexpression. The way in which S100P affects the invasive properties of cells is still not fully understood. However, the results with the NMIIA-containing HeLa A3 cells may suggest that S100P-mediated breakdown of NMIIA filaments is involved in increased cellular invasion. Indeed as stated above, a breakdown in the cytoskeleton of the cell due to S100P-overexpression leads to longer, flatter cells with an increased number of filopodia. This cell shape would make traversing pores in the Boyden chamber membrane and Matrigel layer far easier. Moreover, S100P overexpression has also been shown to affect cell invasion by promoting the secretion of matrix metalloproteinases 5/9 (MMP5/9) [243]. Thus these MMPs, which break down the extracellular matrix, allow for more efficient invasive dissemination through a barrier of collagen-containing, extracellular matrix like Matrigel. Furthermore, S100P has also been shown to enhance plasmin formation, which again promotes degradation of the

extracellular matrix (experiments carried out in house, data not published). From these results it is, therefore, difficult to ascertain fully the role of S100P in cell invasion; however, much of the current literature suggests that S100P does act to promote invasion. Thus, in the absence of NMIIA filaments, it is more likely that there is something novel taking place in the Cos7-S10 cells that results in the observed reduction in invasion due to S100P overexpression. It is worth noting that the observed alterations in migratory and invasive properties due to S100P overexpression were conducted on a 2D surface and, as such, the changes observed may not translate fully to a 3D model system.

3.3.4 The effect of S100P on focal adhesions

S100P-overexpression was shown to result in a significant reduction in the number of stained focal adhesion sites observed using immunofluorescent staining for paxillin and vinculin in HeLa A3 cells. This observation is consistent with previously-published work that noted that same reduction. However, this reduction in stained focal adhesions was not significant in S100P-overexpressing Cos7-S10 cells. These results may, therefore, suggest that the reduction in stained focal adhesions due to S100P overexpression is NMIIA dependent. This conclusion supports the hypothesis that loss of NMIIA filaments due to overexpression of S100P causes a reduction in focal adhesions, which, in turn, results in the loss of adhesive strength. There is also a notable relocalisation of the stained focal adhesions from the main body of the cell in the uninduced control HeLa A3 cells to the cellular periphery in the S100P-overexpressing cells. This relocalisation suggests that mature ventral stress fibres, which normally bind to focal adhesions are not present in the S100P-overexpressing cells. Interestingly the reduction in the focal adhesions in S100P-overexpressing cells seems to be paralleled by the relocalisation of S100P to the nucleus of the cell (Figure 3.12). This result may suggest that S100P may be inducing nuclear events either directly, or more likely indirectly, such as transcription of genes. Moreover, recent studies have shown that the cellular localisation of S100P in early breast cancer is an important prognostic marker, with high nuclear staining yielding the poorest patient outcome [244]. These results suggest that S100P has a role in the nucleus, as well as in the cytoplasm.

When the abundances of integrins and focal adhesion proteins were examined in whole-cell lysates of HeLa A3 cells, there was no significant difference in the levels of any of

these proteins in the S100P-overexpressing cells, compared to the control, uninduced HeLa A3 cells (Figure 3.11, 3.12). Since there are no changes in the global levels of these adhesive proteins, there must be either an alteration in the cellular location of these proteins, and/or a change in the activity state of some of these proteins, such as changes in their phosphorylation, to cause a change in the number/distribution of focal adhesions and the consequent reduction in cellular adhesion.

3.3.5 Does S100P overexpression cause alterations in the abundance of EMT proteins?

When S100P was induced for a short period of time in HeLa A3 cells, and cell lysates were collected 48 hours after the addition of doxycyclin, only very small, if any, changes in the abundance of the main epithelial to mesenchymal transition (EMT) proteins were observed (Figure 5.1). These results, therefore, do not fit the standard criteria for an EMT. Typically EMT is characterised by an increase in N-cadherin, vimentin, Snail and Slug, as well as a reduction in E-cadherin [148]. These results did show an increase in N-cadherin, although there was no change in the abundance of vimentin and Slug, and showed, surprisingly a reduction in the abundance of Snail. Since E-cadherin was not present, these HeLa A3 cells have most likely already undergone a partial EMT prior to S100P-overexpression.

Since the changes in EMT-associated proteins were only very slight if at all, the effect of exposure to S100P long term was assessed to determine if any additional alterations could be observed in the EMT proteins after 48 hours (Figure 5.4). Indeed, there was a large 30-fold reduction in the abundance of Snail, although there were no substantial changes in the levels of N-cadherin or vimentin, when lysates taken from 48 hours and 336 hours after the addition of doxycyclin were compared. This large, significant reduction in the abundance of Snail in the S100P-overexpressing cells is unexpected, since a reduction in Snail has been reported to reduce substantially cell motility, invasion and tumour growth [245, 246]. The effect of an overexpression of Snail in other cell systems due to EMT is downregulating the expression and inhibiting the activity of RhoA, as well as increasing MMP9 expression [247]. Furthermore, there is no published evidence that shows a large reduction in Snail being correlated with any form of negative impact on patient survival. However, there is a possible explanation in that loss of Snail is very strongly associated with a mesenchymal to epithelial transition MET [182]. This process which has been covered in

detail in Section 1.5.3, involves the loss of the mesenchymal characteristics gained by the cells in EMT and their reversion to a more epithelial-like cell. This process is very poorly understood in cancer metastasis, but it is known to be common in cells found at secondary tumour sites. It makes sense that cells become highly motile and have their adhesive properties significantly inhibited during the early stages of cancer metastasis. During this early stage the cells are migrating so as to break away from the primary tumour and disseminate through the surrounding tissue into either the blood and/or lymphatic circulatory systems. However, once cells reach a secondary site, in order for a tumour to grow effectively, it is advantageous if these alterations to cell motility and adhesion can be reversed. It may well be that this process occurs due to long term overexpression of S100P in HeLa A3 cells, and thus has an inhibitory effect on expression of Snail and perhaps mediates an EMT to MET switch. This conclusion is, however, highly speculative and is not supported by the morphological data that shows HeLa A3 cells exposed to S100P continue to become more elongated and mesenchymal-like up to 336 hours after initial induction. Therefore in order to determine the effect of reduced expression of Snail within this cell system due to S100P-overexpression, additional experiments would need to be conducted. The first of these would be Snail knockdowns to determine the effect of a reduction in Snail in the absence of S100P. Once this effect was fully characterised, it may be possible to determine the role S100P plays in snail regulation.

3.3.6 S100P-overexpression affects maturation of focal adhesions through tension-dependent phosphorylation

Upon overexpression of S100P in HeLa A3 cells, there was a significant decrease in the relative levels of phosphorylated FAK Y397, paxillin Y118 and paxillin Y31 compared to the control, uninduced cell lysates (Figure 5.8). Phosphorylation of FAK at Y397 is reportedly mediated by NMIIA-dependent tension and upon phosphorylation at this site, providing FAK is bound to src, FAK phosphorylates paxillin at Y118 and Y31. Paxillin phosphorylation at these sites then causes sequestering of increased vinculin, as well as p130CAS-CRK and G protein-coupled receptor kinase interacting ArfGAP (GIT)–β-Pix to focal adhesions, which, in turn, promotes focal adhesion maturation [99, 122]. Therefore, when the NMIIA filaments are depolymerised in the S100P-overexpressing HeLa A3 cells, cell tension is reduced and this causes a reduction in both of these phosphorylated forms of adhesion-signalling proteins. This reduction and hence loss of activity of such proteins, suggests that

the rate of maturation of focal adhesions is reduced. It is, therefore, probable that this decrease in the rate of maturation of focal adhesions causes, either in whole or in part, the reduction in the number of anti-vinculin/anti-paxillin-stained focal adhesions observed by immunofluorescence in the S100P-induced HeLa A3 cells.

3.4 Conclusions

In this chapter the effects of S100P-overexression on cell morphology, cellular adhesion, migration and invasion were explored using NMIIA positive and NMIIA negative S100P inducible cell systems. Morphologically S100P-overexpressing HeLa A3 cells become more elongated and have increased convex area as the cells are induced over time. This change in morphology seems to take place in two stages, an early stage upto about 48 hours which is NMIIA dependent and then a slow alteration that takes place due to long term overexpression of S100P. In the NMIIA positive, HeLa A3 cells, there was a significant reduction in the rate at which cells adhered, a significant reduction in the strength of cellular adhesion, a significant increase in cell chemotaxic migration and a significant increase in cell invasion due to overexpression of S100P. These changes all seemed to be dependent on the breakdown of filamental NMIIA, since they were not observed significantly in the NMIIA-negative, S100P-inducible Cos7-S10 cells. These observed phenotypic alterations in cellular properties may be explained either, in part or in whole, by an observed loss of the cytoskeletal NMIIA filamental structure when S100P is overexpressed and a significant reduction in the number of paxillin and vinculin-containing focal adhesions. However, the observed changes in cell adhesion are not due to any alterations in the global levels of key focal adhesion or integrin proteins, as determined by whole-cell Western blotting of the HeLa A3 lysates. It was also shown that S100P overexpression does not induce a conventional EMT; however, upon long term exposure to S100P, there is a significant reduction in the abundance of the EMT-related protein Snail. Lastly it was shown that there is a reduction in the relative abundance of phosphorylated FAK (Y397) and paxillin (Y118 and Y31) due to overexpression of S100P. A reduction in phosphorylation at these sites is associated with a reduction in maturation of focal adhesions.

As an additional final point it is worth noting, as mentioned previously, that not all HeLa A3 cells behaved identically upon 48 hours after doxycyclin induction suggesting heterogeneity in the population at this time point. This heterogeneity would likely effect every experiment as either not all cells are responding to doxycyclin equally or responding to S100P equally. Despite this fact it can be assumed that any alterations that take place due to S100P overexpression would only be amplified if the cell population were more homogeneous.

Chapter 4

Adhesome isolation and mass spectrometric analysis

4.1 Introduction

From the results presented in Chapter 3, it is clear that S100P causes alterations in the cells' adhesive, migratory and invasive properties, but that these alterations are not due to a reduction in the overall abundance of any key integrin or focal adhesion protein. To ascertain in more detail, if there were any alterations present within the full cell proteome, LC-MS/MS was selected as the method of analysis. Protein and mRNA array-based techniques were considered, however, since the function of S100P is currently so poorly understood, it was considered that analysing all protein changes due to S100P overexpression was a more thorough approach.

Since the primary aim of this study is to examine the effect of S100P on cellular adhesion, it was necessary to investigate possible methods that could isolate the cell-extracellular matrix fraction. This investigation was undertaken to try and examine specifically, in the absence of all other cellular fractions, what was happening at the cell-extracellular matrix junction due to enhanced levels of S100P.

Many methods have been reported which isolate the cell-extracellular matrix proteins from cells [248-252]. A core element, common to many of these methods is the application of a hydrodynamic shearing force to remove the cell body, organelles and all cytosol leaving only the proteins that were bound tightly to the tissue culture dish. This force is applied in a variety of ways, depending on the specific method, e.g. the use of a Water Pik filled with either sterile PBS or RO water is common. Some methods also utilize triethanolamine (TEA)-containing, low-ionic-strength buffers prior to hydrodynamic

shearing. These buffers promote hypotonic pressure within the cell which weakens the integrity of the plasma membrane. This weakening of the plasma membrane allows the use of less hydrodynamic pressure during shearing, thus minimising any damage to the focal adhesion structures. In some cases cell-permeable, chemical cross-linking agents such as dithiobis-succinimidyl propionate and 1,4-bis[3-(2-pyridyldithio)propionamido]butane have been applied to cells prior to hydrodynamic lysis [250]. These chemicals cross-link lysine and cysteine residues within the cell and this method has been reported to improve the recovery of integrin-based focal adhesions. The aim in each of each of these techniques was to isolate the integrin-containing, cell-extracellular matrix adhesive fraction with as high a purity as possible. However, in all these reported examples, the cells used were fibroblastic cell lines, which are quite different structurally to the epithelial HeLa A3 cells that are used in this study. The main difference is the strong cell-cell adhesions that epithelial cells form, which are not present in fibroblasts. As a result, this may make some of these methods based on shearing of fibroblasts unsuitable for epithelial cells.

4.1.1 Chapter objectives

Using mass spectrometry, it will be determined whether there are observable changes in the abundance of proteins in whole-cell, S100P-induced HeLa A3 cells compared to control, uninduced cells. If there are any proteins that are of particular interest from the whole-cell mass spectrometry data, further investigation will then be conducted on these proteins. Following this, the active cell-extracellular matrix, adhesive fraction of HeLa A3 cells will be isolated from the whole-cell fraction and analysed. The aim is to determine, firstly whether there are any novel proteins present as a result of S100P induction within this fraction, and secondly whether there are alterations in the abundance of known proteins. Similar to the whole-cell mass spectrometry data, any proteins of particular interest will be investigated in further detail.

4.2 Results

4.2.1 Mass spectrometry of whole-cell HeLa A3 extracts

The data shown in Chapter 3 indicated that there were no observable alterations in the abundance of either focal adhesion or integrin proteins due to S100P overexpression in whole HeLa A3 cells. To determine whether there were any alterations in the abundance of any other proteins present within S100P-overexpressing cells, mass spectrometry of whole-cell extracts was undertaken. This high resolution technique allowed most cellular proteins to be examined and their relative abundance compared between the control, uninduced and S100P-induced cells.

When 4 independent cell extracts of uninduced-control and S100P-induced HeLa A3 cells were compared, a total of 1227 protein were identified during mass spectrometric analysis (Appendix 2). Of these proteins, Table 4.1 shows all the proteins that were found to have their relative abundance changed significantly between the uninduced-control and S100P-induced groups. To identify the proteins that had been most substantially altered in their abundance, a cut-off was selected consisting of identification of a particular protein by at least two unique peptides per protein, and a fold change of 1.5 times between the two groups. For the up-regulated proteins in the induced, S100P-expressing HeLa A3 cells, three proteins were identified (0.25% of total proteins identified) that had both the minimum number of peptides required and at least a 1.5-fold increase in abundance. S100P, as anticipated, had the highest fold increase at almost five times (Anova, P < 0.001). RPS29 showed a 2.7-fold increase in abundance in the S100P-overexpressing cells (Anova, P = 0.0027) and is a member of the S14P family of ribosomal proteins, being part of the 40S ribosomal subunit. Oddly, this protein has been associated with Ras-related protein 1A, acting to enhance its tumour suppressor activity. More interestingly, there was a two fold increase in the abundance of asparagine synthetase (ASUS) (Anova, P < 0.001). Overexpression of this protein has been shown to confer resistance to chemotherapeutic agents and apoptosis induced by glucose deprivation [253].

With respect to the significant down-regulated proteins caused by S100P overexpression, ten proteins were identified (0.8% of total proteins identified). These down-regulated proteins affected cell biosynthesis, apoptosis, and cell proliferation (Table 4.1), with the following being of particular note: Histone-binding protein RBBP7 (2.7-fold change, Anova, P = 0.0013); this protein has been shown to interact directly with retinoblastoma protein

and BRCA1, although its function is not well understood. Complement C3 (2.3-fold reduction, Anova, P < 0.001); this protein is crucial in the complement system and as such a reduction may cause a lowering of the surrounding immune response [254, 255]. Programmed cell death protein 4 (2.7-fold reduction, P < 0.001); this protein is an important tumour suppressor, with its reduction being correlated with poor patient outcome in a number of cancers, it also has a role in response to DNA damage [256, 257]. Retrotransposon-derived protein (PEG10) (2.2-fold reduction, Anova, P < 0.001) and endoglin (2.0-fold reduction, Anova, P < 0.001); both proteins are involved in the TGFβ pathway. The former has been shown to be associated with an increase in metastasis and invasion, although its overexpression is positively correlated with these factors rather than the decrease shown in this study [258, 259]. The latter protein, endoglin has a range of effects on cell migration and patient outcome, with some studies suggesting that an increase in cellular endoglin is associated with a metastatic phenotype, and some suggesting the exact opposite [260-262]. CD109 antigen (2.13 fold reduction, Anova, P < 0.001) poses another curiosity, since its overexpression is associated with metastasis and a poor patient outcome in a number of cancers, yet in this system its abundance is decreased due to S100P overexpression [263, 264].

There results pose several questions with regards to the function of S100P within the cell, however, since the aim of this project was to study the effect of S100P on cellular adhesion, most of these differentially-expressed proteins were not studied in any further detail.

Up-regulated proteins in induced S100P-expressing whole-HeLa A3 cells			
Protein / Gene name	UniProt ID	Fold Change Up	Cellular Location
S100 calcium binding protein P (S100P)	P25815	4.9	Cytoplasm
ribosomal protein S29	P62273	2.7	Cytoplasm
asparagine synthetase (glutamine-hydrolyzing)	P08243	1.9	Cytoplasm

Down-regulated proteins in induced S100P-expressing whole-HeLa A3 cells			
Protein / Gene name	UniProt ID	Fold Change Down	Cellular Location
UMP-CMP kinase (CMPK1)	P30085	-2.9	Nucleus
Histone-binding protein RBBP7 (RBBP7)	Q16576	-2.7	Nucleus
Programmed cell death protein 4 (PDCD4)	Q53EL6	-2.7	Nucleus
Mitochondrial carrier homolog 2 (MTCH2)	Q9Y6C9	-2.6	Cytoplasm
Complement C3 (C3)	P01024	-2.3	Extracellular Space
Retrotransposon-derived protein (PEG10)	Q86TG7	-2.2	Nucleus
CD109 antigen (CD109)	Q6YHK3	-2.1	Plasma Membrane
Trifunctional enzyme subunit beta, mitochondrial (HADHB)	P55084	-2.1	Cytoplasm
1-phosphatidylinositol 4,5-bisphosphate phosphodiesterase beta-3 (PLCB3)	Q01970	-2.0	Cytoplasm
Endoglin (ENG)	P17813	-2.0	Plasma Membrane

Table 4.1. Mass spectrometry of S100P-overexpressing whole-HeLa A3 cells. Identification of upregulated and downregulated proteins in whole-cell extracts of S100P-induced and overexpressing HeLa A3 cells relative to uninduced HeLa A3 cells. The fold change in protein levels between control, uninduced and S100P-induced HeLa A3 cells is shown, together with the number of unique peptides used to identify the protein. For inclusion P < 0.05 for each protein selected using Anova and there was a minimum of two unique peptides used for identification. This resulted in a total of 1227 proteins identified, samples used for analysis n = 4. The induced cells were exposed to doxycyclin for 48 hours prior to the experiment. QIAGEN'S Ingenuity Pathway Analysis was used for determining the cellular localisation of each protein.

4.2.1.1 Analysis of endoglin expression

It was decided that the alterations shown in cell morphology and EMT protein abundance which occurred at protracted (>48 hour) times after S100P induction, were probably not due to the breakdown of NMIIA filaments, but a secondary effect of S100P on cell signalling pathways. To explore this aspect, the first protein to be investigated in detail was endoglin, since its expression was shown by mass spectrometry to be reduced in whole-cell extracts of S100P-induced HeLa A3 cells (Table 4.1). A reduction in the expression of endoglin had also been linked with changes in cancer progression in a number of different cancers, as such its role within this S100P system was explored.

4.2.1.2 Western blot validation and siRNA knock-down of endoglin

Before determining the effect that endoglin was having on the S100P overexpressing cells, it was necessary to validate the reduction in endoglin protein levels, which had been observed in whole-cell mass spectrometry (Table 4.1). This validation was undertaken using Western blotting (Figure 4.1 A), followed by densitometric scanning of the proteins bands. These results showed a 2.5-fold decrease (Student's t = 8.05, P < 0.05, n = 3) in immunoreactive endoglin levels in whole-cell, S100P-overexpressing HeLa A3 cells, compared to the control, uninduced cell lysates. This reduction was slightly greater than the 2-fold reduction seen by mass spectrometry (Anova P < 0.0001).

Since the Western blots confirmed the reduction in whole-cell endoglin as a result of S100P overexpression, an endoglin knock-down was performed on control, uninduced HeLa A3 cells. A commercial kit of different endoglin siRNAs numbered 1-6 was used and the cellular knock-down efficiency determined by Western blots of whole-cell lysates at both 24 and 48 hours after siRNA transient transfection. In all cases the knock-downs were more effective after 48 hours compared to 24 hours (Figure 4.1C). Table 4.2 shows the fold decrease in endoglin abundance compared to the abundance of endoglin in cells treated with a scrambled control siRNA. Endoglin siRNA 6 showed the largest 33.7-fold decrease in abundance. Although this was a much larger reduction than that due to overexpression of S100P in the same cell system, this allowed the cellular properties of endoglin to be examined in a more extreme setting, where any alterations it caused to the cells would be

more easily observed. For this reason, endoglin siRNA 6 was used for all further knock-down experiments.
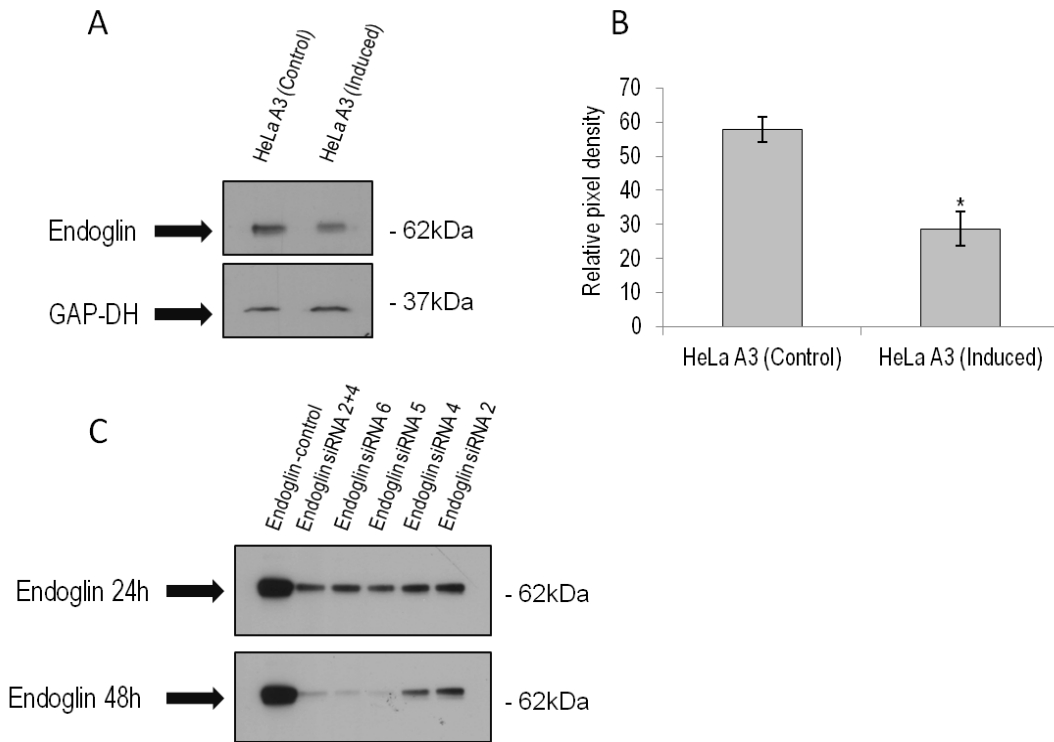
Figure 4.1. Levels of Endoglin in S100P-induced and in siRNA-treated HeLa A3 cells. A) Example of Western blot for endoglin in whole-cell extracts of control, uninduced and doxycyclin-induced, S100P-overexpressing HeLa A3 cells. The induced cells were exposed to doxycyclin for 48 hours prior to the experiment. Ten μg of protein was loaded on 10% (w/v) polyacrylamide gels. B) Quantification of Western blots shows a significant reduction in endoglin in S100P-expressing cells (fold reduction = 2.5, Student's t= 8.05, P < 0.05). Asterisk (*) indicates that the difference between samples is significant (Student's t-test, P < 0.05). C) Western blots showing endoglin siRNA knock-downs in HeLa A3 cells after 24 and 48 hours. The control siRNA used was a scrambled vector control to ensure that the siRNA was not affecting or harming the cells, the different siRNA numbers refer to different siRNAs added.

Endoglin siRNA	Fold decrease compared to siRNA scrambled control at 24h	Fold decrease compared to siRNA scrambled control at 48h
siRNA 2	2.7 fold	3.7 fold
siRNA 4	3.1 fold	5.4 fold
siRNA 5	4.1 fold	27.2 fold
siRNA 6	3.4 fold	33.7 fold
siRNA 2+4	3.0 fold	9.8 fold

Table 4.2. Fold change in endoglin abundance in HeLa A3 cells treated with different endoglin siRNAs. Fold decrease was determined from densitometric scans of Western blots for endoglin shown in Figure 5.5. The siRNA numbers refer to those in the commercial siRNA kit against endoglin (Materials and Methods, Table 2.13).

4.2.1.3 Phenotypic effects of siRNA knock-downs of endoglin in HeLa A3 cells

In order to assess the effect of the endoglin knock-down on the HeLa A3 cells, cell adhesion and migration assays were carried out, since alterations in these key properties are strongly linked with cancer progression. For both assays, cells were incubated with endoglin siRNA 6 for 48 hour before the experiments were started. Thus, when the HeLa A3 control, uninduced cells were transiently transfected with siRNA 6, there was a significant reduction in the rate of cell adhesion (Figure 4.2A) at both 1 hour (1.5-fold reduction, Student's t = 6.66 P = 0.0026, n = 3) and 2 hours (1.1-fold reduction, t = 17.43, P < 0.0001, n = 3) after the cells were seeded. These results are consistent with the known characteristics upon induction of S100P (Figure 3.4). However, when control, uninduced HeLa A3 cells were transfected with endoglin siRNA, there was a significant 1.6-fold decrease in cell migration (Figure 4.2B) (t = 4.9, P < 0.0001, n = 3). This result is the opposite of what was observed when S100P was induced in HeLa A3 cells (Figure 3.6). This result may suggest that the reduction in endoglin due to S100P overexpression may not be having any substantial

effect on the cells' migratory characteristics, or its effect may be masked by the breakdown of the NMIIA filaments.

The phenotypic changes observed in the knock-down experiments (a small reduction in rate of adhesion and a decrease in cell migration not consistent with S100P overexpression) were associated with a 30-fold decrease in endoglin, whereas overexpression of S100P caused a more modest 2-fold decrease in endoglin expression. Thus, it would appear that the changes in cell behaviour due to S100P overexpression were not consistent with endoglin mediating the mechanism, so it was decided that it was not worth pursuing endoglin in any further detail here.
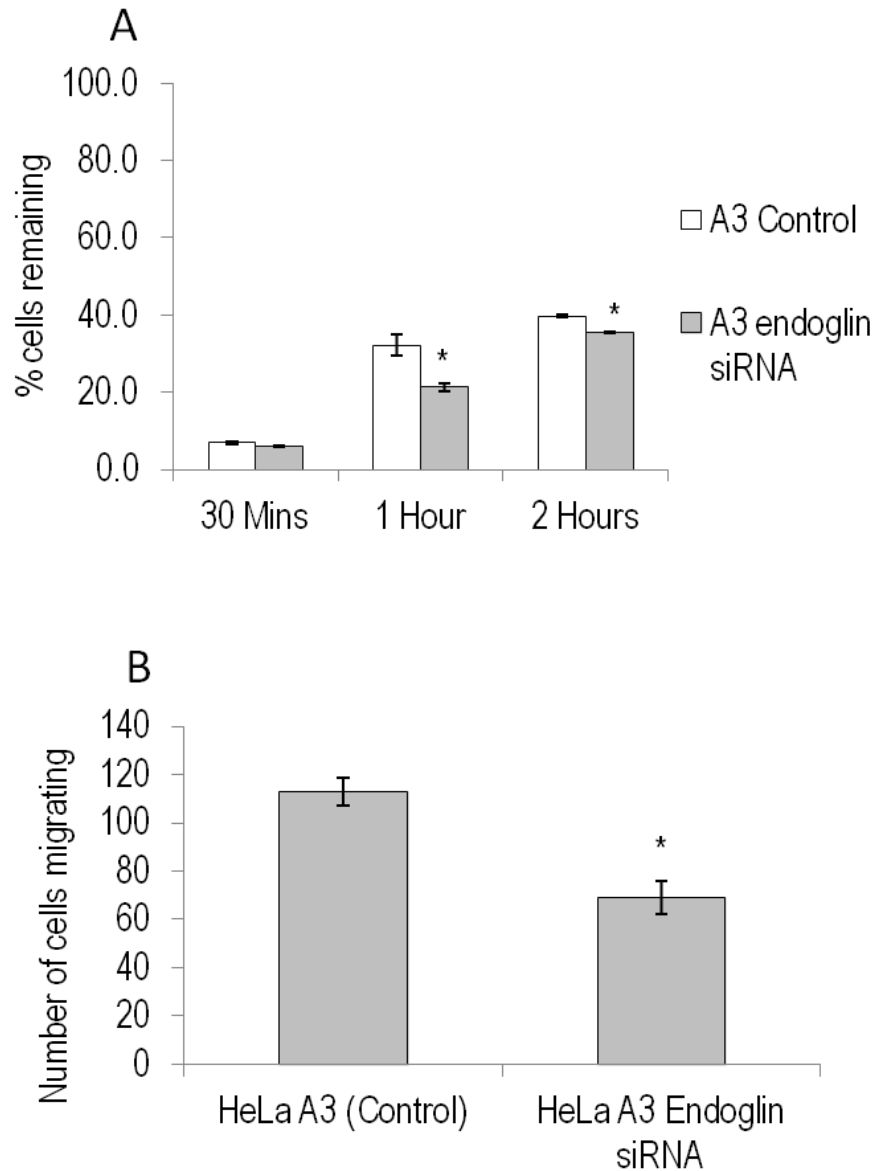
Figure 4.2. Effects of endoglin knockdown on cellular properties. A) Cell adhesion assays show the percentage of cells remaining adhered to tissue culture dishes at different times after initial seeding. Uninduced HeLa A3 cells were seeded at 200k cells per well in each well, using a 24 well culture dish and transiently transfected with a scrambled control siRNA or endoglin siRNA 6. Differences at 30 min Student's t = 3.6, P < 0.05, 1 hour t = 6.66, P < 0.05 and at 2 hours t = 17.43, P < 0.05, n = 3. B) Cell migration assay showing the number of migrating HeLa A3 cells transiently transfected with their scrambled control siRNA or endoglin siRNA 6. Cells were seeded in Boyden chambers and allowed to migrate across a permeable membrane via a 1% to 10% (v/v) serum gradient. The numbers of cells migrated 16 hours after seeding were scored. Student's t = 4.9, P < 0.05, n = 3. Scrambled control siRNA-treated HeLa A3 cells and endoglin siRNA 6-treated HeLa A3 cells were

exposed to the siRNA 48 hours prior to the adhesion or motility assay. Asterisk (*) indicates time points that are significant (Student's t-test, P < 0.05).

4.2.2 Adhesome isolation

As neither Western blots looking for alterations in cytoskeletal or adhesion proteins, nor mass spectrometry of whole cells, gave any indication as to why S100P-overexpressing cells have such a substantially altered phenotype, a more in depth method of studying a cell's adhesive properties was required. Since the immunofluorescent staining for adhesion proteins yielded a quantifiable reduction between the uninduced-control cells and the S100P-induced HeLa A3 cells, a way of isolating and analysing them was sought. To this end a variety of methods were attempted in order to isolated the substratum-cell adhesive fraction of HeLa A3 cells, as follows.

4.2.2.1 Detergent cell lysis

A Triton X-100 PBS solution was added to the cells to cause lysis without removing any Triton-insoluble proteins, such as those of the cytoskeleton and adhesive complexes. Figure 4.3 shows the resultant Western blots using this fraction. A significant reduction in the abundance of talin, shown at 270kDa (fold difference = 2.6, Student's t = 11.98, P = 0.0003, n = 3) and vinculin, shown at 119kDa (fold difference = 1.7, t = 8.55, P = 0.001, n = 3) was observed. No bands were present for paxillin or FAK in any of the blots carried out. Thus, the results for the structural adhesion proteins showed promise, since a decrease was observed in the S100P-overexpressing cells of roughly the same fold as seen by immunofluorescent staining of the same proteins. However, the ability to identify the adhesion signalling proteins using this method was somewhat limited. The inclusion of a Triton X-100 in PBS washing step also made it impossible to analyse this cell fraction using subsequent mass spectrometry due to the detergent's effect on the separation column.
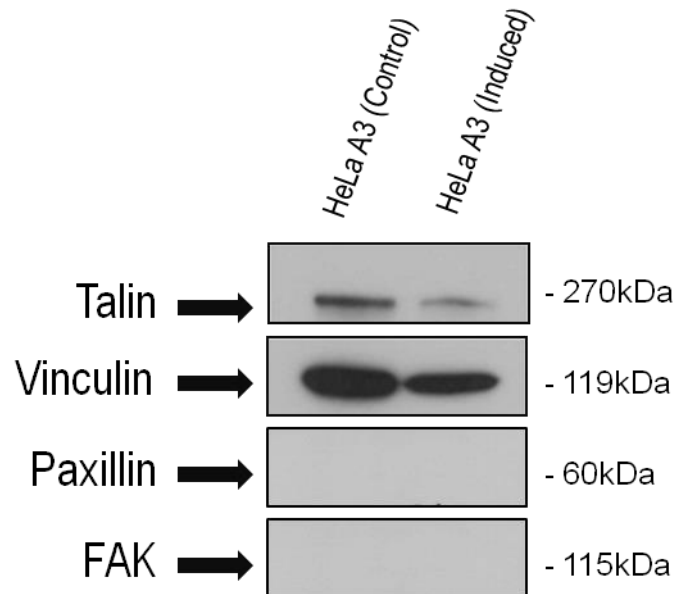
Figure 4.3. Western blotting for focal adhesion proteins in Triton-insoluble cell extracts. Example of Western blots for key focal adhesion proteins in Triton X-100 treated control, uninduced and doxycyclin-induced, S100P-overexpressing HeLa A3 cells is shown. Cells were treated with 0.5% (v/v) Triton X-100 in PBS and the residue solubilised in standard SDS-containing Sample Buffer. A significant reduction is shown in S100P expressing cells for talin (fold difference = 2.6, Student's t = 11.98, P < 0.05, n = 3) and vinculin (fold difference = 1.6, t = 8.55, P < 0.05, n = 3). No bands corresponding to paxillin or FAK were observed in this Triton-insoluble fraction. The induced cells were exposed to doxycyclin for 48 hour prior to the experiment and 4μg of protein was loaded onto an 8% (w/v) polyacrylamide gel.

4.2.2.2 Alternative methods for isolation of adhesion proteins

Due to the limitation of the detergent cell-lysis method described above, several alternative methods were attempted that had been described in the literature at the time.

The first method involved using a triethanolamine-containing low ionic strength buffer to shock hypotonically the cells, which increased cell turgidity. Cells were then exposed to a jet of PBS from a Waterpik to rupture the cells. The dishes were then washed and the adhesive cell residue removed by RIPA buffer and a cell scraper [249]. This method was attempted many times, altering all facets of the protocol; however, in all cases the resultant cell fraction contained substantial cytosolic contamination. The reason for this

contamination may have been that this method had been developed for fibroblastic cells. The increased adhesive strength of the epithelial HeLa A3 cells, together with their cell-cell junctions, meant that it was very difficult to lyse and remove all the cells using the Waterpik. The resulting Western blots showed GAP-DH contamination and very variable results for the abundance of adhesion proteins. This method was therefore deemed to be unsatisfactory.

The use of additional cross-linking agents was also attempted in order to try and anchor the adhesion complexes more firmly to the basal substratum, prior to shearing with a Waterpik. Dithiobis succinimidyl propionate and 1,4-bis[3-(2-pyridyldithio)propionamido]butane were used, these reagents cross-linked any lysine and cysteine residues [250]. Similar to the previous method, however, samples were found to be impure and variable with a large amount of DNA and cytosolic protein remaining in the processed sample.

Data for these experiments is not shown, since, in all cases, Western blots were either completely blank or indistinguishable from whole cell blots. Thus, a new method to isolate focal adhesions was sought, that of hydrodynamic cell shearing.

4.2.2.3 Hydrodynamic shearing

As described in Materials and Methods Section 2.6.2, hydrodynamic shearing of the cells using a focused water shower jet was next attempted to isolate the cell-substratum fraction. This was carried out following collaborative discussions with Professor Martin Humphries and group, who identified this method as a possible technique for isolating the epithelial cell adhesome.

4.2.2.3.1 Whole cell vs. hydrodynamically sheared samples

Figure 4.4 shows an example of a Western blot of the hydrodynamically-sheared residue from HeLa A3 cells compared to that from a whole-cell lysate. Negative controls for marker proteins of other cellular fractions were also blotted to ensure proteins from unwanted cell fractions were removed. These marker proteins were lamin-β1 (for the nuclear fraction), voltage-dependent anion channels (VDAC) (for the mitochondrial fraction) and GAP-DH (for

the cytoplasmic fraction). In all cases bands of 66kDa, 50 kDa and 37 kDa, respectively, corresponding to lamin-β1, VDAC and GAP-GD were observed in whole-cell lysates, but were not detectable in the hydrodynamically-isolated residue. Western blots for the structural adhesion proteins talin and vinculin produced bands corresponding to their reported molecular weights of 270 kDa and 119 kDa, respectively, in the isolated residue. An important improvement in this method is the appearance of paxillin, an adhesion signalling protein, in Western blots, which was absent from all other isolation methods. A clear band of 60 kDa corresponding to paxillin can be observed in the isolated residues, when the blots were exposed to X-ray film for a long exposure time (30 min).

The result of the hydrodynamic shearing procedure is that all unwanted proteins from cell fractions are removed, the structural components of the adhesion proteome (hereafter referred to as the adhesome) are maintained and some of the less strongly-bound signalling proteins of the adhesome are also present.
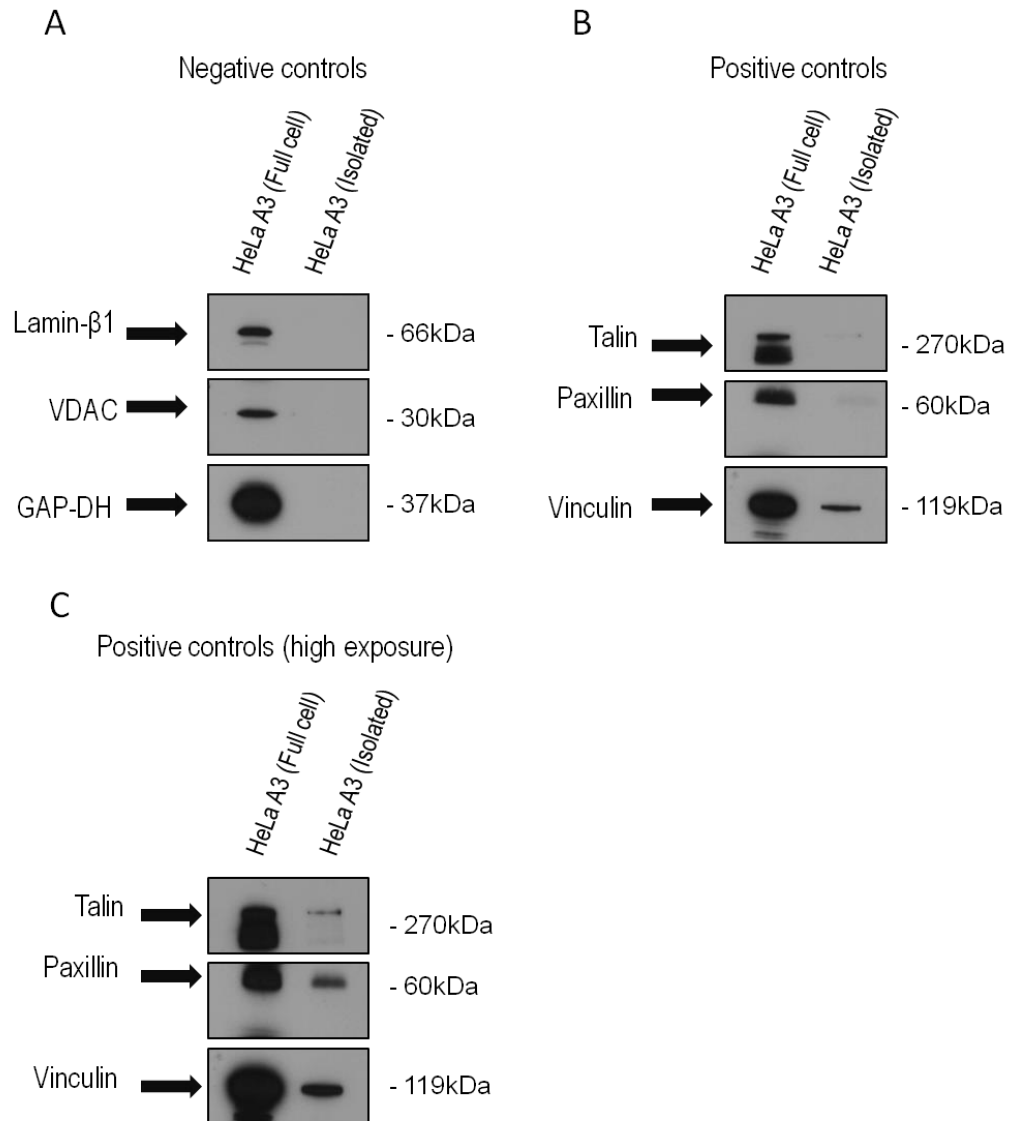
Figure 4.4. Western blotting of isolated residues of hydrodynamically-sheared HeLa A3 cells. Two 10cm diameter tissue culture dishes were exposed to a hydrodynamic force from a standardised shower. The residue was washed with PBS and dissolved in SDS-containing Sample Buffer. Positive and negative control Western blots were used to assess the purity of the residue produced from HeLa A3 cells. A) Negative control protein blots for lamin-β1 (nuclear fraction), voltage-dependent anion channel (VDAC) (mitochondrial fraction) and GAP-DH (cytoplasmic fraction) show no observable marker protein present in the isolated residue. B,C) Positive control protein blots for talin, vinculin and paxillin show the presence of these proteins in the isolated residue. C = double the exposure time of B. A 10% (w/v) polyacrylamide gel was used. For the full, uncropped Western blot see Appendix 5.

4.2.2.3.2 Western blots of hydrodynamically-sheared residues in S100P-overexpressing cells

The hydrodynamically-sheared residues from control, uninduced and S100P-induced HeLa A3 cells were compared on a Coomassie blue-stained SDS polyacrylamide gel, the pattern of protein bands was similar in both samples (Figure 4.5 panel A). Moreover, the overall intensities of the Coomassie blue-stained proteins were almost identical between both residues (1% difference). This was determined by densitometric analysis of the whole lanes. This result suggests that any differences in protein abundance may either be very minor, or it may not be possible to observe these changes using a Coomassie blue stain.

As with the previous samples, all hydrodynamically-sheared residues were analysed using Western blotting for marker proteins to ensure there was no contamination from unwanted cell fractions. Figure 4.5B shows an example of these control blots, where no bands were observed for proteins that would not typically be found in the cell adhesome, suggesting the sample has a very low level of contamination. Figure 4.5C shows an example of Western blots for focal adhesion proteins. Protein bands for talin (fold difference = 1.4, Student's t = 1.75, p = 0.22, n = 3), and vinculin (fold difference = 1.3, t = 3.37, p = 0.08, n = 3) showed no significant reduction between control, uninduced and S100P-induced cell residues. This result was slightly different from the whole-cell immunofluorescence results for vinculin (Figure 3.9) which showed a significant reduction in the number of fluorescent foci in S100P overexpressing cells. Bands for paxillin (fold difference = 1.2, t = 12.19, p = 0.01, n = 3) and FAK (fold difference = 1.3, t = 4.77, p = 0.04, n = 3) showed an apparent significant increase and decrease, respectively, in their intensities in S100P-induced residues compared to the control uninduced residues. The magnitude of these alterations are, however, below most reasonable cut-off points, in this study for example a 1.5 fold cut-off is used for all mass spectrometric experiments, below which any alterations are assumed to have a minimal effect on the cell. Similarly, the results for paxillin are unexpected, since the immunofluorescence results for paxillin (Figure 3.9) showed a significant reduction rather than increase in the number of paxillin-staining foci in S100P-overexpressing cells.
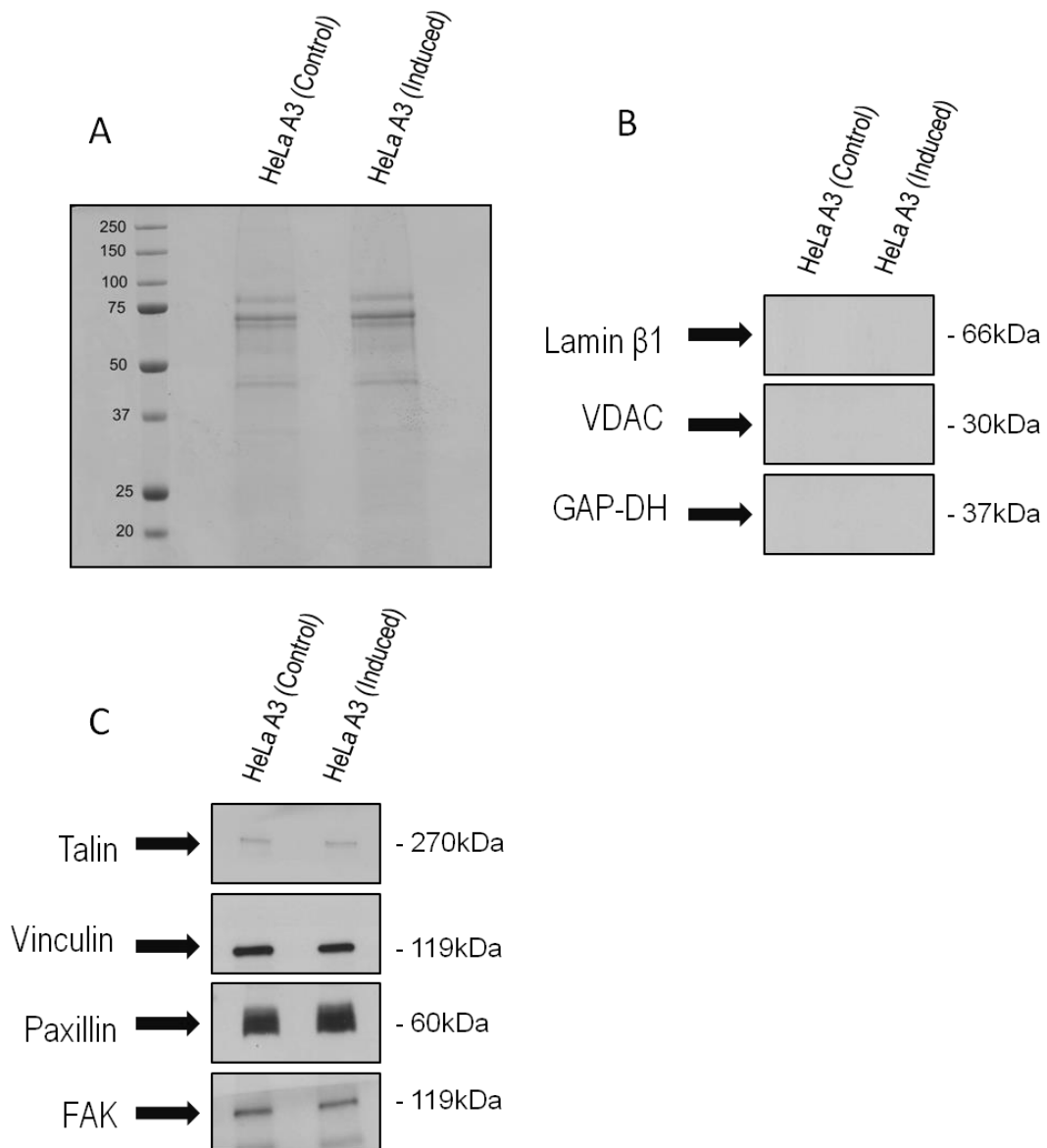
Figure 4.5. Analysis of isolated hydrodynamically-sheared residues in S100P-overexpressing HeLa A3 samples. Two 10 cm diameter tissue culture dishes were exposed to a hydrodynamic force from a standardised shower. The residue was washed with PBS and dissolved in SDS-containing Sample Buffer. Acetone precipitation was then carried out to concentrate the samples, after which the residues were suspended in 30μl of Sample Buffer and each one loaded into a single well. All samples were normalised against the number of cells present on the dish prior to shearing. A) Example of Coomassie Blue-stained gel showing protein bands present in isolated residues from control, uninduced and S100P-induced HeLa A3 cells. B) Example of negative control Western blots for lamin-β1 (nuclear fraction), voltage-dependent anion channel (VDAC) (mitochondrial fraction) and GAP-DH (cytoplasmic fraction) shows no specific subcellular markers present in the

hydrodynamically-sheared residue. C) Positive control protein blots for talin (fold reduction = 1.4, Student's t = 1.75, p = 0.22, n = 3), vinculin (fold reduction = 1.25, t = 3.37, p = 0.08, n = 3), paxillin (fold increase = 1.2, t = 12.19, p < 0.05, n = 3) and FAK (fold reduction = 1.27, t = 4.77, p < 0.05, n = 3) show no significant difference for talin and vinculin and a significant difference in paxillin and FAK in intensity of stained bands between control, uninduced and S100P-induced hydrodynamically-sheared residues from HeLa A3 cells. The induced cells were exposed to doxycyclin for 48 hours prior to the experiment and 10% (w/v) polyacrylamide gels were used.

4.2.2.3.3 Triton X-100 treatment of hydrodynamically-sheared HeLa A3 residues

The results shown in Section 4.2.2.3.1 suggest that upon S100P induction, there was little or no change in the abundance of a subset of focal adhesion proteins present in the hydrodynamically-sheared residue of HeLa A3 cells. However, this result potentially contradicts the results observed in Section 4.2.2.1 when Triton X-100 in a PBS solution was added to whole HeLa A3 cells in order to remove any cytosolic and detergent-soluble proteins, leaving only Triton X-100-insoluble cytoskeletal and adhesion-related proteins. When this Triton X-100 procedure was carried out on whole cells, a reduction was observed in the abundance of talin and vinculin. To determine if the addition of Triton X-100 was having a different effect to hydrodynamic shearing of cells, Triton X-100 in PBS was added to the hydrodynamically-sheared residue of HeLa A3 cells after the standard PBS washes, but prior to residue collection in the SDS-containing lysis buffer. Figure 4.6 shows that indeed, when the hydrodynamically-sheared residue was treated with Triton X-100, a 10-fold reduction in the abundance of talin and a 2.2 fold reduction in vinculin was observed. Moreover no bands corresponding to paxillin and FAK were observed on Western blots. These results may therefore suggest that Triton X-100 is removing more weakly bound components of the cell adhesome in HeLa A3 cells and, as such, may not be an appropriate method for analysing the total cell-extracellular matrix adhesome.
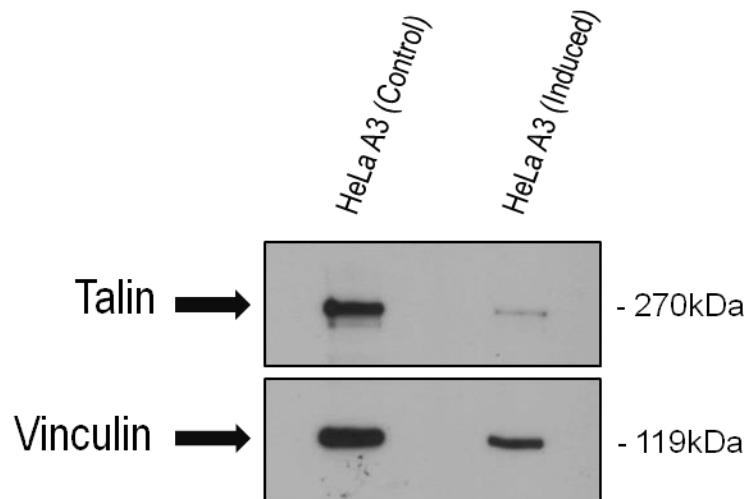
Figure 4.6. Western blotting for focal adhesion proteins in Triton X-100 treated hydrodynamically-sheared HeLa A3 cell residues. Two 10 cm diameter tissue culture dishes were exposed to a hydrodynamic force from a standardised shower. The residues were washed with PBS, then treated with Triton X-100 in PBS, washed again with PBS and then the remaining residue dissolved in SDS-containing Sample Buffer. Acetone precipitation was then carried out to concentrate the samples, after which the residues were resuspended in 30µl of Sample Buffer and each loaded into a single well. Both samples were normalised against the number of cells present on the dish prior to shearing. A 10 fold and 2.2 fold reduction in the intensity of the blotted band for talin and vinculin, respectively, was observed in the S100P-induced HeLa A3 cell residue compared to the control, uninduced cell residue. The induced cells were exposed to doxycyclin for 48 hours prior to the experiment and 10% (w/v) polyacrylamide gels were used.

4.2.2.3.4 Immunofluorescent staining of hydrodynamically-sheared HeLa A3 residues

In order to compare results obtained by Western blots for the hydrodynamically-sheared residues with an *in situ* technique, antibodies to vinculin were used to stain immunofluorescently the adhesion foci, since they gave a stronger signal than antibodies to the other focal adhesion proteins. The results were standardised to the number of cells on each dish prior to shearing, since the outline of the cells was now no longer apparent. Figure 4.7 shows that the hydrodynamically-sheared residues from S100P-induced HeLa A3 cells produced a significantly lower (2.7-fold decrease, Student's t = 12.52, P < 0.0001)

number of punctate structures containing immunoreactive vinculin compared to the control, uninduced cell residues (vinculin control, uninduced mean = 106, SD = 29.9, S100P induced mean = 39, SD = 16.7, t = 12.52, P < 0.0001, foci in 30 fields of view counted in n = 3 experiments). The decrease in the number of immunoreactive vinculin-containing foci was greater than that previously seen in the immunofluorescently-stained whole cells (Figure 3.9), perhaps due to it being easier to count the foci when most of the other cellular components were removed. These results were, however, consistent with the 2.2 fold reduction in Western blots of Triton X-100-treated, hydrodynamically-sheared residues.

A

HeLa A3
(Control)
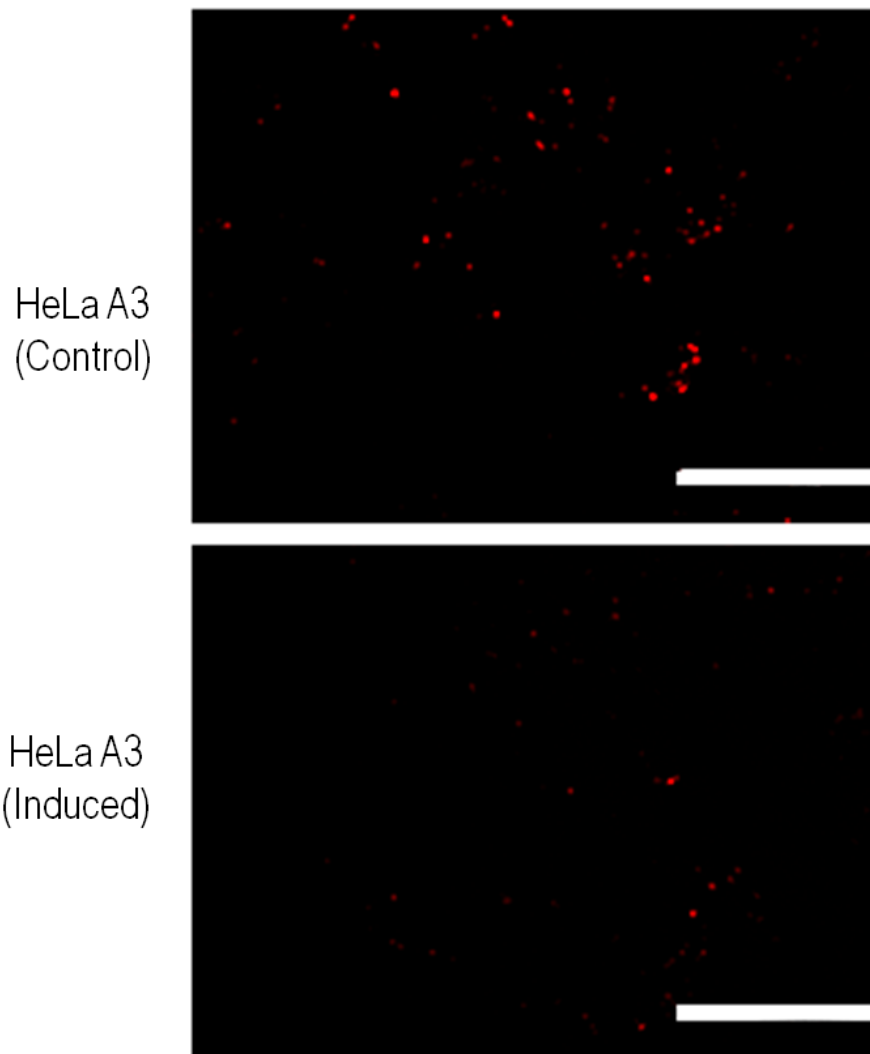
HeLa A3
(Induced)

B
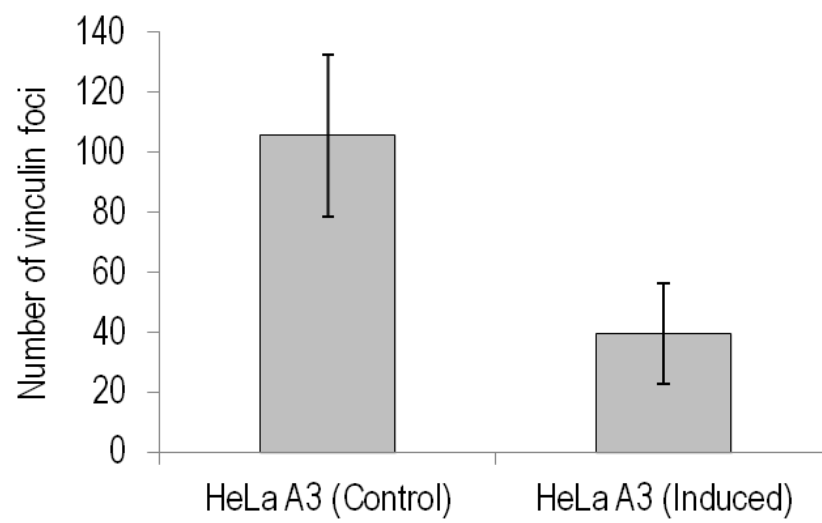
Figure 4.7. Immunofluorescent staining of hydrodynamically-sheared cell residues. A) Uninduced control and S100P-induced HeLa A3 cells were hydrodynamically sheared and the resultant residues were immunofluorescently stained for vinculin. White bars = 100μm. B) The number of foci stained for vinculin per field of view showed a significant 2.7 fold decrease in the S100P-induced HeLa cells compared to the control, uninduced cells (vinculin control uninduced mean = 106, SD = 29.9, S100P-induced mean = 39, SD = 16.7, Student's t = 12.52; P < 0.05, foci in 30 fields of view counted in n = 3 experiments). Values were normalised based on the number of HeLa A3 cells originally adhered to the dishes.

4.2.2.3.5 Mass spectrometry of adhesome residue

Mass spectrometry on the hydrodynamically-sheared cell residues was undertaken for two reasons. Firstly, to determine whether the Western blots for the abundance of focal adhesion proteins reported in Figure 4.5 can be validated using this higher resolution technique. The second reason was to determine if there were any alterations in potentially novel proteins present at the adhesive interface as a result of S100P overexpression.

4.2.2.4.1 Explorative adhesome mass spectrometry

Mass spectrometry was initially performed only on residues from hydrodynamically-sheared control, uninduced HeLa cells. The mass spectrometric analysis yielded a full list of proteins that were present in this cell fraction (Table 4.3). This result gives insight into the diversity of proteins that are present within this cell fraction, the majority being extracellular matrix, cytoskeletal or proteins associated with the plasma membrane. A range of proteins were also present that either bind to these groups of proteins, or are present on the cell membrane and, as such are preserved within the sheared residue. However, there are some nuclear proteins present such as histone H4, which are unexpected in this cell fraction, as they should have been removed during the hydrodynamic shearing process. One explanation for proteins such as this is histones carry a positive charge and, as such, when the cells are lysed, they may have bound adventitiously to heparan sulphate chains or to phosphatidyl inositol membrane patches, both of which are strongly negatively charged [265-267]. An additional important point to note is the lack of focal adhesion signalling proteins such as paxillin and FAK, which, as

previously shown by Western blots are definitely present within the hydrodynamically-sheared protein residue. Even after repeated runs, these signalling proteins were not detected by mass spectrometry, but were routinely observed at low levels in all Western blots. The reason for this is currently unclear, but may reflect a lack of sensitivity of the mass spectrometric technique.

Acetone precipitation-treated hydrodynamically-sheared HeLa A3 cell mass spectrometry			
Protein / gene name	**UniProt ID**	**Cellular location**	**Adhesome Protein**
tubulin, beta 1 class VI	Q9H4B7	Cytoplasm	Yes
four and a half LIM domains 1	Q5JXI8	Cytoplasm	Yes
filamin A, alpha	Q5HY54	Cytoplasm	Yes
tubulin, alpha 1b	P68363	Cytoplasm	Yes
actin, alpha, cardiac muscle 1	P68032	Cytoplasm	Yes
actin, beta	P60709	Cytoplasm	Yes
keratin 2, type II	P35908	Cytoplasm	Yes
myosin, heavy chain 9, non-muscle	P35579	Cytoplasm	Yes
keratin 9, type I	P35527	Cytoplasm	Yes
keratin 5, type II	P13647	Cytoplasm	Yes
keratin 10, type I	P13645	Cytoplasm	Yes
keratin 16, type I	P08779	Cytoplasm	Yes
keratin 1, type II	P04264	Cytoplasm	Yes
keratin 6B, type II	P04259	Cytoplasm	Yes
keratin 14, type I	P02533	Cytoplasm	Yes
actinin, alpha 4	O43707	Cytoplasm	Yes
myosin, light chain 12A, regulatory, non-sarcomeric	J3QRS3	Cytoplasm	Yes
myosin, light chain 6, alkali, smooth muscle and non-muscle	G3V1V0	Cytoplasm	Yes
vimentin	B0YJC4	Cytoplasm	Yes
tubulin, alpha 4a	A8MUB1	Cytoplasm	Yes
stonin 2	Q8WXE9	Cytoplasm	Possible interaction
RAB12, member RAS oncogene family	Q6IQ22	Cytoplasm	Possible Interaction
peptidylprolyl isomerase A (cyclophilin A)	P62937	Cytoplasm	Possible interaction
ribosomal protein S13	P62277	Cytoplasm	Possible interaction
RAP1B, member of RAS oncogene family	P61224	Cytoplasm	Possible interaction
lipoprotein lipase	P06858	Cytoplasm	Possible interaction
quiescin Q6 sulfhydryl oxidase 1	O00391	Cytoplasm	Possible interaction
aldolase A, fructose-bisphosphate	J3KPS3	Cytoplasm	Possible interaction
nucleobindin 1	H7BZI1	Cytoplasm	Possible interaction
nascent polypeptide-associated complex alpha subunit	H0YHX9	Cytoplasm	Possible interaction
heat shock 70kDa protein 8	E9PKE3	Cytoplasm	Possible interaction
triosephosphate isomerase 1	U3KPZ0	Cytoplasm	No
heat shock protein 90kDa alpha (cytosolic), class A member 1	Q86U12	Cytoplasm	No
glyceraldehyde-3-phosphate dehydrogenase	P04406	Cytoplasm	No
lactate dehydrogenase A	P00338	Cytoplasm	No

adaptor-related protein complex 2, alpha 1 subunit	O95782	Cytoplasm	No
biliverdin reductase B	M0QZL1	Cytoplasm	No
adaptor-related protein complex 2, sigma 1 subunit	M0QYZ2	Cytoplasm	No
calpain, small subunit 1	K7EIV0	Cytoplasm	No
ubiquitin B	J3QS39	Cytoplasm	No
pyruvate kinase, muscle	H3BTN5	Cytoplasm	No
signal recognition particle 14kDa (homologous Alu RNA binding protein)	H0YLA2	Cytoplasm	No
adaptor-related protein complex 2, mu 1 subunit	E9PFW3	Cytoplasm	No
family with sequence similarity 179, member A	Q6ZUX3	Cytoplasm	No
S100 calcium binding protein A1	Q5T7Y6	Cytoplasm	Indirect Signalling
profilin 1	P07737	Cytoplasm	Indirect Signalling
enolase 1, (alpha)	P06733	Cytoplasm	Indirect Signalling
thrombospondin, type I, domain containing 4	Q6ZMP0	Cytoplasm	Indirect Signalling
GLI pathogenesis-related 2	Q5VZR0	Cytoplasm	Indirect Signalling
transgelin 2	P37802	Cytoplasm	Indirect Signalling
related RAS viral (r-ras) oncogene homolog	P10301	Cytoplasm	Indirect Signalling
myeloperoxidase	P05164	Cytoplasm	Indirect Signalling
secretory leukocyte peptidase inhibitor	P03973	Cytoplasm	Indirect Signalling
neural precursor cell expressed, developmentally down-regulated 4, E3 ubiquitin protein ligase	H0Y8H4	Cytoplasm	Indirect Signalling
heat shock 27kDa protein 1	F8WE04	Cytoplasm	Indirect Signalling
NME/NM23 nucleoside diphosphate kinase 1	E7ERL0	Cytoplasm	Indirect Signalling
wingless-type MMTV integration site family, member 5A	P41221	Extracellular Space	Yes
TIMP metallopeptidase inhibitor 3	P35625	Extracellular Space	Yes
fibrillin 2	P35556	Extracellular Space	Yes
fibrillin 1	P35555	Extracellular Space	Yes
tenascin C	P24821	Extracellular Space	Yes
collagen, type V, alpha 1	P20908	Extracellular Space	Yes
collagen, type VI, alpha 1	P12109	Extracellular Space	Yes
laminin, gamma 1 (formerly LAMB2)	P11047	Extracellular Space	Yes
thrombospondin 1	P07996	Extracellular Space	Yes
vitronectin	P04004	Extracellular Space	Yes
EGF-like repeats and discoidin I-like domains 3	O43854	Extracellular Space	Yes
laminin, alpha 5	O15230	Extracellular Space	Yes
gelsolin	F5H1A8	Extracellular Space	Yes
inter-alpha-trypsin inhibitor heavy chain 2	Q5T985	Extracellular Space	Possible interaction
bone morphogenetic protein 1	P13497	Extracellular Space	Possible interaction
serpin peptidase inhibitor, clade E (nexin, plasminogen activator inhibitor type 1), member 1	P05121	Extracellular Space	Possible interaction
apolipoprotein H (beta-2-glycoprotein I)	P02749	Extracellular Space	Possible interaction
sema domain, immunoglobulin domain (Ig), short basic domain, secreted, (semaphorin) 3D	O95025	Extracellular Space	Possible interaction
complement factor I	G3XAM2	Extracellular Space	Possible interaction
C-type lectin domain family 3, member B	E9PHK0	Extracellular Space	Possible interaction
inter-alpha-trypsin inhibitor heavy chain 3	E7ET33	Extracellular Space	Possible interaction
serpin peptidase inhibitor, clade F (alpha-2 antiplasmin, pigment epithelium derived factor), member 2	C9JMH6	Extracellular Space	Possible interaction
C1q and tumor necrosis factor related protein 3	Q9BXJ4	Extracellular Space	No
peroxidasin	Q92626	Extracellular Space	No
ribonuclease, RNase A family, 4	P34096	Extracellular Space	No
pregnancy-zone protein	P20742	Extracellular Space	No
complement component 4B (Chido blood group)	P0C0L4	Extracellular Space	No

alpha-2-macroglobulin	P01023	Extracellular Space	No
serpin peptidase inhibitor, clade C (antithrombin), member 1	P01008	Extracellular Space	No
coagulation factor X	P00742	Extracellular Space	No
coagulation factor XIII, A1 polypeptide	P00488	Extracellular Space	No
alpha-fetoprotein	J3KMX3	Extracellular Space	No
albumin	H0YA55	Extracellular Space	No
hemoglobin, alpha 1	G3V1N2	Extracellular Space	No
coagulation factor II (thrombin)	E9PIT3	Extracellular Space	No
lactotransferrin	E7EQB2	Extracellular Space	No
platelet derived growth factor C	B4E3A5	Extracellular Space	No
SPARC related modular calcium binding 1	Q9H4F8	Extracellular Space	Indirect Signalling
HtrA serine peptidase 1	Q92743	Extracellular Space	Indirect Signalling
transforming growth factor, beta-induced, 68kDa	Q15582	Extracellular Space	Indirect Signalling
sema domain, immunoglobulin domain (Ig), short basic domain, secreted, (semaphorin) 3A	Q14563	Extracellular Space	Indirect Signalling
hyaluronan binding protein 2	Q14520	Extracellular Space	Indirect Signalling
HtrA serine peptidase 3	P83110	Extracellular Space	Indirect Signalling
dermcidin	P81605	Extracellular Space	Indirect Signalling
microfibrillar-associated protein 2	P55001	Extracellular Space	Indirect Signalling
lumican	P51884	Extracellular Space	Indirect Signalling
tissue factor pathway inhibitor 2	P48307	Extracellular Space	Indirect Signalling
serpin peptidase inhibitor, clade F (alpha-2 antiplasmin, pigment epithelium derived factor), member 1	P36955	Extracellular Space	Indirect Signalling
connective tissue growth factor	P29279	Extracellular Space	Indirect Signalling
lysyl oxidase	P28300	Extracellular Space	Indirect Signalling
insulin-like growth factor binding protein 5	P24593	Extracellular Space	Indirect Signalling
glutathione peroxidase 3	P22352	Extracellular Space	Indirect Signalling
insulin-like growth factor binding protein 2, 36kDa	P18065	Extracellular Space	Indirect Signalling
insulin-like growth factor binding protein 3	P17936	Extracellular Space	Indirect Signalling
tissue factor pathway inhibitor (lipoprotein-associated coagulation inhibitor)	P10646	Extracellular Space	Indirect Signalling
serpin peptidase inhibitor, clade E (nexin, plasminogen activator inhibitor type 1), member 2	P07093	Extracellular Space	Indirect Signalling
serpin peptidase inhibitor, clade A (alpha-1 antiproteinase, antitrypsin), member 7	P05543	Extracellular Space	Indirect Signalling
histidine-rich glycoprotein	P04196	Extracellular Space	Indirect Signalling
apolipoprotein B	P04114	Extracellular Space	Indirect Signalling
alpha-2-HS-glycoprotein	P02765	Extracellular Space	Indirect Signalling
apolipoprotein E	P02649	Extracellular Space	Indirect Signalling
apolipoprotein A-I	P02647	Extracellular Space	Indirect Signalling
insulin-like growth factor 2	P01344	Extracellular Space	Indirect Signalling
complement component 5	P01031	Extracellular Space	Indirect Signalling
complement component 3	P01024	Extracellular Space	Indirect Signalling
protease, serine, 23	O95084	Extracellular Space	Indirect Signalling
gremlin 1, DAN family BMP antagonist	O60565	Extracellular Space	Indirect Signalling
cysteine-rich, angiogenic inducer, 61	O00622	Extracellular Space	Indirect Signalling
vascular endothelial growth factor A	H0Y2S8	Extracellular Space	Indirect Signalling
cartilage oligomeric matrix protein	G3XAP6	Extracellular Space	Indirect Signalling
latent transforming growth factor beta binding protein 2	G3V3X5	Extracellular Space	Indirect Signalling
midkine (neurite growth-promoting factor 2)	E9PLM6	Extracellular Space	Indirect Signalling
fibrinogen beta chain	D6REL8	Extracellular Space	Indirect Signalling
periostin, osteoblast specific factor	B1ALD9	Extracellular Space	Indirect Signalling

apolipoprotein C-III	B0YIW2	Extracellular Space	Indirect Signalling
histone cluster 1, H2bn	U3KQK0	Nucleus	No
coiled-coil domain containing 80	Q76M96	Nucleus	No
brain abundant, membrane attached signal protein 1	P80723	Nucleus	No
small nuclear ribonucleoprotein D2 polypeptide 16.5kDa	P62316	Nucleus	No
small nuclear ribonucleoprotein polypeptide E	P62304	Nucleus	No
histone cluster 1, H1e	P10412	Nucleus	No
transforming growth factor beta 1 induced transcript 1	O43294	Nucleus	No
ribosomal protein L22	K7EJT5	Nucleus	No
RAN, member RAS oncogene family	H0YFC6	Nucleus	No
Y box binding protein 1	H0Y449	Nucleus	No
small nuclear ribonucleoprotein polypeptide G	F5H013	Nucleus	No
cysteine and glycine-rich protein 1	E9PP21	Nucleus	No
peptidylprolyl isomerase E (cyclophilin E)	E9PEQ6	Nucleus	No
small nuclear ribonucleoprotein polypeptide N	B3KVR1	Nucleus	No
H3 histone, family 3C	Q6NXT2	Nucleus	No
nephronectin	Q6UXI9	Plasma Membrane	Yes
fibronectin type III domain containing 1	Q4ZHG4	Plasma Membrane	Yes
ras-related C3 botulinum toxin substrate 1 (rho family, small GTP binding protein Rac1)	P63000	Plasma Membrane	Yes
LIM and senescent cell antigen-like domains 1	P48059	Plasma Membrane	Yes
basigin (Ok blood group)	P35613	Plasma Membrane	Yes
moesin	P26038	Plasma Membrane	Yes
integrin, beta 5	P18084	Plasma Membrane	Yes
integrin, alpha 5 (fibronectin receptor, alpha polypeptide)	P08648	Plasma Membrane	Yes
integrin, alpha V	P06756	Plasma Membrane	Yes
integrin, beta 1 (fibronectin receptor, beta polypeptide, antigen CD29 includes MDF2, MSK12)	P05556	Plasma Membrane	Yes
integrin, beta 3 (platelet glycoprotein IIIa, antigen CD61)	P05106	Plasma Membrane	Yes
agrin	O00468	Plasma Membrane	Yes
integrin-linked kinase	B7Z1I0	Plasma Membrane	Yes
guanine nucleotide binding protein (G protein), alpha 13	Q14344	Plasma Membrane	Possible interaction
apolipoprotein M	Q5SRP5	Plasma Membrane	No
coagulation factor V (proaccelerin, labile factor)	P12259	Plasma Membrane	No
tumor necrosis factor receptor superfamily, member 11b	O00300	Plasma Membrane	No
transferrin receptor	G3V0E5	Plasma Membrane	No
CD59 molecule, complement regulatory protein	E9PNW4	Plasma Membrane	No
solute carrier family 2 (facilitated glucose transporter), member 1	C9JIM8	Plasma Membrane	No
CD55 molecule, decay accelerating factor for complement (Cromer blood group)	B1AP13	Plasma Membrane	No
guanine nucleotide binding protein (G protein), beta polypeptide 1	B1AKQ8	Plasma Membrane	No
plasminogen activator, urokinase receptor	M0QYR6	Plasma Membrane	Indirect Signalling
solute carrier family 3 (amino acid transporter heavy chain), member 2	J3KPF3	Plasma Membrane	Indirect Signalling
annexin A2	H0YMD0	Plasma Membrane	Indirect Signalling

Table 4.3 Mass spectrometric identification of proteins in hydrodynamically-sheared residue of HeLa A3 cells using acetone precipitation. Three 10 cm diameter tissue culture dishes (6 x10^6 cells) were exposed to a hydrodynamic force from a standardised shower. The residue was washed with PBS and dissolved in SDS-containing sample buffer. SDS was removed using acetone precipitation for sample preparation before liquid chromatography followed by MS-MS mass spectrometry (LC-MS). A total of 171 proteins were identified from two independently isolated samples. Proteins were designated as an adhesome protein (yes) if they were considered to be either an adhesive protein or a protein that directly affects cell adhesion. Proteins noted as having indirect signalling designation have an effect on cellular adhesion via intermediate pathways, complexes or signalling events. Proteins noted as having a possible interaction are those with a uniprot entry that suggests either localisation to sites of adhesion or that have a structure / function that may relate to adhesion but lack substantial evidence. Proteins were only designated as "No" if they had no link to cellular adhesion. QIAGEN'S Ingenuity Pathway Analysis was used for determining the cellular localisation of each protein. The proteins "adhesome" status was determined using the corresponding Uniprot entry.

4.2.2.4.2 Limitations in adhesome analysis

When the explorative mass spectrometric determination of proteins that were present in the hydrodynamically-sheared residue was complete, a comparative experiment to investigate differences in relative amounts of proteins was undertaken between control, uninduced and S100P-overexpressing HeLa A3 cells. Relative comparisons of protein abundance using this method, however, proved to be impossible using the current method of sample preparation due to broadening and time drift of the peaks of the tryptic peptides during LC analysis. Figure 4.8 shows the complete base peak ion chromatogram of tryptic peptides from two control and two S100P-induced sheared cell residue samples. It is clear that there was considerable variability between the two control, and between the two S100P-induced sheared samples, as well as between control and S100P-induced sample peaks. This variability has been exemplified in Figure 4.9, where a single peak of tryptic peptides at a (m/v) of 710.35 has been isolated. This peak elutes at different times between samples and is substantially broad, making peptide identification difficult and relative quantification using the Progenesis programme impossible. It was thought that this

artefact was due to contamination of the samples by SDS resulting from insufficient removal during acetone precipitation and washings.

In order to be able to perform relative quantification on the isolated residues, an alternative method in which all the SDS could be removed was required.
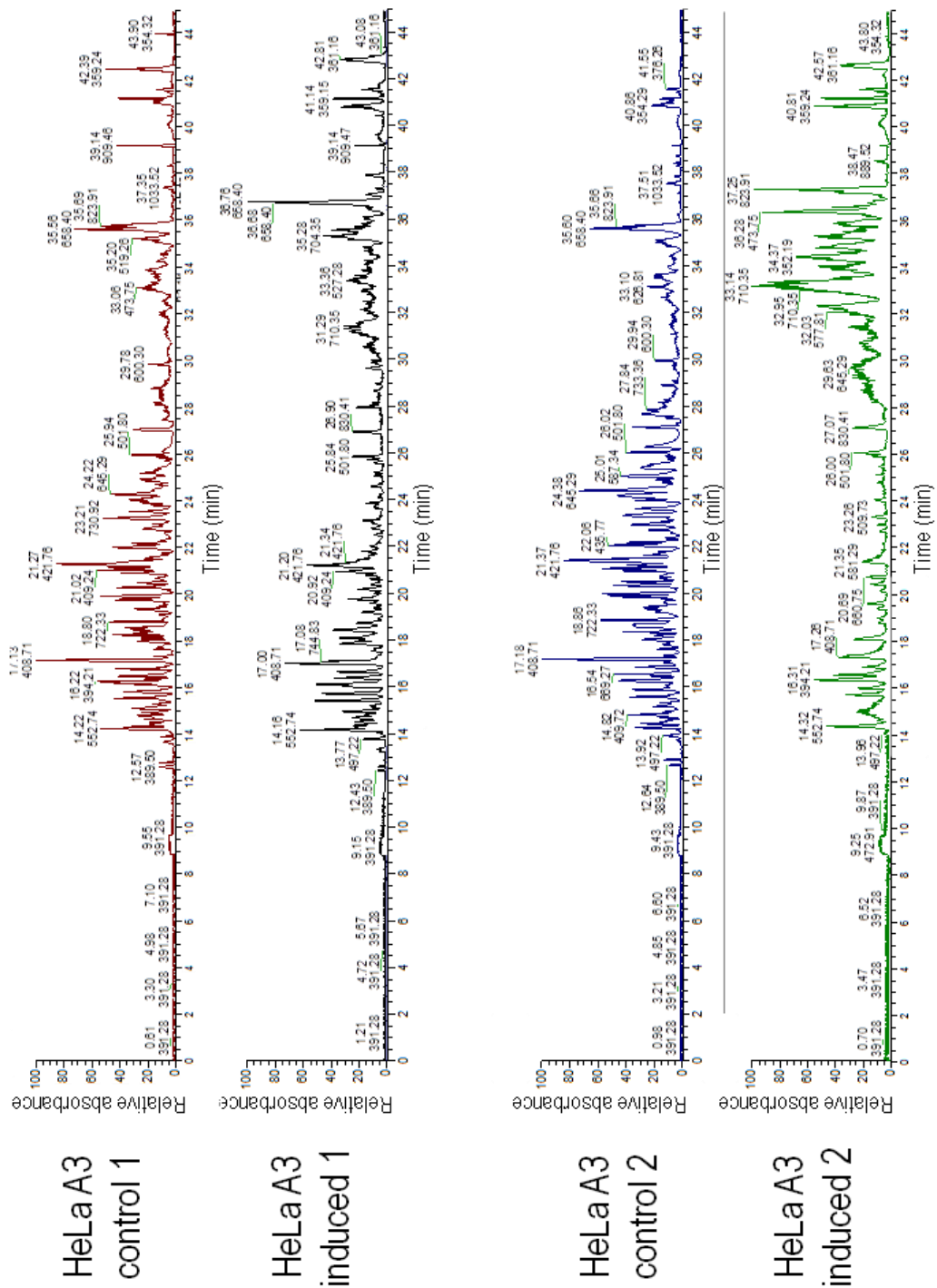
Figure 4.8. Base peak ion chromatogram of tryptic peptides from hydrodynamically-sheared residues of HeLa A3 cells purified using acetone precipitation. Two hydrodynamically-sheared control, uninduced and two S100P-induced HeLa A3 cell residues were run on LC-MS. The relative absorbance of the tryptic peptides, eluted with time is shown together with the m/v of the major peptide peaks and time of elution.

147

Roughly 180 proteins were identified per run. Three 10cm diameter tissue culture dishes (6 x10^6 cells) were exposed to a hydrodynamic force from a standardised shower per sample. The residue was washed with PBS and suspended in SDS-containing sample buffer. The induced cells were exposed to doxycyclin for 48 hours prior to the experiment. SDS was removed by precipitation with acetone before LC-MS.
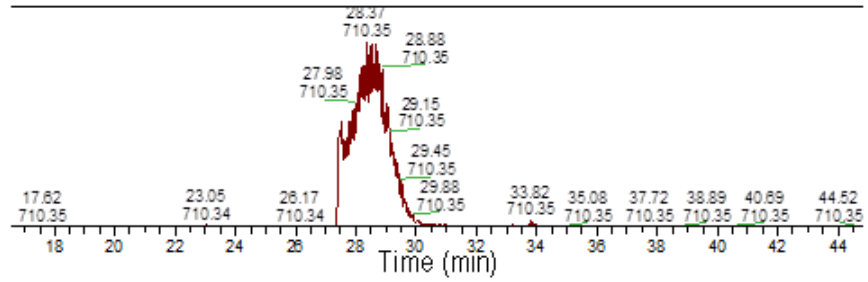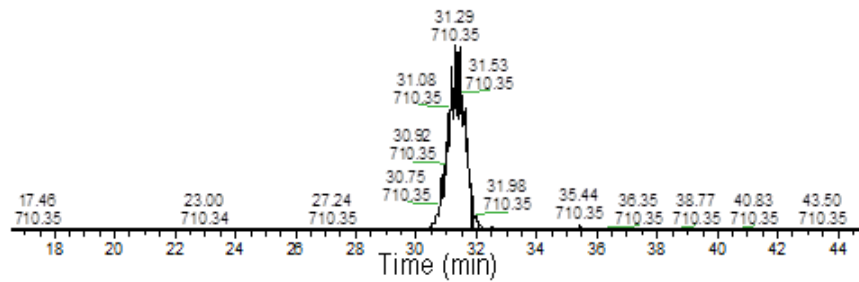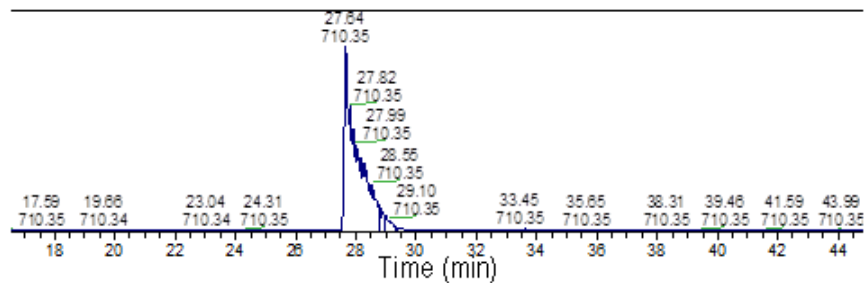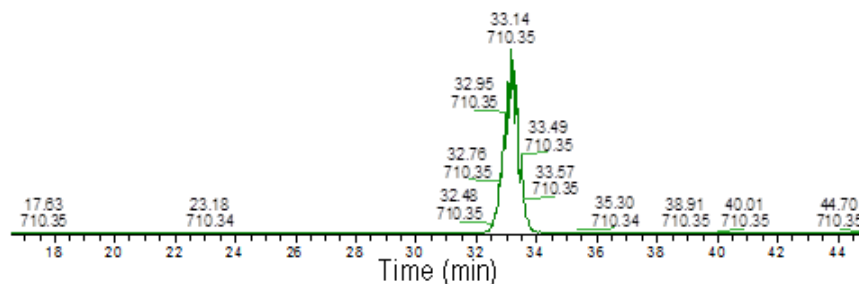
Figure 4.9. Extracted ion chromatogram of acetone precipitated HeLa A3 residues from Figure 4.8 for ion peak 710.35 (m/v). The relative absorbance against time of elution in minutes has been extracted for this tryptic peptide peak at 710.35 (m/v). Peak drift and peak broadening can be observed making label-free quantification using the Progenesis programme impossible. The SDS was removed by precipitation with acetone before LC-MS.

4.2.2.4.3 Use of filter-aided sample preparation (FASP) as a viable method for comparative mass spectrometry

As discussed in Materials and Methods Section 2.7.2.2, FASP was selected as a replacement method instead of precipitation with acetone to remove SDS from the hydrodynamically-sheared residues. When this method was used, the peaks of the tryptic peptides in both the base peak ion chromatogram (Figure 4.10A) and in an extracted ion chromatogram (Figure 4.10B) align, with no peak drift and a suitably sharp peak width. This profile is especially noticeable when compared to the ion chromatograms shown in Figures 4.8 and 4.9.

Moreover, a larger number of proteins were identified by using FASP (488) rather than by acetone precipitation (171). Due to the increased number of proteins, a representative list is presented in Table 4.4 with the full list of proteins obtained from mass spectrometry shown in Appendix 4. Similar to the list of proteins obtained from hydrodynamically-sheared HeLa A3 cells, followed by acetone precipitation, a range of proteins were present from all cellular compartments. As would be expected, there were a number of proteins that would be considered adhesome proteins also present at the plasma membrane, either because they are key adhesion proteins or because they directly affect cell adhesion. The structural focal adhesion proteins talin and vinculin were both present, as well as a number of integrins. However, as with the acetone precipitation method of removing SDS, signalling-based focal adhesion proteins like paxillin and FAK were absent from the list. Cell-cell adhesion proteins were also present, such as the desmosomal proteins: plakophilin, desmocollin and desmoglein. Indirect adhesion signalling proteins that could be localised to the cell membrane were also present such as plasminogen activator, which enables matrix metalloproteinase activity, and annexin, which can act as a membrane scaffolding protein, binding important adhesion-signalling lipids such as PIP2.

Similar to the technique of acetone precipitation several nuclear proteins were also present. It is not possible to say for certain why these proteins occurred in this sheared fraction when all nuclear material should have been removed. However, as stated previously, histones carry a positive charge and, as such, when cells were lysed, they may have bound electrostatically to heparan sulphate chains or phosphatidyl inositol-enriched membrane patches, which are negatively charged. This explanation does not, however explain why some histones are present in the list and not others. For the purposes of this

experiment it is suggested that any nuclear proteins are contaminants and are present due to non-specific binding during cell lysis.

Within the extracellular space fraction a number of extracellular matrix proteins were identified including collagens, laminins, fibrillins and fibronectin. Other extracellular matrix-binding proteins such as heparan sulfate proteoglycan 2 and fibrinogen chains which have a role in cell adhesion were also observed. Several proteins commonly found in cell culture serum (transferrin, alpha-fetoprotein, albumin) were identified; this result shows that trace amounts of serum may have still been present following hydrodynamic shearing. The extracellular proteins also included several matrix metalloproteinases such as plasminogen and several proteins such as osteoglycin which can bind to heparin sulphate chains.

Many cytoskeletal elements found within the cytoplasm were also identified including those of the actin / myosin cytoskeleton and microtubule structures. Furthermore, proteins involved in adhesion and migration signalling such as RAP1 and representatives of members of the S100 proteins were also present. There were several heat shock proteins, which may have a hitherto unsuspected role in adhesion signalling or they may be contaminants. A few ribosomal proteins were also identified. It is not clear whether these are present because they bind negatively charged polymers (rRNA, heparan sulfate, phosphatidyl inositol-enriched membrane patches) and so are contaminants or, since in several cases there has been evidence to suggest that they may localise to sites of cell-extracellular matrix adhesion, that they are a bona fide adhesion proteins.

Based on the quality of both the chromatogram alignment and protein content results, the FASP method was deemed to be suitable for more extensive experiments to determine quantifiable differences between isolated, control and S100P-induced hydrodynamically-sheared cell residues.
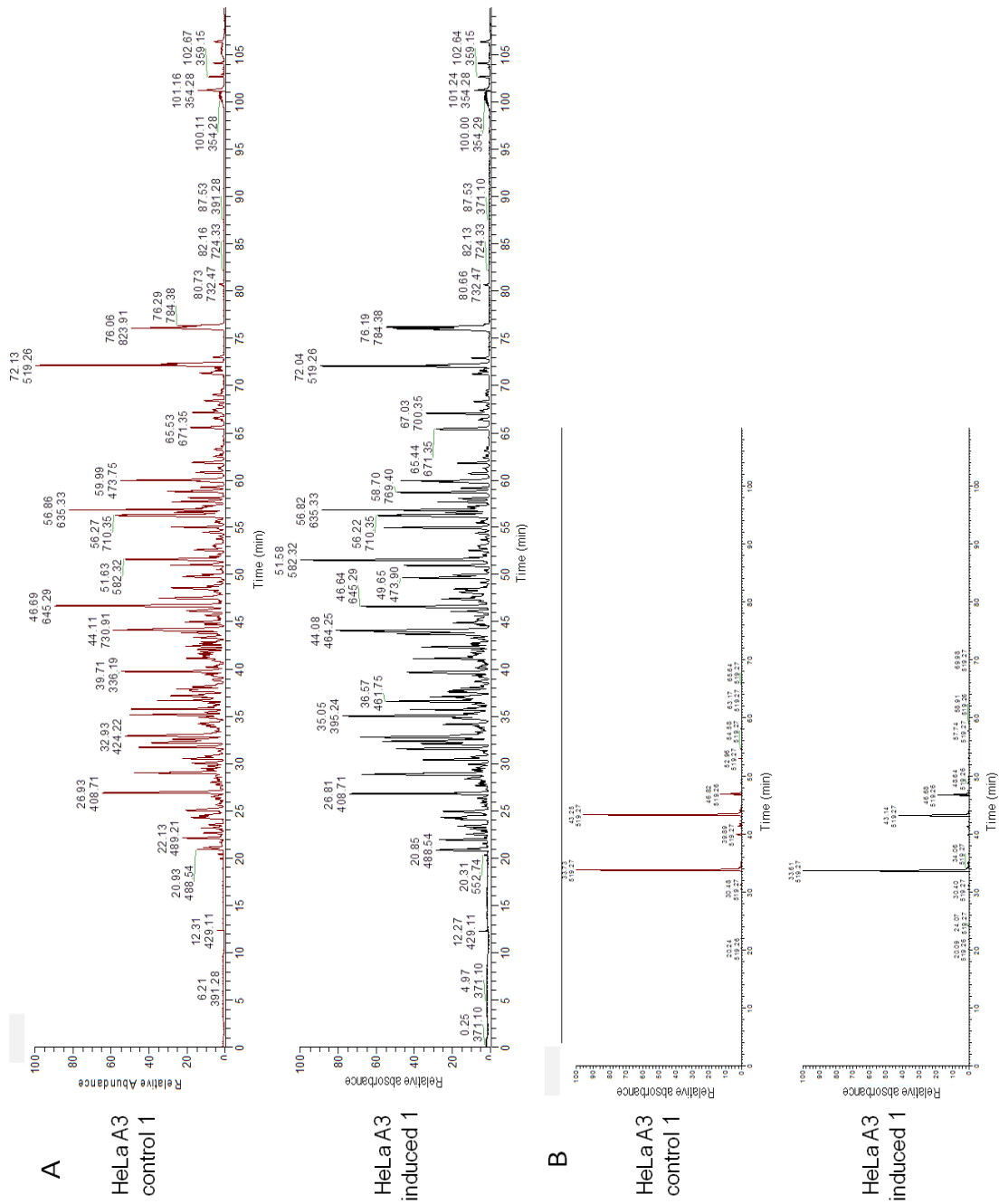
Figure 4.10. Peak ion chromatograms for FASP-treated, hydrodynamically-sheared HeLa A3 cell residues. The relative absorbance at 280nm was recorded using LC for FASP processed, control, uninduced and S100P-induced, HeLa A3 hydrodynamically-sheared cell residues. A) Base peak ion chromatogram from hydrodynamically-sheared, uninduced control and S100P-induced HeLa A3 cell samples. The elution time for the major peaks of tryptic peptides and the mean mass ions (m/v) were recorded on the trace. B) Extracted ion chromatogram from FASP-treated HeLa A3 residues using a peak extracted at 519.27 (m/v).

Using the FASP exchange method the tryptic peptide peaks line up and are suitably sharp, allowing for quantification.

FASP-treated hydrodynamically-sheared HeLa A3 cell mass spectrometry			
Protein / Gene name	**UniProt ID**	**Cellular Location**	**Adhesome protein**
talin 1	Q9Y490	Plasma Membrane	Yes
testin LIM domain protein	Q9UGI8	Plasma Membrane	Yes
nephronectin	Q6UXI9	Plasma Membrane	Yes
plakophilin 1	Q13835	Plasma Membrane	Yes
integrin-linked kinase	Q13418	Plasma Membrane	Yes
desmocollin 1	Q08554	Plasma Membrane	Yes
desmoglein 1	Q02413	Plasma Membrane	Yes
integrin, alpha 3 (antigen CD49C, alpha 3 subunit of VLA-3 receptor)	P26006	Plasma Membrane	Yes
vinculin	P18206	Plasma Membrane	Yes
integrin, beta 5	P18084	Plasma Membrane	Yes
endoglin	P17813	Plasma Membrane	Yes
desmoplakin	P15924	Plasma Membrane	Yes
integrin, alpha 5 (fibronectin receptor, alpha polypeptide)	P08648	Plasma Membrane	Yes
integrin, alpha V	P06756	Plasma Membrane	Yes
integrin, beta 1 (fibronectin receptor, beta polypeptide, antigen CD29 includes MDF2, MSK12)	P05556	Plasma Membrane	Yes
integrin, beta 3 (platelet glycoprotein IIIa, antigen CD61)	P05106	Plasma Membrane	Yes
plasminogen activator, urokinase receptor	Q03405	Plasma Membrane	Indirect Signalling
annexin A2	P07355	Plasma Membrane	Indirect Signalling
H1 histone family, member X	Q92522	Nucleus	No
histone cluster 2, H2bf	Q5QNW6	Nucleus	No
histone cluster 1, H1e	P10412	Nucleus	No
H2A histone family, member Z	P0C0S5	Nucleus	No
histone cluster 1, H2bj	P06899	Nucleus	No
small nuclear ribonucleoprotein polypeptide G	P62308	Nucleus	No
small nuclear ribonucleoprotein polypeptide F	P62306	Nucleus	No
small nuclear ribonucleoprotein polypeptide E	P62304	Nucleus	No
collagen, type XII, alpha 1	Q99715	Extracellular Space	Yes
laminin, alpha 4	Q16363	Extracellular Space	Yes

heparan sulfate proteoglycan 2	P98160	Extracellular Space	Yes
fibrillin 2	P35556	Extracellular Space	Yes
fibrillin 1	P35555	Extracellular Space	Yes
collagen, type VIII, alpha 1	P27658	Extracellular Space	Yes
tenascin C	P24821	Extracellular Space	Yes
collagen, type V, alpha 1	P20908	Extracellular Space	Yes
collagen, type VI, alpha 3	P12111	Extracellular Space	Yes
collagen, type VI, alpha 1	P12109	Extracellular Space	Yes
fibronectin 1	P02751	Extracellular Space	Yes
laminin, alpha 5	O15230	Extracellular Space	Yes
transferrin	P02787	Extracellular Space	No
alpha-fetoprotein	P02771	Extracellular Space	No
albumin	P02768	Extracellular Space	No
fibrinogen gamma chain	P02679	Extracellular Space	Indirect Signalling
fibrinogen beta chain	P02675	Extracellular Space	Indirect Signalling
tissue plasminogen activator	P00750	Extracellular Space	Indirect Signalling
plasminogen activator, urokinase	P00749	Extracellular Space	Indirect Signalling
plasminogen	P00747	Extracellular Space	Indirect Signalling
osteoglycin	P20774	Extracellular Space	Possible interaction
tubulin, alpha 4a	P68366	Cytoplasm	Yes
tubulin, alpha 1b	P68363	Cytoplasm	Yes
actin, beta	P60709	Cytoplasm	Yes
myosin, light chain 9, regulatory	P24844	Cytoplasm	Yes
actinin, alpha 4	O43707	Cytoplasm	Yes
vimentin	P08670	Cytoplasm	Yes
profilin 1	P07737	Cytoplasm	Yes
keratin 8, type II	P05787	Cytoplasm	Yes
keratin 18, type I	P05783	Cytoplasm	Yes
keratin 1, type II	P04264	Cytoplasm	Yes
keratin 6B, type II	P04259	Cytoplasm	Yes
keratin 6A, type II	P02538	Cytoplasm	Yes
keratin 14, type I	P02533	Cytoplasm	Yes
myosin, light chain 12B, regulatory	O14950	Cytoplasm	Yes
ribosomal protein S16	P62249	Cytoplasm	Possible interaction
ribosomal protein S15a	P62244	Cytoplasm	Possible interaction
ribosomal protein S8	P62241	Cytoplasm	Possible interaction
ribosomal protein S3	P23396	Cytoplasm	Possible interaction
ribosomal protein S27a	P62979	Cytoplasm	No

ribosomal protein L11	P62913	Cytoplasm	No
ribosomal protein L30	P62888	Cytoplasm	No
ribosomal protein L35	P42766	Cytoplasm	No
ribosomal protein L13a	P40429	Cytoplasm	No
heat shock protein 90kDa alpha (cytosolic), class B member 1	P08238	Cytoplasm	No
heat shock protein 90kDa alpha (cytosolic), class A member 1	P07900	Cytoplasm	No
glyceraldehyde-3-phosphate dehydrogenase	P04406	Cytoplasm	No
RAP1A, member of RAS oncogene family	P62834	Cytoplasm	Indirect Signalling
ras homolog family member A	P61586	Cytoplasm	Indirect Signalling
RAB10, member RAS oncogene family	P61026	Cytoplasm	Indirect Signalling
S100 calcium binding protein A7	P31151	Cytoplasm	Indirect Signalling
S100 calcium binding protein A4	P26447	Cytoplasm	Indirect Signalling
S100 calcium binding protein A1	P23297	Cytoplasm	Indirect Signalling
S100 calcium binding protein A9	P06702	Cytoplasm	Indirect Signalling
S100 calcium binding protein A8	P05109	Cytoplasm	Indirect Signalling

Table 4.4 Representative sample of proteins obtained from mass spectrometry of hydrodynamically-sheared residue of HeLa A3 cells using FASP SDS removal. Three 10 cm diameter tissue culture dishes (6 x10^6 cells) were exposed to a hydrodynamic force from a standardised shower. The residue was washed with PBS and dissolved in SDS-containing sample buffer. SDS was removed using FASP for sample preparation before liquid chromatography followed by MS-MS mass spectrometry (LC-MS). A total of 488 proteins were identified from four independently isolated samples. Proteins were designated as an adhesome protein (yes) if they were considered to be either an adhesive protein or a protein that directly affects cell adhesion. Proteins noted as having indirect signalling have an effect on cellular adhesion via intermediate pathways, complexes or signalling events. Proteins noted as having a possible interaction are those with a uniprot entry that suggests either localisation to sites of adhesion or that have a structure / function that may relate to adhesion but lack substantial experimental peer-reviewed evidence. Proteins were designated as "No" if these same sources provided no link to cellular adhesion. QIAGEN'S Ingenuity Pathway Analysis was used for determining the cellular localisation of each protein. The proteins "adhesome" status was determined using the corresponding Uniprot entry.

4.2.2.4.4 Comparative mass spectrometry of FASP-treated, hydrodynamically-sheared HeLa A3 residues

When FASP was used to remove SDS contamination, it was possible to acquire a full list of proteins identified by at least two unique tryptic peptides that had their abundance altered

by two-fold or more within the adhesome fraction, as a result of S100P overexpression (Table 4.4). The most obvious point to note is that talin and vinculin were not present in this list, in line with the results obtained by standard Western blots of these cellular residues.

When proteins were up-regulated by S100P overexpression, there appeared to be some contamination in this sheared fraction from other cellular fractions, particularly in nuclear proteins. Of the 11 proteins that were up-regulated, only two could be considered as proteins that should be present within this cellular fraction. The rest are mainly nuclear proteins, transcription factors or ribosomal-interacting proteins. Of the remaining two, Ras GTPase-activating-like protein IQGAP1 (IQGAP1) showed the highest significant increase at 2.81 fold (Anova P = 0.0045). IQGAP1 is a scaffold protein involved in cytoskeletal rearrangement, as well as cell-cell adhesion, cellular motility and cell invasion [218].

Overexpression of IQGAP1 has been shown to increase tumorigenesis and increase cancer cell invasion resulting in metastasis in a number of cancers, including ovarian, colorectal and breast [219, 268-270]. In these cases where cells took on a metastatic phenotype, it was shown that high levels of IQGAP1 occurred localised to the cell membrane. This localisation could explain its increased presence in the sheared residue in S100P-induced cells and its failure to register a difference between control, uninduced and S100P-induced whole cells in the mass spectrometric results shown in Table 4.1.

Growth/differentiation factor 15 (GDF15) was also significantly unregulated by 2.5-fold (Anova P = 0.0043). GDF15 is an extracellular protein growth factor which binds transmembrane receptors [271]. This membrane-binding activity is the likely reason that this protein is present within the adhesome fraction. Similar to IQGAP1, its overexpression has been implicated in the progression of a number of epithelial cancers [272-275].

When proteins were down-regulated by S100P, there would appear to be less contaminating proteins present in the sheared reside than with the up-regulated proteins. The proteins with the largest significant fold change, collagen alpha-1(XII) chain (COL12A1) (fold decrease 3.36, Anova P = 0.00018) and fibrillin-1 (FBN1) (fold decrease 2.65, Anova P = 0.00002) are both extracellular matrix proteins, possibly suggesting that S100P may have a downstream effect on the composition of the extracellular matrix. Another protein of particular note is transforming growth factor-beta-induced protein ig-h3 (TGFβI) (fold decrease 2.19, Anova P = 0.05). This is a secreted protein that has been shown to be

involved in mediating cell to matrix junctions. Crucially, recent evidence may suggest a link between a loss in TGFβI and progression of cancer [276]. Angiopoietin-1 (ANGPT1), a secreted protein shown to promote angiogenesis, is significantly reduced by about two-fold (fold decrease 2.18, Anova P = 0.0004). Curiously, overexpression of this protein has been shown to inhibit tumour growth in breast cancer, despite its known function in angiogenesis [277]. Integrin alpha-5, a crucial cell to matrix binding protein is also significantly reduced by about two-fold (fold decrease 2.2, Anova P = 0.0094). This reduction may be important, since its loss in the adhesive fraction of the S100P-overexpressing cells may explain the reduction in focal adhesions observed using immunofluorescence. Finally the membrane glycoprotein Thy-1 (THY1), a membrane integrin-interacting protein, also showed a two-fold reduction (fold decrease 2.0, Anova P = 0.003). Like many of the proteins in this list, a reduction in this protein has been associated with cancer progression [278].

As a final observation of this dataset, it is worth commenting on the absence of what would be considered to be true adhesion proteins, with the exception of Integrin alpha-5. However, alterations in proteins which have never been linked to S100P were observed in this sheared residue. It is possible that they may be linked by signalling pathways and cause the observed alterations in cell dynamics and loss of cellular adhesion.

Up-regulated proteins in S100P-induced HeLa A3 cell residues				
Protein / Gene name	UniProt ID	Fold Change up	Cellular Location	Adhesome protein
nucleolin	P19338	3.2	Nucleus	No
nucleophosmin (nucleolar phosphoprotein B23, numatrin)	P06748	3.0	Nucleus	No
IQ motif containing GTPase activating protein 1	P46940	2.8	Cytoplasm	Yes
DEK proto-oncogene	P35659	2.8	Nucleus	No
interleukin enhancer binding factor 2	Q12905	2.8	Nucleus	No
histone cluster 1, H1e	P10412	2.8	Nucleus	No
signal recognition particle 14kDa (homologous Alu RNA binding protein)	P37108	2.6	Cytoplasm	No
growth differentiation factor 15	Q99988	2.5	Extracellular Space	Indirect Signalling
nascent polypeptide-associated complex alpha subunit	E9PAV3	2.4	Cytoplasm	Possible interaction
high mobility group box 2	P26583	2.3	Nucleus	No
Y box binding protein 1	P67809	2.2	Nucleus	No

Down-regulated proteins in S100P-induced HeLa A3 cell residues				
Protein / Gene name	UniProt ID	Fold Change down	Cellular Location	Adhesome protein
collagen, type XII, alpha 1	Q99715	3.4	Extracellular Space	Yes
fibrillin 1	P35555	2.7	Extracellular Space	Yes
milk fat globule-EGF factor 8 protein	Q08431	2.6	Extracellular Space	Indirect Signalling
ATPase, Na+/K+ transporting, alpha 1 polypeptide	P05023	2.5	Plasma Membrane	No
microfibrillar-associated protein 2	P55001	2.4	Extracellular Space	Indirect Signalling
transforming growth factor, beta-induced, 68kDa	Q15582	2.2	Extracellular Space	Indirect Signalling
angiopoietin 1	Q15389	2.2	Extracellular Space	Indirect Signalling
integrin, alpha 5 (fibronectin receptor, alpha polypeptide)	P08648	2.2	Plasma Membrane	Yes
solute carrier family 7 (amino acid transporter light chain, L system), member 5	Q01650	2.1	Plasma Membrane	No
Thy-1 cell surface antigen	P04216	2.0	Plasma Membrane	Possible interaction

Table 4.5. Comparative mass spectrometry of residues from hydrodynamically-sheared S100P-overexpressing HeLa A3 cells. The fold change in protein levels between control, uninduced and S100P-induced, HeLa A3 hydrodynamically-sheared residues together with the number of unique peptides used to identify each particular protein during LC-MS analysis are shown. Filter aided sample preparation (FASP) to exchange the SDS for urea

was used before LC-MS. The induced cells were exposed to doxycyclin for 48 hours prior to the experiment. For inclusion the fold change had to be greater than two, at least two unique peptides used for protein determination and P < 0.05 for each protein selected, using Anova for a total of 213 proteins identified. The number of samples used for analysis, n = 4. QIAGEN'S Ingenuity Pathway Analysis was used for determining the cellular localisation of each protein. The proteins "adhesome" status was determined using the corresponding Uniprot entry.

4.2.2.5 Cellular distribution of IQGAP1

Mass spectrometric analysis of hydrodynamically-sheared residues from S100P-overexpressing and control, uninduced HeLa A3 cells showed a 2.8-fold increase in the abundance of IQ motif-containing GTPase activating protein 1 (IQGAP1) in the S100P-overexpressing sheared cell residue (Table 4.4). IQGAP1 is an important scaffold protein involved in a wide range of cellular processes and its expression and cellular localisation have been linked to cancer progression. Since IQGAP1 did not show any alteration in abundance due to S100P-overexpression in the whole-cell mass spectrometric results (Table 4.1), it was probably relocated to the cell- extracellular matrix adhesome of the cell in the S100P-overexpression cells. Therefore, in order to ascertain if this were correct, immunofluorescence staining for IQGAP1 was carried out on S100P-induced HeLa A3 cells. In control, uninduced HeLa A3 cells, the distribution of IQGAP1 staining was primarily perinuclear and cytoskeletal (Figure 4.11A,B). In comparison S100P-overexpressing HeLa A3 cells showed no perinuclear staining and substantially reduced cytoskeletal staining (Figure 4.11C, D). The S100P-overexpressing cells also showed more uniform cytosolic staining with scattered stained foci suggesting that there was a substantial redistribution of IQGAP1 due to the overexpression of S100P, some of which was perhaps relocated to the focal adhesions. However, it was not possible to determine whether this redistribution also occurred in IQGAP1-immunofluorescent staining of hydrodynamically-sheared cell residues.
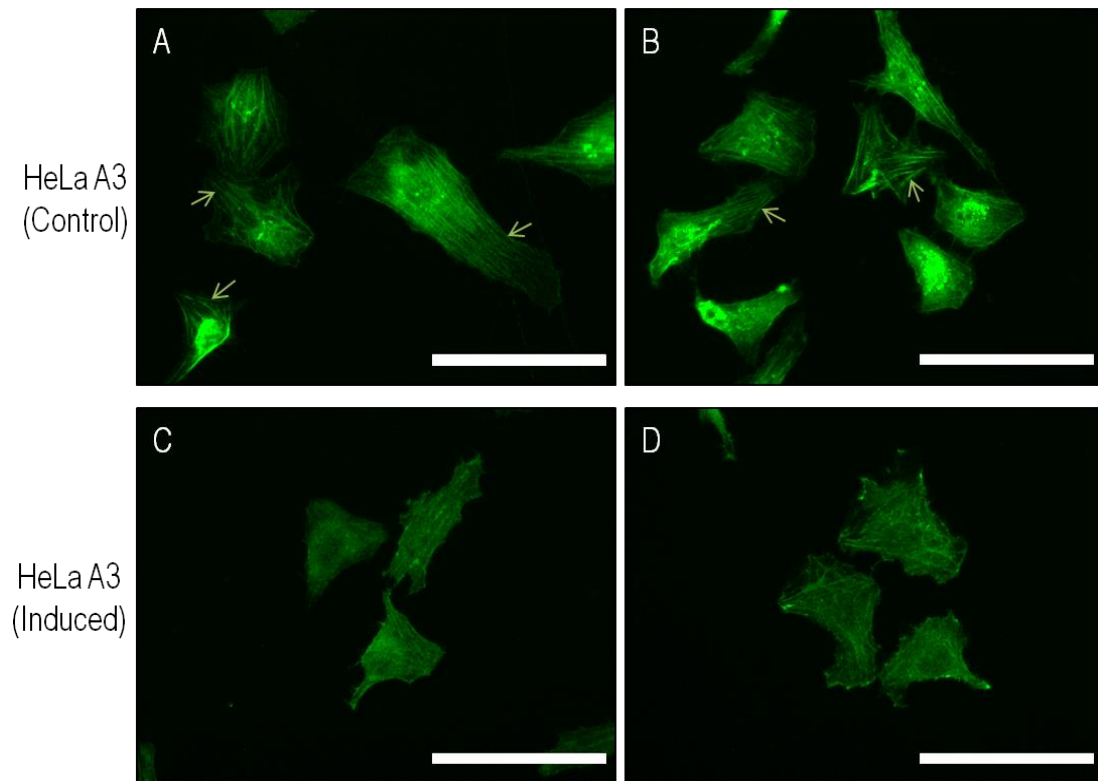
Figure 4.11. Effect of S100P-overexpression on the cellular localisation of IQGAP1. Cells were fixed with 4% (w/v) paraformaldehyde followed by permeabilization using 1% (w/v) Triton X-100 in PBS. HeLa A3 cells were immunofluorescently stained for IQGAP1 (green). Control, uninduced HeLa A3 cells (A,B) show strong filamental cytoskeleton staining (green arrows) and perinuclear staining for IQGAP1. S100P-overexpressing cells (C,D) in comparison, show substantially diminished filamental staining, more cytosolic and punctate staining and no perinuclear staining for IQGAP1. White bar = 100μm.

4.2.2.6 Protein distribution based on normalised abundance

Due to the uniqueness of the isolation method of the adhesome fraction and the complex sample preparation, it was critical to know if the proteins and their relative abundance were generally constant between hydrodynamically-sheared residues from uninduced and S100P-induced HeLa A3 cells. Although alterations in the abundance of some proteins was to be expected, in general the adhesome of both the uninduced control and S100P-induced cell residue should be similar in the proteins present and their abundance. Figure 4.12 shows the Log10 of protein abundance for all 525 proteins present in each of the sheared residues. These abundance values had been normalised using the Progenesis program;

however, due to careful preparation during the initial sample collection, this normalisation change was extremely small. It can be observed that the distribution of all proteins from the sheared residues of both the control, uninduced and S100P-induced HeLa A3 cells followed a similar trend. This indicated that the two sheared residues were relatively similar in overall protein composition and abundance. This result along with the ion chromatograms shown in Figure 4.10 suggested that the method of hydrodynamic shearing followed by FASP sample preparation for comparative adhesome proteomics is a viable technique.
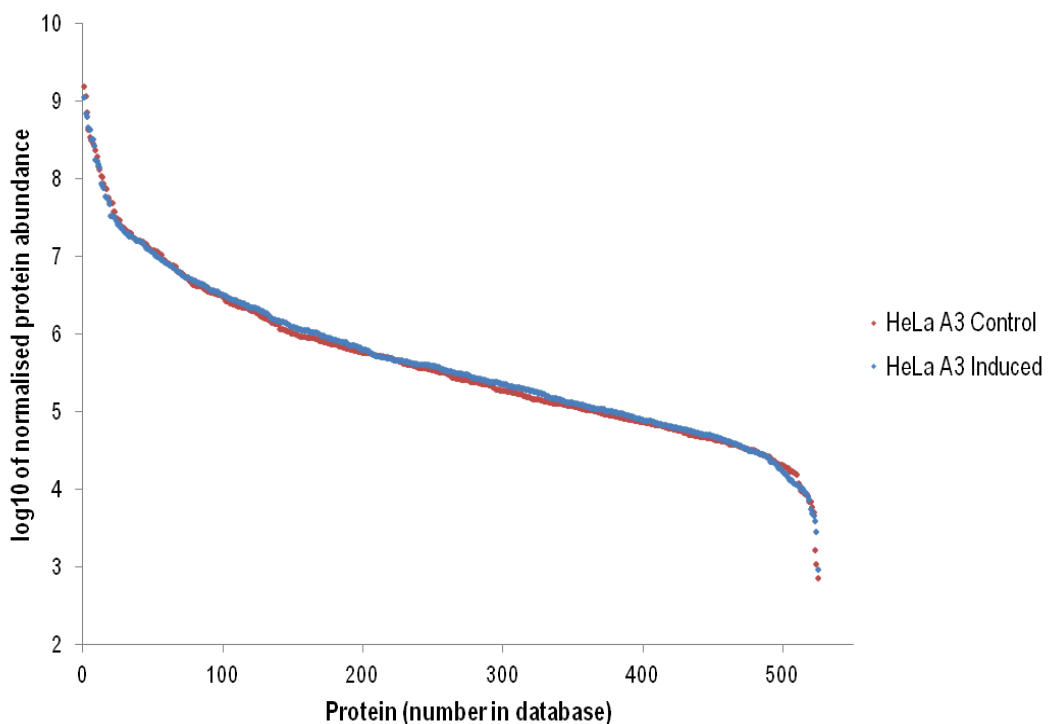
Figure 4.12. The Log$_{10}$ of the normalised protein abundance plotted for each protein present in the hydrodynamically-sheared fraction. Full list of normalised Progenesis proteins from hydrodynamically-sheared control, uninduced and S100P-induced HeLa A3 cells is shown. Protein distribution is consistent between the two isolates indicating sample preparation has conserved the majority of proteins between both of the samples. Total proteins = 525.

4.3 Discussion

As can be seen in Table 4.1 only a very small number of proteins had their abundance significantly altered as a result of 48 hours of S100P overexpression in HeLa A3 cells, when determined by mass spectrometry of whole cells. This may suggest that any of the alterations in cellular properties previously seen in S100P-overexpressing HeLa A3 cells (changes in adhesion, migration and invasion) are not due to major changes in protein expression, but instead are likely to be due to more mechanistic signalling-based alterations. However, it is also worth noting that the total number of proteins obtained from whole cell mass spectrometry of the HeLa A3 cells was considerably lower than that of previous studies. Only 1227 proteins in total were identified in this thesis, in comparison with another study which also used HeLa cells and showed 10255 different proteins encoded by 9207 human genes [279]. It is difficult to determine with certainty why this is the case; however, in that study every effort was made to try and isolate the maximum number of proteins with the abundance of each being of secondary importance. With single pass unlabelled mass spectrometry the total number of identified proteins will be lower, but the proteins observed will be in a larger abundance and as such, any changes that are present due to S100P overexpression can be considered to have a greater potential for causing a biological effect. None of the proteins identified in whole cells which were altered in abundance due to overexpression of S100P were focal adhesion or integrin proteins; although several of them were linked to adhesion and cancer progression. In particular, both PEG10 and endoglin are closely linked to the TGFβ pathway and programmed cell death protein 4 acts as a tumour suppressor [256, 258]. Of the two of these, endoglin is of particular interest, since alterations in its expression have been linked to cancer progression and cell migration [260, 280, 281]. With the relatively high diversity in the function of proteins which change in abundance, it may be that the effect of S100P overexpression on the cell is more substantial than just on the previously described breakdown of filamental NMIIA.

4.3.1 Endoglin expression and effect

Endoglin is a homodimeric membrane glycoprotein which interacts with the TGFβ receptor complex. Binding between endoglin and TGFβ receptor 1, 2 and 3 has been shown, although there is no direct interaction with the TGF-β ligand. Through binding to TGFβ receptor 2, endoglin activates the cytoplasmic kinase activity of the receptor, resulting in the subsequent phosphorylation of TGFβ receptor 1, which then, in turn, interacts with a wide range of downstream signalling proteins including SMADs. However, the exact manner in which endoglin contributes to the activity of the TGFβ receptors and the related downstream pathways are still not fully understood. Upon TGFβ1 binding to the TGFβ receptor, the phosphorylation state of endoglin is reduced [281, 282]. When overexpression studies were carried out on endoglin, it was shown that the normal effect of TGFβ1 binding to its receptor was substantially reduced in the endoglin-overexpressing cells. This reduced binding of TGFβ1 to its receptor resulted in increased cell proliferation and an increase in cellular migration [282, 283]. However, recently the reverse of this has also been shown where overexpression of endoglin results in a decrease in cellular migration and invasion [284-286]. Endoglin is also reported to be important in angiogenesis, since in endoglin-null mice all endoglin knocked down embryos died from defects in vascular development [281, 287]. Furthermore, when tissues were undergoing angiogenesis, they immunohistochemically stained strongly for endoglin compared to adjacent tissues. Thus endoglin probably acts to promote proliferation, migration and angiogenesis through its interactions with TGFβ receptors. In contrast, other studies looking at possible effects of endoglin on cellular adhesion showed this effect was independent of TGFβ [288]. Moreover, these studies showed that the overexpression of endoglin was associated with a reduction in zyxin, an important focal adhesion protein, via a direct interaction. This interaction also resulted in a loss of the zyxin-interacting proteins p130cas and CrkII. The result of these pathway alterations was a reduction in cellular migration [260].

In the context of cancer progression, the role of endoglin is apparently contradictory in several studies [280, 284, 289, 290]. In all cases, however, the studies agreed that endoglin has a significant effect on tumour growth, cellular migration and ultimately cancer metastasis; however, the direction of this effect is controversial. It has been suggested that these contradictory findings may be due to the action of TGFβ as a tumour suppressor in the pre-metastatic tumours, whereas it acts as a tumour enhancer in

advanced metastatic cancers. In line with the latter effect, the abundance of endoglin in blood plasma has been strongly associated with cancer progression, with high levels of soluble endoglin being linked to an increased chance of metastasis in several cancers [280, 291].

In the HeLa A3 cell system, a 2-fold reduction in the abundance of endoglin was observed in the S100P-overexpressing HeLa A3 cells determined by whole-cell mass spectrometry (Table 4.1) and validated using Western blotting. The exact manner in which S100P could cause this reduction is not clear, and it would require further work to try and determine this link. However, in order to ascertain the effect the reduction in endoglin was having on the properties of S100P-overexpressing HeLa A3 cells, siRNA knock-downs were carried out. These knock-downs reduced the levels of endoglin present in HeLa A3 cells by up to 30 fold. This reduction in endoglin resulted in a decrease in the rate of cell adhesion and a decrease in cell migration (Figure 5.6). The reduction in cell adhesion observed here parallels studies which suggest that a reduction in endoglin promotes an increased metastatic phenotype, whereas the decrease in cell migration seen here would seem to suggest the reverse. Ultimately, however, these small alterations in cell adhesion and migration are the result of a large 30-fold change in endoglin in the HeLa A3 cells, whereas S100P-overexpression produces only a 2 - 2.5 fold reduction in endoglin. As a result it is unlikely that the reduction in endoglin in S100P-overexpressing HeLa A3 cells causes a significant impact on cell adhesion and migration in this system. However, this is not to say that the reduction in endoglin is not having any effect on the cell.

4.3.2 Adhesome analysis

In order to try and determine the effect of S100P overexpression on the HeLa A3 cell-extracellular matrix adhesome, a range of different methods were attempted. Of these only two provided reproducible results. The first was the addition of a PBS-Triton X-100 solution to remove the cytosolic and detergent-soluble parts of the cell, in principle leaving only the cytoskeleton and adhesome proteins remaining on the tissue culture dish. The second method involved hydrodynamically shearing cells from the tissue culture dish using a focused water jet, leaving the cell-extracellular matrix proteins remaining on the dish.

4.3.2.1 Triton X-100 treatment vs. hydrodynamic shearing

When utilizing both of these techniques to observe the abundance of key focal adhesion proteins via Western blots a discrepancy arose. Triton X-100-treated cells showed a significant reduction in the structural focal adhesion proteins due to S100P overexpression, whereas the hydrodynamically-sheared samples showed no significant alteration in the abundance of both the structural and signalling-based focal adhesion proteins. This discrepancy was resolved by treating the hydrodynamically-sheared residue from the HeLa A3 cells with the PBS-Triton X-100 solution. Figure 4.4 shows that when HeLa A3 hydrodynamically-sheared cellular residues remaining on the dish were treated with Triton X-100 in PBS a substantial and significant reduction in talin (10 fold decrease) and vinculin (2.2 fold decrease) was observed. Moreover similar to cell samples treated only with Triton X-100, these sheared and Triton X-100-treated residues showed no bands corresponding to paxillin or FAK upon Western blotting. These results may suggest that the Triton X-100 solution is removing more weakly-bound focal adhesion proteins including removing weakly bound signalling-based complexes, leaving only the tightly-bound mature focal adhesions. Thus S100P overexpression in HeLa A3 cells may indeed have an effect, not on the abundance of focal adhesion proteins in the adhesome, but on a reduction in their strength of binding as complexes in the focal adhesions. Since there is a larger reduction in the abundance of talin compared to vinculin, this interpretation has some validity, since there is a greater proportion of talin in immature, nascent adhesions compared to vinculin, the latter accumulates later as focal adhesions mature [42]. Thus, the number of immature focal adhesions would be similar in S100P-induced and non-induced cells, but the number of mature focal adhesions would decrease.

The above hypothesis is in line with that discussed in Section 3.4, whereby loss of NMIIA-mediated tension due to S100P may result in a reduction in maturation of focal adhesions. These less mature, nascent adhesion sites may be more susceptible to non-ionic detergents, due to their overall size being substantially smaller than that of mature focal adhesions. Another explanation is that nascent adhesions are made up of very few integrin proteins and have limited intracellular focal adhesion protein cross-linking [292]. In contrast, mature focal adhesions have high integrin clustering and strong intracellular focal adhesion protein cross-linking [293]. As such, when the plasma membrane is dissolved by Triton X-100, there is very little protein attaching nascent adhesions to the tissue culture dish and holding them together structurally. Subsequent PBS washing steps may, therefore,

dislodge the weakly-bound nascent adhesions, since they now lack plasma membrane support leaving only the mature focal adhesions attached to the dish. Further evidence to support this idea comes from the immunofluorescent staining of hydrodynamically-sheared HeLa A3 cells (Figure 4.5). As part of the immunofluorescence protocol, Triton X-100 was used to treat these hydrodynamically-sheared residues. Thus in this experiment the abundance of focal adhesions stained for immunoreactive vinculin was significantly lower in the hydrodynamically-sheared, Triton X-100-treated residues of S100P-overexpressing HeLa A3 cells compared to those residues from control, uninduced cells. Once again the addition of Triton X-100 may have resulted in some of the more weakly bound focal adhesion proteins in the immature focal adhesions being removed. A repeat of the immunofluorescence experiment using a protocol containing no Triton X-100 would be a method of ascertaining if this were the case. However, all attempts to do so during this study have failed to produce clear immunoreactive foci for vinculin in these samples.

These results, while providing evidence supporting the hypothesis of a decrease in maturation of focal adhesions upon induction of S100P, also highlights that the use of Triton X-100-based solutions to isolate the entire cell-extracellular matrix adhesome of cells is too drastic compared to procedures using hydrodynamic shearing. The use of Triton X-100 also prevents samples from being analysed using routine mass spectrometry without further purification steps, since Triton X-100, like SDS, can cause problems during the trap column and size exclusion column steps. In this way hydrodynamic-shearing is both more effective in preserving what are believed to be adhesome proteins and more convenient for routine mass spectrometric analysis than the use of Triton X-100.

4.3.2.2 Viability of mass spectrometric analysis of hydrodynamically-sheared HeLa A3 residues

Mass spectrometric analysis of the hydrodynamically-sheared HeLa A3 cell residues further validates the Western blots of the residues, since no change is seen in the abundance of talin and vinculin. However, the absence of paxillin and FAK from the mass spectrometry results is somewhat puzzling, even though these proteins are detected in Western blots of the same samples. It is possible that peptides with very low abundance have become obscured by a very high number of peptides detected from more abundant proteins in the sample. There are methods of removing these high abundance peptides, however, their

removal reduces the total amount of protein remaining in the sample and since the hydrodynamically-sheared residues contain little protein to begin with, it was decided that this was not a viable option in this study.

Normalisation of the hydrodynamically-sheared samples was also somewhat difficult, since it was not possible to determine accurately the total amount of protein present in the sheared samples. Instead three methods were used to try and ensure the data was normalised as accurately as possible. Firstly, the samples were normalised against the number of cells on the dishes that were sheared. Secondly, following comparative analysis of the S100P-overexpressing and control, uninduced samples using the Progenesis programme, an estimation of differences in total protein content between the two sheared samples was carried out based on the overall total peak height of the polypeptides in the peak ion chromatograms. In the case of the experiment conducted in Table 4.4, this difference was extremely small suggesting normalisation by cell number despite subsequent sample processing had been accurate. Thirdly the distribution of all proteins based upon their abundance was checked in both S100P-induced and uninduced samples to ensure that they were relatively similar (Figure 4.9). If the two samples showed substantially different patterns of protein abundance, they would be considered to be contaminated and would not be analysed in further detail.

4.3.2.3 The effect of S100P-overexpression on HeLa A3 cell adhesome

Utilizing the hydrodynamic-shearing method, it was possible to ascertain that there was no significant difference in the abundance of focal adhesion proteins in the adhesome of S100P-overexpressing HeLa A3 cells compared to control, uninduced cells, when analysed by both Western blotting and mass spectrometry. However, twelve proteins were significantly altered and these alterations were considered not to be due to contamination. Amongst these there was a 2-fold decrease in the abundance of integrin alpha-5, a fibronectin-binding integrin subunit. The fibronectin-binding integrin, alpha-5 is frequently unregulated in cancer and its upregulation has been reported to be important for metastasis of several different cancers. However, there have also been studies suggesting that a reduction in integrin alpha-5 results in a decrease in cell adhesion, which may actually promote a more metastatic phenotype [294, 295]. This reduction in the levels of integrin alpha-5 is likely to have a substantial effect on the adhesive properties of the

S100P-overexpressing cells. Other adhesion-related proteins such as transforming growth factor-beta-induced protein ig-h3 (TGFβI) were also down regulated. Since one of the functions of TGFβI is the inhibition of cell-extracellular matrix adhesion via TGFβ-mediated signalling linked to a EMT, it is somewhat puzzling that it is down-regulated when S100P is overexpressed in the HeLa A3 cells. Down regulation of this protein has been shown to promote increased cell adhesion, which is the opposite of what is observed in adhesion-based assays on HeLa A3 cells due to S100P overexpression (Figure 3.4 and 3.5). However, more recent studies have shown a decrease in TGFβI results in a poor prognosis in cancer and high TGFβI levels were associated with increased overall survival in patients [276].

As described in Section 2.2.4.3, many of the other observed protein alterations are also associated with cancer progression, the most notable is the complex scaffold protein IQGAP1. Although many of the proteins in the list are associated with either cell adhesion or cancer progression, with the exception of integrin alpha-5 and IQGAP1, none of them interact directly with the assembly of connections between the cell-extracellular matrix or maturation of focal adhesion complexes. This conclusion provides further evidence to support the idea that the alterations observed in cell adhesion due to overexpression of S100P are signalling based, since even at the cell-extracellular matrix interface, there are very few changes in the abundance of focal adhesion proteins. This observation in no way detracts from the importance of the changes obtained from the mass spectrometric analysis of differences in the adhesomes between S100P-induced and uninduced HeLa A3 cells, some of which are likely to contribute to an increased metastatic phenotype due to overexpression of S100P.

4.3.2.4 IQGAP1 expression and effect

IQ motif-containing GTPase activating protein 1 (IQGAP1) is a 190kDa cytoplasmic scaffold protein, which acts as an important mediator of cell properties including cell–cell adhesion, cell-extracellular matrix adhesion and cellular migration via its reorganization of the actin and tubulin cytoskeletons. IQGAP1 accumulates at the leading edge of migrating cells and regulates actin assembly [296]. As well as these structural roles controlling cell dynamics, IQGAP1 has also been shown to be an essential regulator of the Wnt signalling and MAPK pathways, with a result that it has an effect on cell proliferation and cell fate [217, 297]. Biochemically, IQGAP has a vast array of binding partners and protein interactions (more

than 50) making it one of the most complicated scaffold proteins in mammalian systems [298]. Structurally IQGAP1 is complex with six distinct protein-interacting domains. The first is an N-terminal calponin homology (CH) domain which regulates the actin cytoskeleton via binding to Wiskott–Aldrich syndrome protein (N-WASp), as well as directly interacting with F-actin, promoting increased actin polymerization. The second domain is a coiled coil (CC) region which binds ezrin, an important protein involved in cell migration and membrane-associated cell adhesion. Crucially it has been shown that ezrin can interact directly with S100P. The third domain in IQGAP1 is a tryptophan-tryptophan (WW) domain which is able to bind Erk1 and 2. The fourth domain is the central isoleucine-glutamine containing (IQ) domain which is able to bind a wide range of proteins including: S100P, S100B, Rac1, Mek1, PIPK, myosin essential light chains, EGFR, HER2 and many more. The binding of S100P and S100B to IQGAP1 has been shown to be calcium-dependent and it is thought that this binding results in a reduction in IQGAP1 activity, although how this reduction is achieved is still not fully understood. The fifth domain of IQGAP1 contains a GRD domain adjacent to the IQ domain and binds small GTPases such as Rac1 and Cdc42. The final sixth C-terminal domain is a RGCT domain which interacts with the cell-cell junction proteins β-catenin and E-cadherin, as well as several microtubule-binding proteins and PIP2 [214, 215].

IQGAP1 has been shown to be associated with cancer progression in a number of different cancers and it has been suggested that it is a critical component in the metastatic cascade [218]. Moreover, there is increased IQGAP1 expression and significantly altered cellular localisation in samples of tumour tissues, as well as in several different metastatic cancer cell lines [299-301]. This increased expression of IQGAP1 is correlated with a poor patient prognosis in colon, squamous cell, breast, liver, gastric, lung, and ovarian cancers [218, 219]. Since IQGAP1 plays an important role in a wide array of cellular pathways including adhesion and migratory-based networks, it was important to try and determine what effect its increase in the hydrodynamically-sheared fraction of S100P overexpressing HeLa A3 cells would be on the cells (Table 4.3). Since there was no change in levels of IQGAP1 in the whole-cell mass spectrometric results, it is likely that it was modified and/or relocalised in the S100P-overexpressing cells.

The immunostaining results for IQGAP1 have given some clues as to its role, since there were substantial changes in the location of immunostaining for IQGAP1 in the S100P-induced HeLa A3 cells (Figure 5.7). One major change was the absence of perinuclear staining in S100P-overexpressing HeLa A3 cells compared to substantial staining in the

control, uninduced cells. The perinuclear staining is likely to be due to IQGAP1 occurring in the endoplasmic reticulum, since previous studies have shown this to be the case [302, 303]. It has been suggested that the role of perinuclear IQGAP1 may be to tether localised microtubules to perinuclear actin, as well as influencing protein synthesis via interactions with the nuclear translocation complex [304]. IQGAP1 binding may additionally act to regulate the nuclear/microtubule organising centre, which then results in the stabilisation of nuclear positioning for cell polarization during migration of the cell [305]. Thus S100P may be causing a reduction in perinuclear staining of IQGAP1 due to a breakdown in perinuclear actin. S100P-overexpressing HeLa A3 cells also showed diminished immunostaining of the cytoskeleton for IQGAP1, which is also likely to be due to the breakdown of the actin filaments. The effect of this loss in actin bound-IQGAP1 is difficult to envisage without further experimental data, given the complexity of this protein. However, since increased levels of IQGAP1 are detected in the adhesome of S100P-overexpressing HeLa A3 cells using mass spectrometry (Section 4.2.2.4.3), it is logical to assume that the cytoskeletal breakdown due to S100P results in the re-localisation of IQGAP1 from actin filaments to the cell-extracellular matrix interface. Indeed, IQGAP1 has been shown to interact with β1 integrins and Rac1, as well as several other cell surface receptors such as EGFR. Finally the increase in general cytoplasmic fluorescence in S100P-induced HeLa A3 cells may be due to its liberation from actin-containing filaments and perhaps its interaction with the large excess of cytoplasmic S100P produced in these cells [306, 307].

Mechanistically IQGAP1 has been shown to be important in Rac1-mediated directional cell migration via its direct binding to β1 integrins resulting in inhibition of Rac1 activity [306]. As described in detail in Section 1.3.2.3.1, inhibition of Rac1 activity would result in a decrease in focal adhesion formation/maturation and alterations in cell migration. Furthermore, in the context of adhesion, it has been reported that a loss in binding of IQGAP1 to F-actin due to disruption of the actin filaments results in inhibition of the stabilisation of binding of actin to integrin β1 [307] which, in turn, is likely to inhibit the formation of mature focal adhesions and hence substantially reduce cellular adhesion. All of this would be consistent with the observation of enhanced immunofluorescent staining for IQGAP1 in punctate structures, presumably integrin-containing focal adhesions in the S100P-overexpressing HeLa A3 cells. The consequences of the cytoplasmic IQGAP1, either unbound or bound to S100P in this cell system are unknown.

4.4 Conclusions

In this chapter the effects of S100P-overexpression on the whole-cell proteome of HeLa A3 cells 48 hours after S100P-induction was compared to the proteome of control, uninduced cells. Very few alterations in protein levels were found in this whole-cell proteome between the S100P-induced and uninduced HeLa A3 samples, with no changes being observed in focal adhesion or integrin proteins. However, some changes, such as a reduction in endoglin warranted further investigation based on its potential impact on cell adhesion. To this end, it was confirmed by Western blotting that S100P overexpression causes a decrease in endoglin expression in HeLa A3 cells consistent with the mass spectrometric results observed in chapter 4. When endoglin is knocked down, a reduction in cell adhesion is observed, however, these knock-downs also result in a decrease in cell migration, making the biological effect of reduced endoglin due to S100P overexpression somewhat unclear. The adhesome of HeLa A3 cells was also examined to identify protein alterations at the cell-extracellular matrix interface. Using Triton X-100 in PBS it was found that the application of a non-ionic detergent removed weakly-bound focal adhesion proteins resulting in a significant reduction in the levels of structural adhesion proteins present in S100P-induced HeLa A3 cells, compared to control cells. This method, however, resulted in a loss of several important focal adhesion proteins and as such, a second method was developed that utilized hydrodynamic-shearing to isolate the full adhesome fraction. Using this method, mass spectrometric analysis of hydrodynamically-sheared HeLa A3 cells showed that there were several alterations in this fraction, although none of them were core focal adhesion proteins. This result suggests that the changes observed in the adhesive properties of S100P-overexpressing HeLa A3 cells are largely due to signalling alterations rather than a reduction in, or addition of, specific proteins found in the cell adhesome. However, similar to the whole-cell mass spectrometry, some of the proteins identified in the adhesome of the cells did show substantial alterations in abundance due to S100P-overexpression. Several of the proteins identified have reported to be involved in cell adhesion, such as IQGAP1 and, as such, warrant further investigation. To this end it was shown that the cellular location of IQGAP1 upon S100P induction changed, showing a substantial reduction in perinuclear staining of IQGAP1 and a reduction in the intensity of cytoskeletal staining, as well as an apparent increase in staining of punctate structures. Utilizing both the Triton X-100 and hydrodynamic-shearing methods in Western blots and immunofluorescence, it was possible to ascertain that indeed Triton X-100 removed weakly-bound focal adhesions. These results provide further evidence to suggest that

S100P-overexpressing HeLa A3 cells have substantially less strongly-bound mature focal adhesions than uninduced, control cells.

Chapter 5

General Discussion

The work presented in this thesis examined, in detail, the effect of overexpression of S100P on cells and, in particular, the effect of S100P on cellular adhesion. Since S100P overexpression has been associated with a poor patient prognosis in a number of cancers, a greater understanding of the way in which this protein affects cancerous cells could lead to the identification of drug targets in these dangerous S100P-positive cancers.

Within the S100P-inducible HeLa A3 cell system, overexpression of S100P was shown to be associated with a significant decrease in the rate and strength of cell-extracellular matrix adhesion, as well as an increase in cell migration and cell invasion. These alterations were shown to be dependent, in whole or in part, on the presence of NMIIA and to be associated with an alteration in the distribution and abundance of focal adhesion sites, although there were no alterations in the total whole-cell abundance of specific focal adhesion or integrin proteins. In comparative proteomic analysis of S100P-overexpressing whole-HeLa A3 cells and uninduced, control cells, several proteins were identified that had their abundance significantly altered upon overexpression of S100P. Proteomic analysis of the adhesome of HeLa A3 cells isolated by hydrodynamic shearing was then assessed. Similar to the proteome of the whole cell, the protein alterations identified in the adhesome due to overexpression of S100P warrant further investigation, particularly that due to IQGAP1. The effect of S100P on EMT was also investigated and showed that S100P-overexpression does not induce a standard EMT response in cells. Finally the effect of S100P-overexpression on the modification and distribution of several important signalling proteins was established.

Pulling together this data, many of the results form curiosities relating to the possible effect of S100P-overexpression in HeLa A3 cells. However, for most of these results including the change in EMT-related proteins, redistribution of IQGAP1, effect of endoglin and the redistribution of S100P to the nucleus in S100P overexpressing cells, it is difficult to speculate on the effect of these changes beyond what is discussed in their respective sections. However, when the results directly related to cell-extracellular matrix adhesion are combined, they can give a plausible explanation as to some of the effects of S100P-overexpression in HeLa A3 cells.

5.1 The role of S100P in maturation of focal adhesions

Using S100P-inducible HeLa A3 cells, it was shown that S100P-overexpression results in a reduction in both the rate and strength of cell adhesion. It was then shown that overexpression of S100P in HeLa A3 cells caused depolymerisation of NMIIA filaments, but no significant reduction in the total abundance of NMIIA within the cell. Crucially the reduction in cell adhesion and the breakdown of NMIIA filaments were linked, since when S100P was induced in the NMIIA negative Cos7-S10 cell system, no change was observed in the adhesive characteristics of the cells. The number of immunofluorescently-stained focal adhesions was also reduced in S100P-overexpressing HeLa A3 cells, compared to uninduced, control cells. Similar to the change in adhesive characteristics, this alteration was also shown to be dependent on the loss of NMIIA filaments, since this result was not observed in the S100P-induced Cos7-S10 cells. Since NMIIA is a critical component of stress fibres, the reduction in filamental NMIIA would, most likely cause a reduction in cell tension; indeed this has been shown in a number of studies in other systems [239]. Moreover, it has been previously reported that a reduction in stress fibre-mediated tension in epithelial cell systems results in a reduction in phosphorylation of focal adhesion proteins [99]. This relationship was shown to be the case in this system, since S100P-overexpressing HeLa A3 cells showed a significant reduction in the relative levels of phosphorylation at FAK Y397, paxillin Y118 and at paxillin Y31. A number of studies have shown that a reduction in phosphorylation at these sites is associated with a reduction in the recruitment of several important focal adhesion proteins including vinculin and tensin. This reduction in phosphorylation then reportedly results in a significant reduction in the maturation rate of affected focal adhesions [99, 308].

Using the HeLa A3 cell system, it was shown in Chapter 4 that there was a reduction in the abundance of mature focal adhesions in the S100P overexpressing cells. This reduction in mature focal adhesions was suggested because of the manner in which the hydrodynamic shearing and Triton X-100 treatment affected the composition of the HeLa A3 cell's adhesome. The results from Western blots of hydrodynamically-sheared HeLa A3 cell residues showed a reduction in abundance of vinculin and talin when residues were treated with Triton X-100. This was consistent with the immunofluorescent results, however, no changes were observed in the absence of Triton X-100 treatment. Immature nascent adhesions consist of a small number of integrin proteins, in contrast, mature focal adhesions have high levels of integrin clustering and strong intracellular cross-linking of proteins [42, 110]. Thus, when the plasma membrane is dissolved by Triton X-100, the smaller number of uncrosslinked complexes are likely to be removed, whereas those that are strongly cross-linked to the cytoskeleton and extracellular matrix remain attached to the dish. A reduction in the abundance of mature focal adhesions would, therefore, explain both the reduction in the number of observable focal adhesions during immunofluorescent staining, as well as the reduction in the adhesive characteristics of the HeLa A3 cells due to overexpression of S100P. A diagrammatic representation of this is shown in Figure 6.1.

The reduction in the maturation of focal adhesions, as well as the total number of adhesion sites, may also be affected by the redistribution of IQGAP1. As shown in Chapter 4, increased levels of IQGAP1 were detected in the adhesome of S100P-overexpressing HeLa A3 cells using mass spectrometry. Immunostaining for IQGAP1 showed that in control, uninduced cells it was located primarily in the cell perinuclear zone as well as in the cytoskeleton. In the S100P-overexpressing cells this changed to a more uniform cytosolic staining with reduced cytoskeletal and perinuclear IQGAP1 staining, but increased staining of punctate structures. Since S100P-overexpression breaks down the cytoskeleton of the cells it is reasonable to assume that the IQGAP1 bound to the cytoskeleton in control cells is released in the S100P-overexpressing cells and relocalises to the cell-extracellular matrix interface. It is possible that IQGAP1 then binds to β1 integrin and Rac1 complexes in the focal adhesions or potentially other transmembrane surface receptors [306]. The binding to β1 integrin and Rac1 could result in inhibition of Rac1 activity and a subsequent decrease in maturation of focal adhesions, which, in turn, would substantially reduce cellular adhesion [107, 124].

S100P
overexpression

↓

Depolymerisation
of NMIIA

Cytoskeletal
breakdown

Reduced cell
tension

Relocalisation of IQGAP1
from the cytoskeleton to
the cell adhesome

Reduced FAK
Y397
phosphorylation

Increased IQGAP1
to integrin β1
binding

Reduced paxillin
Y118 and Y31
phosphorylation

Inhibition of Rac1
signalling

Reduced
recruitment of FA
proteins

Reduction in rate
of FA maturation

Decreased cell-
extracellular matrix
adhesion

Figure 5.1. The effect of S100P-overexpression on cell-extracellular matrix adhesion.
Upon induction of S100P in HeLa A3 cells NMIIA is depolymerised leading to reduced
cellular tension which inhibits phosphorylation of FAK (Y397) and paxillin (Y118 and Y31).
Reduced phosphorylation at these sites subsequently causes a reduction in the recruitment
of focal adhesion proteins which leads to reduced maturation of focal adhesions. This
reduction in focal adhesion maturation then leads to a decrease in cell-extracellular matrix
adhesion. Dotted arrows indicate a possible secondary effect leading to inhibition of focal
adhesion maturation via IQGAP1 relocalisation and inhibition of Rac1.

5.2 The effect of S100P-overexpression in metastasis

In this thesis it has been demonstrated that the overexpression of S100P results in a
significant decrease in the maturation rate of focal adhesions, which leads to a subsequent
reduction in the rate and strength of adhesion as well as an increase in migration and
invasion in an S100P-inducible human epithelial cancer cell system. The reduction in
adhesion and increase in migration are consistent with the results obtained in S100A4
permanently-overexpressing mouse/rat mammary [309, 310] and bladder [311] carcinoma
cell lines as well as in S100P-overexpressing rat and human carcinoma cell lines [206]. Thus,
the results obtained and conclusions drawn in this thesis are likely to reflect a universal
mechanism for the action of S100 proteins in reducing cell adhesion and in acting to
increase cell migration/invasion, the first and most important step in the process of
metastasis. Overall, a clearer picture of the role of S100P in metastasis is emerging, which
may lead to the development of anti-S100P therapeutic agents to treat S100P positive
cancers.

5.3 Further work

In order to substantiate further the model proposed in Section 6.1, fluorescently tagged
paxillin would need to be transfected into HeLa A3 cells. Confocal time lapse
immunofluorescent microscopy could then be undertaken to visualise in real-time the
changes in formation, maturation and degradation rates of focal adhesions upon induction
of S100P. Alternatively total internal reflection fluorescence microscopy (TIRF) could be

utilized to observe the formation of nascent focal adhesions in cells. Immunofluorescent experiments could also be conducted looking at the distribution of other focal adhesion proteins involved in the later stages of adhesion maturation, one such example would be fluorescently-labelled tensin. Additionally, in order to determine the extent to which the reduction in filamental NMIIA affects cellular tension and rigidity, atomic force microscopy could be carried out. Using this technique it would be possible to quantify the change in tension, rigidity and cell adhesion between control, uninduced and S100P-overexpressing HeLa A3 cells. Several results from this study also warrant further experimentation, in particular quantitative analysis of immunofluorescently-stained focal adhesions with and without Triton X-100 treatment to confirm this treatment is causing a reduction in nascent adhesions. The effect of relocation of S100P to the nucleus upon overexpression also warrants further investigation as well as the curious re-localisation of IQGAP1 to the adhesome in S100P-overexpressing cells. Lastly it would be interesting to investigate if the proteome and adhesome of S100P-overexpressing HeLa A3 cells is significantly different at later time points after induction of S100P. These experiments may help to explain the unexpected results for certain EMT proteins seen after long term overexpression of S100P.

Appendices
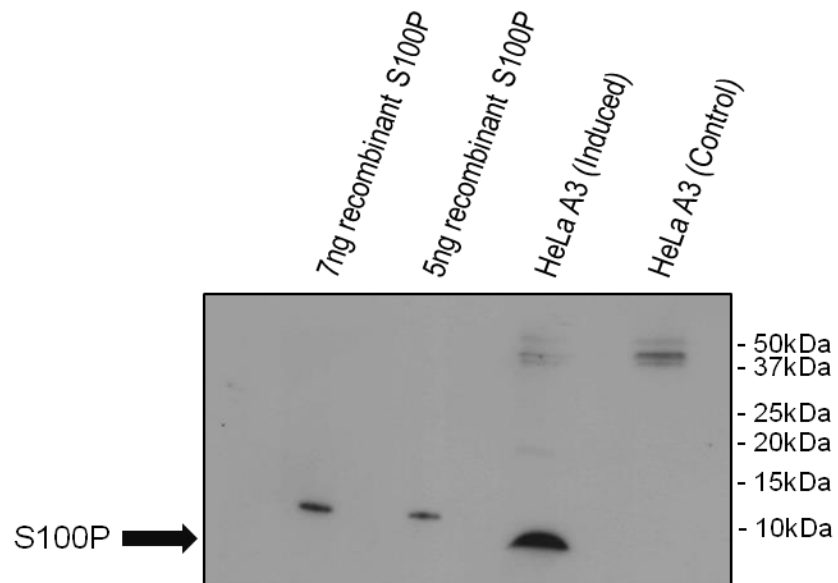
Appendix 1. Whole uncropped Western blot for S100P in HeLa A3 whole-cell lysates. Western blot of S100P expression in HeLa A3 cells 48 hour after addition of 5µg/ml doxycyclin. Twenty µg of protein was loaded per well on a 15% (w/v) polyacrylamide gel. Recombinant S100P bands show a slightly higher molecular weight due to the protein being His-tagged.

Appendicies

Whole-cell mass spectrometry of HeLa A3 cells		
Protein / gene name	UniProt ID	Location
sulfide quinone reductase-like (yeast)	Q9Y6N5	Cytoplasm
basic leucine zipper and W2 domains 2	Q9Y6E2	Cytoplasm
mitochondrial carrier 2	Q9Y6C9	Cytoplasm
phosphoserine aminotransferase 1	Q9Y617	Cytoplasm
signal recognition particle receptor, B subunit	Q9Y5M8	Cytoplasm
translocase of inner mitochondrial membrane 13 homolog (yeast)	Q9Y5L4	Cytoplasm
ubiquitin carboxyl-terminal hydrolase L5	Q9Y5K5	Cytoplasm
SAMM50 sorting and assembly machinery component	Q9Y512	Cytoplasm
hypoxia up-regulated 1	Q9Y4L1	Cytoplasm
ribosomal protein L36	Q9Y3U8	Cytoplasm
RNA exonuclease 2	Q9Y3B8	Cytoplasm
nitric oxide synthase interacting protein	Q9Y314	Cytoplasm
guanine deaminase	Q9Y2T3	Cytoplasm
glutathione S-transferase kappa 1	Q9Y2Q3	Cytoplasm
developmentally regulated GTP binding protein 1	Q9Y295	Cytoplasm
phenylalanyl-tRNA synthetase, alpha subunit	Q9Y285	Cytoplasm
voltage-dependent anion channel 3	Q9Y277	Cytoplasm
nudC nuclear distribution protein	Q9Y266	Cytoplasm
eukaryotic translation initiation factor 3, subunit L	Q9Y262	Cytoplasm
dynamin 3	Q9UQ16	Cytoplasm
NSFL1 (p97) cofactor (p47)	Q9UNZ2	Cytoplasm
WD repeat domain 3	Q9UNX4	Cytoplasm
ribosomal protein L26-like 1	Q9UNX3	Cytoplasm
proteasome (prosome, macropain) 26S subunit, non-ATPase, 13	Q9UNM6	Cytoplasm
GTPase activating protein (SH3 domain) binding protein 2	Q9UN86	Cytoplasm
sorting nexin 12	Q9UMY4	Cytoplasm
coronin, actin binding protein, 1C	Q9ULV4	Cytoplasm
proteasome (prosome, macropain) activator subunit 2 (PA28 beta)	Q9UL46	Cytoplasm
CDV3 homolog (mouse)	Q9UKY7	Cytoplasm
nudix (nucleoside diphosphate linked moiety X)-type motif 5	Q9UKK9	Cytoplasm
MRT4 homolog, ribosome maturation factor	Q9UKD2	Cytoplasm
drebrin-like	Q9UJU6	Cytoplasm
solute carrier family 25 (aspartate/glutamate carrier), member 13	Q9UJS0	Cytoplasm
eukaryotic translation initiation factor 2B, subunit 4 delta, 67kDa	Q9UI10	Cytoplasm
prefoldin subunit 2	Q9UHV9	Cytoplasm
prenylcysteine oxidase 1	Q9UHG3	Cytoplasm
septin 9	Q9UHD8	Cytoplasm
ATP-binding cassette, sub-family F (GCN20), member 2	Q9UG63	Cytoplasm
adducin 3 (gamma)	Q9UEY8	Cytoplasm
ubiquitin-like modifier activating enzyme 2	Q9UBT2	Cytoplasm
DnaJ (Hsp40) homolog, subfamily B, member 11	Q9UBS4	Cytoplasm
cathepsin Z	Q9UBR2	Cytoplasm
eukaryotic translation initiation factor 3, subunit K	Q9UBQ5	Cytoplasm

Appendicies

ataxin 10	Q9UBB4	Cytoplasm
leucyl-tRNA synthetase	Q9P2J5	Cytoplasm
mitochondrial ribosomal protein L15	Q9P015	Cytoplasm
mitochondrial carrier 1	Q9NZJ7	Cytoplasm
FAST kinase domains 2	Q9NYY8	Cytoplasm
UDP-glucose glycoprotein glucosyltransferase 1	Q9NYU2	Cytoplasm
tropomodulin 3 (ubiquitous)	Q9NYL9	Cytoplasm
dipeptidyl-peptidase 3	Q9NY33	Cytoplasm
coiled-coil-helix-coiled-coil-helix domain containing 3	Q9NX63	Cytoplasm
inositol monophosphatase domain containing 1	Q9NX62	Cytoplasm
huntingtin interacting protein K	Q9NX55	Cytoplasm
ATPase family, AAA domain containing 3A	Q9NVI7	Cytoplasm
ubiquinol-cytochrome c reductase complex assembly factor 1	Q9NVA1	Cytoplasm
ethylmalonyl-CoA decarboxylase 1	Q9NTX5	Cytoplasm
Obg-like ATPase 1	Q9NTK5	Cytoplasm
autophagy related 3	Q9NT62	Cytoplasm
phenylalanyl-tRNA synthetase, beta subunit	Q9NSD9	Cytoplasm
translocase of outer mitochondrial membrane 22 homolog (yeast)	Q9NS69	Cytoplasm
diablo, IAP-binding mitochondrial protein	Q9NR28	Cytoplasm
PDZ and LIM domain 7 (enigma)	Q9NR12	Cytoplasm
nitrilase family, member 2	Q9NQR4	Cytoplasm
reticulon 4	Q9NQC3	Cytoplasm
GrpE-like 1, mitochondrial (E. coli)	Q9HAV7	Cytoplasm
Sec61 alpha 2 subunit (S. cerevisiae)	Q9H9S3	Cytoplasm
methyltransferase like 7A	Q9H8H3	Cytoplasm
acyl-CoA dehydrogenase family, member 9	Q9H845	Cytoplasm
dCTP pyrophosphatase 1	Q9H773	Cytoplasm
transcription factor B2, mitochondrial	Q9H5Q4	Cytoplasm
EH-domain containing 1	Q9H4M9	Cytoplasm
arginyl aminopeptidase (aminopeptidase B)	Q9H4A4	Cytoplasm
protein O-fucosyltransferase 1	Q9H488	Cytoplasm
RAB1B, member RAS oncogene family	Q9H0U4	Cytoplasm
integrin-linked kinase-associated serine/threonine phosphatase	Q9H0C8	Cytoplasm
large 60S subunit nuclear export GTPase 1	Q9H089	Cytoplasm
transmembrane protein 126A	Q9H061	Cytoplasm
ubiquitin-like modifier activating enzyme 5	Q9GZZ9	Cytoplasm
N(alpha)-acetyltransferase 50, NatE catalytic subunit	Q9GZZ1	Cytoplasm
WD repeat domain 12	Q9GZL7	Cytoplasm
apoptosis inhibitor 5	Q9BZZ5	Cytoplasm
eukaryotic translation initiation factor 2A, 65kDa	Q9BY44	Cytoplasm
sideroflexin 3	Q9BWM7	Cytoplasm
acetyl-CoA acetyltransferase 2	Q9BWD1	Cytoplasm
HIG1 hypoxia inducible domain family, member 2A	Q9BW72	Cytoplasm
ELOVL fatty acid elongase 1	Q9BW60	Cytoplasm
nucleoporin 85kDa	Q9BW27	Cytoplasm
transmembrane emp24 protein transport domain containing 9	Q9BVK6	Cytoplasm
transmembrane protein 109	Q9BVC6	Cytoplasm
methylthioribose-1-phosphate isomerase 1	Q9BV20	Cytoplasm
latexin	Q9BS40	Cytoplasm

Appendicies

endoplasmic reticulum protein 44	Q9BS26	Cytoplasm
thioredoxin domain containing 17	Q9BRA2	Cytoplasm
coronin, actin binding protein, 1B	Q9BR76	Cytoplasm
tubulin, alpha 1c	Q9BQE3	Cytoplasm
MACRO domain containing 1	Q9BQ69	Cytoplasm
actin related protein 2/3 complex, subunit 5-like	Q9BPX5	Cytoplasm
nipsnap homolog 1 (C. elegans)	Q9BPW8	Cytoplasm
1-acylglycerol-3-phosphate O-acyltransferase 1	Q99943	Cytoplasm
BCL2-associated athanogene	Q99933	Cytoplasm
chaperonin containing TCP1, subunit 7 (eta)	Q99832	Cytoplasm
aconitase 2, mitochondrial	Q99798	Cytoplasm
nucleosome assembly protein 1-like 4	Q99733	Cytoplasm
hydroxysteroid (17-beta) dehydrogenase 10	Q99714	Cytoplasm
prohibitin 2	Q99623	Cytoplasm
DnaJ (Hsp40) homolog, subfamily C, member 7	Q99615	Cytoplasm
family with sequence similarity 129, member B	Q96TA1	Cytoplasm
G elongation factor, mitochondrial 1	Q96RP9	Cytoplasm
VPS35 retromer complex component	Q96QK1	Cytoplasm
CNDP dipeptidase 2 (metallopeptidase M20 family)	Q96KP4	Cytoplasm
up-regulated during skeletal muscle growth 5 homolog (mouse)	Q96IX5	Cytoplasm
succinate-CoA ligase, GDP-forming, beta subunit	Q96I99	Cytoplasm
phosphoglycerate mutase family member 5	Q96HS1	Cytoplasm
endoplasmic reticulum oxidoreductase alpha	Q96HE7	Cytoplasm
phosphoglucomutase 2	Q96G03	Cytoplasm
OTU deubiquitinase, ubiquitin aldehyde binding 1	Q96FW1	Cytoplasm
adaptor-related protein complex 2, mu 1 subunit	Q96CW1	Cytoplasm
optineurin	Q96CV9	Cytoplasm
Fas associated factor family member 2	Q96CS3	Cytoplasm
protein phosphatase 1, regulatory (inhibitor) subunit 14B	Q96C90	Cytoplasm
pyrroline-5-carboxylate reductase family, member 2	Q96C36	Cytoplasm
FK506 binding protein 10, 65 kDa	Q96AY3	Cytoplasm
ribulose-5-phosphate-3-epimerase	Q96AT9	Cytoplasm
leucine rich repeat containing 59	Q96AG4	Cytoplasm
fermitin family member 2	Q96AC1	Cytoplasm
nicalin	Q969V3	Cytoplasm
golgi glycoprotein 1	Q92896	Cytoplasm
CUGBP, Elav-like family member 1	Q92879	Cytoplasm
TRK-fused gene	Q92734	Cytoplasm
phosphatidylinositol glycan anchor biosynthesis, class K	Q92643	Cytoplasm
GCN1 eIF2 alpha kinase activator homolog	Q92616	Cytoplasm
heat shock 105kDa/110kDa protein 1	Q92598	Cytoplasm
stonin 2	Q8WXE9	Cytoplasm
programmed cell death 6 interacting protein	Q8WUM4	Cytoplasm
ATP-binding cassette, sub-family F (GCN20), member 1	Q8NE71	Cytoplasm
SERPINE1 mRNA binding protein 1	Q8NC51	Cytoplasm
SPC24, NDC80 kinetochore complex component	Q8NBT2	Cytoplasm
thioredoxin domain containing 5 (endoplasmic reticulum)	Q8NBS9	Cytoplasm
collagen beta(1-O)galactosyltransferase 1	Q8NBJ5	Cytoplasm
jagunal homolog 1	Q8N5M9	Cytoplasm
phospholipase C, delta 3	Q8N3E9	Cytoplasm
calcium homeostasis endoplasmic reticulum protein	Q8IWX8	Cytoplasm

phospholipase D family, member 3	Q8IV08	Cytoplasm
calcium/calmodulin-dependent protein kinase ID	Q8IU85	Cytoplasm
cullin-associated and neddylation-dissociated 1	Q86VP6	Cytoplasm
metadherin	Q86UE4	Cytoplasm
basic leucine zipper and W2 domains 1	Q7L1Q6	Cytoplasm
La ribonucleoprotein domain family, member 1	Q6PKG0	Cytoplasm
3-hydroxyisobutyryl-CoA hydrolase	Q6NVY1	Cytoplasm
solute carrier family 25 (mitochondrial carrier; phosphate carrier), member 24	Q6NUK1	Cytoplasm
phosphodiesterase 12	Q6L8Q7	Cytoplasm
twinfilin actin binding protein 2	Q6IBS0	Cytoplasm
atlastin GTPase 3	Q6DD88	Cytoplasm
Rho GTPase activating protein 17	Q68EM7	Cytoplasm
KIAA0368	Q5VYK3	Cytoplasm
BRO1 domain and CAAX motif containing	Q5VW32	Cytoplasm
translocase of inner mitochondrial membrane 23 homolog B (yeast)	Q5SRD1	Cytoplasm
COX20 cytochrome c oxidase assembly factor	Q5RI15	Cytoplasm
acylglycerol kinase	Q53H12	Cytoplasm
inverted formin, FH2 and WH2 domain containing	Q27J81	Cytoplasm
inner membrane protein, mitochondrial	Q16891	Cytoplasm
tumor protein D52-like 1	Q16890	Cytoplasm
thioredoxin reductase 1	Q16881	Cytoplasm
UDP-glucose pyrophosphorylase 2	Q16851	Cytoplasm
caseinolytic mitochondrial matrix peptidase proteolytic subunit	Q16740	Cytoplasm
kynureninase	Q16719	Cytoplasm
NADH dehydrogenase (ubiquinone) 1 alpha subcomplex, 5	Q16718	Cytoplasm
mannosidase, alpha, class 2A, member 1	Q16706	Cytoplasm
fascin actin-bundling protein 1	Q16658	Cytoplasm
drebrin 1	Q16643	Cytoplasm
dihydropyrimidinase-like 2	Q16555	Cytoplasm
translocase of outer mitochondrial membrane 34	Q15785	Cytoplasm
thyroid hormone receptor interactor 13	Q15645	Cytoplasm
Sec23 homolog A (S. cerevisiae)	Q15436	Cytoplasm
Ras suppressor protein 1	Q15404	Cytoplasm
transmembrane emp24 domain trafficking protein 2	Q15363	Cytoplasm
reticulocalbin 1, EF-hand calcium binding domain	Q15293	Cytoplasm
prostaglandin E synthase 3 (cytosolic)	Q15185	Cytoplasm
pyrophosphatase (inorganic) 1	Q15181	Cytoplasm
plectin	Q15149	Cytoplasm
phosphoprotein enriched in astrocytes 15	Q15121	Cytoplasm
protein disulfide isomerase family A, member 6	Q15084	Cytoplasm
eukaryotic translation initiation factor 4H	Q15056	Cytoplasm
lysyl-tRNA synthetase	Q15046	Cytoplasm
leucyl-tRNA synthetase 2, mitochondrial	Q15031	Cytoplasm
septin 2	Q15019	Cytoplasm
proteasome (prosome, macropain) 26S subunit, non-ATPase, 6	Q15008	Cytoplasm
LIM and SH3 protein 1	Q14847	Cytoplasm
glucosidase, alpha; neutral AB	Q14697	Cytoplasm
UDP-galactose-4-epimerase	Q14376	Cytoplasm
FK506 binding protein 8, 38kDa	Q14318	Cytoplasm

Appendicies

dynein, cytoplasmic 1, heavy chain 1	Q14204	Cytoplasm
eukaryotic translation initiation factor 3, subunit A	Q14152	Cytoplasm
coactosin-like F-actin binding protein 1	Q14019	Cytoplasm
Ras and Rab interactor 1	Q13671	Cytoplasm
four and a half LIM domains 1	Q13642	Cytoplasm
RAB32, member RAS oncogene family	Q13637	Cytoplasm
RAB31, member RAS oncogene family	Q13636	Cytoplasm
IQ motif containing GTPase activating protein 2	Q13576	Cytoplasm
phosphatidylinositol binding clathrin assembly protein	Q13492	Cytoplasm
PDGFA associated protein 1	Q13442	Cytoplasm
nicotinamide nucleotide transhydrogenase	Q13423	Cytoplasm
eukaryotic translation initiation factor 3, subunit I	Q13347	Cytoplasm
poly(A) binding protein, cytoplasmic 4 (inducible form)	Q13310	Cytoplasm
selenium binding protein 1	Q13228	Cytoplasm
proteasome (prosome, macropain) 26S subunit, non-ATPase, 2	Q13200	Cytoplasm
p21 protein (Cdc42/Rac)-activated kinase 2	Q13177	Cytoplasm
peroxiredoxin 4	Q13162	Cytoplasm
Fas (TNFRSF6)-associated via death domain	Q13158	Cytoplasm
enoyl CoA hydratase 1, peroxisomal	Q13011	Cytoplasm
TNF receptor-associated protein 1	Q12931	Cytoplasm
transducin (beta)-like 3	Q12788	Cytoplasm
peptidase (mitochondrial processing) alpha	Q10713	Cytoplasm
adaptor-related protein complex 1, beta 1 subunit	Q10567	Cytoplasm
cytoskeleton-associated protein 4	Q07065	Cytoplasm
complement component 1, q subcomponent binding protein	Q07021	Cytoplasm
peroxiredoxin 1	Q06830	Cytoplasm
proteasome (prosome, macropain) activator subunit 1 (PA28 alpha)	Q06323	Cytoplasm
caldesmon 1	Q05682	Cytoplasm
protein tyrosine kinase 2	Q05397	Cytoplasm
tyrosine 3-monooxygenase/tryptophan 5-monooxygenase activation protein, eta	Q04917	Cytoplasm
single-stranded DNA binding protein 1, mitochondrial	Q04837	Cytoplasm
aldo-keto reductase family 1, member C2	Q04828	Cytoplasm
glyoxalase I	Q04760	Cytoplasm
keratin 17, type I	Q04695	Cytoplasm
eukaryotic translation initiation factor 4 gamma, 1	Q04637	Cytoplasm
glutathione S-transferase mu 4	Q03013	Cytoplasm
solute carrier family 25 (mitochondrial carrier; oxoglutarate carrier), member 11	Q02978	Cytoplasm
nucleobindin 1	Q02818	Cytoplasm
ribosomal protein L18a	Q02543	Cytoplasm
kinesin family member 23	Q02241	Cytoplasm
transgelin	Q01995	Cytoplasm
phospholipase C, beta 3 (phosphatidylinositol-specific)	Q01970	Cytoplasm
phosphofructokinase, platelet	Q01813	Cytoplasm
fatty acid binding protein 5 (psoriasis-associated)	Q01469	Cytoplasm
sorbitol dehydrogenase	Q00796	Cytoplasm
solute carrier family 25 (mitochondrial carrier; phosphate carrier), member 3	Q00325	Cytoplasm
cytochrome c, somatic	P99999	Cytoplasm
ribosomal protein L19	P84098	Cytoplasm

ras homolog family member G	P84095	Cytoplasm
ribosomal protein L36a	P83881	Cytoplasm
ribosomal protein L24	P83731	Cytoplasm
mitochondrial ribosomal protein S9	P82933	Cytoplasm
chaperonin containing TCP1, subunit 2 (beta)	P78371	Cytoplasm
eukaryotic translation initiation factor 4 gamma, 2	P78344	Cytoplasm
tubulin, alpha 1b	P68363	Cytoplasm
actin, alpha, cardiac muscle 1	P68032	Cytoplasm
thymosin beta 10	P63313	Cytoplasm
guanine nucleotide binding protein (G protein), beta polypeptide 2-like 1	P63244	Cytoplasm
eukaryotic translation initiation factor 5A	P63241	Cytoplasm
ribosomal protein S21	P63220	Cytoplasm
ribosomal protein L38	P63173	Cytoplasm
dynein, light chain, LC8-type 1	P63167	Cytoplasm
tyrosine 3-monooxygenase/tryptophan 5-monooxygenase activation protein, zeta	P63104	Cytoplasm
ribosomal protein S27a	P62979	Cytoplasm
peptidylprolyl isomerase A (cyclophilin A)	P62937	Cytoplasm
ribosomal protein L11	P62913	Cytoplasm
ribosomal protein L32	P62910	Cytoplasm
ribosomal protein L31	P62899	Cytoplasm
ribosomal protein L30	P62888	Cytoplasm
ribosomal protein S28	P62857	Cytoplasm
ribosomal protein S26	P62854	Cytoplasm
ribosomal protein S25	P62851	Cytoplasm
ribosomal protein S24	P62847	Cytoplasm
ribosomal protein S15	P62841	Cytoplasm
ribosomal protein L23	P62829	Cytoplasm
ribosomal protein S6	P62753	Cytoplasm
ribosomal protein L23a	P62750	Cytoplasm
protein phosphatase 2, catalytic subunit, beta isozyme	P62714	Cytoplasm
ribosomal protein S4, X-linked	P62701	Cytoplasm
eukaryotic translation termination factor 1	P62495	Cytoplasm
ribosomal protein L7a	P62424	Cytoplasm
ribosomal protein S11	P62280	Cytoplasm
ribosomal protein S13	P62277	Cytoplasm
ribosomal protein S29	P62273	Cytoplasm
ribosomal protein S18	P62269	Cytoplasm
ribosomal protein S23	P62266	Cytoplasm
ribosomal protein S14	P62263	Cytoplasm
tyrosine 3-monooxygenase/tryptophan 5-monooxygenase activation protein, epsilon	P62258	Cytoplasm
ribosomal protein S16	P62249	Cytoplasm
ribosomal protein S15a	P62244	Cytoplasm
ribosomal protein S8	P62241	Cytoplasm
protein phosphatase 1, catalytic subunit, alpha isozyme	P62136	Cytoplasm
ribosomal protein S7	P62081	Cytoplasm
syntaxin binding protein 1	P61764	Cytoplasm
ras homolog family member A	P61586	Cytoplasm
ribosomal protein L37a	P61513	Cytoplasm
ribosomal protein L27	P61353	Cytoplasm
ribosomal protein L15	P61313	Cytoplasm

Appendicies

ribosomal protein L26	P61254	Cytoplasm
ATP-binding cassette, sub-family E (OABP), member 1	P61221	Cytoplasm
RAB14, member RAS oncogene family	P61106	Cytoplasm
ubiquitin-conjugating enzyme E2K	P61086	Cytoplasm
ubiquitin-conjugating enzyme E2M	P61081	Cytoplasm
RAB10, member RAS oncogene family	P61026	Cytoplasm
signal recognition particle 54kDa	P61011	Cytoplasm
signal peptidase complex subunit 3	P61009	Cytoplasm
destrin (actin depolymerizing factor)	P60981	Cytoplasm
cell division cycle 42	P60953	Cytoplasm
S100 calcium binding protein A10	P60903	Cytoplasm
proteasome (prosome, macropain) subunit, alpha type, 6	P60900	Cytoplasm
ribosomal protein S20	P60866	Cytoplasm
eukaryotic translation initiation factor 4A1	P60842	Cytoplasm
actin, beta	P60709	Cytoplasm
myosin, light chain 6, alkali, smooth muscle and non-muscle	P60660	Cytoplasm
eukaryotic translation initiation factor 3, subunit E	P60228	Cytoplasm
triosephosphate isomerase 1	P60174	Cytoplasm
actin related protein 2/3 complex, subunit 4, 20kDa	P59998	Cytoplasm
epiplakin 1	P58107	Cytoplasm
transmembrane protein 33	P57088	Cytoplasm
eukaryotic translation initiation factor 6	P56537	Cytoplasm
methionyl-tRNA synthetase	P56192	Cytoplasm
eukaryotic translation initiation factor 3, subunit B	P55884	Cytoplasm
aminopeptidase puromycin sensitive	P55786	Cytoplasm
tumor protein D52	P55327	Cytoplasm
hydroxyacyl-CoA dehydrogenase/3-ketoacyl-CoA thiolase/enoyl-CoA hydratase (trifunctional protein), beta subunit	P55084	Cytoplasm
valosin containing protein	P55072	Cytoplasm
eukaryotic translation initiation factor 5	P55010	Cytoplasm
aldehyde dehydrogenase 18 family, member A1	P54886	Cytoplasm
adenylate kinase 2	P54819	Cytoplasm
tyrosyl-tRNA synthetase	P54577	Cytoplasm
arginyl-tRNA synthetase	P54136	Cytoplasm
coatomer protein complex, subunit alpha	P53621	Cytoplasm
methionyl aminopeptidase 1	P53582	Cytoplasm
ATP citrate lyase	P53396	Cytoplasm
biliverdin reductase A	P53004	Cytoplasm
hexokinase 2	P52789	Cytoplasm
spermine synthase	P52788	Cytoplasm
phosphogluconate dehydrogenase	P52209	Cytoplasm
hydroxysteroid (17-beta) dehydrogenase 4	P51659	Cytoplasm
RAB7A, member RAS oncogene family	P51149	Cytoplasm
fragile X mental retardation, autosomal homolog 1	P51114	Cytoplasm
chaperonin containing TCP1, subunit 4 (delta)	P50991	Cytoplasm
chaperonin containing TCP1, subunit 8 (theta)	P50990	Cytoplasm
ribosomal protein L14	P50914	Cytoplasm
palmitoyl-protein thioesterase 1	P50897	Cytoplasm
methionyl aminopeptidase 2	P50579	Cytoplasm
suppression of tumorigenicity 13 (colon carcinoma) (Hsp70 interacting protein)	P50502	Cytoplasm

GDP dissociation inhibitor 2	P50395	Cytoplasm
transmembrane emp24-like trafficking protein 10 (yeast)	P49755	Cytoplasm
acyl-CoA dehydrogenase, very long chain	P49748	Cytoplasm
proteasome (prosome, macropain) subunit, beta type, 2	P49721	Cytoplasm
seryl-tRNA synthetase	P49591	Cytoplasm
histidyl-tRNA synthetase 2, mitochondrial	P49590	Cytoplasm
alanyl-tRNA synthetase	P49588	Cytoplasm
ubiquitin-conjugating enzyme E2A	P49459	Cytoplasm
signal recognition particle 9kDa	P49458	Cytoplasm
Tu translation elongation factor, mitochondrial	P49411	Cytoplasm
chaperonin containing TCP1, subunit 3 (gamma)	P49368	Cytoplasm
deoxyhypusine synthase	P49366	Cytoplasm
fatty acid synthase	P49327	Cytoplasm
lectin, mannose-binding, 1	P49257	Cytoplasm
aldehyde dehydrogenase 9 family, member A1	P49189	Cytoplasm
chaperonin containing TCP1, subunit 5 (epsilon)	P48643	Cytoplasm
glutathione synthetase	P48637	Cytoplasm
serpin peptidase inhibitor, clade B (ovalbumin), member 4	P48594	Cytoplasm
malic enzyme 1, NADP(+)-dependent, cytosolic	P48163	Cytoplasm
ATP synthase, H+ transporting, mitochondrial F1 complex, O subunit	P48047	Cytoplasm
glutaminyl-tRNA synthetase	P47897	Cytoplasm
eukaryotic translation initiation factor 1A, X-linked	P47813	Cytoplasm
capping protein (actin filament) muscle Z-line, beta	P47756	Cytoplasm
capping protein (actin filament) muscle Z-line, alpha 2	P47755	Cytoplasm
phospholipase A2, group IVA (cytosolic, calcium-dependent)	P47712	Cytoplasm
IQ motif containing GTPase activating protein 1	P46940	Cytoplasm
microtubule-associated protein 1B	P46821	Cytoplasm
ribosomal protein S5	P46782	Cytoplasm
ribosomal protein S9	P46781	Cytoplasm
ribosomal protein L21	P46778	Cytoplasm
ribosomal protein L5	P46777	Cytoplasm
ribosomal protein L27a	P46776	Cytoplasm
N-ethylmaleimide-sensitive factor	P46459	Cytoplasm
ubiquitin specific peptidase 5 (isopeptidase T)	P45974	Cytoplasm
voltage-dependent anion channel 2	P45880	Cytoplasm
signal sequence receptor, alpha	P43307	Cytoplasm
leucine-rich pentatricopeptide repeat containing	P42704	Cytoplasm
ribosomal protein S27	P42677	Cytoplasm
aldo-keto reductase family 1, member C3	P42330	Cytoplasm
enoyl-CoA delta isomerase 1	P42126	Cytoplasm
eukaryotic translation initiation factor 1	P41567	Cytoplasm
isoleucyl-tRNA synthetase	P41252	Cytoplasm
glycyl-tRNA synthetase	P41250	Cytoplasm
eukaryotic translation initiation factor 2, subunit 3 gamma, 52kDa	P41091	Cytoplasm
hydroxyacyl-CoA dehydrogenase/3-ketoacyl-CoA thiolase/enoyl-CoA hydratase (trifunctional protein), alpha subunit	P40939	Cytoplasm
malate dehydrogenase 2, NAD (mitochondrial)	P40926	Cytoplasm
malate dehydrogenase 1, NAD (soluble)	P40925	Cytoplasm
ribosomal protein L13a	P40429	Cytoplasm

nicotinamide N-methyltransferase	P40261	Cytoplasm
chaperonin containing TCP1, subunit 6A (zeta 1)	P40227	Cytoplasm
dolichyl-diphosphooligosaccharide--protein glycosyltransferase subunit (non-catalytic)	P39656	Cytoplasm
ribosomal protein S19	P39019	Cytoplasm
heat shock 70kDa protein 9 (mortalin)	P38646	Cytoplasm
electron-transfer-flavoprotein, beta polypeptide	P38117	Cytoplasm
transaldolase 1	P37837	Cytoplasm
transgelin 2	P37802	Cytoplasm
signal recognition particle 14kDa (homologous Alu RNA binding protein)	P37108	Cytoplasm
glutathione peroxidase 4	P36969	Cytoplasm
phosphoglucomutase 1	P36871	Cytoplasm
lon peptidase 1, mitochondrial	P36776	Cytoplasm
ribosomal protein L4	P36578	Cytoplasm
ATP synthase, H+ transporting, mitochondrial F1 complex, gamma polypeptide 1	P36542	Cytoplasm
glutaredoxin (thioltransferase)	P35754	Cytoplasm
adducin 1 (alpha)	P35611	Cytoplasm
sterol O-acyltransferase 1	P35610	Cytoplasm
coatomer protein complex, subunit beta 2 (beta prime)	P35606	Cytoplasm
myosin, heavy chain 10, non-muscle	P35580	Cytoplasm
myosin, heavy chain 9, non-muscle	P35579	Cytoplasm
cystathionine-beta-synthase	P35520	Cytoplasm
radixin	P35241	Cytoplasm
serpin peptidase inhibitor, clade B (ovalbumin), member 6	P35237	Cytoplasm
heat shock 70kDa protein 4	P34932	Cytoplasm
serine hydroxymethyltransferase 2 (mitochondrial)	P34897	Cytoplasm
kinesin family member 5B	P33176	Cytoplasm
guanylate binding protein 2, interferon-inducible	P32456	Cytoplasm
pyrroline-5-carboxylate reductase 1	P32322	Cytoplasm
peroxiredoxin 2	P32119	Cytoplasm
stress-induced phosphoprotein 1	P31948	Cytoplasm
stratifin	P31947	Cytoplasm
tyrosine 3-monooxygenase/tryptophan 5-monooxygenase activation protein, beta	P31946	Cytoplasm
5-aminoimidazole-4-carboxamide ribonucleotide formyltransferase/IMP cyclohydrolase	P31939	Cytoplasm
3-hydroxyisobutyrate dehydrogenase	P31937	Cytoplasm
ubiquinol-cytochrome c reductase core protein I	P31930	Cytoplasm
carbamoyl-phosphate synthase 1, mitochondrial	P31327	Cytoplasm
methionine adenosyltransferase II, alpha	P31153	Cytoplasm
succinate dehydrogenase complex, subunit A, flavoprotein (Fp)	P31040	Cytoplasm
aldehyde dehydrogenase 1 family, member B1	P30837	Cytoplasm
serpin peptidase inhibitor, clade B (ovalbumin), member 1	P30740	Cytoplasm
sorcin	P30626	Cytoplasm
heme oxygenase 2	P30519	Cytoplasm
peptidylprolyl isomerase F	P30405	Cytoplasm
protein phosphatase 2, regulatory subunit A, alpha	P30153	Cytoplasm
protein disulfide isomerase family A, member 3	P30101	Cytoplasm
phosphatidylethanolamine binding protein 1	P30086	Cytoplasm
peroxiredoxin 5	P30044	Cytoplasm
biliverdin reductase B	P30043	Cytoplasm

peroxiredoxin 6	P30041	Cytoplasm
endoplasmic reticulum protein 29	P30040	Cytoplasm
eukaryotic translation elongation factor 1 delta (guanine nucleotide exchange protein)	P29692	Cytoplasm
serpin peptidase inhibitor, clade B (ovalbumin), member 3	P29508	Cytoplasm
cellular retinoic acid binding protein 2	P29373	Cytoplasm
SHC (Src homology 2 domain containing) transforming protein 1	P29353	Cytoplasm
leucine aminopeptidase 3	P28838	Cytoplasm
proteasome (prosome, macropain) subunit, beta type, 5	P28074	Cytoplasm
proteasome (prosome, macropain) subunit, beta type, 4	P28070	Cytoplasm
calnexin	P27824	Cytoplasm
microtubule-associated protein 4	P27816	Cytoplasm
calreticulin	P27797	Cytoplasm
carbamoyl-phosphate synthetase 2, aspartate transcarbamylase, and dihydroorotase	P27708	Cytoplasm
ribosomal protein L10	P27635	Cytoplasm
tyrosine 3-monooxygenase/tryptophan 5-monooxygenase activation protein, theta	P27348	Cytoplasm
FK506 binding protein 2, 13kDa	P26885	Cytoplasm
eukaryotic translation elongation factor 1 gamma	P26641	Cytoplasm
valyl-tRNA synthetase	P26640	Cytoplasm
S100 calcium binding protein A4	P26447	Cytoplasm
S100 calcium binding protein P	P25815	Cytoplasm
proteasome (prosome, macropain) subunit, alpha type, 4	P25789	Cytoplasm
proteasome (prosome, macropain) subunit, alpha type, 2	P25787	Cytoplasm
ATP synthase, H+ transporting, mitochondrial F1 complex, alpha subunit 1, cardiac muscle	P25705	Cytoplasm
ribosomal protein S12	P25398	Cytoplasm
myosin, light chain 9, regulatory	P24844	Cytoplasm
acetyl-CoA acetyltransferase 1	P24752	Cytoplasm
eukaryotic translation elongation factor 1 beta 2	P24534	Cytoplasm
KDEL (Lys-Asp-Glu-Leu) endoplasmic reticulum protein retention receptor 1	P24390	Cytoplasm
eukaryotic translation initiation factor 4B	P23588	Cytoplasm
adenosylhomocysteinase	P23526	Cytoplasm
glycine cleavage system protein H (aminomethyl carrier)	P23434	Cytoplasm
ribosomal protein S3	P23396	Cytoplasm
tryptophanyl-tRNA synthetase	P23381	Cytoplasm
peptidylprolyl isomerase B (cyclophilin B)	P23284	Cytoplasm
ubiquinol-cytochrome c reductase core protein II	P22695	Cytoplasm
ubiquitin-like modifier activating enzyme 1	P22314	Cytoplasm
sterol carrier protein 2	P22307	Cytoplasm
phosphoribosylaminoimidazole carboxylase, phosphoribosylaminoimidazole succinocarboxamide synthetase	P22234	Cytoplasm
phosphoribosylglycinamide formyltransferase, phosphoribosylglycinamide synthetase, phosphoribosylaminoimidazole synthetase	P22102	Cytoplasm
protein-L-isoaspartate (D-aspartate) O-methyltransferase	P22061	Cytoplasm
transglutaminase 2	P21980	Cytoplasm
catechol-O-methyltransferase	P21964	Cytoplasm
voltage-dependent anion channel 1	P21796	Cytoplasm
aconitase 1, soluble	P21399	Cytoplasm
filamin A, alpha	P21333	Cytoplasm

Appendicies

glutathione S-transferase mu 3 (brain)	P21266	Cytoplasm
IMP (inosine 5'-monophosphate) dehydrogenase 1	P20839	Cytoplasm
calpastatin	P20810	Cytoplasm
proteasome (prosome, macropain) subunit, beta type, 1	P20618	Cytoplasm
MX dynamin-like GTPase 1	P20591	Cytoplasm
RAB6A, member RAS oncogene family	P20340	Cytoplasm
eukaryotic translation initiation factor 2, subunit 2 beta, 38kDa	P20042	Cytoplasm
spermidine synthase	P19623	Cytoplasm
eukaryotic translation initiation factor 2-alpha kinase 2	P19525	Cytoplasm
regulator of chromosome condensation 1	P18754	Cytoplasm
phosphoglycerate mutase 1 (brain)	P18669	Cytoplasm
ribosomal protein L17	P18621	Cytoplasm
protein tyrosine phosphatase, non-receptor type 1	P18031	Cytoplasm
t-complex 1	P17987	Cytoplasm
calpain 2, (m/II) large subunit	P17655	Cytoplasm
glutamic-oxaloacetic transaminase 1, soluble	P17174	Cytoplasm
stathmin 1	P16949	Cytoplasm
ATPase, Ca++ transporting, cardiac muscle, slow twitch 2	P16615	Cytoplasm
P450 (cytochrome) oxidoreductase	P16435	Cytoplasm
carbonyl reductase 1	P16152	Cytoplasm
ribosomal protein S2	P15880	Cytoplasm
NAD(P)H dehydrogenase, quinone 1	P15559	Cytoplasm
NME/NM23 nucleoside diphosphate kinase 1	P15531	Cytoplasm
ubiquitin carboxyl-terminal esterase L3 (ubiquitin thiolesterase)	P15374	Cytoplasm
ATPase, H+ transporting, lysosomal 56/58kDa, V1 subunit B1	P15313	Cytoplasm
UDP-Gal:betaGlcNAc beta 1,4- galactosyltransferase, polypeptide 1	P15291	Cytoplasm
G1 to S phase transition 1	P15170	Cytoplasm
aldo-keto reductase family 1, member B1 (aldose reductase)	P15121	Cytoplasm
ubiquinol-cytochrome c reductase binding protein	P14927	Cytoplasm
aspartyl-tRNA synthetase	P14868	Cytoplasm
cyclin B1	P14635	Cytoplasm
heat shock protein 90kDa beta (Grp94), member 1	P14625	Cytoplasm
pyruvate kinase, muscle	P14618	Cytoplasm
aldo-keto reductase family 1, member A1 (aldehyde reductase)	P14550	Cytoplasm
farnesyl diphosphate synthase	P14324	Cytoplasm
protein kinase C substrate 80K-H	P14314	Cytoplasm
protein kinase, cAMP-dependent, regulatory, type II, alpha	P13861	Cytoplasm
acylaminoacyl-peptide hydrolase	P13798	Cytoplasm
plastin 3	P13797	Cytoplasm
tumor protein, translationally-controlled 1	P13693	Cytoplasm
prolyl 4-hydroxylase, alpha polypeptide I	P13674	Cytoplasm
protein disulfide isomerase family A, member 4	P13667	Cytoplasm
eukaryotic translation elongation factor 2	P13639	Cytoplasm
actinin, alpha 1	P12814	Cytoplasm
annexin A3	P12429	Cytoplasm
creatine kinase, brain	P12277	Cytoplasm
IMP (inosine 5'-monophosphate) dehydrogenase 2	P12268	Cytoplasm
solute carrier family 25 (mitochondrial carrier; adenine	P12236	Cytoplasm

Appendicies

nucleotide translocator), member 6		
poly(A) binding protein, cytoplasmic 1	P11940	Cytoplasm
phosphoribosyl pyrophosphate synthetase 2	P11908	Cytoplasm
methylenetetrahydrofolate dehydrogenase (NADP+ dependent) 1, methenyltetrahydrofolate cyclohydrolase, formyltetrahydrofolate synthetase	P11586	Cytoplasm
pyruvate carboxylase	P11498	Cytoplasm
glucose-6-phosphate dehydrogenase	P11413	Cytoplasm
acyl-CoA dehydrogenase, C-4 to C-12 straight chain	P11310	Cytoplasm
v-ral simian leukemia viral oncogene homolog A (ras related)	P11233	Cytoplasm
pyruvate dehydrogenase (lipoamide) beta	P11177	Cytoplasm
heat shock 70kDa protein 8	P11142	Cytoplasm
heat shock 70kDa protein 5 (glucose-regulated protein, 78kDa)	P11021	Cytoplasm
heat shock 60kDa protein 1 (chaperonin)	P10809	Cytoplasm
protein kinase, cAMP-dependent, regulatory, type I, alpha	P10644	Cytoplasm
ribosomal protein S17	P0CW22	Cytoplasm
ubiquinol-cytochrome c reductase, Rieske iron-sulfur polypeptide 1 pseudogene 1	P0C7P4	Cytoplasm
aldolase C, fructose-bisphosphate	P09972	Cytoplasm
leukotriene A4 hydrolase	P09960	Cytoplasm
cytochrome c oxidase subunit VIc	P09669	Cytoplasm
dihydrolipoamide dehydrogenase	P09622	Cytoplasm
tropomyosin 1 (alpha)	P09493	Cytoplasm
glutathione S-transferase pi 1	P09211	Cytoplasm
signal recognition particle 19kDa	P09132	Cytoplasm
ribosomal protein SA	P08865	Cytoplasm
guanine nucleotide binding protein (G protein), alpha inhibiting activity polypeptide 3	P08754	Cytoplasm
keratin 7, type II	P08729	Cytoplasm
vimentin	P08670	Cytoplasm
cytochrome c-1	P08574	Cytoplasm
asparagine synthetase (glutamine-hydrolyzing)	P08243	Cytoplasm
heat shock protein 90kDa alpha (cytosolic), class B member 1	P08238	Cytoplasm
phosphofructokinase, muscle	P08237	Cytoplasm
ubiquinol-cytochrome c reductase hinge protein	P07919	Cytoplasm
heat shock protein 90kDa alpha (cytosolic), class A member 1	P07900	Cytoplasm
glutamyl-prolyl-tRNA synthetase	P07814	Cytoplasm
profilin 1	P07737	Cytoplasm
calpain 1, (mu/I) large subunit	P07384	Cytoplasm
cathepsin D	P07339	Cytoplasm
prolyl 4-hydroxylase, beta polypeptide	P07237	Cytoplasm
lactate dehydrogenase B	P07195	Cytoplasm
epoxide hydrolase 1, microsomal (xenobiotic)	P07099	Cytoplasm
tropomyosin 3	P06753	Cytoplasm
phosphorylase, glycogen, liver	P06737	Cytoplasm
enolase 1, (alpha)	P06733	Cytoplasm
S100 calcium binding protein A6	P06703	Cytoplasm
ATP synthase, H+ transporting, mitochondrial F1 complex, beta polypeptide	P06576	Cytoplasm
uroporphyrinogen decarboxylase	P06132	Cytoplasm
keratin 8, type II	P05787	Cytoplasm

keratin 18, type I	P05783	Cytoplasm
ribosomal protein, large, P2	P05387	Cytoplasm
ribosomal protein, large, P1	P05386	Cytoplasm
eukaryotic translation initiation factor 2, subunit 1 alpha, 35kDa	P05198	Cytoplasm
solute carrier family 25 (mitochondrial carrier; adenine nucleotide translocator), member 5	P05141	Cytoplasm
S100 calcium binding protein A8	P05109	Cytoplasm
ribophorin II	P04844	Cytoplasm
ribophorin I	P04843	Cytoplasm
heat shock 27kDa protein 1	P04792	Cytoplasm
glyceraldehyde-3-phosphate dehydrogenase	P04406	Cytoplasm
tubulin, beta 4A class IVa	P04350	Cytoplasm
ornithine aminotransferase	P04181	Cytoplasm
cystatin B (stefin B)	P04080	Cytoplasm
aldolase A, fructose-bisphosphate	P04075	Cytoplasm
glucosidase, beta, acid	P04062	Cytoplasm
catalase	P04040	Cytoplasm
NADH dehydrogenase, subunit 5 (complex I)	P03915	Cytoplasm
NADH dehydrogenase, subunit 4 (complex I)	P03905	Cytoplasm
hemoglobin, zeta	P02008	Cytoplasm
argininosuccinate synthase 1	P00966	Cytoplasm
adenylate kinase 1	P00568	Cytoplasm
phosphoglycerate kinase 1	P00558	Cytoplasm
glutamic-oxaloacetic transaminase 2, mitochondrial	P00505	Cytoplasm
hypoxanthine phosphoribosyltransferase 1	P00492	Cytoplasm
superoxide dismutase 1, soluble	P00441	Cytoplasm
cytochrome c oxidase subunit II	P00403	Cytoplasm
cytochrome b5 reductase 3	P00387	Cytoplasm
glutamate dehydrogenase 1	P00367	Cytoplasm
lactate dehydrogenase A	P00338	Cytoplasm
cytochrome b5 type A (microsomal)	P00167	Cytoplasm
translocase of outer mitochondrial membrane 40 homolog (yeast)	O96008	Cytoplasm
thioredoxin domain containing 12 (endoplasmic reticulum)	O95881	Cytoplasm
adaptor-related protein complex 2, alpha 1 subunit	O95782	Cytoplasm
AHA1, activator of heat shock 90kDa protein ATPase homolog 1 (yeast)	O95433	Cytoplasm
6-phosphogluconolactonase	O95336	Cytoplasm
leucine zipper-EF-hand containing transmembrane protein 1	O95202	Cytoplasm
ubiquitination factor E4B	O95155	Cytoplasm
SEC31 homolog A, COPII coating complex component	O94979	Cytoplasm
adaptor-related protein complex 2, alpha 2 subunit	O94973	Cytoplasm
glutaminase	O94925	Cytoplasm
translocase of outer mitochondrial membrane 70 homolog A (S. cerevisiae)	O94826	Cytoplasm
glutaredoxin 3	O76003	Cytoplasm
trio Rho guanine nucleotide exchange factor	O75962	Cytoplasm
ATP synthase, H+ transporting, mitochondrial Fo complex, subunit d	O75947	Cytoplasm
ADP-ribosylation factor-like 6 interacting protein 5	O75915	Cytoplasm
isocitrate dehydrogenase 1 (NADP+), soluble	O75874	Cytoplasm
eukaryotic translation initiation factor 3, subunit J	O75822	Cytoplasm

Appendicies

cell division cycle 123	O75794	Cytoplasm
lysophospholipase I	O75608	Cytoplasm
cold shock domain containing E1, RNA-binding	O75534	Cytoplasm
SEC22 vesicle trafficking protein homolog B (S. cerevisiae) (gene/pseudogene)	O75396	Cytoplasm
citrate synthase	O75390	Cytoplasm
peroxisomal biogenesis factor 14	O75381	Cytoplasm
filamin B, beta	O75369	Cytoplasm
tubulin folding cofactor A	O75347	Cytoplasm
programmed cell death 6	O75340	Cytoplasm
NADH dehydrogenase (ubiquinone) Fe-S protein 2, 49kDa (NADH-coenzyme Q reductase)	O75306	Cytoplasm
gamma-glutamylcyclotransferase	O75223	Cytoplasm
clustered mitochondria (cluA/CLU1) homolog	O75153	Cytoplasm
Rho-associated, coiled-coil containing protein kinase 2	O75116	Cytoplasm
ATP-binding cassette, sub-family B (MDR/TAP), member 7	O75027	Cytoplasm
eukaryotic translation initiation factor 5B	O60841	Cytoplasm
perilipin 3	O60664	Cytoplasm
procollagen-lysine, 2-oxoglutarate 5-dioxygenase 3	O60568	Cytoplasm
acyl-CoA synthetase long-chain family member 4	O60488	Cytoplasm
translocase of inner mitochondrial membrane 8 homolog A (yeast)	O60220	Cytoplasm
NADH dehydrogenase (ubiquinone) Fe-S protein 5, 15kDa (NADH-coenzyme Q reductase)	O43920	Cytoplasm
adenosylhomocysteinase-like 1	O43865	Cytoplasm
calumenin	O43852	Cytoplasm
myosin IB	O43795	Cytoplasm
asparaginyl-tRNA synthetase	O43776	Cytoplasm
endosulfine alpha	O43768	Cytoplasm
actinin, alpha 4	O43707	Cytoplasm
tumor protein D52-like 2	O43399	Cytoplasm
thioredoxin-like 1	O43396	Cytoplasm
eukaryotic translation elongation factor 1 epsilon 1	O43324	Cytoplasm
3'-phosphoadenosine 5'-phosphosulfate synthase 1	O43252	Cytoplasm
phosphoglycerate dehydrogenase	O43175	Cytoplasm
cytochrome b5 type B (outer mitochondrial membrane)	O43169	Cytoplasm
actin related protein 2/3 complex, subunit 5, 16kDa	O15511	Cytoplasm
eukaryotic translation initiation factor 3, subunit H	O15372	Cytoplasm
eukaryotic translation initiation factor 3, subunit D	O15371	Cytoplasm
actin related protein 2/3 complex, subunit 2, 34kDa	O15144	Cytoplasm
actin related protein 2/3 complex, subunit 1B, 41kDa	O15143	Cytoplasm
phosphoribosylformylglycinamidine synthase	O15067	Cytoplasm
solute carrier family 27 (fatty acid transporter), member 2	O14975	Cytoplasm
myosin, light chain 12B, regulatory	O14950	Cytoplasm
ubiquinol-cytochrome c reductase, complex III subunit VII, 9.5kDa	O14949	Cytoplasm
interferon-induced protein with tetratricopeptide repeats 3	O14879	Cytoplasm
tripeptidyl peptidase I	O14773	Cytoplasm
protein arginine methyltransferase 5	O14744	Cytoplasm
inositol(myo)-1(or 4)-monophosphatase 2	O14732	Cytoplasm
prostaglandin E synthase	O14684	Cytoplasm
adaptor-related protein complex 3, delta 1 subunit	O14617	Cytoplasm
pyridoxal (pyridoxine, vitamin B6) kinase	O00764	Cytoplasm

Appendicies

ubiquitin-conjugating enzyme E2C	O00762	Cytoplasm
DEAD (Asp-Glu-Ala-Asp) box helicase 3, X-linked	O00571	Cytoplasm
proteasome (prosome, macropain) 26S subunit, non-ATPase, 14	O00487	Cytoplasm
procollagen-lysine, 2-oxoglutarate 5-dioxygenase 2	O00469	Cytoplasm
dynamin 1-like	O00429	Cytoplasm
insulin-like growth factor 2 mRNA binding protein 3	O00425	Cytoplasm
eukaryotic translation initiation factor 3, subunit F	O00303	Cytoplasm
proteasome (prosome, macropain) 26S subunit, non-ATPase, 11	O00231	Cytoplasm
myosin IC	O00159	Cytoplasm
acyl-CoA thioesterase 7	O00154	Cytoplasm
PDZ and LIM domain 1	O00151	Cytoplasm
kinesin heavy chain member 2A	O00139	Cytoplasm
nascent polypeptide-associated complex alpha subunit	E9PAV3	Cytoplasm
cofilin 2 (muscle)	Q9Y281	Extracellular Space
sushi domain containing 2	Q9UGT4	Extracellular Space
family with sequence similarity 49, member B	Q9NUQ9	Extracellular Space
coiled-coil domain containing 47	Q96A33	Extracellular Space
myosin, heavy chain 14, non-muscle	Q7Z406	Extracellular Space
tumor necrosis factor, alpha-induced protein 2	Q03169	Extracellular Space
mesencephalic astrocyte-derived neurotrophic factor	P55145	Extracellular Space
hepatoma-derived growth factor	P51858	Extracellular Space
serpin peptidase inhibitor, clade H (heat shock protein 47), member 1, (collagen binding protein 1)	P50454	Extracellular Space
nicotinamide phosphoribosyltransferase	P43490	Extracellular Space
wingless-type MMTV integration site family, member 5A	P41221	Extracellular Space
chitinase 3-like 1 (cartilage glycoprotein-39)	P36222	Extracellular Space
granulin	P28799	Extracellular Space
thymidine phosphorylase	P19971	Extracellular Space
lectin, galactoside-binding, soluble, 3	P17931	Extracellular Space
laminin, gamma 1 (formerly LAMB2)	P11047	Extracellular Space
lectin, galactoside-binding, soluble, 1	P09382	Extracellular Space
fibroblast growth factor 2 (basic)	P09038	Extracellular Space
prosaposin	P07602	Extracellular Space
glucose-6-phosphate isomerase	P06744	Extracellular Space
ISG15 ubiquitin-like modifier	P05161	Extracellular Space
vitronectin	P04004	Extracellular Space

194

Appendicies

complement component 9	P02748	Extracellular Space
complement component 3	P01024	Extracellular Space
WD repeat domain 1	O75083	Extracellular Space
RNA binding motif protein 8A	Q9Y5S9	Nucleus
UTP18 small subunit (SSU) processome component homolog (yeast)	Q9Y5J1	Nucleus
suppressor of Ty 16 homolog (S. cerevisiae)	Q9Y5B9	Nucleus
talin 2	Q9Y4G6	Nucleus
SAM domain and HD domain 1	Q9Y3Z3	Nucleus
chromatin target of PRMT1	Q9Y3Y2	Nucleus
NOC2-like nucleolar associated transcriptional repressor	Q9Y3T9	Nucleus
NOP16 nucleolar protein	Q9Y3C1	Nucleus
ribosomal RNA processing 15 homolog	Q9Y3B9	Nucleus
NOP58 ribonucleoprotein	Q9Y2X3	Nucleus
RuvB-like AAA ATPase 1	Q9Y265	Nucleus
peptidylprolyl cis/trans isomerase, NIMA-interacting 4	Q9Y237	Nucleus
chromosome 14 open reading frame 166	Q9Y224	Nucleus
structural maintenance of chromosomes 3	Q9UQE7	Nucleus
proliferation-associated 2G4, 38kDa	Q9UQ80	Nucleus
serine/arginine repetitive matrix 2	Q9UQ35	Nucleus
Fas (TNFRSF6) associated factor 1	Q9UNN5	Nucleus
nucleolar protein 7, 27kDa	Q9UMY1	Nucleus
pre-mRNA processing factor 19	Q9UMS4	Nucleus
NIN1/RPN12 binding protein 1 homolog	Q9ULX3	Nucleus
RALY heterogeneous nuclear ribonucleoprotein	Q9UKM9	Nucleus
LSM7 homolog, U6 small nuclear RNA and mRNA degradation associated	Q9UK45	Nucleus
bromodomain adjacent to zinc finger domain, 1B	Q9UIG0	Nucleus
poly-U binding splicing factor 60KDa	Q9UHX1	Nucleus
mortality factor 4 like 1	Q9UBU8	Nucleus
BRCA2 and CDKN1A interacting protein	Q9P287	Nucleus
regulator of chromosome condensation 2	Q9P258	Nucleus
myoferlin	Q9NZM1	Nucleus
apoptosis antagonizing transcription factor	Q9NY61	Nucleus
GAR1 homolog, ribonucleoprotein	Q9NY12	Nucleus
testis expressed 10	Q9NXF1	Nucleus
NHP2 ribonucleoprotein	Q9NX24	Nucleus
RNA binding motif protein 22	Q9NW64	Nucleus
RNA binding motif protein 28	Q9NW13	Nucleus
anti-silencing function 1B histone chaperone	Q9NVP2	Nucleus
structural maintenance of chromosomes 4	Q9NTJ3	Nucleus
DEAD (Asp-Glu-Ala-Asp) box helicase 21	Q9NR30	Nucleus
steroid receptor RNA activator 1	Q9HD15	Nucleus
calcyclin binding protein	Q9HB71	Nucleus
coiled-coil domain containing 86	Q9H6F5	Nucleus
HEAT repeat containing 1	Q9H583	Nucleus
activating signal cointegrator 1 complex subunit 2	Q9H1I8	Nucleus
N-acetyltransferase 10 (GCN5-related)	Q9H0A0	Nucleus
fat mass and obesity associated	Q9C0B1	Nucleus
transducin (beta)-like 1 X-linked receptor 1	Q9BZK7	Nucleus

Appendicies

GTP binding protein 4	Q9BZE4	Nucleus
serrate, RNA effector molecule	Q9BXP5	Nucleus
splicing factor 3b, subunit 5, 10kDa	Q9BWJ5	Nucleus
guanine nucleotide binding protein-like 3 (nucleolar)	Q9BVP2	Nucleus
heterogeneous nuclear ribonucleoprotein U-like 1	Q9BUJ2	Nucleus
transmembrane protein 43	Q9BTV4	Nucleus
acidic (leucine-rich) nuclear phosphoprotein 32 family, member E	Q9BTT0	Nucleus
nucleolar protein 10	Q9BSC4	Nucleus
MYB binding protein (P160) 1a	Q9BQG0	Nucleus
WD repeat domain 77	Q9BQA1	Nucleus
elaC ribonuclease Z 2	Q9BQ52	Nucleus
protein arginine methyltransferase 1	Q99873	Nucleus
EBNA1 binding protein 2	Q99848	Nucleus
copine I	Q99829	Nucleus
heterogeneous nuclear ribonucleoprotein A/B	Q99729	Nucleus
translin-associated factor X	Q99598	Nucleus
nucleoporin 88kDa	Q99567	Nucleus
parkinson protein 7	Q99497	Nucleus
prefoldin subunit 5	Q99471	Nucleus
cell division cycle 5-like	Q99459	Nucleus
myeloid-associated differentiation marker	Q96S97	Nucleus
RNA binding motif protein 14	Q96PK6	Nucleus
zinc finger RNA binding protein	Q96KR1	Nucleus
far upstream element (FUSE) binding protein 3	Q96I24	Nucleus
DEAD (Asp-Glu-Ala-Asp) box polypeptide 27	Q96GQ7	Nucleus
small nuclear ribonucleoprotein 40kDa (U5)	Q96DI7	Nucleus
cirrhosis, autosomal recessive 1A (cirhin)	Q969X6	Nucleus
ubiquitin specific peptidase 7 (herpes virus-associated)	Q93009	Nucleus
transportin 1	Q92973	Nucleus
KH-type splicing regulatory protein	Q92945	Nucleus
UPF1 regulator of nonsense transcripts homolog (yeast)	Q92900	Nucleus
DEAD (Asp-Glu-Ala-Asp) box helicase 17	Q92841	Nucleus
histone deacetylase 2	Q92769	Nucleus
N-myc downstream regulated 1	Q92597	Nucleus
H1 histone family, member X	Q92522	Nucleus
DEAD (Asp-Glu-Ala-Asp) box helicase 1	Q92499	Nucleus
ataxin 2-like	Q8WWM7	Nucleus
importin 4	Q8TEX9	Nucleus
gem (nuclear organelle) associated protein 5	Q8TEQ6	Nucleus
UTP15, U3 small nucleolar ribonucleoprotein, homolog (S. cerevisiae)	Q8TED0	Nucleus
cleavage and polyadenylation specific factor 7, 59kDa	Q8N684	Nucleus
serine/arginine repetitive matrix 1	Q8IYB3	Nucleus
FtsJ homolog 3 (E. coli)	Q8IY81	Nucleus
WD repeat domain 75	Q8IWA0	Nucleus
histone cluster 2, H2ab	Q8IUE6	Nucleus
Aly/REF export factor	Q86V81	Nucleus
poly(A) binding protein, nuclear 1	Q86U42	Nucleus
NOP9 nucleolar protein	Q86U38	Nucleus
paternally expressed 10	Q86TG7	Nucleus
DEAH (Asp-Glu-Ala-His) box helicase 30	Q7L2E3	Nucleus

Appendicies

DEAD (Asp-Glu-Ala-Asp) box polypeptide 46	Q7L014	Nucleus
staphylococcal nuclease and tudor domain containing 1	Q7KZF4	Nucleus
WD repeat domain 74	Q6RFH5	Nucleus
BRCA1-associated ATM activator 1	Q6PJG6	Nucleus
pre-mRNA processing factor 8	Q6P2Q9	Nucleus
cell division cycle 73	Q6P1J9	Nucleus
polymerase I and transcript release factor	Q6NZI2	Nucleus
ubiquitin protein ligase E3 component n-recognin 4	Q5T4S7	Nucleus
heterochromatin protein 1, binding protein 3	Q5SSJ5	Nucleus
histone cluster 2, H2bf	Q5QNW6	Nucleus
deoxynucleotidyltransferase, terminal, interacting protein 2	Q5QJE6	Nucleus
ribosomal RNA processing 12 homolog	Q5JTH9	Nucleus
programmed cell death 4 (neoplastic transformation inhibitor)	Q53EL6	Nucleus
smu-1 suppressor of mec-8 and unc-52 homolog (C. elegans)	Q2TAY7	Nucleus
TSR1, 20S rRNA accumulation, homolog (S. cerevisiae)	Q2NL82	Nucleus
heterogeneous nuclear ribonucleoprotein U-like 2	Q1KMD3	Nucleus
interferon, gamma-inducible protein 16	Q16666	Nucleus
cleavage and polyadenylation specific factor 6, 68kDa	Q16630	Nucleus
serine/arginine-rich splicing factor 7	Q16629	Nucleus
retinoblastoma binding protein 7	Q16576	Nucleus
damage-specific DNA binding protein 1, 127kDa	Q16531	Nucleus
cysteine and glycine-rich protein 2	Q16527	Nucleus
neural precursor cell expressed, developmentally down-regulated 8	Q15843	Nucleus
splicing factor 1	Q15637	Nucleus
splicing factor 3a, subunit 1, 120kDa	Q15459	Nucleus
splicing factor 3b, subunit 4, 49kDa	Q15427	Nucleus
scaffold attachment factor B	Q15424	Nucleus
splicing factor 3b, subunit 3, 130kDa	Q15393	Nucleus
transcription elongation factor B (SIII), polypeptide 2 (18kDa, elongin B)	Q15370	Nucleus
transcription elongation factor B (SIII), polypeptide 1 (15kDa, elongin C)	Q15369	Nucleus
poly(rC) binding protein 2	Q15366	Nucleus
RNA binding protein S1, serine-rich domain	Q15287	Nucleus
PWP2 periodic tryptophan protein homolog (yeast)	Q15269	Nucleus
non-POU domain containing, octamer-binding	Q15233	Nucleus
WD repeat domain 43	Q15061	Nucleus
ribosome biogenesis regulator homolog	Q15050	Nucleus
elongation factor Tu GTP binding domain containing 2	Q15029	Nucleus
nuclear mitotic apparatus protein 1	Q14980	Nucleus
nucleolar and coiled-body phosphoprotein 1	Q14978	Nucleus
karyopherin (importin) beta 1	Q14974	Nucleus
DR1-associated protein 1 (negative cofactor 2 alpha)	Q14919	Nucleus
major vault protein	Q14764	Nucleus
lamin B receptor	Q14739	Nucleus
protein phosphatase 2, regulatory subunit B', delta	Q14738	Nucleus
BMS1 ribosome biogenesis factor	Q14692	Nucleus
structural maintenance of chromosomes 1A	Q14683	Nucleus
minichromosome maintenance complex component 6	Q14566	Nucleus
RNA binding motif protein 39	Q14498	Nucleus

Appendicies

block of proliferation 1	Q14137	Nucleus
heterogeneous nuclear ribonucleoprotein D (AU-rich element RNA binding protein 1, 37kDa)	Q14103	Nucleus
cytoskeleton associated protein 5	Q14008	Nucleus
exosome component 2	Q13868	Nucleus
DEAD (Asp-Glu-Ala-Asp) box polypeptide 39B	Q13838	Nucleus
KRR1, small subunit (SSU) processome component, homolog (yeast)	Q13601	Nucleus
peptidylprolyl cis/trans isomerase, NIMA-interacting 1	Q13526	Nucleus
Treacher Collins-Franceschetti syndrome 1	Q13428	Nucleus
tripartite motif containing 28	Q13263	Nucleus
serine/arginine-rich splicing factor 5	Q13243	Nucleus
serine/arginine-rich splicing factor 9	Q13242	Nucleus
chromobox homolog 3	Q13185	Nucleus
heterogeneous nuclear ribonucleoprotein A0	Q13151	Nucleus
interleukin enhancer binding factor 3, 90kDa	Q12906	Nucleus
interleukin enhancer binding factor 2	Q12905	Nucleus
interferon-related developmental regulator 2	Q12894	Nucleus
AHNAK nucleoprotein	Q09666	Nucleus
NOP2/Sun RNA methyltransferase family, member 2	Q08J23	Nucleus
structure specific recognition protein 1	Q08945	Nucleus
DEAH (Asp-Glu-Ala-His) box helicase 9	Q08211	Nucleus
serine/arginine-rich splicing factor 4	Q08170	Nucleus
serine/arginine-rich splicing factor 1	Q07955	Nucleus
KH domain containing, RNA binding, signal transduction associated 1	Q07666	Nucleus
lamin B2	Q03252	Nucleus
ribosomal protein L6	Q02878	Nucleus
FK506 binding protein 4, 59kDa	Q02790	Nucleus
exosome component 10	Q01780	Nucleus
down-regulator of transcription 1, TBP-binding (negative cofactor 2)	Q01658	Nucleus
serine/arginine-rich splicing factor 2	Q01130	Nucleus
SET nuclear proto-oncogene	Q01105	Nucleus
U2 small nuclear RNA auxiliary factor 1	Q01081	Nucleus
heterogeneous nuclear ribonucleoprotein U (scaffold attachment factor A)	Q00839	Nucleus
FK506 binding protein 3, 25kDa	Q00688	Nucleus
high density lipoprotein binding protein	Q00341	Nucleus
serine/arginine-rich splicing factor 3	P84103	Nucleus
SAP domain containing ribonucleoprotein	P82979	Nucleus
brain abundant, membrane attached signal protein 1	P80723	Nucleus
protein kinase, DNA-activated, catalytic polypeptide	P78527	Nucleus
ribonucleic acid export 1	P78406	Nucleus
general transcription factor IIi	P78347	Nucleus
ubiquitin-conjugating enzyme E2L 3	P68036	Nucleus
Y box binding protein 1	P67809	Nucleus
ubiquitin-conjugating enzyme E2I	P63279	Nucleus
small ubiquitin-like modifier 1	P63165	Nucleus
transformer 2 beta homolog (Drosophila)	P62995	Nucleus
ribosomal protein L10a	P62906	Nucleus
RAN, member RAS oncogene family	P62826	Nucleus
proteasome (prosome, macropain) 26S subunit, ATPase, 6	P62333	Nucleus

Appendicies

small nuclear ribonucleoprotein D3 polypeptide 18kDa	P62318	Nucleus
small nuclear ribonucleoprotein D2 polypeptide 16.5kDa	P62316	Nucleus
small nuclear ribonucleoprotein D1 polypeptide 16kDa	P62314	Nucleus
small nuclear ribonucleoprotein polypeptide F	P62306	Nucleus
small nuclear ribonucleoprotein polypeptide E	P62304	Nucleus
proteasome (prosome, macropain) 26S subunit, ATPase, 5	P62195	Nucleus
nuclear transport factor 2	P61970	Nucleus
WD repeat domain 5	P61964	Nucleus
ribosomal protein S3A	P61247	Nucleus
WD repeat domain 4	P57081	Nucleus
heterogeneous nuclear ribonucleoprotein H2 (H')	P55795	Nucleus
SNU13 homolog, small nuclear ribonucleoprotein (U4/U6.U5)	P55769	Nucleus
adenosine deaminase, RNA-specific	P55265	Nucleus
adenosine kinase	P55263	Nucleus
nucleosome assembly protein 1-like 1	P55209	Nucleus
CSE1 chromosome segregation 1-like (yeast)	P55060	Nucleus
RAD23 homolog B, nucleotide excision repair protein	P54727	Nucleus
SUB1 homolog (S. cerevisiae)	P53999	Nucleus
nucleoporin 98kDa	P52948	Nucleus
heterogeneous nuclear ribonucleoprotein F	P52597	Nucleus
polymerase (RNA) II (DNA directed) polypeptide H	P52434	Nucleus
karyopherin alpha 2 (RAG cohort 1, importin alpha 1)	P52292	Nucleus
heterogeneous nuclear ribonucleoprotein M	P52272	Nucleus
SWI/SNF related, matrix associated, actin dependent regulator of chromatin, subfamily a, member 4	P51532	Nucleus
annexin A11	P50995	Nucleus
MRE11 homolog A, double strand break repair nuclease	P49959	Nucleus
guanine monphosphate synthase	P49915	Nucleus
RAN binding protein 2	P49792	Nucleus
RNA binding motif protein 25	P49756	Nucleus
minichromosome maintenance complex component 2	P49736	Nucleus
primase, DNA, polypeptide 2 (58kDa)	P49643	Nucleus
nuclear autoantigenic sperm protein (histone-binding)	P49321	Nucleus
Yes-associated protein 1	P46937	Nucleus
BCL2-associated athanogene 6	P46379	Nucleus
NOP2 nucleolar protein	P46087	Nucleus
Ran GTPase activating protein 1	P46060	Nucleus
marker of proliferation Ki-67	P46013	Nucleus
chromobox homolog 5	P45973	Nucleus
RAN binding protein 1	P43487	Nucleus
mutS homolog 2	P43246	Nucleus
matrin 3	P43243	Nucleus
cyclin-dependent kinase inhibitor 2A	P42771	Nucleus
superkiller viralicidic activity 2-like 2 (S. cerevisiae)	P42285	Nucleus
signal transducer and activator of transcription 1, 91kDa	P42224	Nucleus
thymopoietin	P42167	Nucleus
BUD31 homolog	P41223	Nucleus
signal transducer and activator of transcription 3 (acute-phase response factor)	P40763	Nucleus
flap structure-specific endonuclease 1	P39748	Nucleus
ribosomal protein L3	P39023	Nucleus
eukaryotic translation initiation factor 4A3	P38919	Nucleus

RNA binding motif protein, X-linked	P38159	Nucleus
polymerase (RNA) II (DNA directed) polypeptide I, 14.5kDa	P36954	Nucleus
protein phosphatase 1, catalytic subunit, gamma isozyme	P36873	Nucleus
tripartite motif containing 23	P36406	Nucleus
proteasome (prosome, macropain) 26S subunit, ATPase, 2	P35998	Nucleus
DEK proto-oncogene	P35659	Nucleus
FUS RNA binding protein	P35637	Nucleus
ribosomal protein L22	P35268	Nucleus
prohibitin	P35232	Nucleus
minichromosome maintenance complex component 7	P33993	Nucleus
minichromosome maintenance complex component 5	P33992	Nucleus
minichromosome maintenance complex component 4	P33991	Nucleus
deoxyuridine triphosphatase	P33316	Nucleus
ribosomal protein L9	P32969	Nucleus
cytidine deaminase	P32320	Nucleus
heterogeneous nuclear ribonucleoprotein H1 (H)	P31943	Nucleus
heterogeneous nuclear ribonucleoprotein H3 (2H9)	P31942	Nucleus
DnaJ (Hsp40) homolog, subfamily A, member 1	P31689	Nucleus
ribonucleotide reductase M2	P31350	Nucleus
cytidine monophosphate (UMP-CMP) kinase 1, cytosolic	P30085	Nucleus
ribosomal protein L12	P30050	Nucleus
polymerase (DNA directed), delta 1, catalytic subunit	P28340	Nucleus
APEX nuclease (multifunctional DNA repair enzyme) 1	P27695	Nucleus
replication protein A1, 70kDa	P27694	Nucleus
threonyl-tRNA synthetase	P26639	Nucleus
polypyrimidine tract binding protein 1	P26599	Nucleus
ribosomal protein L13	P26373	Nucleus
U2 small nuclear RNA auxiliary factor 2	P26368	Nucleus
DNA (cytosine-5-)-methyltransferase 1	P26358	Nucleus
DEAD (Asp-Glu-Ala-Asp) box helicase 6	P26196	Nucleus
DnaJ (Hsp40) homolog, subfamily B, member 1	P25685	Nucleus
nuclear transcription factor Y, beta	P25208	Nucleus
minichromosome maintenance complex component 3	P25205	Nucleus
ribonucleotide reductase M1	P23921	Nucleus
cofilin 1 (non-muscle)	P23528	Nucleus
splicing factor proline/glutamine-rich	P23246	Nucleus
transcription elongation factor A (SII), 1	P23193	Nucleus
heterogeneous nuclear ribonucleoprotein A2/B1	P22626	Nucleus
fibrillarin	P22087	Nucleus
cysteine and glycine-rich protein 1	P21291	Nucleus
parathymosin	P20962	Nucleus
lamin B1	P20700	Nucleus
basic transcription factor 3	P20290	Nucleus
nucleolin	P19338	Nucleus
ligase I, DNA, ATP-dependent	P18858	Nucleus
SON DNA binding protein	P18583	Nucleus
ribosomal protein L7	P18124	Nucleus
proteasome (prosome, macropain) 26S subunit, ATPase, 3	P17980	Nucleus
DEAD (Asp-Glu-Ala-Asp) box helicase 5	P17844	Nucleus
CTP synthase 1	P17812	Nucleus
high mobility group AT-hook 1	P17096	Nucleus
Y box binding protein 3	P16989	Nucleus

Appendicies

histone cluster 1, H1b	P16401	Nucleus
heterogeneous nuclear ribonucleoprotein L	P14866	Nucleus
small nuclear ribonucleoprotein polypeptides B and B1	P14678	Nucleus
X-ray repair complementing defective repair in Chinese hamster cells 5 (double-strand-break rejoining)	P13010	Nucleus
X-ray repair complementing defective repair in Chinese hamster cells 6	P12956	Nucleus
translocated promoter region, nuclear basket protein	P12270	Nucleus
proliferating cell nuclear antigen	P12004	Nucleus
cyclin-dependent kinase 4	P11802	Nucleus
topoisomerase (DNA) II alpha 170kDa	P11388	Nucleus
topoisomerase (DNA) I	P11387	Nucleus
TROVE domain family, member 2	P10155	Nucleus
poly (ADP-ribose) polymerase 1	P09874	Nucleus
small nuclear ribonucleoprotein polypeptide A'	P09661	Nucleus
heterogeneous nuclear ribonucleoprotein A1	P09651	Nucleus
high mobility group box 1	P09429	Nucleus
nuclear factor I/C (CCAAT-binding transcription factor)	P08651	Nucleus
H1 histone family, member 0	P07305	Nucleus
nucleophosmin (nucleolar phosphoprotein B23, numatrin)	P06748	Nucleus
cyclin-dependent kinase 1	P06493	Nucleus
prothymosin, alpha	P06454	Nucleus
Sjogren syndrome antigen B (autoantigen La)	P05455	Nucleus
lamin A/C	P02545	Nucleus
purine nucleoside phosphorylase	P00491	Nucleus
actin-like 6A	O96019	Nucleus
3'(2'), 5'-bisphosphate nucleotidase 1	O95861	Nucleus
importin 7	O95373	Nucleus
LUC7-like 3 pre-mRNA splicing factor	O95232	Nucleus
pre-mRNA processing factor 6	O94906	Nucleus
metastasis associated 1 family, member 2	O94776	Nucleus
signal recognition particle 72kDa	O76094	Nucleus
ribosomal L1 domain containing 1	O76021	Nucleus
survival motor neuron domain containing 1	O75940	Nucleus
DnaJ (Hsp40) homolog, subfamily C, member 8	O75937	Nucleus
breast carcinoma amplified sequence 2	O75934	Nucleus
nucleoporin 155kDa	O75694	Nucleus
surfeit 6	O75683	Nucleus
small nuclear ribonucleoprotein 200kDa (U5)	O75643	Nucleus
splicing factor 3b, subunit 1, 155kDa	O75533	Nucleus
barrier to autointegration factor 1	O75531	Nucleus
PC4 and SFRS1 interacting protein 1	O75475	Nucleus
PRP40 pre-mRNA processing factor 40 homolog A	O75400	Nucleus
H2A histone family, member Y	O75367	Nucleus
dyskeratosis congenita 1, dyskerin	O60832	Nucleus
polyglutamine binding protein 1	O60828	Nucleus
synaptotagmin binding, cytoplasmic RNA interacting protein	O60506	Nucleus
aquarius intron-binding spliceosomal factor	O60306	Nucleus
SWI/SNF related, matrix associated, actin dependent regulator of chromatin, subfamily a, member 5	O60264	Nucleus
nudix (nucleoside diphosphate linked moiety X)-type motif 21	O43809	Nucleus

Appendicies

HIV-1 Tat specific factor 1	O43719	Nucleus
BUB3 mitotic checkpoint protein	O43684	Nucleus
pleiotropic regulator 1	O43660	Nucleus
2'-deoxynucleoside 5'-phosphate N-hydrolase 1	O43598	Nucleus
exportin, tRNA	O43592	Nucleus
heterogeneous nuclear ribonucleoprotein R	O43390	Nucleus
transforming growth factor beta 1 induced transcript 1	O43294	Nucleus
zw10 kinetochore protein	O43264	Nucleus
ribosomal RNA processing 8, methyltransferase, homolog (yeast)	O43159	Nucleus
DEAH (Asp-Glu-Ala-His) box helicase 15	O43143	Nucleus
CD3e molecule, epsilon associated protein	O15446	Nucleus
progesterone receptor membrane component 2	O15173	Nucleus
polymerase (RNA) I polypeptide C, 30kDa	O15160	Nucleus
exportin 1	O14980	Nucleus
heterogeneous nuclear ribonucleoprotein D-like	O14979	Nucleus
histone acetyltransferase 1	O14929	Nucleus
transcription elongation regulator 1	O14776	Nucleus
karyopherin alpha 4 (importin alpha 3)	O00629	Nucleus
NOP56 ribonucleoprotein	O00567	Nucleus
pescadillo ribosomal biogenesis factor 1	O00541	Nucleus
bridging integrator 1	O00499	Nucleus
importin 5	O00410	Nucleus
chloride intracellular channel 1	O00299	Nucleus
DNA fragmentation factor, 45kDa, alpha polypeptide	O00273	Nucleus
aryl hydrocarbon receptor interacting protein	O00170	Nucleus
DEAD (Asp-Glu-Ala-Asp) box polypeptide 39A	O00148	Nucleus
protein phosphatase methylesterase 1	Q9Y570	Other
LUC7-like 2 pre-mRNA splicing factor	Q9Y383	Other
thioredoxin-related transmembrane protein 2	Q9Y320	Other
cysteine and histidine-rich domain (CHORD) containing 1	Q9UHD1	Other
family with sequence similarity 105, member A	Q9NUU6	Other
acidic residue methyltransferase 1	Q9H993	Other
replication termination factor 2 domain containing 1	Q9BY42	Other
eukaryotic translation initiation factor 3, subunit C	Q99613	Other
pseudouridylate synthase 7 (putative)	Q96PZ0	Other
ubiquitin protein ligase E3 component n-recognin 7 (putative)	Q8N806	Other
eukaryotic translation initiation factor 3, subunit M	Q7L2H7	Other
La ribonucleoprotein domain family, member 4	Q71RC2	Other
RNA binding motif, single stranded interacting protein 3	Q6XE24	Other
5'-nucleotidase domain containing 1	Q5TFE4	Other
ubiquitin associated protein 2-like	Q14157	Other
G protein pathway suppressor 1	Q13098	Other
cyclin-dependent kinase 3	Q00526	Other
ribosomal protein L8	P62917	Other
acidic (leucine-rich) nuclear phosphoprotein 32 family, member A	P39687	Other
tropomyosin 2 (beta)	P07951	Other
hemoglobin, delta	P02042	Other
phosphoribosyl pyrophosphate synthetase-associated protein 2	O60256	Other
phosphoglycolate phosphatase	A6NDG6	Other

Appendicies

chloride intracellular channel 4	Q9Y696	Plasma Membrane
talin 1	Q9Y490	Plasma Membrane
canopy FGF signaling regulator 2	Q9Y2B0	Plasma Membrane
stomatin (EPB72)-like 2	Q9UJZ1	Plasma Membrane
testin LIM domain protein	Q9UGI8	Plasma Membrane
prostaglandin F2 receptor inhibitor	Q9P2B2	Plasma Membrane
sema domain, seven thrombospondin repeats (type 1 and type 1-like), transmembrane domain (TM) and short cytoplasmic domain, (semaphorin) 5B	Q9P283	Plasma Membrane
transmembrane protein 14C	Q9P0S9	Plasma Membrane
VAMP (vesicle-associated membrane protein)-associated protein A, 33kDa	Q9P0L0	Plasma Membrane
cornichon family AMPA receptor auxiliary protein 4	Q9P003	Plasma Membrane
olfactory receptor, family 5, subfamily AC, member 2	Q9NZP5	Plasma Membrane
podocalyxin-like 2	Q9NZ53	Plasma Membrane
trans-2,3-enoyl-CoA reductase	Q9NZ01	Plasma Membrane
FAT atypical cadherin 2	Q9NYQ8	Plasma Membrane
Ly1 antibody reactive	Q9NX58	Plasma Membrane
adipocyte plasma membrane associated protein	Q9HDC9	Plasma Membrane
pinin, desmosome associated protein	Q9H307	Plasma Membrane
tweety family member 3	Q9C0H2	Plasma Membrane
solute carrier family 38, member 2	Q96QD8	Plasma Membrane
membrane bound O-acyltransferase domain containing 7	Q96N66	Plasma Membrane
potassium channel tetramerization domain containing 12	Q96CX2	Plasma Membrane
solute carrier family 38, member 5	Q8WUX1	Plasma Membrane
kinectin 1 (kinesin receptor)	Q86UP2	Plasma Membrane
zinc finger CCCH-type, antiviral 1	Q7Z2W4	Plasma Membrane
CD109 molecule	Q6YHK3	Plasma Membrane
vasorin	Q6EMK4	Plasma Membrane
tensin 3	Q68CZ2	Plasma Membrane
STEAP family member 4	Q687X5	Plasma Membrane
annexin A8-like 1	Q5VT79	Plasma Membrane
GNAS complex locus	Q5JWF2	Plasma Membrane

Appendicies

NODAL modulator 1	Q5JPE7	Plasma Membrane
zyxin	Q15942	Plasma Membrane
vesicle-associated membrane protein 3	Q15836	Plasma Membrane
solute carrier family 1 (neutral amino acid transporter), member 5	Q15758	Plasma Membrane
solute carrier family 9, subfamily A (NHE3, cation proton antiporter 3), member 3 regulator 2	Q15599	Plasma Membrane
paraoxonase 2	Q15165	Plasma Membrane
plastin 1	Q14651	Plasma Membrane
cell cycle associated protein 1	Q14444	Plasma Membrane
flotillin 2	Q14254	Plasma Membrane
cortactin	Q14247	Plasma Membrane
desmoglein 2	Q14126	Plasma Membrane
spectrin, alpha, non-erythrocytic 1	Q13813	Plasma Membrane
four and a half LIM domains 3	Q13643	Plasma Membrane
trophoblast glycoprotein	Q13641	Plasma Membrane
tissue specific transplantation antigen P35B	Q13630	Plasma Membrane
integrin-linked kinase	Q13418	Plasma Membrane
aminoacyl tRNA synthetase complex-interacting multifunctional protein 2	Q13155	Plasma Membrane
bone marrow stromal cell antigen 2	Q10589	Plasma Membrane
caveolin 1, caveolae protein, 22kDa	Q03135	Plasma Membrane
solute carrier family 7 (amino acid transporter light chain, L system), member 5	Q01650	Plasma Membrane
interferon induced transmembrane protein 3	Q01628	Plasma Membrane
CAP, adenylate cyclase-associated protein 1 (yeast)	Q01518	Plasma Membrane
spectrin, beta, non-erythrocytic 1	Q01082	Plasma Membrane
clathrin, heavy chain (Hc)	Q00610	Plasma Membrane
Dab, mitogen-responsive phosphoprotein, homolog 2 (Drosophila)	P98082	Plasma Membrane
guanine nucleotide binding protein (G protein), gamma 5	P63218	Plasma Membrane
ras-related C3 botulinum toxin substrate 1 (rho family, small GTP binding protein Rac1)	P63000	Plasma Membrane
guanine nucleotide binding protein (G protein), beta polypeptide 2	P62879	Plasma Membrane
guanine nucleotide binding protein (G protein), beta polypeptide 1	P62873	Plasma Membrane
chemokine (C-X-C motif) receptor 4	P61073	Plasma Membrane
chloride channel, nucleotide-sensitive, 1A	P54105	Plasma Membrane

Appendicies

solute carrier family 16 (monocarboxylate transporter), member 1	P53985	Plasma Membrane
basal cell adhesion molecule (Lutheran blood group)	P50895	Plasma Membrane
CD151 molecule (Raph blood group)	P48509	Plasma Membrane
STT3A, subunit of the oligosaccharyltransferase complex (catalytic)	P46977	Plasma Membrane
melanoma cell adhesion molecule	P43121	Plasma Membrane
ATPase, H+ transporting, lysosomal 70kDa, V1 subunit A	P38606	Plasma Membrane
basigin (Ok blood group)	P35613	Plasma Membrane
catenin (cadherin-associated protein), alpha 1, 102kDa	P35221	Plasma Membrane
glypican 1	P35052	Plasma Membrane
L1 cell adhesion molecule	P32004	Plasma Membrane
transmembrane 4 L six family member 1	P30408	Plasma Membrane
myristoylated alanine-rich protein kinase C substrate	P29966	Plasma Membrane
stomatin	P27105	Plasma Membrane
moesin	P26038	Plasma Membrane
cadherin 2, type 1, N-cadherin (neuronal)	P19022	Plasma Membrane
vinculin	P18206	Plasma Membrane
endoglin	P17813	Plasma Membrane
CD44 molecule (Indian blood group)	P16070	Plasma Membrane
mucin 1, cell surface associated	P15941	Plasma Membrane
folate receptor 1 (adult)	P15328	Plasma Membrane
ezrin	P15311	Plasma Membrane
alanyl (membrane) aminopeptidase	P15144	Plasma Membrane
junction plakoglobin	P14923	Plasma Membrane
CD99 molecule	P14209	Plasma Membrane
CD59 molecule, complement regulatory protein	P13987	Plasma Membrane
lysosomal-associated membrane protein 2	P13473	Plasma Membrane
annexin A4	P09525	Plasma Membrane
annexin A5	P08758	Plasma Membrane
solute carrier family 3 (amino acid transporter heavy chain), member 2	P08195	Plasma Membrane
CD55 molecule, decay accelerating factor for complement (Cromer blood group)	P08174	Plasma Membrane
ras homolog family member C	P08134	Plasma Membrane

annexin A6	P08133	Plasma Membrane
annexin A2	P07355	Plasma Membrane
integrin, alpha V	P06756	Plasma Membrane
alkaline phosphatase, liver/bone/kidney	P05186	Plasma Membrane
ATPase, Na+/K+ transporting, alpha 1 polypeptide	P05023	Plasma Membrane
guanine nucleotide binding protein (G protein), alpha inhibiting activity polypeptide 2	P04899	Plasma Membrane
annexin A1	P04083	Plasma Membrane
transferrin receptor	P02786	Plasma Membrane
neuroblastoma RAS viral (v-ras) oncogene homolog	P01111	Plasma Membrane
epidermal growth factor receptor	P00533	Plasma Membrane
VAMP (vesicle-associated membrane protein)-associated protein B and C	O95292	Plasma Membrane
ER lipid raft associated 2	O94905	Plasma Membrane
flotillin 1	O75955	Plasma Membrane
ER lipid raft associated 1	O75477	Plasma Membrane
solute carrier family 16 (monocarboxylate transporter), member 7	O60669	Plasma Membrane
diaphanous-related formin 1	O60610	Plasma Membrane
LanC lantibiotic synthetase component C-like 1 (bacterial)	O43813	Plasma Membrane
erythrocyte membrane protein band 4.1-like 2	O43491	Plasma Membrane
solute carrier family 16 (monocarboxylate transporter), member 3	O15427	Plasma Membrane
leptin receptor overlapping transcript	O15243	Plasma Membrane
solute carrier family 9, subfamily A (NHE3, cation proton antiporter 3), member 3 regulator 1	O14745	Plasma Membrane
progesterone receptor membrane component 1	O00264	Plasma Membrane

Appendix 2. Full list of proteins obtained from whole-cell mass spectrometry of HeLa A3 cells. Identification of proteins in the whole cell proteome of HeLa A3 cells. For inclusion P < 0.05 for each protein selected using Anova and there was a minimum of two unique peptides used for identification. Total proteins identified = 1227. QIAGEN'S Ingenuity Pathway Analysis was used for determining the cellular localisation of each protein.
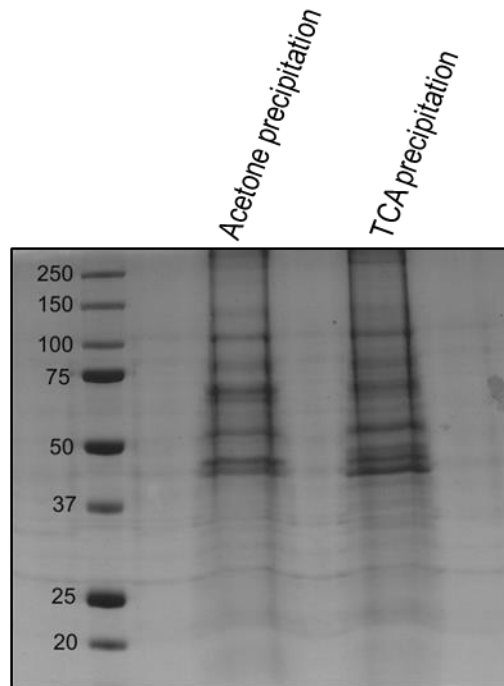
Appendix 3. Coomassie blue-stained gel showing acetone vs. TCA precipitation of hydrodynamically-sheared HeLa A3 cell residues. Six 10 cm diameter tissue culture dishes were exposed to a hydrodynamic force from a standardised shower. The residues were washed with PBS and dissolved in SDS-containing Sample Buffer. Acetone precipitation or TCA precipitation was then carried out to concentrate the samples after which the residues were suspended in 30µl of Sample Buffer and each one loaded into a single well. A 10% (w/v) polyacrylamide gel was used.

Appendices

FASP-treated hydrodynamically-sheared HeLa A3 cell mass spectrometry			
Protein / gene name	**UniProt ID**	**Cellular location**	**Adhesome protein**
LIM domain and actin binding 1	Q9UHB6	Cytoplasm	Yes
PDZ and LIM domain 7 (enigma)	Q9NR12	Cytoplasm	Yes
tubulin, beta 1 class VI	Q9H4B7	Cytoplasm	Yes
BRICK1, SCAR/WAVE actin-nucleating complex subunit	Q8WUW1	Cytoplasm	Yes
cell migration inducing protein, hyaluronan binding	Q8WUJ3	Cytoplasm	Yes
keratin 78, type II	Q8N1N4	Cytoplasm	Yes
fermitin family member 3	Q86UX7	Cytoplasm	Yes
keratin 77, type II	Q7Z794	Cytoplasm	Yes
keratin 71, type II	Q3SY84	Cytoplasm	Yes
keratin 31, type I	Q15323	Cytoplasm	Yes
LIM and SH3 protein 1	Q14847	Cytoplasm	Yes
four and a half LIM domains 1	Q13642	Cytoplasm	Yes
myosin IE	Q12965	Cytoplasm	Yes
caldesmon 1	Q05682	Cytoplasm	Yes
keratin 17, type I	Q04695	Cytoplasm	Yes
keratin 76, type II	Q01546	Cytoplasm	Yes
sushi-repeat containing protein, X-linked	P78539	Cytoplasm	Yes
tubulin, beta 4B class IVb	P68371	Cytoplasm	Yes
tubulin, alpha 4a	P68366	Cytoplasm	Yes
tubulin, alpha 1b	P68363	Cytoplasm	Yes
actin, alpha 2, smooth muscle, aorta	P62736	Cytoplasm	Yes
actin, beta	P60709	Cytoplasm	Yes
myosin, light chain 6, alkali, smooth muscle and non-muscle	P60660	Cytoplasm	Yes
capping protein (actin filament) muscle Z-line, alpha 2	P47755	Cytoplasm	Yes
IQ motif containing GTPase activating protein 1	P46940	Cytoplasm	Yes
keratin 2, type II	P35908	Cytoplasm	Yes
myosin, heavy chain 9, non-muscle	P35579	Cytoplasm	Yes
keratin 9, type I	P35527	Cytoplasm	Yes
coronin, actin binding protein, 1A	P31146	Cytoplasm	yes
CAP-GLY domain containing linker protein 1	P30622	Cytoplasm	Yes
myosin, light chain 9, regulatory	P24844	Cytoplasm	Yes
filamin A, alpha	P21333	Cytoplasm	Yes
keratin 4, type II	P19013	Cytoplasm	Yes
calpain 2, (m/II) large subunit	P17655	Cytoplasm	Yes
plastin 3	P13797	Cytoplasm	Yes
keratin 5, type II	P13647	Cytoplasm	Yes
keratin 13, type I	P13646	Cytoplasm	Yes
keratin 10, type I	P13645	Cytoplasm	Yes
actinin, alpha 1	P12814	Cytoplasm	Yes
keratin 3, type II	P12035	Cytoplasm	Yes
keratin 16, type I	P08779	Cytoplasm	Yes
vimentin	P08670	Cytoplasm	Yes
pleckstrin	P08567	Cytoplasm	Yes
profilin 1	P07737	Cytoplasm	Yes
tubulin, beta class I	P07437	Cytoplasm	Yes
enolase 1, (alpha)	P06733	Cytoplasm	Yes

keratin 8, type II	P05787	Cytoplasm	Yes
keratin 18, type I	P05783	Cytoplasm	Yes
keratin 1, type II	P04264	Cytoplasm	Yes
keratin 6B, type II	P04259	Cytoplasm	Yes
keratin 6A, type II	P02538	Cytoplasm	Yes
keratin 14, type I	P02533	Cytoplasm	Yes
adaptor-related protein complex 2, alpha 2 subunit	O94973	Cytoplasm	Yes
keratin 34, type I	O76011	Cytoplasm	Yes
filamin B, beta	O75369	Cytoplasm	Yes
keratin 86, type II	O43790	Cytoplasm	Yes
actinin, alpha 4	O43707	Cytoplasm	Yes
myosin, light chain 12B, regulatory	O14950	Cytoplasm	Yes
myosin IC	O00159	Cytoplasm	Yes
cofilin 1 (non-muscle)	P23528	Cytoplasm	Yes
GULP, engulfment adaptor PTB domain containing 1	Q9UBP9	Cytoplasm	Possible interaction
stonin 2	Q8WXE9	Cytoplasm	Possible interaction
SERPINE1 mRNA binding protein 1	Q8NC51	Cytoplasm	Possible interaction
coiled-coil domain containing 146	Q8IYE0	Cytoplasm	Possible interaction
hornerin	Q86YZ3	Cytoplasm	Possible interaction
filaggrin family member 2	Q5D862	Cytoplasm	Possible interaction
RAB11B, member RAS oncogene family	Q15907	Cytoplasm	Possible interaction
Ras suppressor protein 1	Q15404	Cytoplasm	Possible interaction
peptidylprolyl isomerase A (cyclophilin A)	P62937	Cytoplasm	Possible interaction
ribosomal protein S4, X-linked	P62701	Cytoplasm	Possible interaction
tyrosine 3-monooxygenase/tryptophan 5-monooxygenase activation protein, epsilon	P62258	Cytoplasm	Possible interaction
ribosomal protein S16	P62249	Cytoplasm	Possible interaction
ribosomal protein S15a	P62244	Cytoplasm	Possible interaction
ribosomal protein S8	P62241	Cytoplasm	Possible interaction
RAP1B, member of RAS oncogene family	P61224	Cytoplasm	Possible interaction
ribosomal protein L29	P47914	Cytoplasm	Possible interaction
epidermal growth factor receptor pathway substrate 15	P42566	Cytoplasm	Possible interaction
ribosomal protein S3	P23396	Cytoplasm	Possible interaction
poly(A) binding protein, cytoplasmic 1	P11940	Cytoplasm	Possible interaction
heat shock 70kDa protein 8	P11142	Cytoplasm	Possible interaction
heat shock 70kDa protein 5 (glucose-regulated protein, 78kDa)	P11021	Cytoplasm	Possible interaction
prolyl 4-hydroxylase, beta polypeptide	P07237	Cytoplasm	Possible interaction
lipoprotein lipase	P06858	Cytoplasm	Possible interaction
ribosomal protein, large, P2	P05387	Cytoplasm	Possible interaction
arginase 1	P05089	Cytoplasm	Possible interaction
aldolase A, fructose-bisphosphate	P04075	Cytoplasm	Possible interaction
Kirsten rat sarcoma viral oncogene homolog	P01116	Cytoplasm	Possible interaction
torsin family 1, member B (torsin B)	O14657	Cytoplasm	Possible interaction
quiescin Q6 sulfhydryl oxidase 1	O00391	Cytoplasm	Possible interaction
nascent polypeptide-associated complex alpha subunit	E9PAV3	Cytoplasm	Possible interaction
keratin associated protein 2-3	P0C7H8	Cytoplasm	Possible interaction
ribosomal protein L36	Q9Y3U8	Cytoplasm	No
MRT4 homolog, ribosome maturation factor	Q9UKD2	Cytoplasm	No
cysteine-rich secretory protein LCCL domain containing 1	Q9H336	Cytoplasm	No

cysteine-rich secretory protein LCCL domain containing 2	Q9H0B8	Cytoplasm	No
adaptor-related protein complex 2, mu 1 subunit	Q96CW1	Cytoplasm	No
programmed cell death 6 interacting protein	Q8WUM4	Cytoplasm	No
chromosome 3 open reading frame 58	Q8NDZ4	Cytoplasm	No
chromosome 1 open reading frame 68	Q5T750	Cytoplasm	No
keratinocyte proline-rich protein	Q5T749	Cytoplasm	No
eukaryotic translation initiation factor 4A2	Q14240	Cytoplasm	No
bleomycin hydrolase	Q13867	Cytoplasm	No
phosphatidylinositol binding clathrin assembly protein	Q13492	Cytoplasm	No
transcription factor A, mitochondrial	Q00059	Cytoplasm	No
ribosomal protein L24	P83731	Cytoplasm	No
hemoglobin, beta	P68871	Cytoplasm	No
ribosomal protein S27a	P62979	Cytoplasm	No
ribosomal protein L11	P62913	Cytoplasm	No
ribosomal protein L30	P62888	Cytoplasm	No
Finkel-Biskis-Reilly murine sarcoma virus (FBR-MuSV) ubiquitously expressed	P62861	Cytoplasm	No
ribosomal protein S23	P62266	Cytoplasm	No
ADP-ribosylation factor 3	P61204	Cytoplasm	No
triosephosphate isomerase 1	P60174	Cytoplasm	No
adaptor-related protein complex 2, sigma 1 subunit	P53680	Cytoplasm	No
suppression of tumorigenicity 13 (colon carcinoma) (Hsp70 interacting protein)	P50502	Cytoplasm	No
signal recognition particle 9kDa	P49458	Cytoplasm	No
ribosomal protein L34	P49207	Cytoplasm	No
ATP synthase, H+ transporting, mitochondrial F1 complex, O subunit	P48047	Cytoplasm	No
peptidylprolyl isomerase C (cyclophilin C)	P45877	Cytoplasm	No
ribosomal protein L35	P42766	Cytoplasm	No
ribosomal protein L13a	P40429	Cytoplasm	No
hippocalcin-like 1	P37235	Cytoplasm	No
signal recognition particle 14kDa (homologous Alu RNA binding protein)	P37108	Cytoplasm	No
caspase 14, apoptosis-related cysteine peptidase	P31944	Cytoplasm	No
biliverdin reductase B	P30043	Cytoplasm	No
adenosylhomocysteinase	P23526	Cytoplasm	No
peptidylprolyl isomerase B (cyclophilin B)	P23284	Cytoplasm	No
eukaryotic translation initiation factor 2, subunit 2 beta, 38kDa	P20042	Cytoplasm	No
ribosomal protein S2	P15880	Cytoplasm	No
pyruvate kinase, muscle	P14618	Cytoplasm	No
aldo-keto reductase family 1, member A1 (aldehyde reductase)	P14550	Cytoplasm	No
eukaryotic translation elongation factor 2	P13639	Cytoplasm	No
glutathione S-transferase pi 1	P09211	Cytoplasm	No
guanine nucleotide binding protein (G protein), alpha inhibiting activity polypeptide 3	P08754	Cytoplasm	No
heat shock protein 90kDa alpha (cytosolic), class B member 1	P08238	Cytoplasm	No
heat shock protein 90kDa alpha (cytosolic), class A member 1	P07900	Cytoplasm	No
lactate dehydrogenase B	P07195	Cytoplasm	No
creatine kinase, muscle	P06732	Cytoplasm	No

Appendices

calpain, small subunit 1	P04632	Cytoplasm	No
glyceraldehyde-3-phosphate dehydrogenase	P04406	Cytoplasm	No
phosphoglycerate kinase 1	P00558	Cytoplasm	No
lactate dehydrogenase A	P00338	Cytoplasm	No
adaptor-related protein complex 2, alpha 1 subunit	O95782	Cytoplasm	No
beta-1,4-glucuronyltransferase 1	O43505	Cytoplasm	No
metallothionein 1M	Q8N339	Cytoplasm	No
numb homolog (Drosophila)-like	Q9Y6R0	Cytoplasm	Indirect Signalling
developmentally regulated GTP binding protein 1	Q9Y295	Cytoplasm	Indirect Signalling
protein kinase C and casein kinase substrate in neurons 2	Q9UNF0	Cytoplasm	Indirect Signalling
adducin 3 (gamma)	Q9UEY8	Cytoplasm	Indirect Signalling
calmodulin-like 5	Q9NZT1	Cytoplasm	Indirect Signalling
tropomodulin 2 (neuronal)	Q9NZR1	Cytoplasm	Indirect Signalling
GLI pathogenesis-related 2	Q9H4G4	Cytoplasm	Indirect Signalling
thioredoxin interacting protein	Q9H3M7	Cytoplasm	Indirect Signalling
spectrin, beta, non-erythrocytic 4	Q9H254	Cytoplasm	Indirect Signalling
neural precursor cell expressed, developmentally down-regulated 4-like, E3 ubiquitin protein ligase	Q96PU5	Cytoplasm	Indirect Signalling
protein tyrosine phosphatase type IVA, member 1	Q93096	Cytoplasm	Indirect Signalling
thrombospondin, type I, domain containing 4	Q6ZMP0	Cytoplasm	Indirect Signalling
coactosin-like F-actin binding protein 1	Q14019	Cytoplasm	Indirect Signalling
peroxiredoxin 1	Q06830	Cytoplasm	Indirect Signalling
transgelin	Q01995	Cytoplasm	Indirect Signalling
RAP1A, member of RAS oncogene family	P62834	Cytoplasm	Indirect Signalling
ras homolog family member A	P61586	Cytoplasm	Indirect Signalling
RAB10, member RAS oncogene family	P61026	Cytoplasm	Indirect Signalling
cell division cycle 42	P60953	Cytoplasm	Indirect Signalling
phosphatidylinositol-5-phosphate 4-kinase, type II, alpha	P48426	Cytoplasm	Indirect Signalling
transgelin 2	P37802	Cytoplasm	Indirect Signalling
peroxiredoxin 2	P32119	Cytoplasm	Indirect Signalling
S100 calcium binding protein A7	P31151	Cytoplasm	Indirect Signalling
phosphatidylethanolamine binding protein 1	P30086	Cytoplasm	Indirect Signalling
peroxiredoxin 6	P30041	Cytoplasm	Indirect Signalling
serpin peptidase inhibitor, clade B (ovalbumin), member 3	P29508	Cytoplasm	Indirect Signalling
calmodulin-like 3	P27482	Cytoplasm	Indirect Signalling
S100 calcium binding protein A4	P26447	Cytoplasm	Indirect Signalling
S100 calcium binding protein A1	P23297	Cytoplasm	Indirect Signalling
RAB5A, member RAS oncogene family	P20339	Cytoplasm	Indirect Signalling
ADP-ribosylation factor 4	P18085	Cytoplasm	Indirect Signalling
NME/NM23 nucleoside diphosphate kinase 1	P15531	Cytoplasm	Indirect Signalling
UDP-Gal:betaGlcNAc beta 1,4- galactosyltransferase, polypeptide 1	P15291	Cytoplasm	Indirect Signalling
enolase 3 (beta, muscle)	P13929	Cytoplasm	Indirect Signalling
v-ral simian leukemia viral oncogene homolog A (ras related)	P11233	Cytoplasm	Indirect Signalling
clusterin	P10909	Cytoplasm	Indirect Signalling
related RAS viral (r-ras) oncogene homolog	P10301	Cytoplasm	Indirect Signalling
calpain 1, (mu/I) large subunit	P07384	Cytoplasm	Indirect Signalling
S100 calcium binding protein A9	P06702	Cytoplasm	Indirect Signalling
ATP synthase, H+ transporting, mitochondrial F1 complex, beta polypeptide	P06576	Cytoplasm	Indirect Signalling

myeloperoxidase	P05164	Cytoplasm	Indirect Signalling
S100 calcium binding protein A8	P05109	Cytoplasm	Indirect Signalling
heat shock 27kDa protein 1	P04792	Cytoplasm	Indirect Signalling
epsin 2	O95208	Cytoplasm	Indirect Signalling
copine III	O75131	Cytoplasm	Indirect Signalling
spondin 1, extracellular matrix protein	Q9HCB6	Extracellular Space	Yes
collagen, type XII, alpha 1	Q99715	Extracellular Space	Yes
laminin, alpha 4	Q16363	Extracellular Space	Yes
keratin 33B, type I	Q14525	Extracellular Space	Yes
collagen, type XIV, alpha 1	Q05707	Extracellular Space	Yes
heparan sulfate proteoglycan 2	P98160	Extracellular Space	Yes
keratin 85, type II	P78386	Extracellular Space	Yes
laminin, beta 2 (laminin S)	P55268	Extracellular Space	Yes
wingless-type MMTV integration site family, member 5A	P41221	Extracellular Space	Yes
TIMP metallopeptidase inhibitor 3	P35625	Extracellular Space	Yes
fibrillin 2	P35556	Extracellular Space	Yes
fibrillin 1	P35555	Extracellular Space	Yes
thrombospondin 4	P35443	Extracellular Space	Yes
collagen, type VIII, alpha 1	P27658	Extracellular Space	Yes
tenascin C	P24821	Extracellular Space	Yes
brain-derived neurotrophic factor	P23560	Extracellular Space	Yes
anosmin 1	P23352	Extracellular Space	Yes
fibulin 1	P23142	Extracellular Space	Yes
collagen, type V, alpha 1	P20908	Extracellular Space	Yes
collagen, type VI, alpha 3	P12111	Extracellular Space	Yes
collagen, type VI, alpha 1	P12109	Extracellular Space	Yes
laminin, gamma 1 (formerly LAMB2)	P11047	Extracellular Space	Yes
collagen, type IV, alpha 2	P08572	Extracellular Space	Yes
collagen, type I, alpha 2	P08123	Extracellular Space	Yes
thrombospondin 1	P07996	Extracellular Space	Yes
laminin, beta 1	P07942	Extracellular Space	Yes
gelsolin	P06396	Extracellular Space	Yes
vitronectin	P04004	Extracellular	Yes

		Space	
fibronectin 1	P02751	Extracellular Space	Yes
collagen, type III, alpha 1	P02461	Extracellular Space	Yes
collagen, type I, alpha 1	P02452	Extracellular Space	Yes
transforming growth factor, beta 1	P01137	Extracellular Space	Yes
keratin 33A, type I	O76009	Extracellular Space	Yes
WD repeat domain 1	O75083	Extracellular Space	Yes
EGF-like repeats and discoidin I-like domains 3	O43854	Extracellular Space	Yes
chondroadherin	O15335	Extracellular Space	Yes
laminin, alpha 5	O15230	Extracellular Space	Yes
matrilin 2	O00339	Extracellular Space	Yes
inter-alpha-trypsin inhibitor heavy chain family, member 4	Q14624	Extracellular Space	Possible interaction
inter-alpha-trypsin inhibitor heavy chain 3	Q06033	Extracellular Space	Possible interaction
serpin peptidase inhibitor, clade H (heat shock protein 47), member 1, (collagen binding protein 1)	P50454	Extracellular Space	Possible interaction
osteoglycin	P20774	Extracellular Space	Possible interaction
inter-alpha-trypsin inhibitor heavy chain 1	P19827	Extracellular Space	Possible interaction
inter-alpha-trypsin inhibitor heavy chain 2	P19823	Extracellular Space	Possible interaction
bone morphogenetic protein 1	P13497	Extracellular Space	Possible interaction
serpin peptidase inhibitor, clade F (alpha-2 antiplasmin, pigment epithelium derived factor), member 2	P08697	Extracellular Space	Possible interaction
complement component 8, beta polypeptide	P07358	Extracellular Space	Possible interaction
C-type lectin domain family 3, member B	P05452	Extracellular Space	Possible interaction
complement factor I	P05156	Extracellular Space	Possible interaction
serpin peptidase inhibitor, clade G (C1 inhibitor), member 1	P05155	Extracellular Space	Possible interaction
serpin peptidase inhibitor, clade A (alpha-1 antiproteinase, antitrypsin), member 5	P05154	Extracellular Space	Possible interaction
serpin peptidase inhibitor, clade E (nexin, plasminogen activator inhibitor type 1), member 1	P05121	Extracellular Space	Possible interaction
group-specific component (vitamin D binding protein)	P02774	Extracellular Space	Possible interaction
apolipoprotein H (beta-2-glycoprotein I)	P02749	Extracellular Space	Possible interaction
complement component 9	P02748	Extracellular Space	Possible interaction
sema domain, immunoglobulin domain (Ig), short basic domain, secreted, (semaphorin) 3D	O95025	Extracellular Space	Possible interaction
C-type lectin domain family 11, member A	Q9Y240	Extracellular Space	No
phospholipase A2, group IID	Q9UNK4	Extracellular	No

		Space	
platelet derived growth factor C	Q9NRA1	Extracellular Space	No
C1q and tumor necrosis factor related protein 3	Q9BXJ4	Extracellular Space	No
peroxidasin	Q92626	Extracellular Space	No
ADAM metallopeptidase with thrombospondin type 1 motif, 13	Q76LX8	Extracellular Space	No
dermokine	Q6E0U4	Extracellular Space	No
keratinocyte differentiation-associated protein	P60985	Extracellular Space	No
afamin	P43652	Extracellular Space	No
ribonuclease, RNase A family, 4	P34096	Extracellular Space	No
pregnancy-zone protein	P20742	Extracellular Space	No
carboxypeptidase N, polypeptide 1	P15169	Extracellular Space	No
carboxypeptidase A1 (pancreatic)	P15085	Extracellular Space	No
complement component 4B (Chido blood group)	P0C0L4	Extracellular Space	No
protein S (alpha)	P07225	Extracellular Space	No
coagulation factor XIII, B polypeptide	P05160	Extracellular Space	No
sex hormone-binding globulin	P04278	Extracellular Space	No
lecithin-cholesterol acyltransferase	P04180	Extracellular Space	No
lactotransferrin	P02788	Extracellular Space	No
transferrin	P02787	Extracellular Space	No
alpha-fetoprotein	P02771	Extracellular Space	No
albumin	P02768	Extracellular Space	No
alpha-2-macroglobulin	P01023	Extracellular Space	No
serpin peptidase inhibitor, clade C (antithrombin), member 1	P01008	Extracellular Space	No
coagulation factor X	P00742	Extracellular Space	No
coagulation factor IX	P00740	Extracellular Space	No
coagulation factor II (thrombin)	P00734	Extracellular Space	No
coagulation factor XIII, A1 polypeptide	P00488	Extracellular Space	No
dickkopf WNT signaling pathway inhibitor 1	O94907	Extracellular Space	No
cytokine receptor-like factor 1	O75462	Extracellular Space	No
angiopoietin-like 3	Q9Y5C1	Extracellular Space	Indirect Signalling
lysyl oxidase-like 2	Q9Y4K0	Extracellular Space	Indirect Signalling

angiopoietin-like 2	Q9UKU9	Extracellular Space	Indirect Signalling
ADAM metallopeptidase with thrombospondin type 1 motif, 1	Q9UHI8	Extracellular Space	Indirect Signalling
netrin 4	Q9HB63	Extracellular Space	Indirect Signalling
gremlin 2, DAN family BMP antagonist	Q9H772	Extracellular Space	Indirect Signalling
SPARC related modular calcium binding 1	Q9H4F8	Extracellular Space	Indirect Signalling
angiopoietin-like 4	Q9BY76	Extracellular Space	Indirect Signalling
R-spondin 3	Q9BXY4	Extracellular Space	Indirect Signalling
growth differentiation factor 15	Q99988	Extracellular Space	Indirect Signalling
sema domain, immunoglobulin domain (Ig), short basic domain, secreted, (semaphorin) 3C	Q99985	Extracellular Space	Indirect Signalling
proteoglycan 4	Q92954	Extracellular Space	Indirect Signalling
frizzled-related protein	Q92765	Extracellular Space	Indirect Signalling
HtrA serine peptidase 1	Q92743	Extracellular Space	Indirect Signalling
ADAM metallopeptidase with thrombospondin type 1 motif, 15	Q8TE58	Extracellular Space	Indirect Signalling
latent transforming growth factor beta binding protein 4	Q8N2S1	Extracellular Space	Indirect Signalling
plexin domain containing 2	Q6UX71	Extracellular Space	Indirect Signalling
transforming growth factor, beta-induced, 68kDa	Q15582	Extracellular Space	Indirect Signalling
angiopoietin 1	Q15389	Extracellular Space	Indirect Signalling
periostin, osteoblast specific factor	Q15063	Extracellular Space	Indirect Signalling
latent transforming growth factor beta binding protein 2	Q14767	Extracellular Space	Indirect Signalling
latent transforming growth factor beta binding protein 1	Q14766	Extracellular Space	Indirect Signalling
sema domain, immunoglobulin domain (Ig), short basic domain, secreted, (semaphorin) 3A	Q14563	Extracellular Space	Indirect Signalling
hyaluronan binding protein 2	Q14520	Extracellular Space	Indirect Signalling
sema domain, immunoglobulin domain (Ig), short basic domain, secreted, (semaphorin) 3F	Q13275	Extracellular Space	Indirect Signalling
noggin	Q13253	Extracellular Space	Indirect Signalling
sema domain, immunoglobulin domain (Ig), short basic domain, secreted, (semaphorin) 3B	Q13214	Extracellular Space	Indirect Signalling
multimerin 1	Q13201	Extracellular Space	Indirect Signalling
secreted phosphoprotein 2, 24kDa	Q13103	Extracellular Space	Indirect Signalling
EGF containing fibulin-like extracellular matrix protein 1	Q12805	Extracellular Space	Indirect Signalling
milk fat globule-EGF factor 8 protein	Q08431	Extracellular Space	Indirect Signalling
lysyl oxidase-like 1	Q08397	Extracellular Space	Indirect Signalling
HGF activator	Q04756	Extracellular	Indirect Signalling

		Space	
HtrA serine peptidase 3	P83110	Extracellular Space	Indirect Signalling
dermcidin	P81605	Extracellular Space	Indirect Signalling
transforming growth factor, beta 2	P61812	Extracellular Space	Indirect Signalling
lysozyme	P61626	Extracellular Space	Indirect Signalling
protease, serine, 12 (neurotrypsin, motopsin)	P56730	Extracellular Space	Indirect Signalling
phospholipid transfer protein	P55058	Extracellular Space	Indirect Signalling
microfibrillar-associated protein 2	P55001	Extracellular Space	Indirect Signalling
lumican	P51884	Extracellular Space	Indirect Signalling
cartilage oligomeric matrix protein	P49747	Extracellular Space	Indirect Signalling
mannan-binding lectin serine peptidase 1 (C4/C2 activating component of Ra-reactive factor)	P48740	Extracellular Space	Indirect Signalling
tissue factor pathway inhibitor 2	P48307	Extracellular Space	Indirect Signalling
serpin peptidase inhibitor, clade F (alpha-2 antiplasmin, pigment epithelium derived factor), member 1	P36955	Extracellular Space	Indirect Signalling
chitinase 3-like 1 (cartilage glycoprotein-39)	P36222	Extracellular Space	Indirect Signalling
connective tissue growth factor	P29279	Extracellular Space	Indirect Signalling
lysyl oxidase	P28300	Extracellular Space	Indirect Signalling
macrophage stimulating 1	P26927	Extracellular Space	Indirect Signalling
insulin-like growth factor binding protein 5	P24593	Extracellular Space	Indirect Signalling
bone morphogenetic protein 6	P22004	Extracellular Space	Indirect Signalling
midkine (neurite growth-promoting factor 2)	P21741	Extracellular Space	Indirect Signalling
bone morphogenetic protein 7	P18075	Extracellular Space	Indirect Signalling
insulin-like growth factor binding protein 2, 36kDa	P18065	Extracellular Space	Indirect Signalling
insulin-like growth factor binding protein 3	P17936	Extracellular Space	Indirect Signalling
vascular endothelial growth factor A	P15692	Extracellular Space	Indirect Signalling
chemokine (C-C motif) ligand 5	P13501	Extracellular Space	Indirect Signalling
tissue factor pathway inhibitor (lipoprotein-associated coagulation inhibitor)	P10646	Extracellular Space	Indirect Signalling
serpin peptidase inhibitor, clade E (nexin, plasminogen activator inhibitor type 1), member 2	P07093	Extracellular Space	Indirect Signalling
serpin peptidase inhibitor, clade A (alpha-1 antiproteinase, antitrypsin), member 7	P05543	Extracellular Space	Indirect Signalling
histidine-rich glycoprotein	P04196	Extracellular Space	Indirect Signalling
apolipoprotein B	P04114	Extracellular Space	Indirect Signalling
alpha-2-HS-glycoprotein	P02765	Extracellular	Indirect Signalling

		Space	
alpha-1-microglobulin/bikunin precursor	P02760	Extracellular Space	Indirect Signalling
fibrinogen gamma chain	P02679	Extracellular Space	Indirect Signalling
fibrinogen beta chain	P02675	Extracellular Space	Indirect Signalling
apolipoprotein C-III	P02656	Extracellular Space	Indirect Signalling
apolipoprotein E	P02649	Extracellular Space	Indirect Signalling
apolipoprotein A-I	P02647	Extracellular Space	Indirect Signalling
insulin-like growth factor 2	P01344	Extracellular Space	Indirect Signalling
complement component 5	P01031	Extracellular Space	Indirect Signalling
complement component 3	P01024	Extracellular Space	Indirect Signalling
plasminogen activator, tissue	P00750	Extracellular Space	Indirect Signalling
plasminogen activator, urokinase	P00749	Extracellular Space	Indirect Signalling
plasminogen	P00747	Extracellular Space	Indirect Signalling
protease, serine, 23	O95084	Extracellular Space	Indirect Signalling
gremlin 1, DAN family BMP antagonist	O60565	Extracellular Space	Indirect Signalling
cysteine-rich, angiogenic inducer, 61	O00622	Extracellular Space	Indirect Signalling
peptidylprolyl isomerase E (cyclophilin E)	Q9UNP9	Nucleus	No
GAR1 homolog, ribonucleoprotein	Q9NY12	Nucleus	No
copine I	Q99829	Nucleus	No
S100 calcium binding protein A16	Q96FQ6	Nucleus	No
ADP-ribosyltransferase 4 (Dombrock blood group)	Q93070	Nucleus	No
H1 histone family, member X	Q92522	Nucleus	No
Aly/REF export factor	Q86V81	Nucleus	No
poly(A) binding protein, nuclear 1	Q86U42	Nucleus	No
coiled-coil domain containing 80	Q76M96	Nucleus	No
histone cluster 2, H2bf	Q5QNW6	Nucleus	No
serine/arginine-rich splicing factor 7	Q16629	Nucleus	No
interleukin enhancer binding factor 2	Q12905	Nucleus	No
AHNAK nucleoprotein	Q09666	Nucleus	No
serine/arginine-rich splicing factor 3	P84103	Nucleus	No
brain abundant, membrane attached signal protein 1	P80723	Nucleus	No
Y box binding protein 1	P67809	Nucleus	No
transformer 2 beta homolog (Drosophila)	P62995	Nucleus	No
RAN, member RAS oncogene family	P62826	Nucleus	No
small nuclear ribonucleoprotein D3 polypeptide 18kDa	P62318	Nucleus	No
small nuclear ribonucleoprotein D2 polypeptide 16.5kDa	P62316	Nucleus	No
small nuclear ribonucleoprotein D1 polypeptide 16kDa	P62314	Nucleus	No
small nuclear ribonucleoprotein polypeptide G	P62308	Nucleus	No
small nuclear ribonucleoprotein polypeptide F	P62306	Nucleus	No

Appendices

small nuclear ribonucleoprotein polypeptide E	P62304	Nucleus	No
ribosomal protein S3A	P61247	Nucleus	No
SUB1 homolog (S. cerevisiae)	P53999	Nucleus	No
ArfGAP with FG repeats 1	P52594	Nucleus	No
BUD31 homolog	P41223	Nucleus	No
RNA binding motif protein, X-linked	P38159	Nucleus	No
DEK proto-oncogene	P35659	Nucleus	No
high mobility group box 2	P26583	Nucleus	No
cysteine and glycine-rich protein 1	P21291	Nucleus	No
basic transcription factor 3	P20290	Nucleus	No
nucleolin	P19338	Nucleus	No
small nuclear ribonucleoprotein polypeptides B and B1	P14678	Nucleus	No
X-ray repair complementing defective repair in Chinese hamster cells 6	P12956	Nucleus	No
histone cluster 1, H1e	P10412	Nucleus	No
H2A histone family, member Z	P0C0S5	Nucleus	No
high mobility group box 1	P09429	Nucleus	No
small nuclear ribonucleoprotein polypeptide A	P09012	Nucleus	No
small nuclear ribonucleoprotein polypeptide B	P08579	Nucleus	No
heterogeneous nuclear ribonucleoprotein C (C1/C2)	P07910	Nucleus	No
histone cluster 1, H2bj	P06899	Nucleus	No
nucleophosmin (nucleolar phosphoprotein B23, numatrin)	P06748	Nucleus	No
ribosomal L1 domain containing 1	O76021	Nucleus	No
synaptotagmin binding, cytoplasmic RNA interacting protein	O60506	Nucleus	No
LUC7-like 2 pre-mRNA splicing factor	Q9Y383	Nucleus	No
basic transcription factor 3-like 4	Q96K17	Nucleus	No
heterogeneous nuclear ribonucleoprotein A1-like 2	Q32P51	Nucleus	No
talin 1	Q9Y490	Plasma Membrane	Yes
testin LIM domain protein	Q9UGI8	Plasma Membrane	Yes
cadherin, EGF LAG seven-pass G-type receptor 3	Q9NYQ7	Plasma Membrane	Yes
CUB domain containing protein 1	Q9H5V8	Plasma Membrane	Yes
fibroblast growth factor receptor-like 1	Q8N441	Plasma Membrane	Yes
nephronectin	Q6UXI9	Plasma Membrane	Yes
fibronectin type III domain containing 1	Q4ZHG4	Plasma Membrane	Yes
protein tyrosine phosphatase, receptor type, K	Q15262	Plasma Membrane	Yes
plakophilin 1	Q13835	Plasma Membrane	Yes
integrin-linked kinase	Q13418	Plasma Membrane	Yes
contactin 1	Q12860	Plasma Membrane	Yes
desmocollin 1	Q08554	Plasma Membrane	Yes
desmoglein 1	Q02413	Plasma Membrane	Yes
ras-related C3 botulinum toxin substrate 1 (rho	P63000	Plasma	Yes

|			
family, small GTP binding protein Rac1)		Membrane	
CD81 molecule	P60033	Plasma Membrane	Yes
dynamin 2	P50570	Plasma Membrane	Yes
vasodilator-stimulated phosphoprotein	P50552	Plasma Membrane	Yes
numb homolog (Drosophila)	P49757	Plasma Membrane	Yes
LIM and senescent cell antigen-like domains 1	P48059	Plasma Membrane	Yes
melanoma cell adhesion molecule	P43121	Plasma Membrane	Yes
basigin (Ok blood group)	P35613	Plasma Membrane	Yes
integrin, alpha 3 (antigen CD49C, alpha 3 subunit of VLA-3 receptor)	P26006	Plasma Membrane	Yes
vinculin	P18206	Plasma Membrane	Yes
integrin, beta 5	P18084	Plasma Membrane	Yes
endoglin	P17813	Plasma Membrane	Yes
CD44 molecule (Indian blood group)	P16070	Plasma Membrane	Yes
desmoplakin	P15924	Plasma Membrane	Yes
junction plakoglobin	P14923	Plasma Membrane	Yes
microtubule-associated protein 2	P11137	Plasma Membrane	Yes
integrin, alpha 5 (fibronectin receptor, alpha polypeptide)	P08648	Plasma Membrane	Yes
integrin, alpha V	P06756	Plasma Membrane	Yes
integrin, beta 1 (fibronectin receptor, beta polypeptide, antigen CD29 includes MDF2, MSK12)	P05556	Plasma Membrane	Yes
integrin, beta 3 (platelet glycoprotein IIIa, antigen CD61)	P05106	Plasma Membrane	Yes
agrin	O00468	Plasma Membrane	Yes
prostaglandin F2 receptor inhibitor	Q9P2B2	Plasma Membrane	Possible interaction
insulin-like growth factor 2 receptor	P11717	Plasma Membrane	Possible interaction
Thy-1 cell surface antigen	P04216	Plasma Membrane	Possible interaction
epsin 1	Q9Y6I3	Plasma Membrane	No
guanine nucleotide binding protein (G protein), gamma 12	Q9UBI6	Plasma Membrane	No
tweety family member 3	Q9C0H2	Plasma Membrane	No
plasmalemma vesicle associated protein	Q9BX97	Plasma Membrane	No
G protein-coupled receptor, class C, group 5, member A	Q8NFJ5	Plasma Membrane	No
solute carrier family 1 (neutral amino acid transporter), member 5	Q15758	Plasma Membrane	No
solute carrier family 7 (amino acid transporter light chain, L system), member 5	Q01650	Plasma Membrane	No

clathrin, heavy chain (Hc)	Q00610	Plasma Membrane	No
guanine nucleotide binding protein (G protein), gamma 5	P63218	Plasma Membrane	No
adaptor-related protein complex 2, beta 1 subunit	P63010	Plasma Membrane	No
guanine nucleotide binding protein (G protein), beta polypeptide 2	P62879	Plasma Membrane	No
guanine nucleotide binding protein (G protein), beta polypeptide 1	P62873	Plasma Membrane	No
alanyl (membrane) aminopeptidase	P15144	Plasma Membrane	No
carboxypeptidase M	P14384	Plasma Membrane	No
CD59 molecule, complement regulatory protein	P13987	Plasma Membrane	No
coagulation factor V (proaccelerin, labile factor)	P12259	Plasma Membrane	No
solute carrier family 2 (facilitated glucose transporter), member 1	P11166	Plasma Membrane	No
clathrin, light chain A	P09496	Plasma Membrane	No
membrane metallo-endopeptidase	P08473	Plasma Membrane	No
CD55 molecule, decay accelerating factor for complement (Cromer blood group)	P08174	Plasma Membrane	No
alkaline phosphatase, liver/bone/kidney	P05186	Plasma Membrane	No
ATPase, Na+/K+ transporting, alpha 1 polypeptide	P05023	Plasma Membrane	No
guanine nucleotide binding protein (G protein), alpha inhibiting activity polypeptide 2	P04899	Plasma Membrane	No
annexin A1	P04083	Plasma Membrane	No
transferrin receptor	P02786	Plasma Membrane	No
major histocompatibility complex, class I, A	P01891	Plasma Membrane	No
apolipoprotein M	O95445	Plasma Membrane	No
tumor necrosis factor receptor superfamily, member 11b	O00300	Plasma Membrane	No
immunoglobulin lambda-like polypeptide 1	B9A064	Plasma Membrane	No
notch 3	Q9UM47	Plasma Membrane	Indirect Signalling
mannose receptor, C type 2	Q9UBG0	Plasma Membrane	Indirect Signalling
epidermal growth factor receptor pathway substrate 15-like 1	Q9UBC2	Plasma Membrane	Indirect Signalling
EH-domain containing 4	Q9H223	Plasma Membrane	Indirect Signalling
immunoglobulin superfamily, member 8	Q969P0	Plasma Membrane	Indirect Signalling
low density lipoprotein receptor-related protein 1	Q07954	Plasma Membrane	Indirect Signalling
plasminogen activator, urokinase receptor	Q03405	Plasma Membrane	Indirect Signalling
interferon induced transmembrane protein 3	Q01628	Plasma Membrane	Indirect Signalling
CAP, adenylate cyclase-associated protein 1 (yeast)	Q01518	Plasma	Indirect Signalling

		Membrane	
Dab, mitogen-responsive phosphoprotein, homolog 2 (Drosophila)	P98082	Plasma Membrane	Indirect Signalling
ADP-ribosylation factor 6	P62330	Plasma Membrane	Indirect Signalling
EPH receptor B4	P54760	Plasma Membrane	Indirect Signalling
AXL receptor tyrosine kinase	P30530	Plasma Membrane	Indirect Signalling
stomatin	P27105	Plasma Membrane	Indirect Signalling
moesin	P26038	Plasma Membrane	Indirect Signalling
CD63 molecule	P08962	Plasma Membrane	Indirect Signalling
solute carrier family 3 (amino acid transporter heavy chain), member 2	P08195	Plasma Membrane	Indirect Signalling
ras homolog family member C	P08134	Plasma Membrane	Indirect Signalling
annexin A2	P07355	Plasma Membrane	Indirect Signalling

Appendix 4. Full list of proteins obtained from mass spectrometry of hydrodynamically-sheared HeLa A3 cells treated with FASP. Proteins were designated as an adhesome protein (yes) if they were considered to be either an adhesive protein or a protein that directly affects cell adhesion. Proteins noted as having indirect signalling have an effect on cellular adhesion via intermediate pathways, complexes or signalling events. Proteins noted as having a possible interaction are those with a uniprot entry that suggests either localisation to sites of adhesion or that have a structure / function that may relate to adhesion but lack substantial evidence. Proteins were only designated as "No" if they had no link to cellular adhesion.
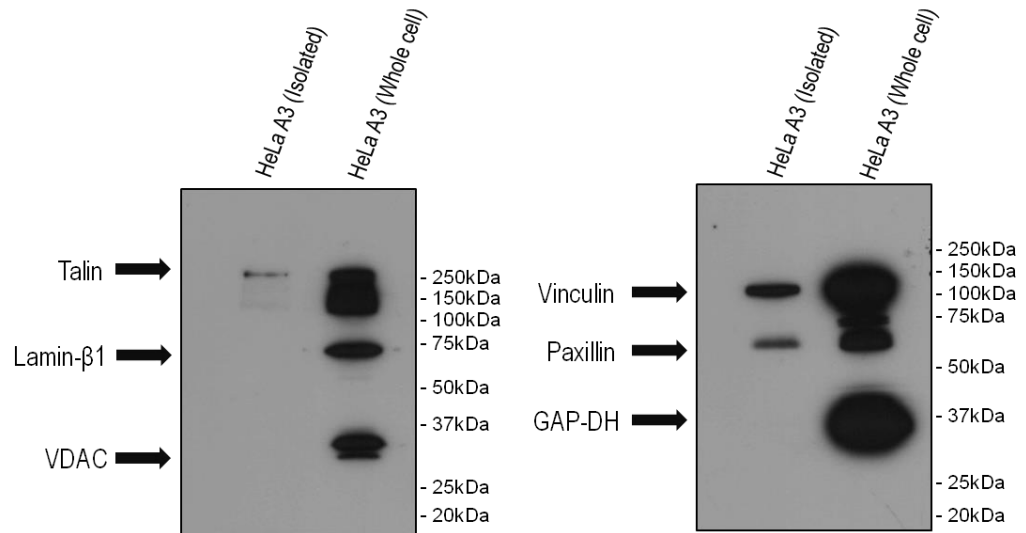
Appendix 5. Whole, uncropped Western blots for negative and positive control proteins used to determine the purity of hydrodynamically-sheared cell residues. Two 10cm diameter tissue culture dishes were exposed to a hydrodynamic force from a standardised shower. The residue was washed with PBS and dissolved in SDS-containing Sample Buffer. Negative control protein blots for lamin-β1 (nuclear fraction), voltage-dependent anion channel (VDAC) (mitochondrial fraction) and GAP-DH (cytoplasmic fraction). Positive control protein blots for talin, vinculin and paxillin. A 10% (w/v) polyacrylamide gel was used.

References

1   Hanahan, D. and Weinberg, R. A. (2011) Hallmarks of cancer: the next generation. Cell. **144**, 646-674

2   Bos, J. L. (1989) ras oncogenes in human cancer: a review. Cancer research. **49**, 4682-4689

3   Croce, C. M. (2008) Oncogenes and cancer. The New England journal of medicine. **358**, 502-511

4   Knudson, A. G., Jr. (1971) Mutation and cancer: statistical study of retinoblastoma. Proceedings of the National Academy of Sciences of the United States of America. **68**, 820-823

5   Surget, S., Khoury, M. P. and Bourdon, J. C. (2013) Uncovering the role of p53 splice variants in human malignancy: a clinical perspective. OncoTargets and therapy. **7**, 57-68

6   Jemal, A., Bray, F., Center, M. M., Ferlay, J., Ward, E. and Forman, D. (2011) Global cancer statistics. CA: a cancer journal for clinicians. **61**, 69-90

7   Steeg, P. S. (2006) Tumor metastasis: mechanistic insights and clinical challenges. Nature medicine. **12**, 895-904

8   Larue, L. and Bellacosa, A. (2005) Epithelial-mesenchymal transition in development and cancer: role of phosphatidylinositol 3' kinase/AKT pathways. Oncogene. **24**, 7443-7454

9   Knights, A. J., Funnell, A. P., Crossley, M. and Pearson, R. C. (2012) Holding Tight: Cell Junctions and Cancer Spread. Trends in cancer research. **8**, 61-69

10   Neunlist, M., Van Landeghem, L., Mahe, M. M., Derkinderen, P., des Varannes, S. B. and Rolli-Derkinderen, M. (2013) The digestive neuronal-glial-epithelial unit: a new actor in gut health and disease. Nature reviews. Gastroenterology & hepatology. **10**, 90-100

11   Gooding, J. M., Yap, K. L. and Ikura, M. (2004) The cadherin-catenin complex as a focal point of cell adhesion and signalling: new insights from three-dimensional structures. BioEssays : news and reviews in molecular, cellular and developmental biology. **26**, 497-511

12   Niessen, C. M., Leckband, D. and Yap, A. S. (2011) Tissue organization by cadherin adhesion molecules: dynamic molecular and cellular mechanisms of morphogenetic regulation. Physiological reviews. **91**, 691-731

13   Menke, A. and Giehl, K. (2012) Regulation of adherens junctions by Rho GTPases and p120-catenin. Archives of biochemistry and biophysics. **524**, 48-55

14   Tepass, U., Truong, K., Godt, D., Ikura, M. and Peifer, M. (2000) Cadherins in embryonic and neural morphogenesis. Nature reviews. Molecular cell biology. **1**, 91-100

15   Pokutta, S., Herrenknecht, K., Kemler, R. and Engel, J. (1994) Conformational changes of the recombinant extracellular domain of E-cadherin upon calcium binding. European journal of biochemistry / FEBS. **223**, 1019-1026

16   Beavon, I. R. (2000) The E-cadherin-catenin complex in tumour metastasis: structure, function and regulation. Eur J Cancer. **36**, 1607-1620

17   Derycke, L. D. and Bracke, M. E. (2004) N-cadherin in the spotlight of cell-cell adhesion, differentiation, embryogenesis, invasion and signalling. The International journal of developmental biology. **48**, 463-476

18   Shapiro, L. and Weis, W. I. (2009) Structure and biochemistry of cadherins and catenins. Cold Spring Harbor perspectives in biology. **1**, a003053

19   Nagafuchi, A., Ishihara, S. and Tsukita, S. (1994) The roles of catenins in the cadherin-mediated cell adhesion: functional analysis of E-cadherin-alpha catenin fusion molecules. The Journal of cell biology. **127**, 235-245

20   Rangarajan, E. S. and Izard, T. (2012) The cytoskeletal protein alpha-catenin unfurls upon binding to vinculin. The Journal of biological chemistry. **287**, 18492-18499

21   Campbell, I. D. and Humphries, M. J. (2011) Integrin structure, activation, and interactions. Cold Spring Harbor perspectives in biology. **3**

22   Hartsock, A. and Nelson, W. J. (2008) Adherens and tight junctions: structure, function and connections to the actin cytoskeleton. Biochimica et biophysica acta. **1778**, 660-669

23   Tang, V. W. and Goodenough, D. A. (2003) Paracellular ion channel at the tight junction. Biophysical journal. **84**, 1660-1673

24   Paris, L., Tonutti, L., Vannini, C. and Bazzoni, G. (2008) Structural organization of the tight junctions. Biochimica et biophysica acta. **1778**, 646-659

25   Fanning, A. S., Jameson, B. J., Jesaitis, L. A. and Anderson, J. M. (1998) The tight junction protein ZO-1 establishes a link between the transmembrane protein occludin and the actin cytoskeleton. The Journal of biological chemistry. **273**, 29745-29753

26   Garrod, D. and Chidgey, M. (2008) Desmosome structure, composition and function. Biochimica et biophysica acta. **1778**, 572-587

27   van Tintelen, J. P. and Hauer, R. N. (2009) Cardiomyopathies: New test for arrhythmogenic right ventricular cardiomyopathy. Nature reviews. Cardiology. **6**, 450-451

28   Chitaev, N. A. and Troyanovsky, S. M. (1997) Direct Ca2+-dependent heterophilic interaction between desmosomal cadherins, desmoglein and desmocollin, contributes to cell-cell adhesion. The Journal of cell biology. **138**, 193-201

29   Marcozzi, C., Burdett, I. D., Buxton, R. S. and Magee, A. I. (1998) Coexpression of both types of desmosomal cadherin and plakoglobin confers strong intercellular adhesion. Journal of cell science. **111 (Pt 4)**, 495-509

30   Howard, S., Deroo, T., Fujita, Y. and Itasaki, N. (2011) A positive role of cadherin in Wnt/beta-catenin signalling during epithelial-mesenchymal transition. PloS one. **6**, e23899

31   Tobioka, H., Isomura, H., Kokai, Y., Tokunaga, Y., Yamaguchi, J. and Sawada, N. (2004) Occludin expression decreases with the progression of human endometrial carcinoma. Human pathology. **35**, 159-164

32   Kominsky, S. L., Argani, P., Korz, D., Evron, E., Raman, V., Garrett, E., Rein, A., Sauter, G., Kallioniemi, O. P. and Sukumar, S. (2003) Loss of the tight junction protein claudin-7 correlates with histological grade in both ductal carcinoma in situ and invasive ductal carcinoma of the breast. Oncogene. **22**, 2021-2033

33   Lee, S. K., Moon, J., Park, S. W., Song, S. Y., Chung, J. B. and Kang, J. K. (2005) Loss of the tight junction protein claudin 4 correlates with histological growth-pattern and differentiation in advanced gastric adenocarcinoma. Oncology reports. **13**, 193-199

34   Yang, L., Chen, Y., Cui, T., Knosel, T., Zhang, Q., Albring, K. F., Huber, O. and Petersen, I. (2012) Desmoplakin acts as a tumor suppressor by inhibition of the Wnt/beta-catenin signaling pathway in human lung cancer. Carcinogenesis. **33**, 1863-1870

35   Chidgey, M. and Dawson, C. (2007) Desmosomes: a role in cancer? British journal of cancer. **96**, 1783-1787

36   Kundu, S. T., Gosavi, P., Khapare, N., Patel, R., Hosing, A. S., Maru, G. B., Ingle, A., Decaprio, J. A. and Dalal, S. N. (2008) Plakophilin3 downregulation leads to a decrease in cell adhesion and promotes metastasis. International journal of cancer. Journal international du cancer. **123**, 2303-2314

37   Chun, M. G. and Hanahan, D. (2010) Genetic deletion of the desmosomal component desmoplakin promotes tumor microinvasion in a mouse model of pancreatic neuroendocrine carcinogenesis. PLoS genetics. **6**, e1001120

38   Robertson, J., Jacquemet, G., Byron, A., Jones, M. C., Warwood, S., Selley, J. N., Knight, D., Humphries, J. D. and Humphries, M. J. (2015) Defining the phospho-adhesome through the phosphoproteomic analysis of integrin signalling. Nature communications. **6**, 6265

39   Winograd-Katz, S. E., Fassler, R., Geiger, B. and Legate, K. R. (2014) The integrin adhesome: from genes and proteins to human disease. Nature reviews. Molecular cell biology. **15**, 273-288

40   Zaidel-Bar, R., Itzkovitz, S., Ma'ayan, A., Iyengar, R. and Geiger, B. (2007) Functional atlas of the integrin adhesome. Nature cell biology. **9**, 858-867

41   Berrier, A. L. and Yamada, K. M. (2007) Cell-matrix adhesion. Journal of cellular physiology. **213**, 565-573

42   Parsons, J. T., Horwitz, A. R. and Schwartz, M. A. (2010) Cell adhesion: integrating cytoskeletal dynamics and cellular tension. Nature reviews. Molecular cell biology. **11**, 633-643

43   Webb, D. J., Parsons, J. T. and Horwitz, A. F. (2002) Adhesion assembly, disassembly and turnover in migrating cells -- over and over and over again. Nature cell biology. **4**, E97-100

44   Ponti, A., Machacek, M., Gupton, S. L., Waterman-Storer, C. M. and Danuser, G. (2004) Two distinct actin networks drive the protrusion of migrating cells. Science. **305**, 1782-1786

45   Vicente-Manzanares, M., Choi, C. K. and Horwitz, A. R. (2009) Integrins in cell migration--the actin connection. Journal of cell science. **122**, 199-206

46   Humphries, M. J. (2000) Integrin structure. Biochemical Society transactions. **28**, 311-339

47   Hynes, R. O. (2002) Integrins: bidirectional, allosteric signaling machines. Cell. **110**, 673-687

48   D'Souza, S. E., Ginsberg, M. H. and Plow, E. F. (1991) Arginyl-glycyl-aspartic acid (RGD): a cell adhesion motif. Trends in biochemical sciences. **16**, 246-250

49   Ye, F., Kim, C. and Ginsberg, M. H. (2011) Molecular mechanism of inside-out integrin regulation. Journal of thrombosis and haemostasis : JTH. **9 Suppl 1**, 20-25

50   Anthis, N. J. and Campbell, I. D. (2011) The tail of integrin activation. Trends in biochemical sciences. **36**, 191-198

51   Shattil, S. J., Kim, C. and Ginsberg, M. H. (2010) The final steps of integrin activation: the end game. Nature reviews. Molecular cell biology. **11**, 288-300

52   Bouvard, D., Brakebusch, C., Gustafsson, E., Aszodi, A., Bengtsson, T., Berna, A. and Fassler, R. (2001) Functional consequences of integrin gene mutations in mice. Circulation research. **89**, 211-223

53   Humphries, J. D., Byron, A. and Humphries, M. J. (2006) Integrin ligands at a glance. Journal of cell science. **119**, 3901-3903

54   Ratnikov, B. I., Partridge, A. W. and Ginsberg, M. H. (2005) Integrin activation by talin. Journal of thrombosis and haemostasis : JTH. **3**, 1783-1790

55   Calderwood, D. A., Yan, B., de Pereda, J. M., Alvarez, B. G., Fujioka, Y., Liddington, R. C. and Ginsberg, M. H. (2002) The phosphotyrosine binding-like domain of talin activates integrins. The Journal of biological chemistry. **277**, 21749-21758

56   Calderwood, D. A., Fujioka, Y., de Pereda, J. M., Garcia-Alvarez, B., Nakamoto, T., Margolis, B., McGlade, C. J., Liddington, R. C. and Ginsberg, M. H. (2003) Integrin beta cytoplasmic domain interactions with phosphotyrosine-binding domains: a structural prototype for diversity in integrin signaling. Proceedings of the National Academy of Sciences of the United States of America. **100**, 2272-2277

57   Calderwood, D. A., Campbell, I. D. and Critchley, D. R. (2013) Talins and kindlins: partners in integrin-mediated adhesion. Nature reviews. Molecular cell biology. **14**, 503-517

58   Goult, B. T., Bouaouina, M., Elliott, P. R., Bate, N., Patel, B., Gingras, A. R., Grossmann, J. G., Roberts, G. C., Calderwood, D. A., Critchley, D. R. and Barsukov, I. L. (2010) Structure of a double ubiquitin-like domain in the talin head: a role in integrin activation. The EMBO journal. **29**, 1069-1080

59   Elliott, P. R., Goult, B. T., Kopp, P. M., Bate, N., Grossmann, J. G., Roberts, G. C., Critchley, D. R. and Barsukov, I. L. (2010) The Structure of the talin head reveals a novel extended conformation of the FERM domain. Structure. **18**, 1289-1299

60   Papagrigoriou, E., Gingras, A. R., Barsukov, I. L., Bate, N., Fillingham, I. J., Patel, B., Frank, R., Ziegler, W. H., Roberts, G. C., Critchley, D. R. and Emsley, J. (2004) Activation of a vinculin-binding site in the talin rod involves rearrangement of a five-helix bundle. The EMBO journal. **23**, 2942-2951

61   Fillingham, I., Gingras, A. R., Papagrigoriou, E., Patel, B., Emsley, J., Critchley, D. R., Roberts, G. C. and Barsukov, I. L. (2005) A vinculin binding domain from the talin rod unfolds to form a complex with the vinculin head. Structure. **13**, 65-74

62   Gingras, A. R., Bate, N., Goult, B. T., Hazelwood, L., Canestrelli, I., Grossmann, J. G., Liu, H., Putz, N. S., Roberts, G. C., Volkmann, N., Hanein, D., Barsukov, I. L. and Critchley, D. R. (2008) The structure of the C-terminal actin-binding domain of talin. The EMBO journal. **27**, 458-469

63   Petrich, B. G. (2009) Talin-dependent integrin signalling in vivo. Thrombosis and haemostasis. **101**, 1020-1024

64   Anthis, N. J., Wegener, K. L., Ye, F., Kim, C., Goult, B. T., Lowe, E. D., Vakonakis, I., Bate, N., Critchley, D. R., Ginsberg, M. H. and Campbell, I. D. (2009) The structure of an integrin/talin complex reveals the basis of inside-out signal transduction. The EMBO journal. **28**, 3623-3632

65   Wegener, K. L., Partridge, A. W., Han, J., Pickford, A. R., Liddington, R. C., Ginsberg, M. H. and Campbell, I. D. (2007) Structural basis of integrin activation by talin. Cell. **128**, 171-182

66   Song, X., Yang, J., Hirbawi, J., Ye, S., Perera, H. D., Goksoy, E., Dwivedi, P., Plow, E. F., Zhang, R. and Qin, J. (2012) A novel membrane-dependent on/off switch mechanism of talin FERM domain at sites of cell adhesion. Cell research. **22**, 1533-1545

67   Goksoy, E., Ma, Y. Q., Wang, X., Kong, X., Perera, D., Plow, E. F. and Qin, J. (2008) Structural basis for the autoinhibition of talin in regulating integrin activation. Molecular cell. **31**, 124-133

68   Goldmann, W. H., Bremer, A., Haner, M., Aebi, U. and Isenberg, G. (1994) Native talin is a dumbbell-shaped homodimer when it interacts with actin. Journal of structural biology. **112**, 3-10

69   Legate, K. R., Takahashi, S., Bonakdar, N., Fabry, B., Boettiger, D., Zent, R. and Fassler, R. (2011) Integrin adhesion and force coupling are independently regulated by localized PtdIns(4,5)2 synthesis. The EMBO journal. **30**, 4539-4553

70   Wynne, J. P., Wu, J., Su, W., Mor, A., Patsoukis, N., Boussiotis, V. A., Hubbard, S. R. and Philips, M. R. (2012) Rap1-interacting adapter molecule (RIAM) associates with the plasma membrane via a proximity detector. The Journal of cell biology. **199**, 317-330

71   Lee, H. S., Lim, C. J., Puzon-McLaughlin, W., Shattil, S. J. and Ginsberg, M. H. (2009) RIAM activates integrins by linking talin to ras GTPase membrane-targeting sequences. The Journal of biological chemistry. **284**, 5119-5127

72   Kloeker, S., Major, M. B., Calderwood, D. A., Ginsberg, M. H., Jones, D. A. and Beckerle, M. C. (2004) The Kindler syndrome protein is regulated by transforming growth

factor-beta and involved in integrin-mediated adhesion. The Journal of biological chemistry. **279**, 6824-6833

73   Ma, Y. Q., Qin, J., Wu, C. and Plow, E. F. (2008) Kindlin-2 (Mig-2): a co-activator of beta3 integrins. The Journal of cell biology. **181**, 439-446

74   Goult, B. T., Bouaouina, M., Harburger, D. S., Bate, N., Patel, B., Anthis, N. J., Campbell, I. D., Calderwood, D. A., Barsukov, I. L., Roberts, G. C. and Critchley, D. R. (2009) The structure of the N-terminus of kindlin-1: a domain important for alphaiibbeta3 integrin activation. Journal of molecular biology. **394**, 944-956

75   Margadant, C., Kreft, M., de Groot, D. J., Norman, J. C. and Sonnenberg, A. (2012) Distinct roles of talin and kindlin in regulating integrin alpha5beta1 function and trafficking. Current biology : CB. **22**, 1554-1563

76   Bledzka, K., Liu, J., Xu, Z., Perera, H. D., Yadav, S. P., Bialkowska, K., Qin, J., Ma, Y. Q. and Plow, E. F. (2012) Spatial coordination of kindlin-2 with talin head domain in interaction with integrin beta cytoplasmic tails. The Journal of biological chemistry. **287**, 24585-24594

77   Harburger, D. S. and Calderwood, D. A. (2009) Integrin signalling at a glance. Journal of cell science. **122**, 159-163

78   Legate, K. R., Wickstrom, S. A. and Fassler, R. (2009) Genetic and cell biological analysis of integrin outside-in signaling. Genes & development. **23**, 397-418

79   Multhaupt, H. A., Yoneda, A., Whiteford, J. R., Oh, E. S., Lee, W. and Couchman, J. R. (2009) Syndecan signaling: when, where and why? Journal of physiology and pharmacology : an official journal of the Polish Physiological Society. **60 Suppl 4**, 31-38

80   Leonova, E. I. and Galzitskaya, O. V. (2013) Structure and functions of syndecans in vertebrates. Biochemistry. Biokhimiia. **78**, 1071-1085

81   Woods, A., Longley, R. L., Tumova, S. and Couchman, J. R. (2000) Syndecan-4 binding to the high affinity heparin-binding domain of fibronectin drives focal adhesion formation in fibroblasts. Archives of biochemistry and biophysics. **374**, 66-72

82   Wilcox-Adelman, S. A., Denhez, F. and Goetinck, P. F. (2002) Syndecan-4 modulates focal adhesion kinase phosphorylation. The Journal of biological chemistry. **277**, 32970-32977

83   Woods, A. and Couchman, J. R. (2001) Syndecan-4 and focal adhesion function. Current opinion in cell biology. **13**, 578-583

84   Yang, X., Pursell, B., Lu, S., Chang, T. K. and Mercurio, A. M. (2009) Regulation of beta 4-integrin expression by epigenetic modifications in the mammary gland and during the epithelial-to-mesenchymal transition. Journal of cell science. **122**, 2473-2480

85   Jones, J. L., Royall, J. E., Critchley, D. R. and Walker, R. A. (1997) Modulation of myoepithelial-associated alpha6beta4 integrin in a breast cancer cell line alters invasive potential. Experimental cell research. **235**, 325-333

86   Maschler, S., Wirl, G., Spring, H., Bredow, D. V., Sordat, I., Beug, H. and Reichmann, E. (2005) Tumor cell invasiveness correlates with changes in integrin expression and localization. Oncogene. **24**, 2032-2041

87   Akiyama, S. K., Olden, K. and Yamada, K. M. (1995) Fibronectin and integrins in invasion and metastasis. Cancer metastasis reviews. **14**, 173-189

88   Schittenhelm, J., Klein, A., Tatagiba, M. S., Meyermann, R., Fend, F., Goodman, S. L. and Sipos, B. (2013) Comparing the expression of integrins alphavbeta3, alphavbeta5, alphavbeta6, alphavbeta8, fibronectin and fibrinogen in human brain metastases and their corresponding primary tumors. International journal of clinical and experimental pathology. **6**, 2719-2732

89   Aluwihare, P., Mu, Z., Zhao, Z., Yu, D., Weinreb, P. H., Horan, G. S., Violette, S. M. and Munger, J. S. (2009) Mice that lack activity of alphavbeta6- and alphavbeta8-integrins reproduce the abnormalities of Tgfb1- and Tgfb3-null mice. Journal of cell science. **122**, 227-232

90   Cruz-Monserrate, Z., Qiu, S., Evers, B. M. and O'Connor, K. L. (2007) Upregulation and redistribution of integrin alpha6beta4 expression occurs at an early stage in pancreatic adenocarcinoma progression. Modern pathology : an official journal of the United States and Canadian Academy of Pathology, Inc. **20**, 656-667

91   Bon, G., Folgiero, V., Di Carlo, S., Sacchi, A. and Falcioni, R. (2007) Involvement of alpha6beta4 integrin in the mechanisms that regulate breast cancer progression. Breast cancer research : BCR. **9**, 203

92   Beaulieu, J. F. (2010) Integrin alpha6beta4 in colorectal cancer. World journal of gastrointestinal pathophysiology. **1**, 3-11

93   Brown, M. C. and Turner, C. E. (2004) Paxillin: adapting to change. Physiological reviews. **84**, 1315-1339

94   Parsons, J. T. (2003) Focal adhesion kinase: the first ten years. Journal of cell science. **116**, 1409-1416

95   Ziegler, W. H., Liddington, R. C. and Critchley, D. R. (2006) The structure and regulation of vinculin. Trends in cell biology. **16**, 453-460

96   Humphries, J. D., Wang, P., Streuli, C., Geiger, B., Humphries, M. J. and Ballestrem, C. (2007) Vinculin controls focal adhesion formation by direct interactions with talin and actin. The Journal of cell biology. **179**, 1043-1057

97   Sjoblom, B., Salmazo, A. and Djinovic-Carugo, K. (2008) Alpha-actinin structure and regulation. Cellular and molecular life sciences : CMLS. **65**, 2688-2701

98   Turner, C. E. (2000) Paxillin and focal adhesion signalling. Nature cell biology. **2**, E231-236

99   Pasapera, A. M., Schneider, I. C., Rericha, E., Schlaepfer, D. D. and Waterman, C. M. (2010) Myosin II activity regulates vinculin recruitment to focal adhesions through FAK-mediated paxillin phosphorylation. The Journal of cell biology. **188**, 877-890

100   Hall, J. E., Fu, W. and Schaller, M. D. (2011) Focal adhesion kinase: exploring Fak structure to gain insight into function. International review of cell and molecular biology. **288**, 185-225

101   Lietha, D., Cai, X., Ceccarelli, D. F., Li, Y., Schaller, M. D. and Eck, M. J. (2007) Structural basis for the autoinhibition of focal adhesion kinase. Cell. **129**, 1177-1187

102   Mitra, S. K., Hanson, D. A. and Schlaepfer, D. D. (2005) Focal adhesion kinase: in command and control of cell motility. Nature reviews. Molecular cell biology. **6**, 56-68

103   Frame, M. C. (2002) Src in cancer: deregulation and consequences for cell behaviour. Biochimica et biophysica acta. **1602**, 114-130

104   Mitra, S. K. and Schlaepfer, D. D. (2006) Integrin-regulated FAK-Src signaling in normal and cancer cells. Current opinion in cell biology. **18**, 516-523

105   Parsons, S. J. and Parsons, J. T. (2004) Src family kinases, key regulators of signal transduction. Oncogene. **23**, 7906-7909

106   Amano, M., Chihara, K., Kimura, K., Fukata, Y., Nakamura, N., Matsuura, Y. and Kaibuchi, K. (1997) Formation of actin stress fibers and focal adhesions enhanced by Rho-kinase. Science. **275**, 1308-1311

107   Narumiya, S., Tanji, M. and Ishizaki, T. (2009) Rho signaling, ROCK and mDia1, in transformation, metastasis and invasion. Cancer metastasis reviews. **28**, 65-76

108   Katoh, K., Kano, Y. and Ookawara, S. (2007) Rho-kinase dependent organization of stress fibers and focal adhesions in cultured fibroblasts. Genes to cells : devoted to molecular & cellular mechanisms. **12**, 623-638

109   Bhatt, A., Kaverina, I., Otey, C. and Huttenlocher, A. (2002) Regulation of focal complex composition and disassembly by the calcium-dependent protease calpain. Journal of cell science. **115**, 3415-3425

110   Zamir, E., Katz, B. Z., Aota, S., Yamada, K. M., Geiger, B. and Kam, Z. (1999) Molecular diversity of cell-matrix adhesions. Journal of cell science. **112 (Pt 11)**, 1655-1669

111   Haynie, D. T. (2014) Molecular physiology of the tensin brotherhood of integrin adaptor proteins. Proteins. **82**, 1113-1127

112   Yoshigi, M., Hoffman, L. M., Jensen, C. C., Yost, H. J. and Beckerle, M. C. (2005) Mechanical force mobilizes zyxin from focal adhesions to actin filaments and regulates cytoskeletal reinforcement. The Journal of cell biology. **171**, 209-215

113   Kang, F., Purich, D. L. and Southwick, F. S. (1999) Profilin promotes barbed-end actin filament assembly without lowering the critical concentration. The Journal of biological chemistry. **274**, 36963-36972

114   Gutsche-Perelroizen, I., Lepault, J., Ott, A. and Carlier, M. F. (1999) Filament assembly from profilin-actin. The Journal of biological chemistry. **274**, 6234-6243

115   Da Silva, J. S., Medina, M., Zuliani, C., Di Nardo, A., Witke, W. and Dotti, C. G. (2003) RhoA/ROCK regulation of neuritogenesis via profilin IIa-mediated control of actin stability. The Journal of cell biology. **162**, 1267-1279

116   Legate, K. R., Montanez, E., Kudlacek, O. and Fassler, R. (2006) ILK, PINCH and parvin: the tIPP of integrin signalling. Nature reviews. Molecular cell biology. **7**, 20-31

117   Huang, R. Y., Guilford, P. and Thiery, J. P. (2012) Early events in cell adhesion and polarity during epithelial-mesenchymal transition. Journal of cell science. **125**, 4417-4422

118   Vicente-Manzanares, M., Ma, X., Adelstein, R. S. and Horwitz, A. R. (2009) Non-muscle myosin II takes centre stage in cell adhesion and migration. Nature reviews. Molecular cell biology. **10**, 778-790

119   Geiger, B. and Yamada, K. M. (2011) Molecular architecture and function of matrix adhesions. Cold Spring Harbor perspectives in biology. **3**

120   Burridge, K. (2005) Foot in mouth: do focal adhesions disassemble by endocytosis? Nature cell biology. **7**, 545-547

121   Katoh, K., Kano, Y. and Noda, Y. (2011) Rho-associated kinase-dependent contraction of stress fibres and the organization of focal adhesions. Journal of the Royal Society, Interface / the Royal Society. **8**, 305-311

122   Sachdev, S., Bu, Y. and Gelman, I. H. (2009) Paxillin-Y118 phosphorylation contributes to the control of Src-induced anchorage-independent growth by FAK and adhesion. BMC cancer. **9**, 12

123   Ridley, A. J. and Hall, A. (1992) The small GTP-binding protein rho regulates the assembly of focal adhesions and actin stress fibers in response to growth factors. Cell. **70**, 389-399

124   Huveneers, S. and Danen, E. H. (2009) Adhesion signaling - crosstalk between integrins, Src and Rho. Journal of cell science. **122**, 1059-1069

125   Goeckeler, Z. M., Masaracchia, R. A., Zeng, Q., Chew, T. L., Gallagher, P. and Wysolmerski, R. B. (2000) Phosphorylation of myosin light chain kinase by p21-activated kinase PAK2. The Journal of biological chemistry. **275**, 18366-18374

126   Alexandrova, A. Y., Arnold, K., Schaub, S., Vasiliev, J. M., Meister, J. J., Bershadsky, A. D. and Verkhovsky, A. B. (2008) Comparative dynamics of retrograde actin flow and focal adhesions: formation of nascent adhesions triggers transition from fast to slow flow. PloS one. **3**, e3234

127   Welf, E. S. and Haugh, J. M. (2011) Signaling pathways that control cell migration: models and analysis. Wiley interdisciplinary reviews. Systems biology and medicine. **3**, 231-240

128   Ridley, A. J. (2011) Life at the leading edge. Cell. **145**, 1012-1022

129   Guo, W. H. and Wang, Y. L. (2007) Retrograde fluxes of focal adhesion proteins in response to cell migration and mechanical signals. Molecular biology of the cell. **18**, 4519-4527

130   Ji, L., Lim, J. and Danuser, G. (2008) Fluctuations of intracellular forces during cell protrusion. Nature cell biology. **10**, 1393-1400

131   Wolfenson, H., Bershadsky, A., Henis, Y. I. and Geiger, B. (2011) Actomyosin-generated tension controls the molecular kinetics of focal adhesions. Journal of cell science. **124**, 1425-1432

132   Choi, C. K., Vicente-Manzanares, M., Zareno, J., Whitmore, L. A., Mogilner, A. and Horwitz, A. R. (2008) Actin and alpha-actinin orchestrate the assembly and maturation of nascent adhesions in a myosin II motor-independent manner. Nature cell biology. **10**, 1039-1050

133   Pellegrin, S. and Mellor, H. (2007) Actin stress fibres. Journal of cell science. **120**, 3491-3499

134   Tojkander, S., Gateva, G. and Lappalainen, P. (2012) Actin stress fibers--assembly, dynamics and biological roles. Journal of cell science. **125**, 1855-1864

135   Small, J. V., Rottner, K., Kaverina, I. and Anderson, K. I. (1998) Assembling an actin cytoskeleton for cell attachment and movement. Biochimica et biophysica acta. **1404**, 271-281

136   Vallenius, T. (2013) Actin stress fibre subtypes in mesenchymal-migrating cells. Open biology. **3**, 130001

137   Hotulainen, P. and Lappalainen, P. (2006) Stress fibers are generated by two distinct actin assembly mechanisms in motile cells. The Journal of cell biology. **173**, 383-394

138   Kovac, B., Teo, J. L., Makela, T. P. and Vallenius, T. (2013) Assembly of non-contractile dorsal stress fibers requires alpha-actinin-1 and Rac1 in migrating and spreading cells. Journal of cell science. **126**, 263-273

139   Tojkander, S., Gateva, G., Schevzov, G., Hotulainen, P., Naumanen, P., Martin, C., Gunning, P. W. and Lappalainen, P. (2011) A molecular pathway for myosin II recruitment to stress fibers. Current biology : CB. **21**, 539-550

140   Yilmaz, M. and Christofori, G. (2010) Mechanisms of motility in metastasizing cells. Molecular cancer research : MCR. **8**, 629-642

141   Chrzanowska-Wodnicka, M. and Burridge, K. (1996) Rho-stimulated contractility drives the formation of stress fibers and focal adhesions. The Journal of cell biology. **133**, 1403-1415

142   Yang, X., Zheng, F., Zhang, S. and Lu, J. (2015) Loss of RhoA expression prevents proliferation and metastasis of SPCA1 lung cancer cells in vitro. Biomedicine & pharmacotherapy = Biomedecine & pharmacotherapie. **69**, 361-366

143   Kalluri, R. and Weinberg, R. A. (2009) The basics of epithelial-mesenchymal transition. The Journal of clinical investigation. **119**, 1420-1428

144   Etienne-Manneville, S. (2013) Microtubules in cell migration. Annual review of cell and developmental biology. **29**, 471-499

145   Akhshi, T. K., Wernike, D. and Piekny, A. (2014) Microtubules and actin crosstalk in cell migration and division. Cytoskeleton (Hoboken). **71**, 1-23

146   Wehrle-Haller, B. and Imhof, B. A. (2003) Actin, microtubules and focal adhesion dynamics during cell migration. The international journal of biochemistry & cell biology. **35**, 39-50

147   Thiery, J. P., Acloque, H., Huang, R. Y. and Nieto, M. A. (2009) Epithelial-mesenchymal transitions in development and disease. Cell. **139**, 871-890

148   Lamouille, S., Xu, J. and Derynck, R. (2014) Molecular mechanisms of epithelial-mesenchymal transition. Nature reviews. Molecular cell biology. **15**, 178-196

149   Yan, C., Grimm, W. A., Garner, W. L., Qin, L., Travis, T., Tan, N. and Han, Y. P. (2010) Epithelial to mesenchymal transition in human skin wound healing is induced by tumor necrosis factor-alpha through bone morphogenic protein-2. The American journal of pathology. **176**, 2247-2258

150   Kim, Y. S., Yi, B. R., Kim, N. H. and Choi, K. C. (2014) Role of the epithelial-mesenchymal transition and its effects on embryonic stem cells. Experimental & molecular medicine. **46**, e108

151   Yilmaz, M. and Christofori, G. (2009) EMT, the cytoskeleton, and cancer cell invasion. Cancer metastasis reviews. **28**, 15-33

152   Toivola, D. M., Tao, G. Z., Habtezion, A., Liao, J. and Omary, M. B. (2005) Cellular integrity plus: organelle-related and protein-targeting functions of intermediate filaments. Trends in cell biology. **15**, 608-617

153   Mendez, M. G., Kojima, S. and Goldman, R. D. (2010) Vimentin induces changes in cell shape, motility, and adhesion during the epithelial to mesenchymal transition. FASEB journal : official publication of the Federation of American Societies for Experimental Biology. **24**, 1838-1851

154   Tomita, K., van Bokhoven, A., van Leenders, G. J., Ruijter, E. T., Jansen, C. F., Bussemakers, M. J. and Schalken, J. A. (2000) Cadherin switching in human prostate cancer progression. Cancer research. **60**, 3650-3654

155   Theveneau, E. and Mayor, R. (2012) Cadherins in collective cell migration of mesenchymal cells. Current opinion in cell biology. **24**, 677-684

156   Cavallaro, U. and Christofori, G. (2004) Cell adhesion and signalling by cadherins and Ig-CAMs in cancer. Nature reviews. Cancer. **4**, 118-132

157   Lehembre, F., Yilmaz, M., Wicki, A., Schomber, T., Strittmatter, K., Ziegler, D., Kren, A., Went, P., Derksen, P. W., Berns, A., Jonkers, J. and Christofori, G. (2008) NCAM-induced focal adhesion assembly: a functional switch upon loss of E-cadherin. The EMBO journal. **27**, 2603-2615

158   de Caestecker, M. (2004) The transforming growth factor-beta superfamily of receptors. Cytokine & growth factor reviews. **15**, 1-11

159   Dumont, N. and Arteaga, C. L. (2000) Transforming growth factor-beta and breast cancer: Tumor promoting effects of transforming growth factor-beta. Breast cancer research : BCR. **2**, 125-132

160   Feng, X. H. and Derynck, R. (2005) Specificity and versatility in tgf-beta signaling through Smads. Annual review of cell and developmental biology. **21**, 659-693

161   Massague, J. (2012) TGFbeta signalling in context. Nature reviews. Molecular cell biology. **13**, 616-630

162   Schmierer, B. and Hill, C. S. (2007) TGFbeta-SMAD signal transduction: molecular specificity and functional flexibility. Nature reviews. Molecular cell biology. **8**, 970-982

163   Ikushima, H. and Miyazono, K. (2010) TGFbeta signalling: a complex web in cancer progression. Nature reviews. Cancer. **10**, 415-424

164   Deckers, M., van Dinther, M., Buijs, J., Que, I., Lowik, C., van der Pluijm, G. and ten Dijke, P. (2006) The tumor suppressor Smad4 is required for transforming growth factor beta-induced epithelial to mesenchymal transition and bone metastasis of breast cancer cells. Cancer research. **66**, 2202-2209

165   Yang, Y. C., Piek, E., Zavadil, J., Liang, D., Xie, D., Heyer, J., Pavlidis, P., Kucherlapati, R., Roberts, A. B. and Bottinger, E. P. (2003) Hierarchical model of gene regulation by transforming growth factor beta. Proceedings of the National Academy of Sciences of the United States of America. **100**, 10269-10274

166   Kaimori, A., Potter, J., Kaimori, J. Y., Wang, C., Mezey, E. and Koteish, A. (2007) Transforming growth factor-beta1 induces an epithelial-to-mesenchymal transition state in mouse hepatocytes in vitro. The Journal of biological chemistry. **282**, 22089-22101

167   Bhowmick, N. A., Ghiassi, M., Bakin, A., Aakre, M., Lundquist, C. A., Engel, M. E., Arteaga, C. L. and Moses, H. L. (2001) Transforming growth factor-beta1 mediates epithelial to mesenchymal transdifferentiation through a RhoA-dependent mechanism. Molecular biology of the cell. **12**, 27-36

168   Ozdamar, B., Bose, R., Barrios-Rodiles, M., Wang, H. R., Zhang, Y. and Wrana, J. L. (2005) Regulation of the polarity protein Par6 by TGFbeta receptors controls epithelial cell plasticity. Science. **307**, 1603-1609

169   Terry, S., Nie, M., Matter, K. and Balda, M. S. (2010) Rho signaling and tight junction functions. Physiology (Bethesda). **25**, 16-26

170   Bellovin, D. I., Simpson, K. J., Danilov, T., Maynard, E., Rimm, D. L., Oettgen, P. and Mercurio, A. M. (2006) Reciprocal regulation of RhoA and RhoC characterizes the EMT and identifies RhoC as a prognostic marker of colon carcinoma. Oncogene. **25**, 6959-6967

171   Izzi, L. and Attisano, L. (2006) Ubiquitin-dependent regulation of TGFbeta signaling in cancer. Neoplasia. **8**, 677-688

172   Gui, T., Sun, Y., Shimokado, A. and Muragaki, Y. (2012) The Roles of Mitogen-Activated Protein Kinase Pathways in TGF-beta-Induced Epithelial-Mesenchymal Transition. Journal of signal transduction. **2012**, 289243

173   Naber, H. P., Drabsch, Y., Snaar-Jagalska, B. E., ten Dijke, P. and van Laar, T. (2013) Snail and Slug, key regulators of TGF-beta-induced EMT, are sufficient for the induction of single-cell invasion. Biochemical and biophysical research communications. **435**, 58-63

174   Kim, E. S., Kim, M. S. and Moon, A. (2004) TGF-beta-induced upregulation of MMP-2 and MMP-9 depends on p38 MAPK, but not ERK signaling in MCF10A human breast epithelial cells. International journal of oncology. **25**, 1375-1382

175   Medici, D., Hay, E. D. and Olsen, B. R. (2008) Snail and Slug promote epithelial-mesenchymal transition through beta-catenin-T-cell factor-4-dependent expression of transforming growth factor-beta3. Molecular biology of the cell. **19**, 4875-4887

176   Wang, Y., Shi, J., Chai, K., Ying, X. and Zhou, B. P. (2013) The Role of Snail in EMT and Tumorigenesis. Current cancer drug targets. **13**, 963-972

177   Sanchez-Tillo, E., Siles, L., de Barrios, O., Cuatrecasas, M., Vaquero, E. C., Castells, A. and Postigo, A. (2011) Expanding roles of ZEB factors in tumorigenesis and tumor progression. American journal of cancer research. **1**, 897-912

178   Cano, A. and Portillo, F. (2010) An emerging role for class I bHLH E2-2 proteins in EMT regulation and tumor progression. Cell adhesion & migration. **4**, 56-60

179   Leptin, M. (1991) twist and snail as positive and negative regulators during Drosophila mesoderm development. Genes & development. **5**, 1568-1576

180   Barrallo-Gimeno, A. and Nieto, M. A. (2005) The Snail genes as inducers of cell movement and survival: implications in development and cancer. Development. **132**, 3151-3161

181   Wang, H., Fang, R., Wang, X. F., Zhang, F., Chen, D. Y., Zhou, B., Wang, H. S., Cai, S. H. and Du, J. (2013) Stabilization of Snail through AKT/GSK-3beta signaling pathway is required for TNF-alpha-induced epithelial-mesenchymal transition in prostate cancer PC3 cells. European journal of pharmacology. **714**, 48-55

182   Yao, D., Dai, C. and Peng, S. (2011) Mechanism of the mesenchymal-epithelial transition and its relationship with metastatic tumor formation. Molecular cancer research : MCR. **9**, 1608-1620

183   Chaffer, C. L., Brennan, J. P., Slavin, J. L., Blick, T., Thompson, E. W. and Williams, E. D. (2006) Mesenchymal-to-epithelial transition facilitates bladder cancer metastasis: role of fibroblast growth factor receptor-2. Cancer research. **66**, 11271-11278

184   Oltean, S., Febbo, P. G. and Garcia-Blanco, M. A. (2008) Dunning rat prostate adenocarcinomas and alternative splicing reporters: powerful tools to study epithelial plasticity in prostate tumors in vivo. Clinical & experimental metastasis. **25**, 611-619

185   Wells, A., Yates, C. and Shepard, C. R. (2008) E-cadherin as an indicator of mesenchymal to epithelial reverting transitions during the metastatic seeding of disseminated carcinomas. Clinical & experimental metastasis. **25**, 621-628

186   Clarke, C., Rudland, P. and Barraclough, R. (2015) The metastasis-inducing protein AGR2 is O-glycosylated upon secretion from mammary epithelial cells. Molecular and cellular biochemistry. **408**, 245-252

187   Shojaei, F., Scott, N., Kang, X., Lappin, P. B., Fitzgerald, A. A., Karlicek, S., Simmons, B. H., Wu, A., Lee, J. H., Bergqvist, S. and Kraynov, E. (2012) Osteopontin induces growth of metastatic tumors in a preclinical model of non-small lung cancer. Journal of experimental & clinical cancer research : CR. **31**, 26

188   Gross, S. R., Sin, C. G., Barraclough, R. and Rudland, P. S. (2014) Joining S100 proteins and migration: for better or for worse, in sickness and in health. Cellular and molecular life sciences : CMLS. **71**, 1551-1579

189   Donato, R. (2003) Intracellular and extracellular roles of S100 proteins. Microscopy research and technique. **60**, 540-551

190   Fritz, G., Botelho, H. M., Morozova-Roche, L. A. and Gomes, C. M. (2010) Natural and amyloid self-assembly of S100 proteins: structural basis of functional diversity. The FEBS journal. **277**, 4578-4590

191   Lukanidin, E. and Sleeman, J. P. (2012) Building the niche: the role of the S100 proteins in metastatic growth. Seminars in cancer biology. **22**, 216-225

192   Davies, B. R., Davies, M. P., Gibbs, F. E., Barraclough, R. and Rudland, P. S. (1993) Induction of the metastatic phenotype by transfection of a benign rat mammary epithelial cell line with the gene for p9Ka, a rat calcium-binding protein, but not with the oncogene EJ-ras-1. Oncogene. **8**, 999-1008

193   Wang, G., Platt-Higgins, A., Carroll, J., de Silva Rudland, S., Winstanley, J., Barraclough, R. and Rudland, P. S. (2006) Induction of metastasis by S100P in a rat mammary model and its association with poor survival of breast cancer patients. Cancer research. **66**, 1199-1207

194   Zimmer, D. B., Eubanks, J. O., Ramakrishnan, D. and Criscitiello, M. F. (2013) Evolution of the S100 family of calcium sensor proteins. Cell calcium. **53**, 170-179

195   Barraclough, R., Gibbs, F., Smith, J. A., Haynes, G. A. and Rudland, P. S. (1990) Calcium-ion binding by the potential calcium-ion-binding protein, p9Ka. Biochemical and biophysical research communications. **169**, 660-666

196   Heizmann, C. W., Fritz, G. and Schafer, B. W. (2002) S100 proteins: structure, functions and pathology. Frontiers in bioscience : a journal and virtual library. **7**, d1356-1368

197   Gribenko, A. V. and Makhatadze, G. I. (1998) Oligomerization and divalent ion binding properties of the S100P protein: a Ca2+/Mg2+-switch model. Journal of molecular biology. **283**, 679-694

198   Bresnick, A. R., Weber, D. J. and Zimmer, D. B. (2015) S100 proteins in cancer. Nature reviews. Cancer. **15**, 96-109

199   Parkkila, S., Pan, P. W., Ward, A., Gibadulinova, A., Oveckova, I., Pastorekova, S., Pastorek, J., Martinez, A. R., Helin, H. O. and Isola, J. (2008) The calcium-binding protein S100P in normal and malignant human tissues. BMC clinical pathology. **8**, 2

200   Boye, K. and Maelandsmo, G. M. (2010) S100A4 and metastasis: a small actor playing many roles. The American journal of pathology. **176**, 528-535

201   Arumugam, T. and Logsdon, C. D. (2011) S100P: a novel therapeutic target for cancer. Amino acids. **41**, 893-899

202   Tong, X. M., Lin, X. N., Song, T., Liu, L. and Zhang, S. Y. (2010) Calcium-binding protein S100P is highly expressed during the implantation window in human endometrium. Fertility and sterility. **94**, 1510-1518

203   Austermann, J., Nazmi, A. R., Muller-Tidow, C. and Gerke, V. (2008) Characterization of the Ca2+ -regulated ezrin-S100P interaction and its role in tumor cell migration. The Journal of biological chemistry. **283**, 29331-29340

204   Hapangama, D. K., Raju, R. S., Valentijn, A. J., Barraclough, D., Hart, A., Turner, M. A., Platt-Higgins, A., Barraclough, R. and Rudland, P. S. (2012) Aberrant expression of metastasis-inducing proteins in ectopic and matched eutopic endometrium of women with endometriosis: implications for the pathogenesis of endometriosis. Hum Reprod. **27**, 394-407

205   Barry, S., Chelala, C., Lines, K., Sunamura, M., Wang, A., Marelli-Berg, F. M., Brennan, C., Lemoine, N. R. and Crnogorac-Jurcevic, T. (2013) S100P is a metastasis-associated gene that facilitates transendothelial migration of pancreatic cancer cells. Clinical & experimental metastasis. **30**, 251-264

206   Du, M., Wang, G., Ismail, T. M., Gross, S., Fernig, D. G., Barraclough, R. and Rudland, P. S. (2012) S100P dissociates myosin IIA filaments and focal adhesion sites to reduce cell adhesion and enhance cell migration. The Journal of biological chemistry. **287**, 15330-15344

207   Whiteman, H. J., Weeks, M. E., Dowen, S. E., Barry, S., Timms, J. F., Lemoine, N. R. and Crnogorac-Jurcevic, T. (2007) The role of S100P in the invasion of pancreatic cancer cells is mediated through cytoskeletal changes and regulation of cathepsin D. Cancer research. **67**, 8633-8642

208   Koltzscher, M., Neumann, C., Konig, S. and Gerke, V. (2003) Ca2+-dependent binding and activation of dormant ezrin by dimeric S100P. Molecular biology of the cell. **14**, 2372-2384

209   Smith, W. J., Nassar, N., Bretscher, A., Cerione, R. A. and Karplus, P. A. (2003) Structure of the active N-terminal domain of Ezrin. Conformational and mobility changes identify keystone interactions. The Journal of biological chemistry. **278**, 4949-4956

210   Bretscher, A. (1999) Regulation of cortical structure by the ezrin-radixin-moesin protein family. Current opinion in cell biology. **11**, 109-116

211   Haas, M. A., Vickers, J. C. and Dickson, T. C. (2007) Rho kinase activates ezrin-radixin-moesin (ERM) proteins and mediates their function in cortical neuron growth, morphology and motility in vitro. Journal of neuroscience research. **85**, 34-46

212   Crepaldi, T., Gautreau, A., Comoglio, P. M., Louvard, D. and Arpin, M. (1997) Ezrin is an effector of hepatocyte growth factor-mediated migration and morphogenesis in epithelial cells. The Journal of cell biology. **138**, 423-434

213   Heil, A., Nazmi, A. R., Koltzscher, M., Poeter, M., Austermann, J., Assard, N., Baudier, J., Kaibuchi, K. and Gerke, V. (2011) S100P is a novel interaction partner and regulator of IQGAP1. The Journal of biological chemistry. **286**, 7227-7238

214   Briggs, M. W. and Sacks, D. B. (2003) IQGAP proteins are integral components of cytoskeletal regulation. EMBO reports. **4**, 571-574

215   Kurella, V. B., Richard, J. M., Parke, C. L., Lecour, L. F., Jr., Bellamy, H. D. and Worthylake, D. K. (2009) Crystal structure of the GTPase-activating protein-related domain from IQGAP1. The Journal of biological chemistry. **284**, 14857-14865

216   Noritake, J., Watanabe, T., Sato, K., Wang, S. and Kaibuchi, K. (2005) IQGAP1: a key regulator of adhesion and migration. Journal of cell science. **118**, 2085-2092

217   Jameson, K. L., Mazur, P. K., Zehnder, A. M., Zhang, J., Zarnegar, B., Sage, J. and Khavari, P. A. (2013) IQGAP1 scaffold-kinase interaction blockade selectively targets RAS-MAP kinase-driven tumors. Nature medicine. **19**, 626-630

218   Johnson, M., Sharma, M. and Henderson, B. R. (2009) IQGAP1 regulation and roles in cancer. Cellular signalling. **21**, 1471-1478

219   Jadeski, L., Mataraza, J. M., Jeong, H. W., Li, Z. and Sacks, D. B. (2008) IQGAP1 stimulates proliferation and enhances tumorigenesis of human breast epithelial cells. The Journal of biological chemistry. **283**, 1008-1017

220   Penumutchu, S. R., Chou, R. H. and Yu, C. (2014) Structural insights into calcium-bound S100P and the V domain of the RAGE complex. PloS one. **9**, e103947

221   Arumugam, T., Ramachandran, V., Gomez, S. B., Schmidt, A. M. and Logsdon, C. D. (2012) S100P-derived RAGE antagonistic peptide reduces tumor growth and metastasis. Clinical cancer research : an official journal of the American Association for Cancer Research. **18**, 4356-4364

222   Mercado-Pimentel, M. E., Onyeagucha, B. C., Li, Q., Pimentel, A. C., Jandova, J. and Nelson, M. A. (2015) The S100P/RAGE signaling pathway regulates expression of microRNA-21 in colon cancer cells. FEBS letters. **589**, 2388-2393

223   Wu, Z., Boonmars, T., Nagano, I., Boonjaraspinyo, S., Srinontong, P., Ratasuwan, P., Narong, K., Nielsen, P. S. and Maekawa, Y. (2015) Significance of S100P as a biomarker in diagnosis, prognosis and therapy of opisthorchiasis-associated cholangiocarcinoma. International journal of cancer. Journal international du cancer

224   Ge, F., Wang, C., Wang, W. and Wu, B. (2013) S100P predicts prognosis and drug resistance in gastric cancer. The International journal of biological markers. **28**, e387-392

225   Bartling, B., Rehbein, G., Schmitt, W. D., Hofmann, H. S., Silber, R. E. and Simm, A. (2007) S100A2-S100P expression profile and diagnosis of non-small cell lung carcinoma: impairment by advanced tumour stages and neoadjuvant chemotherapy. Eur J Cancer. **43**, 1935-1943

226   Yuan, R. H., Chang, K. T., Chen, Y. L., Hsu, H. C., Lee, P. H., Lai, P. L. and Jeng, Y. M. (2013) S100P expression is a novel prognostic factor in hepatocellular carcinoma and predicts survival in patients with high tumor stage or early recurrent tumors. PloS one. **8**, e65501

227   Schor, A. P., Carvalho, F. M., Kemp, C., Silva, I. D. and Russo, J. (2006) S100P calcium-binding protein expression is associated with high-risk proliferative lesions of the breast. Oncology reports. **15**, 3-6

228   Jiang, L., Lai, Y. K., Zhang, J., Wang, H., Lin, M. C., He, M. L. and Kung, H. F. (2011) Targeting S100P inhibits colon cancer growth and metastasis by Lentivirus-mediated RNA interference and proteomic analysis. Mol Med. **17**, 709-716

229   Hamada, S., Satoh, K., Hirota, M., Fujibuchi, W., Kanno, A., Umino, J., Ito, H., Satoh, A., Kikuta, K., Kume, K., Masamune, A. and Shimosegawa, T. (2009) Expression of the calcium-binding protein S100P is regulated by bone morphogenetic protein in pancreatic duct epithelial cell lines. Cancer science. **100**, 103-110

230   (1952) SCIENTIFIC proceedings: American Association for Cancer Research, Inc., New York, N.Y., April 11-13, 1952. Cancer research. **12**, 243-312

231   Scherer, W. F., Syverton, J. T. and Gey, G. O. (1953) Studies on the propagation in vitro of poliomyelitis viruses. IV. Viral multiplication in a stable strain of human malignant epithelial cells (strain HeLa) derived from an epidermoid carcinoma of the cervix. The Journal of experimental medicine. **97**, 695-710

232   Jensen, F. C., Girardi, A. J., Gilden, R. V. and Koprowski, H. (1964) Infection of Human and Simian Tissue Cultures with Rous Sarcoma Virus. Proceedings of the National Academy of Sciences of the United States of America. **52**, 53-59

233   Arumugam, T., Simeone, D. M., Van Golen, K. and Logsdon, C. D. (2005) S100P promotes pancreatic cancer growth, survival, and invasion. Clinical cancer research : an official journal of the American Association for Cancer Research. **11**, 5356-5364

234   Chandramouli, A., Mercado-Pimentel, M. E., Hutchinson, A., Gibadulinova, A., Olson, E. R., Dickinson, S., Shanas, R., Davenport, J., Owens, J., Bhattacharyya, A. K., Regan, J. W., Pastorekova, S., Arumugam, T., Logsdon, C. D. and Nelson, M. A. (2010) The induction of S100p expression by the Prostaglandin E(2) (PGE(2))/EP4 receptor signaling pathway in colon cancer cells. Cancer biology & therapy. **10**, 1056-1066

235   Onyeagucha, B. C., Mercado-Pimentel, M. E., Hutchison, J., Flemington, E. K. and Nelson, M. A. (2013) S100P/RAGE signaling regulates microRNA-155 expression via AP-1 activation in colon cancer. Experimental cell research. **319**, 2081-2090

236   Lo, J. F., Yu, C. C., Chiou, S. H., Huang, C. Y., Jan, C. I., Lin, S. C., Liu, C. J., Hu, W. Y. and Yu, Y. H. (2011) The epithelial-mesenchymal transition mediator S100A4 maintains cancer-initiating cells in head and neck cancers. Cancer research. **71**, 1912-1923

237   Schneider, M., Hansen, J. L. and Sheikh, S. P. (2008) S100A4: a common mediator of epithelial-mesenchymal transition, fibrosis and regeneration in diseases? J Mol Med (Berl). **86**, 507-522

238   Worthylake, R. A., Lemoine, S., Watson, J. M. and Burridge, K. (2001) RhoA is required for monocyte tail retraction during transendothelial migration. The Journal of cell biology. **154**, 147-160

239   Shutova, M., Yang, C., Vasiliev, J. M. and Svitkina, T. (2012) Functions of nonmuscle myosin II in assembly of the cellular contractile system. PloS one. **7**, e40814

240   Betapudi, V., Licate, L. S. and Egelhoff, T. T. (2006) Distinct roles of nonmuscle myosin II isoforms in the regulation of MDA-MB-231 breast cancer cell spreading and migration. Cancer research. **66**, 4725-4733

241   Xia, Z. K., Yuan, Y. C., Yin, N., Yin, B. L., Tan, Z. P. and Hu, Y. R. (2012) Nonmuscle myosin IIA is associated with poor prognosis of esophageal squamous cancer. Diseases of the esophagus : official journal of the International Society for Diseases of the Esophagus / I.S.D.E. **25**, 427-436

242   Saleem, M., Kweon, M. H., Johnson, J. J., Adhami, V. M., Elcheva, I., Khan, N., Bin Hafeez, B., Bhat, K. M., Sarfaraz, S., Reagan-Shaw, S., Spiegelman, V. S., Setaluri, V. and Mukhtar, H. (2006) S100A4 accelerates tumorigenesis and invasion of human prostate cancer through the transcriptional regulation of matrix metalloproteinase 9. Proceedings of the National Academy of Sciences of the United States of America. **103**, 14825-14830

243   Dakhel, S., Padilla, L., Adan, J., Masa, M., Martinez, J. M., Roque, L., Coll, T., Hervas, R., Calvis, C., Messeguer, R., Mitjans, F. and Hernandez, J. L. (2014) S100P antibody-mediated therapy as a new promising strategy for the treatment of pancreatic cancer. Oncogenesis. **3**, e92

244   Maciejczyk, A., Lacko, A., Ekiert, M., Jagoda, E., Wysocka, T., Matkowski, R., Halon, A., Gyorffy, B., Lage, H. and Surowiak, P. (2013) Elevated nuclear S100P expression is associated with poor survival in early breast cancer patients. Histology and histopathology. **28**, 513-524

245   Zhang, A., Wang, Q., Han, Z., Hu, W., Xi, L., Gao, Q., Wang, S., Zhou, J., Xu, G., Meng, L., Chen, G. and Ma, D. (2013) Reduced expression of Snail decreases breast cancer cell motility by downregulating the expression and inhibiting the activity of RhoA GTPase. Oncology letters. **6**, 339-346

246   Jin, H., Yu, Y., Zhang, T., Zhou, X., Zhou, J., Jia, L., Wu, Y., Zhou, B. P. and Feng, Y. (2010) Snail is critical for tumor growth and metastasis of ovarian carcinoma. International journal of cancer. Journal international du cancer. **126**, 2102-2111

247   Lin, C. Y., Tsai, P. H., Kandaswami, C. C., Lee, P. P., Huang, C. J., Hwang, J. J. and Lee, M. T. (2011) Matrix metalloproteinase-9 cooperates with transcription factor Snail to induce epithelial-mesenchymal transition. Cancer science. **102**, 815-827

248   Geiger, T. and Zaidel-Bar, R. (2012) Opening the floodgates: proteomics and the integrin adhesome. Current opinion in cell biology. **24**, 562-568

249   Kuo, J. C., Han, X., Hsiao, C. T., Yates, J. R., 3rd and Waterman, C. M. (2011) Analysis of the myosin-II-responsive focal adhesion proteome reveals a role for beta-Pix in negative regulation of focal adhesion maturation. Nature cell biology. **13**, 383-393

250   Schiller, H. B., Friedel, C. C., Boulegue, C. and Fassler, R. (2011) Quantitative proteomics of the integrin adhesome show a myosin II-dependent recruitment of LIM domain proteins. EMBO reports. **12**, 259-266

251   Humphries, J. D., Byron, A., Bass, M. D., Craig, S. E., Pinney, J. W., Knight, D. and Humphries, M. J. (2009) Proteomic analysis of integrin-associated complexes identifies RCC2 as a dual regulator of Rac1 and Arf6. Science signaling. **2**, ra51

252   Ajeian, J. N., Horton, E. R., Astudillo, P., Byron, A., Askari, J. A., Millon-Fremillon, A., Knight, D., Kimber, S. J., Humphries, M. J. and Humphries, J. D. (2015) Proteomic analysis of integrin-associated complexes from mesenchymal stem cells. Proteomics. Clinical applications

253   Cui, H., Darmanin, S., Natsuisaka, M., Kondo, T., Asaka, M., Shindoh, M., Higashino, F., Hamuro, J., Okada, F., Kobayashi, M., Nakagawa, K. and Koide, H. (2007) Enhanced expression of asparagine synthetase under glucose-deprived conditions protects pancreatic cancer cells from apoptosis induced by glucose deprivation and cisplatin. Cancer research. **67**, 3345-3355

254   Lin, K., He, S., He, L., Chen, J., Cheng, X., Zhang, G. and Zhu, B. (2014) Complement component 3 is a prognostic factor of non-small cell lung cancer. Molecular Medicine Reports. **10**, 811-817

255   Rutkowski, M. J., Sughrue, M. E., Kane, A. J., Mills, S. A. and Parsa, A. T. (2010) Cancer and the complement cascade. Molecular cancer research : MCR. **8**, 1453-1465

256   Chen, Y., Knosel, T., Kristiansen, G., Pietas, A., Garber, M. E., Matsuhashi, S., Ozaki, I. and Petersen, I. (2003) Loss of PDCD4 expression in human lung cancer correlates with tumour progression and prognosis. The Journal of pathology. **200**, 640-646

257   Singh, P., Marikkannu, R., Bitomsky, N. and Klempnauer, K. H. (2009) Disruption of the Pdcd4 tumor suppressor gene in chicken DT40 cells reveals its role in the DNA-damage response. Oncogene. **28**, 3758-3764

258   Deng, X., Hu, Y., Ding, Q., Han, R., Guo, Q., Qin, J., Li, J., Xiao, R., Tian, S., Hu, W., Zhang, Q. and Xiong, J. (2014) PEG10 plays a crucial role in human lung cancer proliferation, progression, prognosis and metastasis. Oncology reports. **32**, 2159-2167

259   Zang, W., Wang, T., Huang, J., Li, M., Wang, Y., Du, Y., Chen, X. and Zhao, G. (2015) Long noncoding RNA PEG10 regulates proliferation and invasion of esophageal cancer cells. Cancer gene therapy. **22**, 138-144

260   Conley, B. A., Koleva, R., Smith, J. D., Kacer, D., Zhang, D., Bernabeu, C. and Vary, C. P. (2004) Endoglin controls cell migration and composition of focal adhesions: function of the cytosolic domain. The Journal of biological chemistry. **279**, 27440-27449

261   Kershaw, R. M., Siddiqui, Y. H., Roberts, D., Jayaraman, P. S. and Gaston, K. (2014) PRH/HHex inhibits the migration of breast and prostate epithelial cells through direct transcriptional regulation of Endoglin. Oncogene. **33**, 5592-5600

262   Perez-Gomez, E., Villa-Morales, M., Santos, J., Fernandez-Piqueras, J., Gamallo, C., Dotor, J., Bernabeu, C. and Quintanilla, M. (2007) A role for endoglin as a suppressor of malignancy during mouse skin carcinogenesis. Cancer research. **67**, 10268-10277

263   Hashimoto, M., Ichihara, M., Watanabe, T., Kawai, K., Koshikawa, K., Yuasa, N., Takahashi, T., Yatabe, Y., Murakumo, Y., Zhang, J. M., Nimura, Y. and Takahashi, M. (2004) Expression of CD109 in human cancer. Oncogene. **23**, 3716-3720

264   Emori, M., Tsukahara, T., Murase, M., Kano, M., Murata, K., Takahashi, A., Kubo, T., Asanuma, H., Yasuda, K., Kochin, V., Kaya, M., Nagoya, S., Nishio, J., Iwasaki, H., Sonoda, T., Hasegawa, T., Torigoe, T., Wada, T., Yamashita, T. and Sato, N. (2013) High expression of CD109 antigen regulates the phenotype of cancer stem-like cells/cancer-initiating cells in the novel epithelioid sarcoma cell line ESX and is related to poor prognosis of soft tissue sarcoma. PloS one. **8**, e84187

265   Bannister, A. J. and Kouzarides, T. (2011) Regulation of chromatin by histone modifications. Cell research. **21**, 381-395

266   Sarrazin, S., Lamanna, W. C. and Esko, J. D. (2011) Heparan sulfate proteoglycans. Cold Spring Harbor perspectives in biology. **3**

267   Heo, W. D., Inoue, T., Park, W. S., Kim, M. L., Park, B. O., Wandless, T. J. and Meyer, T. (2006) PI(3,4,5)P3 and PI(4,5)P2 lipids target proteins with polybasic clusters to the plasma membrane. Science. **314**, 1458-1461

268   Dong, P., Nabeshima, K., Nishimura, N., Kawakami, T., Hachisuga, T., Kawarabayashi, T. and Iwasaki, H. (2006) Overexpression and diffuse expression pattern of IQGAP1 at invasion fronts are independent prognostic parameters in ovarian carcinomas. Cancer letters. **243**, 120-127

269   Nabeshima, K., Shimao, Y., Inoue, T. and Koono, M. (2002) Immunohistochemical analysis of IQGAP1 expression in human colorectal carcinomas: its overexpression in carcinomas and association with invasion fronts. Cancer letters. **176**, 101-109

270   Sakurai-Yageta, M., Recchi, C., Le Dez, G., Sibarita, J. B., Daviet, L., Camonis, J., D'Souza-Schorey, C. and Chavrier, P. (2008) The interaction of IQGAP1 with the exocyst complex is required for tumor cell invasion downstream of Cdc42 and RhoA. The Journal of cell biology. **181**, 985-998

271   Vanhara, P., Hampl, A., Kozubik, A. and Soucek, K. (2012) Growth/differentiation factor-15: prostate cancer suppressor or promoter? Prostate cancer and prostatic diseases. **15**, 320-328

272   Wollmann, W., Goodman, M. L., Bhat-Nakshatri, P., Kishimoto, H., Goulet, R. J., Jr., Mehrotra, S., Morimiya, A., Badve, S. and Nakshatri, H. (2005) The macrophage inhibitory cytokine integrates AKT/PKB and MAP kinase signaling pathways in breast cancer cells. Carcinogenesis. **26**, 900-907

273   Park, Y. J., Lee, H. and Lee, J. H. (2010) Macrophage inhibitory cytokine-1 transactivates ErbB family receptors via the activation of Src in SK-BR-3 human breast cancer cells. BMB reports. **43**, 91-96

274   Boyle, G. M., Pedley, J., Martyn, A. C., Banducci, K. J., Strutton, G. M., Brown, D. A., Breit, S. N. and Parsons, P. G. (2009) Macrophage inhibitory cytokine-1 is overexpressed in malignant melanoma and is associated with tumorigenicity. The Journal of investigative dermatology. **129**, 383-391

275   Kim, I. Y., Park, S. Y., Kang, Y., Thapa, D., Choi, H. G. and Kim, J. A. (2011) Role of nonsteroidal anti-inflammatory drug-activated gene-1 in docetaxel-induced cell death of human colorectal cancer cells with different p53 status. Archives of pharmacal research. **34**, 323-330

276   Pajares, M. J., Agorreta, J., Salvo, E., Behrens, C., Wistuba, II, Montuenga, L. M., Pio, R. and Rouzaut, A. (2014) TGFBI expression is an independent predictor of survival in adjuvant-treated lung squamous cell carcinoma patients. British journal of cancer. **110**, 1545-1551

277   Hayes, A. J., Huang, W. Q., Yu, J., Maisonpierre, P. C., Liu, A., Kern, F. G., Lippman, M. E., McLeskey, S. W. and Li, L. Y. (2000) Expression and function of angiopoietin-1 in breast cancer. British journal of cancer. **83**, 1154-1160

278   Abeysinghe, H. R., Cao, Q., Xu, J., Pollock, S., Veyberman, Y., Guckert, N. L., Keng, P. and Wang, N. (2003) THY1 expression is associated with tumor suppression of human ovarian cancer. Cancer genetics and cytogenetics. **143**, 125-132

279   Nagaraj, N., Wisniewski, J. R., Geiger, T., Cox, J., Kircher, M., Kelso, J., Paabo, S. and Mann, M. (2011) Deep proteome and transcriptome mapping of a human cancer cell line. Molecular systems biology. **7**, 548

280   Li, C., Guo, B., Wilson, P. B., Stewart, A., Byrne, G., Bundred, N. and Kumar, S. (2000) Plasma levels of soluble CD105 correlate with metastasis in patients with breast cancer. International journal of cancer. Journal international du cancer. **89**, 122-126

281   Nassiri, F., Cusimano, M. D., Scheithauer, B. W., Rotondo, F., Fazio, A., Yousef, G. M., Syro, L. V., Kovacs, K. and Lloyd, R. V. (2011) Endoglin (CD105): a review of its role in

angiogenesis and tumor diagnosis, progression and therapy. Anticancer research. **31**, 2283-2290

282   Koleva, R. I., Conley, B. A., Romero, D., Riley, K. S., Marto, J. A., Lux, A. and Vary, C. P. (2006) Endoglin structure and function: Determinants of endoglin phosphorylation by transforming growth factor-beta receptors. The Journal of biological chemistry. **281**, 25110-25123

283   Perez-Gomez, E., Del Castillo, G., Juan Francisco, S., Lopez-Novoa, J. M., Bernabeu, C. and Quintanilla, M. (2010) The role of the TGF-beta coreceptor endoglin in cancer. TheScientificWorldJournal. **10**, 2367-2384

284   Liu, Y., Jovanovic, B., Pins, M., Lee, C. and Bergan, R. C. (2002) Over expression of endoglin in human prostate cancer suppresses cell detachment, migration and invasion. Oncogene. **21**, 8272-8281

285   Guerrero-Esteo, M., Lastres, P., Letamendia, A., Perez-Alvarez, M. J., Langa, C., Lopez, L. A., Fabra, A., Garcia-Pardo, A., Vera, S., Letarte, M. and Bernabeu, C. (1999) Endoglin overexpression modulates cellular morphology, migration, and adhesion of mouse fibroblasts. European journal of cell biology. **78**, 614-623

286   Lee, N. Y., Ray, B., How, T. and Blobe, G. C. (2008) Endoglin promotes transforming growth factor beta-mediated Smad 1/5/8 signaling and inhibits endothelial cell migration through its association with GIPC. The Journal of biological chemistry. **283**, 32527-32533

287   Nomura-Kitabayashi, A., Anderson, G. A., Sleep, G., Mena, J., Karabegovic, A., Karamath, S., Letarte, M. and Puri, M. C. (2009) Endoglin is dispensable for angiogenesis, but required for endocardial cushion formation in the midgestation mouse embryo. Developmental biology. **335**, 66-77

288   Rossi, E., Lopez-Novoa, J. M. and Bernabeu, C. (2014) Endoglin involvement in integrin-mediated cell adhesion as a putative pathogenic mechanism in hereditary hemorrhagic telangiectasia type 1 (HHT1). Frontiers in genetics. **5**, 457

289   Kopczynska, E. and Makarewicz, R. (2012) Endoglin - a marker of vascular endothelial cell proliferation in cancer. Contemp Oncol (Pozn). **16**, 68-71

290   Chakhachiro, Z. I., Zuo, Z., Aladily, T. N., Kantarjian, H. M., Cortes, J. E., Alayed, K., Nguyen, M. H., Medeiros, L. J. and Bueso-Ramos, C. (2013) CD105 (endoglin) is highly overexpressed in a subset of cases of acute myeloid leukemias. American journal of clinical pathology. **140**, 370-378

291   Kopczynska, E., Dancewicz, M., Kowalewski, J., Makarewicz, R., Kardymowicz, H., Kaczmarczyk, A. and Tyrakowski, T. (2012) Influence of surgical resection on plasma endoglin (CD105) level in nonsmall cell lung cancer patients. Experimental oncology. **34**, 53-56

292   Vicente-Manzanares, M., Webb, D. J. and Horwitz, A. R. (2005) Cell migration at a glance. Journal of cell science. **118**, 4917-4919

293   Huttenlocher, A. and Horwitz, A. R. (2011) Integrins in cell migration. Cold Spring Harbor perspectives in biology. **3**, a005074

294   Murillo, C. A., Rychahou, P. G. and Evers, B. M. (2004) Inhibition of alpha5 integrin decreases PI3K activation and cell adhesion of human colon cancers. Surgery. **136**, 143-149

295   Mierke, C. T., Frey, B., Fellner, M., Herrmann, M. and Fabry, B. (2011) Integrin alpha5beta1 facilitates cancer cell invasion through enhanced contractile forces. Journal of cell science. **124**, 369-383

296   Brown, M. D. and Sacks, D. B. (2006) IQGAP1 in cellular signaling: bridging the GAP. Trends in cell biology. **16**, 242-249

297   Goto, T., Sato, A., Adachi, S., Iemura, S., Natsume, T. and Shibuya, H. (2013) IQGAP1 protein regulates nuclear localization of beta-catenin via importin-beta5 protein in Wnt signaling. The Journal of biological chemistry. **288**, 36351-36360

298   White, C. D., Erdemir, H. H. and Sacks, D. B. (2012) IQGAP1 and its binding proteins control diverse biological functions. Cellular signalling. **24**, 826-834

299   Takemoto, H., Doki, Y., Shiozaki, H., Imamura, H., Utsunomiya, T., Miyata, H., Yano, M., Inoue, M., Fujiwara, Y. and Monden, M. (2001) Localization of IQGAP1 is inversely correlated with intercellular adhesion mediated by e-cadherin in gastric cancers. International journal of cancer. Journal international du cancer. **91**, 783-788

300   Wang, X. X., Li, X. Z., Zhai, L. Q., Liu, Z. R., Chen, X. J. and Pei, Y. (2013) Overexpression of IQGAP1 in human pancreatic cancer. Hepatobiliary & pancreatic diseases international : HBPD INT. **12**, 540-545

301   Hayashi, H., Nabeshima, K., Aoki, M., Hamasaki, M., Enatsu, S., Yamauchi, Y., Yamashita, Y. and Iwasaki, H. (2010) Overexpression of IQGAP1 in advanced colorectal cancer correlates with poor prognosis-critical role in tumor invasion. International journal of cancer. Journal international du cancer. **126**, 2563-2574

302   Osman, M. (2010) An emerging role for IQGAP1 in regulating protein traffic. TheScientificWorldJournal. **10**, 944-953

303   Rigothier, C., Auguste, P., Welsh, G. I., Lepreux, S., Deminiere, C., Mathieson, P. W., Saleem, M. A., Ripoche, J. and Combe, C. (2012) IQGAP1 interacts with components of the slit diaphragm complex in podocytes and is involved in podocyte migration and permeability in vitro. PloS one. **7**, e37695

304   Rittmeyer, E. N., Daniel, S., Hsu, S. C. and Osman, M. A. (2008) A dual role for IQGAP1 in regulating exocytosis. Journal of cell science. **121**, 391-403

305   Johnson, M. A. and Henderson, B. R. (2012) The scaffolding protein IQGAP1 co-localizes with actin at the cytoplasmic face of the nuclear envelope: implications for cytoskeletal regulation. Bioarchitecture. **2**, 138-142

306   Jacquemet, G., Morgan, M. R., Byron, A., Humphries, J. D., Choi, C. K., Chen, C. S., Caswell, P. T. and Humphries, M. J. (2013) Rac1 is deactivated at integrin activation sites through an IQGAP1-filamin-A-RacGAP1 pathway. Journal of cell science. **126**, 4121-4135

307   Suzuki, K., Chikamatsu, Y. and Takahashi, K. (2005) Requirement of protein phosphatase 2A for recruitment of IQGAP1 to Rac-bound beta1 integrin. Journal of cellular physiology. **203**, 487-492

308   Zaidel-Bar, R., Milo, R., Kam, Z. and Geiger, B. (2007) A paxillin tyrosine phosphorylation switch regulates the assembly and form of cell-matrix adhesions. Journal of cell science. **120**, 137-148

309   Jenkinson, S. R., Barraclough, R., West, C. R. and Rudland, P. S. (2004) S100A4 regulates cell motility and invasion in an in vitro model for breast cancer metastasis. British journal of cancer. **90**, 253-262

310   Ismail, T. M., Fernig, D. G., Rudland, P. S., Terry, C. J., Wang, G. and Barraclough, R. (2008) The basic C-terminal amino acids of calcium-binding protein S100A4 promote metastasis. Carcinogenesis. **29**, 2259-2266

311   Levett, D., Flecknell, P. A., Rudland, P. S., Barraclough, R., Neal, D. E., Mellon, J. K. and Davies, B. R. (2002) Transfection of S100A4 produces metastatic variants of an orthotopic model of bladder cancer. The American journal of pathology. **160**, 693-700